

Light-Induced and Supramolecular Ligation to Design Macromolecules in Solution and on Surfaces

Zur Erlangung des akademischen Grades eines

DOKTORS DER NATURWISSENSCHAFTEN

(Dr. rer. nat.)

Fakultät für Chemie und Biowissenschaften

Karlsruher Institut für Technologie (KIT) - Universitätsbereich

genehmigte

DISSERTATION

von

Dipl.-Chem. Astrid Franziska Hirschbiel

aus

Karlsruhe, Deutschland

Dekan: Prof. Dr. Willem M. Klopper

Referent: Prof. Dr. Christopher Barner-Kowollik

Korreferent: Prof. Dr. Hans-Achim Wagenknecht

Tag der mündlichen Prüfung: 23.10.2015

Die vorliegende Arbeit wurde von August 2012 bis September 2015 unter Anleitung von Prof. Christopher Barner-Kowollik am Karlsruher Institut für Technologie (KIT) – Universitätsbereich angefertigt.

Erklärung

Ich erkläre hiermit, dass ich die vorliegende Arbeit im Rahmen der Betreuung durch Prof. Dr. Christopher Barner-Kowollik selbstständig verfasst und keine anderen als die angegebenen Quellen und Hilfsmittel verwendet habe. Wörtlich oder inhaltlich übernommenen Stellen sind als solche kenntlich gemacht und die Satzung des Karlsruher Instituts für Technologie (KIT) zur Sicherung guter wissenschaftlicher Praxis wurde beachtet.

Des Weiteren erkläre ich, dass ich mich derzeit in keinem weiteren laufenden Promotionsverfahren befinde und auch keine vorausgegangenen Promotionsversuche unternommen habe.

Karlsruhe, den 04.09.2015

Astrid Hirschbiel

Für meine Familie

Abstract

Light-induced reactions offer a wide spectrum of possible applications in synthetic chemistry. Simply, by means of irradiation, bonds can be formed or already existing conjunctions can be cleaved without the need of additional catalysts, thus yielding a versatile and clean method to design macromolecules in solution and on surfaces. In the course of the present thesis, the light-induced reactivity of *o*-nitrobenzyl and 2-methoxy-6-methylbenzaldehyde (photoenol, PE) is applied to design patterned surfaces for biological applications as well as to form complex macromolecular architectures in combination with supramolecular host-guest interactions. Such novel and effective techniques to form complex macromolecular architectures aid in the design of advanced functional materials.

By means of a photolithographic approach, spatially resolved functionalized polycarbonate (PC) films are generated and employed in the context of cell culture and guiding. The combination of photopatterning via the cleavage of an *o*-nitrobenzyl derivative and the surface-initiated polymerization of an oligo(ethylene glycol) (OEG) derivative creates micropatterns of passivated and non-passivated areas on the film. In the non-passivated areas carboxylic acid functionalities increase the adhesiveness of the PC surface and lead to cell/protein attachment on the film, whereas the poly(OEG) forms a biorepellent layer. Specific areas of the polymeric substrate can thus be made accessible for biological impact, such as strongly fouling

sera (fetal calf serum (FCS)), proteins (enhanced green fluorescent protein (eGFP)) and specific cell attachment. In addition, the patterned PC substrates are thermoformed into 3D microchannels and cell guiding within the 3D structure is achieved.

Moreover, for the first time the photoenol Diels-Alder reaction and β -cyclodextrin (CD) host-guest interactions are combined as an innovative tool for the modular design of sophisticated polymer architectures. The PE unit enables the light-induced reaction with a reactive double bond and β -CD is able to form strong inclusion complexes with suitable guest molecules. In this context several chain transfer agents (CTA) are synthesized and equipped with supramolecular recognition units (*tert*-butyl phenyl and adamantyl), a photoactive unit (photoenol, PE), and a molecule with a reactive double bond (maleimide), respectively. By means of reversible-addition fragmentation chain transfer (RAFT) polymerization of water soluble acrylamides – *N*-isopropylacrylamide (NiPAAm), *N,N'*-dimethylacrylamide (DMAAm), *N,N'*-diethylacrylamide (DEAAm), and *N*-hydroxyethylacrylamide (HOEAAm) – the functionalities attached to the CTAs are transferred onto the chain termini of well-defined polymer blocks with narrow size distributions. The generated multifunctional blocks are combined to di-, tri-, and tetrablock copolymers. Thus, partially covalent and partially supramolecularly ligated multiblock copolymers are obtained and in-depth analyzed via size exclusion chromatography (SEC), high resolution (Orbitrap) electrospray ionization mass spectrometry, dynamic light scattering (DLS) and nuclear Overhauser effect spectroscopy (NOESY).

Furthermore, a variation of this block building technique is employed for the design of stimuli responsive nanoparticles. The approach is based on the formation of a supramolecularly connected diblock copolymer of β -CD functionalized poly(DMAAm) and adamantyl bearing poly(NiPAAm), which has PE crosslinking units incorporated in its side chain. In aqueous solution, micellization of the diblock copolymer occurs when heated above the lower critical solution temperature (LCST) of the thermoresponsive poly(NiPAAm) block, which is subsequently cross-linked in its core. The statistically incorporated PE units enable photo-induced reactions with

the maleimide end-groups of the linker molecule. The linker is encapsulated in the micelle during the self-assembly of the diblock copolymer. The cross-linked cores of the micelles yield the thermoresponsive nanoparticles that are released from their micellar scaffold via the removal of the β -CD arms with trifluoroacetic acid (TFA) featuring a trigger temperature around 30 °C. Among other characterization techniques, DLS and atomic force microscopy (AFM) are applied to analyze micelles and nanoparticles in detail. In summary, the efficiency of light-induced reactions to design surfaces and complex polymer architectures is demonstrated.

Zusammenfassung

Lichtinduzierte Reaktionen haben eine große Bandbreite an Anwendungsmöglichkeiten in der synthetischen Chemie. Durch einfache Bestrahlung und ohne die Zugabe von Katalysatoren können neue chemische Bindungen geknüpft werden oder vorhandene Bindungen gespalten werden. Dadurch sind photoinduzierte Reaktionen eine vielfältige und saubere Methode, um makromolekulare Architekturen in Lösung und auf Oberflächen aufzubauen. Im Verlauf der vorliegenden Arbeit wird die durch Licht induzierte Reaktivität von *o*-Nitrobenzyl und 2-Methoxy-6-methylbenzaldehyd (Photoenol, PE) genutzt, um strukturierte Oberflächen für biologische Anwendungen zu gestalten, und um in Kombination mit supramolekularen Wirt-Gast-Wechselwirkungen komplexe makromolekulare Architekturen aufzubauen. Derart neue und wirkungsvolle Verknüpfungstechniken zum Aufbau komplexer Polymerstrukturen sind die Grundlage für die Entwicklung von fortschrittlichen und funktionellen Materialien. Mittels eines photolithographischen Ansatzes werden orts aufgelöst funktionalisierte Polycarbonat(PC)-Filme erzeugt, die für Zellkulturen und Zellführungs-Untersuchungen eingesetzt werden. Durch die Kombination aus photochemischer Abspaltung eines *o*-Nitrobenzyl-Derivats mit der oberflächeninitiierten Polymerisation eines Oligoethylenglykol-Derivats werden Mikrostrukturen von passivierten und nichtpassivierten Bereichen auf dem Film generiert. In den nichtpassivierten Bereichen erhöhen Carbonsäure-Funktionalitäten die Haftfähigkeit der PC-Oberfläche und führen zu Protein- und Zellanlagerungen auf dem Film, wohingegen das Poly(OEG) eine bioabweisende Schicht bildet. Dadurch werden bestimmte Bereiche des Polymersubstrats für biologische Einflüsse

zugänglich, wie z.B. für Fetales Kälberserum (FCS), grün fluoreszierendes Protein (GFP) und für spezifische Zellanhaftung. Zudem werden die strukturierten Oberflächen thermisch in einen dreidimensionalen Mikrokanal umgeformt, um die Zellführung innerhalb der 3D-Struktur zu untersuchen.

Darüber hinaus wird erstmalig die photoinduzierte Diels–Alder Reaktion in Kombination mit β -Cyclodextrin (CD) Wirt-Gast-Beziehungen eingesetzt, um auf modulare Weise anspruchsvolle Polymerarchitekturen aufzubauen. Die PE-Einheit ermöglicht die lichtinduzierte Reaktion mit reaktiven Doppelbindungen, und β -CD kann stabile Einschlusskomplexe mit geeigneten Gastmolekülen ausbilden. Zu diesem Zweck werden sogenannte RAFT-Reagenzien (s.u.) synthetisiert, die jeweils mit supramolekularen Erkennungseinheiten (*tert*-Butyl phenyl), photoaktiven Einheiten (Photoenol, PE) und Molekülen mit einer reaktiven Doppelbindung (Maleimid) ausgestattet sind. Mittels reversibler Additions-Fragmentierungs-Kettentransfer(RAFT)-Polymerisation von wasserlöslichen Acrylamiden – *N*-Isopropylacrylamid (NiPAAm), *N,N'*-Dimethylacrylamid (DMAAm), *N,N'*-Diethylacrylamid (DEAAm) und *N*-hydroxyethylacrylamid (HOEAAm) – werden die funktionellen Gruppen der RAFT-Reagenzien auf die Kettenenden von Polymerblöcken mit kontrollierter Kettenlänge übertragen. Die so erzeugten multifunktionellen Blöcke werden zu Di-, Tri- und Tetrablockcopolymeren vereint. Dadurch entstehen teils kovalent gebundene und teils supramolekular verknüpfte Multiblockcopolymere, die eingehend mittels Größenausschlusschromatographie, hoch auflösender (Orbitrap-)Elektrospray-Ionisations-Massenspektrometrie (ESI-MS), dynamischer Lichtstreuung (DLS) und Kern-Overhauser-Effekt-Spektroskopie analysiert werden.

Zusätzlich werden die modularen Bausteine für die Entwicklung thermoresponsiver Nanopartikel eingesetzt. Der Ansatz basiert auf der Herstellung von supramolekular verbundenen Diblockcopolymeren, bestehenden aus einer β -CD-funktionalisierten Poly(DMAAm)-Einheit und eines Adamantyl-funktionalisierten Poly(NiPAAm)-Blocks mit zusätzlich eingebauten PE-Vernetzungspunkten in der Seitenkette. In erhitzter wässriger Lösung ordnen sich die Diblockcopolymere zu Mizellen an, wenn die untere kritische Lösungstemperatur (LCST) des thermoresponsiven Poly(NiPAAm)-Blocks erreicht wird. Die Mizellen werden anschließend durch

Bestrahlung in ihrem Inneren vernetzt. Dabei ermöglichen die statistisch eingebauten PE-Einheiten die photoinduzierte Reaktion mit den Maleimid-Endgruppen eines während der Mizellenbildung eingeschlossenen Linkermoleküls. Die quervernetzten Kerne der Mizellen ergeben die thermoresponsiven Nanopartikel, mit einer kritischen Kontraktionstemperatur von 30 °C, die durch das Entfernen der β -CD-funktionalisierten Arme, mittels Zugabe von Trifluoressigsäure (TFA), aus ihrem Mizellengerüst befreit werden. Neben anderen Charakterisierungsmethoden werden dynamische Lichtstreuung (DLS) und Rasterkraftmikroskopie (AFM) eingesetzt, um Mizellen und Nanopartikel eingehend zu untersuchen.

Im Allgemeinen wird gezeigt, dass lichtinduzierte Reaktionen äußerst wirkungsvoll sind, um Oberflächen zu bearbeiten und komplexe makromolekulare Architekturen zu konstruieren.

Publications Arising from this Dissertation

- [1] ***Photolithographic Patterning of 3D-Formed Polycarbonate Films for Targeted Cell Guiding***
Hirschbiel, A. F.; Geyer, S.; Yameen, B.; Welle, A.; Nikolov, P.; Giselbrecht, S.; Scholpp, S.; Delaittre, G.; Barner-Kowollik, C. *Advanced Materials* **2015**, *27*, 2621-2626.
- [2] ***Photochemical Design of Stimuli Responsive Nanoparticles Prepared by Supramolecular Host-Guest Chemistry***
Hirschbiel, A. F.; Schmidt, B. V. K.; Krolla-Sidenstein, P.; Blinco, J.; Barner-Kowollik, C. *Macromolecules* **2015**, *48*, 4410-4420.
- [3] ***Access to Multiblock Copolymers via Supramolecular Host-Guest Chemistry and Photochemical Ligation***
Hirschbiel, A. F.; Konrad, W.; Schulze-Suenninghausen, D.; Wiedmann, S.; Luy, B.; Schmidt, B. V. K.; Barner-Kowollik, C. *ACS Macro Letters* **2015**, *4*, 1062-1066.

Contents

1. Introduction	1
2. Theoretical Background and Literature Overview	5
2.1 Light-Induced Reactions	6
2.1.1 Photochemistry – a Brief History	6
2.1.2 Photo-Induced Diels–Alder Reactions	11
2.1.3 Photolabile Protecting Groups	16
2.2 Radical Polymerization	20
2.2.1 Free Radical Polymerization (FRP)	20
2.2.2 Controlled/Living Radical Polymerizations (CRP)	22
2.3 Cyclodextrins	30
2.3.1 The Structure of Cyclodextrins	31
2.3.2 Complex Formation of Cyclodextrins	32
2.4 Spatially Resolved Surface Design	37
2.4.1 Photolithographic Surface Patterning	39
2.5 Modular Ligation of Polymers	43
2.5.1 <i>Click</i> Chemistry	44
2.5.2 Diels–Alder Reaction	46
2.5.3 Azide-Alkyne Cycloaddition	51
3. Light-Induced Surface Modification for Guided Cell Attachment	55
3.1 Motivation	56
3.2 Results and Discussion	57
3.2.1 Modification of Polycarbonate Surfaces	57
3.2.2 Protein Adhesion on the Polycarbonate Film	63
3.2.3 Cell Guiding on the Polycarbonate Film in 2D	65
3.2.4 Thermoforming and Cell Guiding in 3D	67

Contents

3.3	Conclusion.....	70
3.4	Experimental Section	71
3.4.1	Materials	71
3.4.2	Instrumentation.....	71
3.4.3	Syntheses.....	73
3.4.4	Surface Reactions.....	75
3.4.5	Protein adhesion studies	76
3.4.6	Thermoforming.....	77
3.4.7	Cell Guiding Experiments	78
4.	Complex Macromolecular Architectures via Supramolecular Chemistry and Photochemical Ligation.....	79
4.1	Motivation	80
4.2	Results and Discussion	81
4.2.1	Synthesis of Chain Transfer Agents	81
4.2.2	Generation of Multifunctional Polymeric Building Blocks.....	86
4.2.3	Modular Ligation of Polymer Chains to Multi- block Copolymers.....	96
4.2.4	Development of Thermoresponsive Nanoparticles from Complex Macromolecular Architectures	102
4.3	Conclusion.....	119
4.4	Experimental Section	120
4.4.1	Materials	120
4.4.2	Instrumentation.....	121
4.4.3	Small Molecule Syntheses	123
4.4.4	Polymer Syntheses	129
4.4.5	Multiblock Copolymer Formation.....	134
4.4.6	Nanoparticle Design.....	135
5.	Conclusion and Outlook	137
	References.....	141
	Appendix A.....	163
	Appendix B.....	167

1

Introduction

Nature has inspired scientists at the beginning of the 20th century to employ light as an energy source to trigger chemical reactions.^{1,2} Since that time, a plethora of research on photochemical reactions has been performed in organic chemistry and polymer science alike and has led to a wide application range, due to their advanced features.³⁻⁵ Light-induced chemical reactions provide spatial and temporal control over covalent bond formation or molecular cleavage, by focusing the light beam on specific areas and with defined exposure times. The wavelength and the intensity of the incident light can be varied to trigger reactions that are susceptible to a certain range of the electromagnetic spectrum only, thus providing a level of selectivity and orthogonality,⁶ also towards light-insensitive units, which is not achievable with conventional thermally induced reactions. Since light-induced reactions proceed at ambient temperature without the need of additional reagents and toxic catalysts,

they can be applied to highly sensitive systems, e.g. in bio-orthogonal conjugations.^{7,8,9} Furthermore, photo-triggered reactions can proceed with high yields and minimum side reactions which simplifies or even prevents the need for purification of the sample.⁵

The present thesis exploits photo-induced reactions for the design of patterned surfaces aimed towards advanced applications and the construction of complex macromolecular architectures in solution. Thus, the study is divided into two major chapters: Chapter 3) The modification of chemical surfaces via photo-induced deprotection and Chapter 4) The design of complex macromolecular architectures, combining light-induced reactions with supramolecular chemistry (Figure 1.1). Although photochemical reactions have already been extensively employed in polymer science, the range of these reactions is still not exhausted, especially in combination with other ligation techniques and novel substrates.

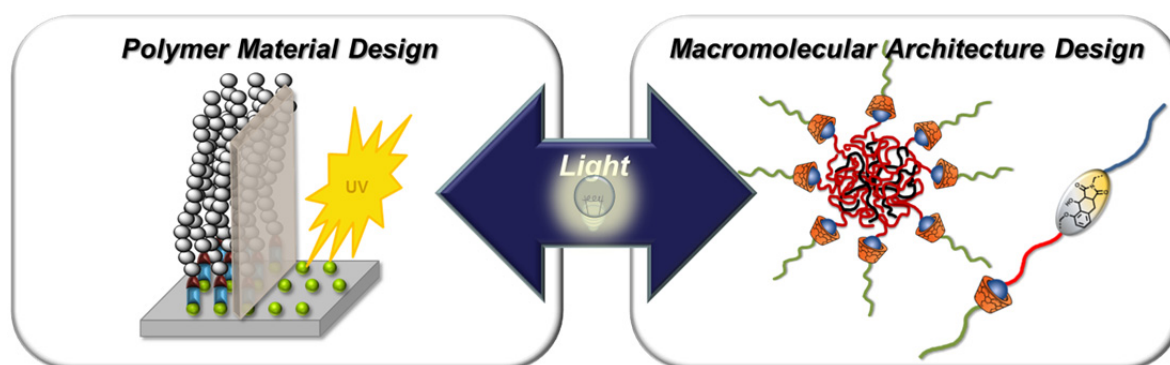


Figure 1.1. Draft of the projects presented in the present dissertation.

There is an emerging need in biological research to develop microscavolds which can mimic organs as structural subunits of the body, e.g. hollow tubes that can resemble the central nervous system (CNS) or non-tubular structures such as the heart.^{10, 11} To further advance the biological platform or to study defined co-cultures, boundaries have to be introduced as they are naturally occurring in a living system.¹²⁻¹⁴ Part of the current study has the aim to develop a general method for spatially functionalizing polycarbonate (PC) films for advanced cell culture and guiding experiments, followed by a thermoforming step (the so-called SMART method).¹⁵⁻¹⁷ The hollow microchannel structures that are generated in this manner

can simulate the neural channels of zebra fish. Since light-induced reactions provide a mild and efficient tool to precisely introduce defined patterns onto a surface, a photolithographic approach is employed to modify the PC films. Accordingly, a photo-active moiety, acting simultaneously as an initiator for controlled radical polymerization, is covalently attached to the surface and subsequently released in defined areas, by means of soft UV irradiation and a photomask. Followed by the surface-initiated polymerization of a biorepellent polymer – evolving at the remaining initiator – micro-patterns of polymer brushes in the non-irradiated areas and hydrophilic moieties in the irradiated areas are generated. Thus, certain areas on the substrate are activated for cell attachment, whereas other areas have biorepellent properties. Furthermore, a 3D microchannel is shaped on the photo-patterned polycarbonate film via a thermoforming process. In cooperation with a biology research group, specific cell-attachment to the pre-defined areas on the patterned film is investigated, on the 2D substrate and in the 3D shaped microchannel.

The second part of the present dissertation addresses the development of complex polymer architectures, which has been driving polymer scientists in recent years.^{18,19,20} Since the emergence of reversible deactivation radical polymerization methods, also referred to as controlled radical polymerization (CRP), it is possible to synthesize well-defined polymer chains with regard to molecular weight, size distribution and end-group functionality.²¹ In combination with highly efficient organic reactions, summarized under the term *click* reactions, a toolbox of polymeric building blocks can be compiled, which allows for the access of tailor-made functional materials and sophisticated macromolecular architectures.²²⁻²⁴

The study is motivated by the strong demand for the simple design of macromolecular architectures via the versatile coupling opportunities offered by light-induced and supramolecular chemistry. In particular, host-guest interactions of cyclodextrins (CD) have found broad application in polymer science as an important tool for non-covalent conjunctions, e.g. in drug delivery systems²⁵ or self-healing materials.²⁶ By merging the efficient light-induced Diels–Alder *click* reactions with supramolecular host-guest interactions of CDs, materials with new and improved

properties can be developed. Both linking techniques have the advantage of orthogonal and quantitative conversion without the need of further reactants and purification steps. Since the supramolecular host-guest complexes of CDs are generally formed in water, a set of water soluble polymer building blocks is synthesized with CRP protocols, to be precise with reversible addition-fragmentation chain transfer polymerization (RAFT). Thus, a range of newly designed chain transfer agents (CTA) is employed to introduce the desired functionalities – supramolecular recognition sites and light-responsive units – into the polymer blocks. By means of irradiation and supramolecular self-assembly, tri- and tetrablock copolymer structures are obtained. Moreover, a variation of this block building technique is employed in the design of stimuli responsive nanoparticles from thermoresponsive monomers.

The methods introduced in the course of the present thesis critically expand the field of photochemical reactions by associating them with other ligation techniques such as supramolecular chemistry or with innovative substrates, e.g. thermoformable PC films. Thus, a valuable contribution is provided to readily construct complex macromolecular architectures with advanced features and to design biological platforms.

2

Theoretical Background and Literature Overview

In the following chapter a brief overview on the theoretical background of the methods which were employed in the course of the present dissertation is given. First, the development of light-induced reactions is summarized, followed by specific examples of photochemically activated reactions. Subsequently, an outline on radical polymerization techniques is given, with a focus on applied syntheses. In addition to light-induced reactions, supramolecular host-guest interactions of cyclodextrins were utilized to ligate polymer building blocks and are therefore described. Furthermore, surface modification approaches are presented. Finally, a general view on modular ligation techniques for polymeric building blocks is given along with possible architectures that can be obtained via modular ligation. The individual

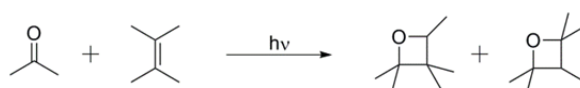
topics are briefly summarized and the reader is referred to the literature for further coverage of the topic.

2.1 Light-Induced Reactions

The thesis addresses novel applications of light-induced reactions in the context of surface modifications and macromolecular design. Therefore, a brief description of the development of photochemical reactions is given, along with the theoretical background that is needed in order to understand the processes occurring after photochemical activation. Moreover, the reaction mechanism of the applied photochemistry together with a literature overview is presented.

2.1.1 Photochemistry – a Brief History

The pioneers in the field of photochemistry were Trommsdorf, who was the first to hypothesize that light interacts with matter and can induce chemical reactions²⁷ and Einstein with the discovery of the laws governing the photoelectric effect and the quantum equivalence.^{28,29} Followed by Planck and its quantum hypothesis as well as Bodenstein and Stark who gave insight into the kinetics of radiated molecules,^{30,29} the foundation for light-induced chemical reactions was laid. The first systematic study on the influence of light on organic compounds was performed by Ciamician and Silber with the intention to employ sunlight for chemical reactions.^{1,2,31-33} Furthermore, the combined work of Paternò and Büchi, known as the famous *Paternò-Büchi* reaction, described the photochemically induced [2+2]-cycloaddition of a carbonyl with olefins to oxetans (Scheme 2.1).³ The *Paternò-Büchi* reaction is to this date the most widely used method for oxetanes synthesis.³⁴



Scheme 2.1. Paternò-Büchi reaction: Addition of an excited-state carbonyl compound to an olefin to form an oxetan.³

Furthermore, Norrish and coworkers investigated the photochemical decomposition of carbonyl compounds and thus, gave insight into the occurring photochemical processes, using laser flash photolysis.³⁵⁻³⁸ Their discoveries (depicted in Scheme 2.3 and Scheme 2.4) are referred to as the Norrish Type I and Norrish Type II reaction and will be explained in more detail later in the current section. Firstly, however the processes occurring in a photochemically excited molecule are explained.

Photochemical reactions occur through absorption of a photon by a compound, which initially leads to the excitation of electrons from the electronic singlet ground state of the molecule to its excited singlet state from which further electron transitions can occur. Such electron transitions can be visualized by a Jablonski diagram, depicted in Figure 2.1.³⁹

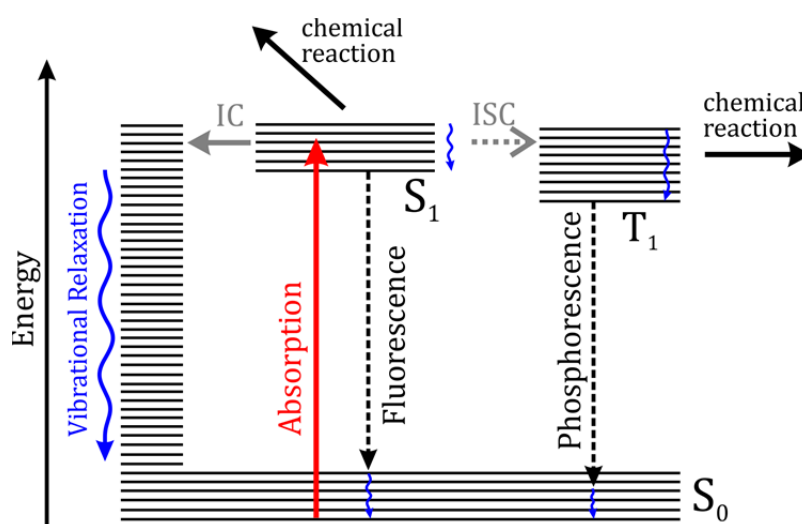


Figure 2.1. Jablonski diagram of a three level system, with singlet ground state (S_0), excited singlet state (S_1) and an excited triplet state (T_1). The following photochemical processes are shown: Excitation of an electron via absorption (red), internal conversion (IC) and vibrational loss (non-radiative), fluorescence, intersystem crossing (ISC), phosphorescence and chemical reactions.

After absorption, the excited molecule can now undergo several radiative or non-radiative deactivations:

Internal conversion (IC) and vibrational relaxation: The absorbed energy is released via a radiationless transition from the excited singlet state to the singlet ground state. Since the transfer occurs between two states with equal spin multiplicity, IC

2. Theoretical Background and Literature Overview

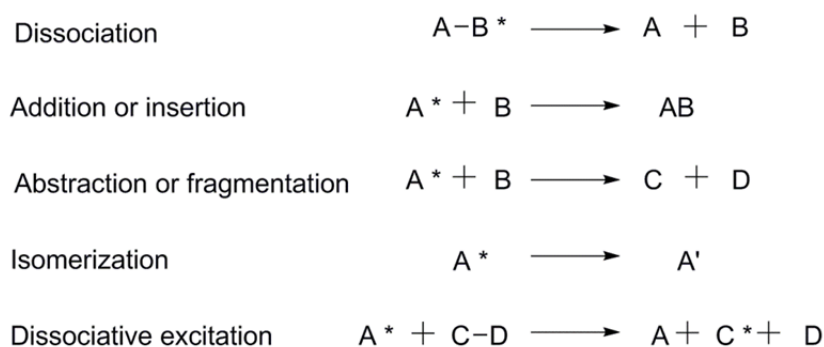
occurs relatively fast and the energy is released into the environment via collisions or vibrational relaxation.

Fluorescence: After excitation into the excited singlet state, the molecule releases a part of its energy via collisions with its environment. Through this radiationless deactivation, the molecule can reach its excited singlet ground state. Since the remaining energy is too high to be absorbed by the environment and to deactivate the molecule, the energy is released by spontaneous emission of a photon (fluorescence).

Intersystem crossing (ISC): The molecule undergoes radiationless spin conversion from the excited singlet into an energetically lower excited triplet state, characterized by the presence of two unpaired electrons with parallel spin. Especially in molecules where the S_1 - T_1 energy gap is low (e.g. ketones) ISC rates are enhanced.

Phosphorescence: After ISC, the molecule is located in its triplet state. Here, as well as in the excited singlet state, some of the energy is released by vibrational relaxation until the ground level of the excited triplet state is reached. As it was the case for fluorescence, the energy of the molecule is too high to be absorbed by the environment. As a consequence, emission of a photon (phosphorescence) from the triplet ground state occurs, yet is rather slow, since the probability of a spin change from triplet to singlet is reduced. The latter restriction results in longer emission times even after the light source has already been removed. Furthermore, the molecule can return to the S_0 ground state via chemical reaction.

Chemical reactions and dissociation: Chemical reactions can either occur from the excited singlet state or the excited triplet state, depending on the absorbing molecule. An overview of possible chemical reactions which can occur after photochemical excitation is summarized in Scheme 2.2.



Scheme 2.2. Overview of chemical processes which can occur after photochemical excitation. A, B, C, and D are arbitrary molecules.⁴⁰

Especially light triggered isomerization is important for the photo-induced reactions employed in the current thesis and will be further discussed in sections 2.1.2 and 2.1.3.

In order to quantify photochemical reactions, the quantity of the incident light absorbed by the sample needs to be determined. In general, light absorption is quantified through Beer-Lambert's law which is the relationship between absorbance and the concentration of an absorber of electromagnetic radiation:

$$\log\left(\frac{I_t}{I_0}\right) = -\varepsilon[J]l$$

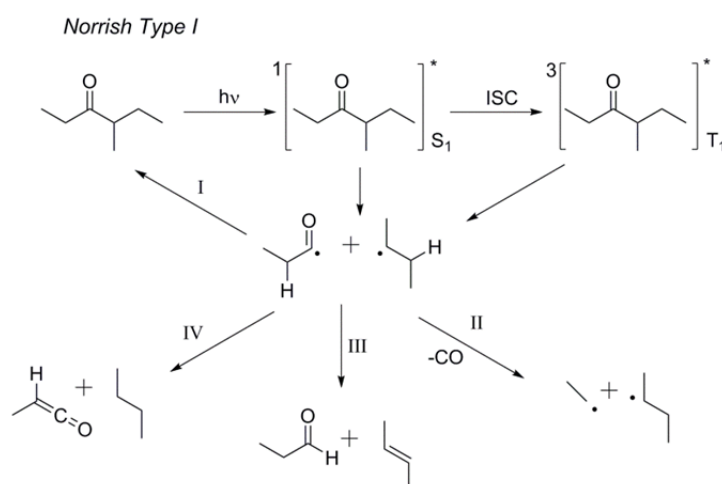
I_0 = Intensity of the incident light
 I_t = Intensity of the transmitted light
 ε = molar extinction coefficient
 l = path length of the light
 $[J]$ = concentration of the absorbing species.

Equation 2.1. Beer-Lambert's law.⁴⁰

To measure the absorption, the intensity of irradiation before (I_0) and after passing through a sample (I_t) is determined. After calculation of the negative logarithm of the ratio of both intensities and plotting against sample concentration and path length, the molar extinction coefficient can be determined. The later characterizes the absorbance of a molecule.⁴⁰

2. Theoretical Background and Literature Overview

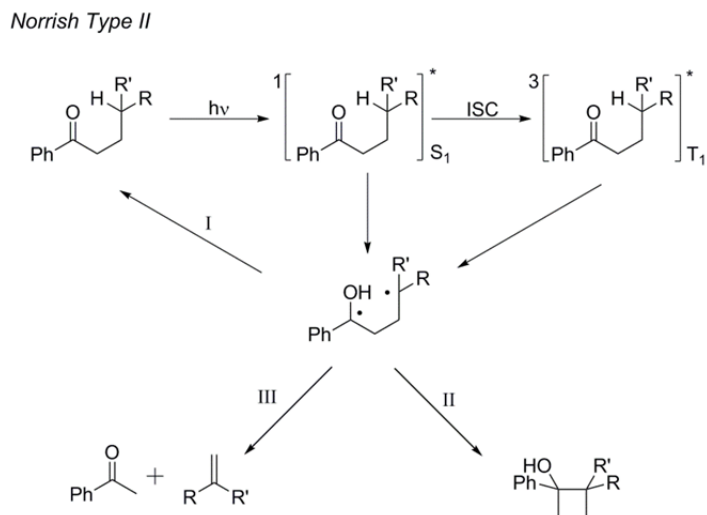
Norrish and coworkers revealed that the electron transition in carbonyls derives from the excitation of an electron stemming from the free electron pair at the oxygen (n) into an unoccupied antibonding π^* -orbital of the carbonyl double bond. This transition is referred to as $n \rightarrow \pi^*$ excitation, which is in fact symmetry forbidden. However, due to the small triplet-singlet energy gap, the ISC rates of carbonyls are high. Thus, photochemical reactions from the excited singlet state can occur, yet reactions from the excited triplet state are more likely. The cleavage of a carbon-carbon bond in α -position to the carbonyl group, resulting in two radicals, is shown in Scheme 2.3, and is referred to as Norrish Type I reaction. Subsequently, the formed acyl- and alkyl- radicals, which are obtained either from the excited singlet or the excited triplet state, can undergo several reactions to yield in a variety of possible products: Recombination of the radicals to the starting compound (I), decarboxylation (II), intermolecular hydrogen transfer (III) and intramolecular hydrogen transfer (IV).^{34,41} For example, radical initiation methods in polymer chemistry, such as the light-induced decomposition of benzoin into benzoyl- and benzyl alcohol radicals, follow a Norrish Type I mechanism.⁴²



Scheme 2.3. Norrish Type I reaction: intramolecular α -cleavage. 4-Methyl-3-hexanone was exemplarily chosen to demonstrate the processes described in literature.^{41,34}

Furthermore, a second dissociation mechanism was itemized by Norrish. The Norrish Type II reaction, shown in Scheme 2.4, describes the intramolecular abstraction of a hydrogen atom from the γ -position, generating a 1,4-diradical which

can recombine to its initial state (I), cyclize to cyclobutanol (II) or undergo cleavage to give an alkene and an enol (III).



Scheme 2.4. Norrish Type II reaction: Intramolecular hydrogen abstraction from a carbon-hydrogen bond in γ -position to the carbonyl bond.⁴³

The background information, given in the past section, aids to understand the photoenolisation mechanism of *o*-methyl substituted aromatic ketones and aldehydes as they were applied in the course of the present thesis.

2.1.2 Photo-Induced Diels–Alder Reactions

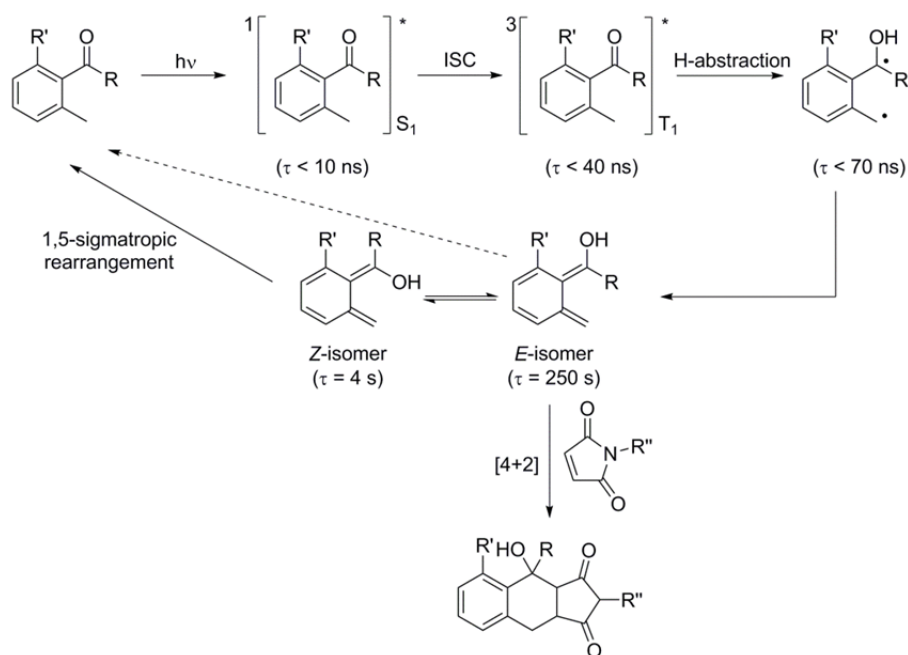
The photo-ligation strategy employed in Chapter 4 is based on the light-induced isomerization reaction of 2-methoxy-6-methylbenzaldehyde, which forms an extremely reactive diene, a so called *o*-quinodimethane (photoenol), upon irradiation with UV light. The so formed diene can further react in a [4+2] cycloaddition (Diels–Alder reaction) in the presence of a dienophile. This light induced Diels–Alder (DA) reaction is highly orthogonal towards other ligation methods, e.g. conventional DA reactions or copper catalyzed azide alkyne cycloaddition. Furthermore, light as trigger provides spatial and temporal control over the chemical reactions.

Only light-induced Diels–Alder (DA) reactions are addressed in the following paragraph. A summary on DA reactions in general is given later on in this chapter (see section 2.5.2) in the context of modular ligation strategies.

2.1.2.1 Photoenol Chemistry

In 1961, Yang and Rivas reported the photo-induced enolization of *o*-alkyl benzophenones, which were trapped in a DA reaction in the presence of a dienophile, thus giving the base for photoenol *click* chemistry.⁴⁴⁻⁴⁶ The term *click* chemistry is discussed in more detail in section 2.5.1. The actual mechanism of the photoenolization reaction was finally revealed by Tchir and Porter on the example of 2,5-dimethyl benzophenone via flash photolysis and is depicted in Scheme 2.5.⁴⁷⁻⁵¹

Via irradiation, the *o*-methyl substituted carbonyl is excited to a transient singlet state through an $n \rightarrow \pi^*$ transition of the carbonyl, followed by fast ISC to the excited triplet state. From the excited triplet state, abstraction of the γ -hydrogen (Norrish Type II reaction) takes place, resulting in a conjugated 1,4-biradical. The biradical relaxes into two possible conformations, the *E*- and *Z*-isomer of the photoenol. The lifetime of the *Z*-isomer is much shorter compared to the *E*-isomer and thus rapidly rearranges to the starting compound via a (1,5)-sigmatropic proton shift. Due to its increased lifetime the *E*-isomer of photoenol can subsequently react in a thermally induced DA reaction with a dienophile or rearrange to the *o*-methyl carbonyl.⁵² In fact, to avoid misunderstandings, the photoenol DA reaction is not triggered via irradiation, since according to the Woodward-Hoffmann rules (see section 2.5.2) the [4+2] cycloadditions are thermally activated. Light, in this context, only generates the reactive diene – the photoenol – and the actual DA reaction proceeds at ambient temperature.



Scheme 2.5. Mechanism of the photo-induced formation of *o*-quinomethanes (photoenol, PE). The mechanism was adapted from Tchir and Porter who measured 2,4-dimethyl benzophenone in degassed cyclohexane.⁴⁷

Furthermore, the group of Barner-Kowollik investigated the influence of the substituent (R) on the reactivity of the photoenol. Two photoenol derivatives – 2-methyl benzophenone and 2-methoxy-6-methyl benzaldehyde – showed high reactivity, also in the context of polymer conjugation.⁵³⁻⁵⁵ However, only the 2-methoxy-6-methyl benzaldehyde derivative was employed for the studies in Chapter 4 of this dissertation. Compared to 2-methyl benzophenone, the synthesis of 2-methoxy-6-methyl benzaldehyde is straightforward and it showed higher reactivity, even towards less activated dienophiles.

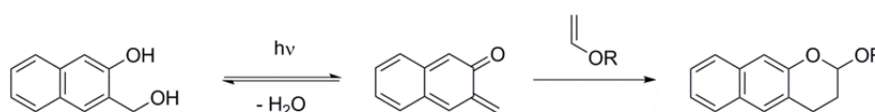
The rapid and orthogonal reaction of the photoenol, resulting in high yields without any side products has led to a broad variety of applications. For example, photoenols were utilized by Barner-Kowollik and team in the spatially resolved modification of silicon wafers,⁵⁶ gold surfaces⁵⁷ and cellulose.⁵⁸ They were also employed by the same group for the preparation of single chain nanoparticles⁵⁹ or for the generation of polymeric Janus spheres, in combination with reversible addition-fragmentation chain transfer (RAFT) polymerization.⁶⁰

2. Theoretical Background and Literature Overview

Two alternative approaches to the photoenol chemistry are given below which also generate highly reactive intermediates triggered by light and then are able to undergo DA reactions.

2.1.2.2 *o*-Naphthoquinone Methides (NQM)

An alternative to the photoenol DA reaction is given by *o*-naphthoquinone methides (*o*NQMs). *o*NQMs can undergo photo-induced hetero Diels–Alder (HDA) reactions upon irradiation with light. The general mechanism is shown in Scheme 2.6. *o*NQMs are formed via irradiation of 3-hydroxy-2-naphthalenemethanol under abstraction of a water molecule. An equilibrium is established in which the reactive *o*NQM can either be rehydrated or react in a [4+2]-cycloaddition reaction.⁶¹ In contrast to the photoenol, the formed diene is electron deficient, thus it only reacts with electron rich dienophiles, e.g. vinyl ethers and enamines.⁶²

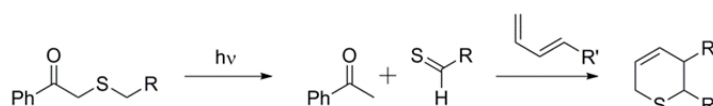


Scheme 2.6. General mechanism of the photoactivation of 2-naphthoquinone-3-methides (*o*NQMs) and subsequent Diels–Alder reaction.⁶²

The research group around Popik employed the light-induced HDA reactions of *o*NQMs in several reactions,⁶²⁻⁷⁰ especially for surface grafting approaches in order to produce patterned surfaces.^{62,64,65} In this way, Popik and coworkers were able to immobilize fluorescent markers on glass substrates.⁶⁵ In addition, they employed the photo-induced *o*NQM reaction in combination with azide alkyne *click* chemistry, featuring high orthogonality.^{66,71} Moreover, it was discovered that NQMs can undergo Michael additions with nucleophilic groups (e.g. thiols).⁶⁶ Although, the possibility to undergo Michael addition adds to the versatility of *o*NQMs, the reaction loses its orthogonality.⁶⁴

2.1.2.3 Thioaldehydes

Furthermore, photochemical activation cannot only generate reactive dienes, such as photoenol and *o*NMQ, but also form reactive dienophiles for DA reactions. The photo-fragmentation of phenacyl sulfide into a thioaldehyde, shown in Scheme 2.7, yields such reactive dienophiles which can be trapped in HDA reactions.^{72,73}



Scheme 2.7. Photo-induced generation of a thioaldehyde and subsequent HDA reaction.⁷⁴

The light-induced formation of thioaldehydes has been employed for the spatially resolved surface patterning of silicon wafers by our team.⁷⁴ In this study, phenacyl sulfide was covalently attached to the silicon surface and thioaldehydes were generated in defined areas (on the surface) via irradiation with a shadow mask. Thus, cyclopentadiene-functionalized poly(ethylene glycol) could be grafted to the reactive dienophiles on the surface. In the same manner, cellulose substrates could be modified with diene end-capped peptides and polymers by us.⁵⁸

Similar to *o*NQMs, the reactive thioaldehyde intermediates also react with many other functional groups, which leads to side-product formation. Therefore, also no orthogonality is given.⁷⁵

In conclusion, thioaldehydes and *o*-naphthoquinone methides are versatile light-triggered intermediates. However, high orthogonality is only given via photo-induced reactions with photoenols.

2.1.3 Photolabile Protecting Groups

Photolabile protecting groups (PPGs) which can be simply removed via irradiation are highly attractive to protect the functionalities of sensitive molecules.^{76,77} Thus, compounds which are incompatible with harsh treatment conditions, such as acidic or basic ones, can be easily protected under the mild conditions of PPGs, which do not require addition of further compounds.⁷⁸ Employing light as trigger to release PPGs also allows for temporal and spatial control over the deactivated species and is therefore often applied for the modification of solid substrates.^{76,79} In general, PPGs should guarantee full protection of the targeted functionality in a molecule. Moreover, the deprotection reaction should proceed in a fast, efficient, clean and orthogonal manner, preferably solvent independent. Furthermore, wavelengths in the soft UV range – above 320 nm – are desired in order to prevent degradative side reactions, e.g. in sensitive biological systems. Possible side-products generated in the course of the deprotection should be chemically inert and not interfere with the photolysis.⁸⁰ So far, no PPG system has been developed which fulfills all mentioned criteria, yet this does not affect the wide applications of PPGs, especially on surfaces,^{77,81,82} and in biological systems.⁸³⁻⁸⁵ In the context of biochemistry, PPGs are often referred to as *caged* compounds, that is to say that the deprotected biomolecule is released from a cage or, in other words, is “*uncaged*”.⁹ The efficiency of the deprotection reaction strongly depends on the quantum yield Φ (ratio of the number of photons emitted to the number of photons absorbed) and the absorption coefficient ϵ of the PPG. As a consequence, photoreactions occur if high quantum yields and strong absorbance is reached with the excitation wavelength.⁸⁰

For a more detailed background the reader should refer to the numerous reviews published on PPGs.^{4,8,9,67,76-80,85-93} An overview of simplified basic structures of selected examples of PPGs is depicted in Figure 2.2 to demonstrate the versatility of compounds which can be employed in photodegradation reactions.

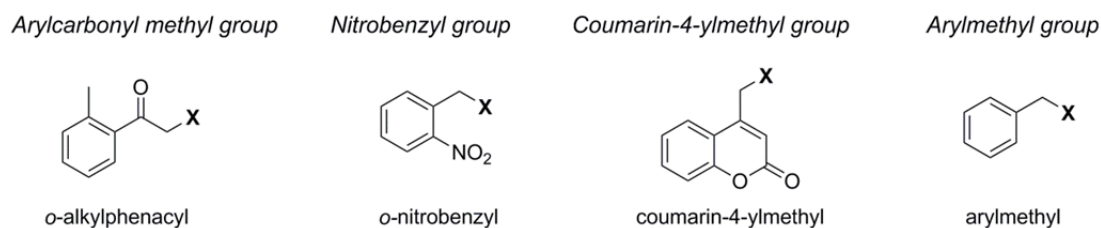


Figure 2.2. Selected examples of photoremovable protecting groups (PPGs), which were summarized by Klán *et al.* in a very detailed review.⁶⁷

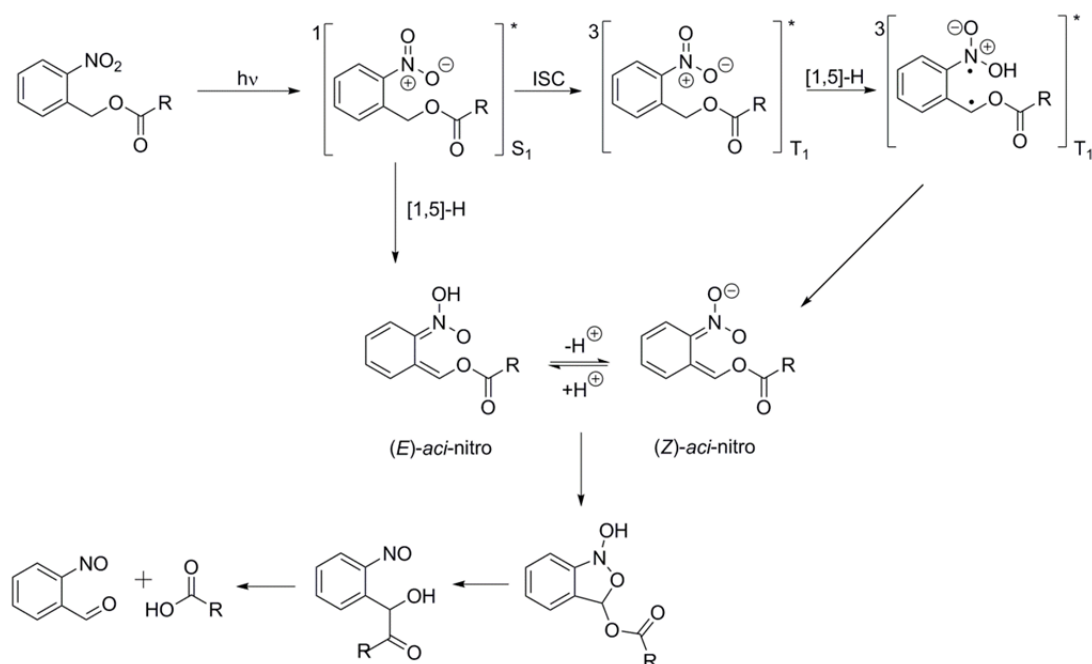
The following section only focuses on *o*-nitrobenzyl derivatives, which were employed in Chapter 3 to pattern the surface of a polycarbonate (PC) film in association with cell cultures. An approach based on *o*-nitrobenzyl derivatives was chosen, since they can be activated by soft UVA irradiation (i.e. 320-365 nm) and their synthesis is rather facile.⁹⁴

2.1.3.1 *o*-Nitrobenzyl Photoprotecting Group

The *o*-nitrobenzyl (*o*NB) group is a well-known photo-removable protecting group which reacts in a photoisomerization reaction, resulting in *o*-nitrobenzylaldehydes and simultaneously releasing carboxylic acids.⁷⁸ The photoisomerization of *o*-nitrobenzylaldehyde to *o*-nitrobenzoic acid was already observed by Ciamician and Silber in 1901.³¹ The first applications of the *o*NB were later reported by Woodward and coworkers in the 1970s.⁹⁰

The mechanism, depicted in Scheme 2.8, illustrates the excitation of *o*NB to the excited singlet state, where either ISC to the excited triplet state or a hydrogen transfer from the *o*-alkyl substituent can occur. Hydrogen transfer can also occur from the excited triplet state but is less likely. As a result, *aci*-nitro intermediates are formed in an *E/Z*-mixture, which undergo irreversible cyclization. The cyclic intermediate ring-opens to a hemiacetal intermediate and finally releases methanol under hydrolysis.⁶⁷

2. Theoretical Background and Literature Overview



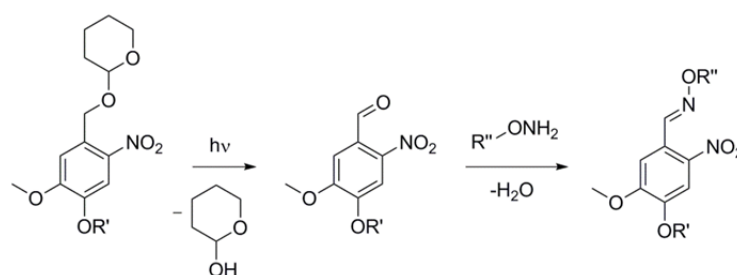
Scheme 2.8. Mechanism of the photoisomerization of *o*-nitrobenzyl alcohol derivatives, forming the corresponding *o*-nitrobenzaldehyde and simultaneously releasing a carboxylic acid.^{67,94,95}

In some applications, the formation of the highly reactive *o*-nitrobenzylaldehyde can lead to undesired side products.⁸⁰ Nevertheless, *o*NBs are still frequently employed, e.g. in the context of polymer science, since their absorption wavelength can be fine-tuned according to the substituent attached to the aromatic ring or at the benzylic position.^{96,97} In this way, *o*NBs have been employed as cross-linkers in photodegradable networks,⁹⁸⁻¹⁰⁰ for the side chain functionalization of polymers¹⁰¹⁻¹⁰³ and in many biological applications as mild protecting group.^{7,104,105} Furthermore, *o*NBs have been applied as photocleavable junctions in block copolymers,¹⁰⁶⁻¹⁰⁸ and for thin film patterning.¹⁰⁹⁻¹¹¹

Due to the mild and orthogonal conditions for the *o*NB photodeprotection, the system is ideal for the surface modification of thin thermoformable polycarbonate films, described in Chapter 3.

Furthermore, a variation of photodeprotection of *o*NB derivatives has been successfully employed to produce patterned surfaces. Paulöhrl *et al.* introduced the photo-triggered oxime ligation where an *o*NB acetal is irradiated with UV light and releases an aldehyde moiety (Scheme 2.9).¹¹² The aldehyde, which is usually formed

as a byproduct in the *o*NB deprotection reaction is, in this regard, the actual product and subsequently participates in an oxime ligation reaction with reactive nucleophiles (e.g. hydroxyl amines). In this way, the photo-triggered oxime ligation was employed to graft molecules and peptides onto an 2-[(4,5-dimethoxy-2-nitro-benzyl)oxy]tetrahydro-2H-pyranyl functionalized silicon surfaces, producing molecular patterns in the deprotected areas on the surface.



Scheme 2.9. Photo-triggered oxime ligation.¹¹²

2.2 Radical Polymerization

Due to facilitated reaction conditions and the high tolerance towards a broad variety of vinyl monomers, radical polymerizations are applied to a high extent for the development of industrial manufactured plastics, e.g. polyethylene (PE), polystyrene (PS) and poly(vinyl chloride) (PVC).¹¹³ The following paragraph comprises an outline of conventional free radical polymerization in comparison to its advanced version, the controlled/living radical polymerization (CRP). Furthermore, the three fundamental CRP techniques – nitroxide mediated polymerization (NMP), atom-transfer radical polymerization (ATRP) and reversible addition-fragmentation (RAFT) polymerization – are briefly discussed.

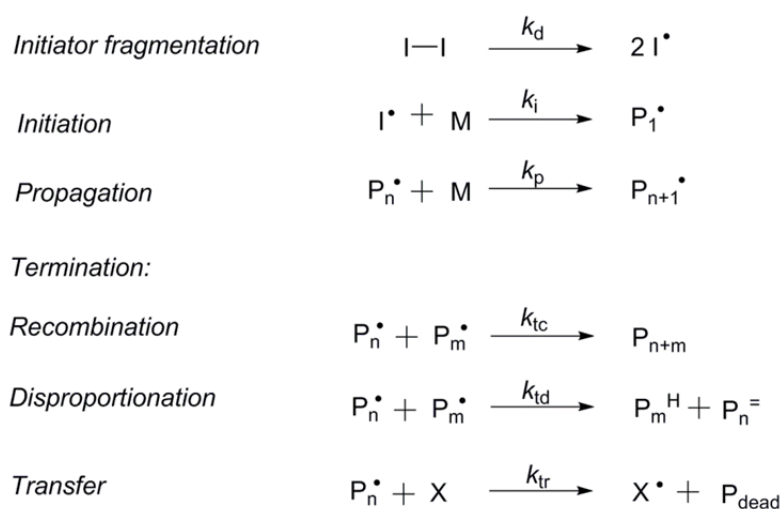
In the scope of the present thesis, ATRP (section 2.2.2.2) and RAFT polymerization (section 2.2.2.3) techniques were employed for the generation of well-defined polymer chains. The surface-initiated (SI) ATRP of biorepellent polymers from polycarbonate surfaces is described in Chapter 3. In addition, the synthesis of chain-end-functionalized polymer blocks via RAFT polymerization and their modular ligation to block copolymers is addressed in Chapter 4.

2.2.1 Free Radical Polymerization (FRP)

In free radical polymerization (FRP), a large range of monomers are polymerizable. Furthermore, FRP can be performed in bulk, suspension, emulsion and solution which usually can be easily purified. Additionally, facile copolymerization of various vinyl monomers is possible due to their similar reactivity. Moreover, radicals are in general tolerant towards many functional groups, e.g. acidic, hydroxyl- and amino groups, wherefore this polymerization technique is very attractive for industrial applications.¹¹⁴

The mechanism of a FRP is depicted in Scheme 2.10 and comprises four elemental steps: Initiation, propagation, termination and transfer. The reaction starts with the initiator fragmentation as part of the initiation step, thus generating primary radicals ($I\cdot$). Initiator fragmentation can be generated for example via thermal or

photoactivated dissociation. Two regularly employed initiators are, e.g. 2,2'-azobis(2-methylpropionitrile) (AIBN) or dibenzoyl peroxide (DBPO). Subsequently, the initiating radicals ($I\cdot$) react with monomer (M), thus starting the propagation step. During propagation the growing radicals repetitively add to monomers, elongating the growing polymer chain ($P_{n+1}\cdot$). Finally, termination of the growing polymer chains can either occur via the coupling of two radicals (recombination) or by transfer reactions, i.e. transfer to the monomer (X) or disproportionation, resulting in a saturated (P_m^H) and an unsaturated polymer chain ($P_n^=$). Furthermore, transfer reactions can result in branching or crosslinking of the polymer chains.¹¹⁴



Scheme 2.10. Mechanism of a free radical polymerization. (I = Initiator, M = Monomer, P_n and P_m = growing polymer chains, X = small molecule (e.g. monomer, solvent), P_{dead} = non-functional/dead polymer chain).¹¹⁵ In general, k_{tc} and k_{td} are dependent on the chain length of the terminating radicals, since in contrast to k_p they are diffusion controlled.

The reaction mixtures of radical polymerizations must be deoxygenated to avoid radical quenching by oxygen. Gases such as nitrogen or argon are usually employed to create an inert atmosphere for radical polymerizations. In FRP, high molecular weight polymers are obtained at an early stage of the polymerization in relatively short reaction times.¹¹⁴ Usually, FRP yields atactic polymers, since radicals add to the less substituted carbon of the monomer. However, conventional FRP also comprises some drawbacks. The major disadvantage of FRP is the high frequency of termination reactions, due to the high radical concentration. Even though the radical

concentration of the reaction mixture can be reduced via dilution – since termination is diffusion controlled – most of the polymer chains are dead and cannot be further modified.¹¹⁵ Ultimately, no control over polymer chain lengths, their architectures and their size distributions – as can be obtained via anionic polymerization¹¹⁶ – is accessible via FRP. Thus, research was inspired to adjust FRP in order to obtain well-defined polymers. Finally, controlled/living polymerization protocols managed to combine the versatility of FRP with some attributes of anionic polymerization, described in the following paragraph.

2.2.2 Controlled/Living Radical Polymerizations (CRP)

Controlled living radical polymerization (CRP) techniques were developed to eliminate the limitations noted above for FRP. The IUPAC term for these kinds of reactions is reversible deactivation radical polymerization (RDRP) – according to the control mechanism of the polymerization – but in this section they are still referred to as CRP. The term living polymerization was introduced by Szwarc in the context of anionic polymerization, stating that *living* polymerizations are molecular chain growth processes without termination or transfer reactions.¹¹⁷ Moreover, the living character of a polymerization is defined by linear evolution of molecular weight with increasing monomer conversion, narrow weight dispersity (\mathcal{D}) and – importantly – the possibility of chain extension.¹¹⁵

In order to minimize the termination reactions of FRPs and thus gaining control over the polymerization process, reversible deactivation techniques were introduced. The three most commonly employed methods are nitroxide mediated polymerization (NMP), atom-transfer radical polymerization (ATRP) and reversible addition-fragmentation chain transfer (RAFT) polymerization and are shortly discussed in the present section. The principle of CRPs is based on a dynamic equilibrium between growing radicals and dormant species, thus minimizing the possibility of termination. However, termination cannot be completely avoided in CRPs, which is why they are rather referred to as controlled polymerizations than living ones. Two types of equilibria exist: i) In a deactivation/activation process

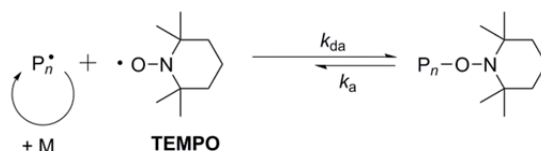
radicals are reversibly trapped (see NMP and ATRP) or ii) the radicals undergo a degenerative exchange process (see RAFT polymerization). The reversible trapping of the radical – as it is performed in NMP¹¹⁸ or ATRP^{119,120} – relies on the persistent radical effect in which newly generated radicals are trapped, e.g. by a stable nitroxide radical. Subsequently, the trapped species is reactivated, either thermally, light-induced, catalytic or spontaneously.¹¹⁵ Since the growth of the radical polymer chain is controlled through constant activation and deactivation, the radical concentration is reduced which results in lower termination rates. Furthermore, termination is reduced since the growing radical species more likely reacts with the trapping species than with itself.^{121, 122} In addition, simultaneous polymer growth is obtained via efficient initiators, since initiation is faster than termination. The resulting polymer chains are only deactivated and can be reactivated at any time again, leading to a wide variety of possibilities for further functionalization. In contrast to NMP and ATRP, RAFT polymerization is based on a degenerative chain transfer mechanism.¹²³⁻¹²⁵ In this process the polymer chains are reversibly transferred to a so-called chain transfer agent (CTA), which provides control over the polymerisation. Similar to FRP, slow initiation and fast termination are observed and the radical concentration is not reduced.

In contrast to FRP, CRP protocols allow for well-defined polymers with control over architecture, chain length, polydispersity and end-group-functionality.

2.2.2.1 Nitroxide Mediated Polymerization (NMP)

As mentioned earlier, nitroxide mediated polymerization (NMP) relies on the persistent radical effect.¹²² In NMP, stable nitroxide radicals such as 2,2,6,6-tetramethyl-1-piperidinyloxy (TEMPO) and its derivatives activate and deactivate the growing radicals by forming a relatively weak covalent bond with the polymer chain, yielding an alkoxyamine.¹²⁶ The chains are reactivated by the thermally induced reversible homolytic cleavage of the polymer-nitroxide bond, thus regenerating the growing radicals (see Scheme 2.11).¹²⁷ NMP can be initiated with conventional initiators (e.g. AIBN, DBPO) or with specially designed alkoxyamine initiators which thermally decompose to form the stable nitroxide radical. Crucial

for the control of the polymerization is that the controlling species only reversibly react with the propagating polymer chains but neither with themselves nor in any side reaction.



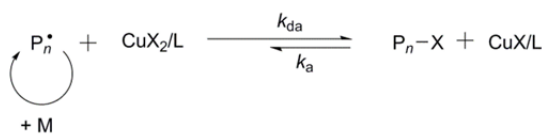
Scheme 2.11. Mechanism of NMP exemplarily shown with TEMPO (P_n^{\bullet} = growing polymer chain, k_{da} = rate coefficient of deactivation, k_a = rate coefficient of activation).¹¹⁸

Compared to other CRP methods, NMP is the least versatile technique since it is limited to monomers which form stable radicals (e.g. styrene, acrylamides etc.) so that the equilibrium can return to the active species. Besides, NMP requires high polymerization temperatures in order to cleave the covalent bond of the alkoxyamine. In addition, further modifications of the alkoxyamine-terminated polymer chains are indeed possible, but are rather difficult to perform.¹¹⁵

2.2.2.2 Atom Transfer Radical Polymerization (ATRP)

Atom transfer radical polymerization (ATRP) was first reported in 1994 by Matyjaszewski¹²¹ and Sawamoto.¹²⁸ The same controlling principle which was described for NMP applies as well for atom transfer radical polymerization (ATRP). In the case of ATRP, a transition metal complex (CuX/L) – for example $CuBr/bpy_2$ – reversibly cleaves an alkyl halide bond (P_n-X), as depicted in Scheme 2.12.¹²⁰ In the reaction with the halogen atom the metal halide complex is oxidized (CuX_2/L), simultaneously allowing the formation of a growing radical chain (P_n^{\bullet}). The propagating chains are formed *in situ* due to thermal decomposition of the so-called ATRP initiators, which are small organic compounds (e.g. 2-bromo-2-methylpropionyl bromide). Thus, no addition of radical starters is necessary. As explained previously, termination reactions in ATRP are suppressed by the persistent radical effect.¹²² However, at the same time the radical concentration is

decreased and the equilibrium is shifted towards the dormant species, resulting in reduced propagation rates.



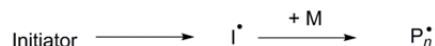
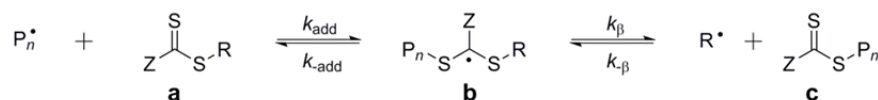
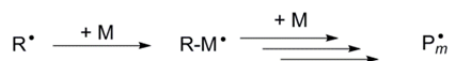
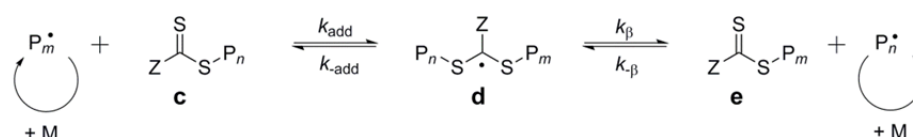
Scheme 2.12. Mechanism of atom-transfer radical polymerization (ATRP).¹²⁹

Even though ATRP can be catalyzed by many transition metals,¹²⁰ copper is by far the most efficient catalyst in ATRP.¹¹³ Usually, the copper complexes are formed with polydentate alkyl amines (e.g. *N,N,N',N'',N'''*-pentamethyldiethylenetriamine (PMDETA)), which provide better catalyst solubility and can adjust the ATRP equilibrium. Possible side reactions in ATRP are solvent or monomer coordination to the transition metal, oxidation or reduction of radicals to carbanions or carbocations or HBr elimination.¹¹⁵ In addition, ATRP has some limitations towards nitrogen containing monomers, since they have a higher tendency to form complexes with the transition metal catalyst.¹¹⁵ However, a wide range of reaction conditions can be employed for ATRP such as temperatures reaching from the subzero region up to 130 °C, or a variety of solvents (e.g. organic, aqueous). Resulting from that, the quantity of polymerizable monomers for ATRP is much higher than in NMP. Furthermore, ATRP polymers retain their halide functionality which can be readily modified in post-polymerization reactions.

Surface initiated ATRP (SI-ATRP) was employed in Chapter 3 in order to grow biorepellent polymer brushes with controlled thickness and density from a polycarbonate film. ATRP was chosen for the surface modification since it proceeds in aqueous solution at ambient temperature and no addition of radical starter is necessary, as such conditions as well as organic solvents could potentially harm the thin and un-crosslinked polycarbonate film.¹³⁰

2.2.2.3 Reversible Addition-Fragmentation Chain-Transfer Polymerization (RAFT)

In Chapter 4, modular polymeric building blocks are synthesized via RAFT. Among all CRP methods available, RAFT polymerization is one of the most versatile polymer design strategies, since it can directly introduce end-group functionalities without the need of post-polymerization modifications. The core principle of RAFT is a significant suppression of irreversible chain termination events.¹²⁴ The overall mechanism of a typical RAFT process is depicted in Scheme 2.13. A radical initiator, such as AIBN, generates primary free radicals ($I\cdot$) which then react with the monomer species (M) to produce growing chains ($P_n\cdot$) (i). In the first step of the chain growth, a pre-equilibrium (ii) is created in which the RAFT agent (**a**) is converted into its polymeric form, i.e. the so called macro-RAFT-agent (**c**). The macro RAFT agent **c** is integral to the main equilibrium. The growing radical ($P_n\cdot$) adds to the carbon-sulfur-double bond and produces a carbon centered intermediate radical (**b**). The intermediate radical releases a new radical by β -scission, which again initiates a growing radical chain (iii). The following addition fragmentation steps constitute a main equilibrium (iv) between the growing chains $P_n\cdot$, $P_m\cdot$ and the periodically inactive thiocarbonylthio-compound (**d**). Control of the polymerization process is provided by a fast establishment of the equilibrium in which there is a constant and rapid exchange between active and inactive species. At the end of the polymerization process the majority of chains carry a thiocarbonylthio-functional group with only a small amount of conventionally terminated material or “dead” (non-functional) polymer (**v**).¹³¹ During RAFT polymerization, the radical concentration is ideally not reduced, thus keeping the reaction rate high and comparable to FRP, but also enhancing the chance of termination.

i) *Initiation*ii) *Reversible Chain Transfer*iii) *Reinitiation*iv) *Chain Equilibration*v) *Termination*

Scheme 2.13. The basic mechanism of reversible addition fragmentation chain transfer (RAFT) polymerization: Initiation of the polymerization (i), the formation of the macro RAFT agent (**c**) in the pre-equilibrium (ii), the release of a new radical (R^\bullet) (iii), the chain growth in the main equilibrium (iv) and finally the termination of the polymerization, which still occurs to a certain percentage (v).^{132,131}

Depending on the choice of the chain transfer agent (CTA), consisting of thiocarbonyl thio compounds (shown in Figure 2.3), a broad variety of monomers can be polymerized. In general, CTAs should provide fast addition and fast fragmentation of the growing polymer chains. Therefore, the constitution of the CTA needs to be selected carefully as the chemical structures of the R- and the Z-group play an important role for the control over the polymerization.

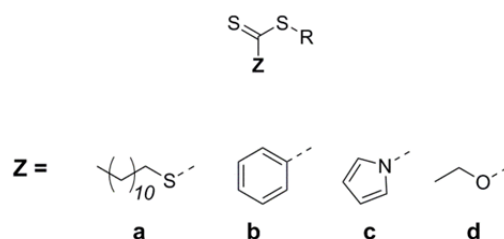


Figure 2.3. General structure of RAFT agents: Trithiocarbonates **a**, dithioester **b**, dithiocarbamate **c** and xanthate **d**.

2. Theoretical Background and Literature Overview

The influence of the R- and the Z-group is demonstrated in Figure 2.4.¹³² Strongly stabilizing Z-groups (e.g. a phenyl group) efficiently control the polymerization of styrene or methacrylate (which form tertiary radicals), however they decelerate or even inhibit the polymerization of acrylates. For monomers which form less stable radicals, weaker stabilizing groups such as dithiocarbamates or xanthates are employed.¹³² The selection of the R-group also depends on the radical structure of the monomer. It is important that the R-radical can efficiently initiate polymerization and while being more stable than the polymer radical to be able to be formed. However, the stability of the generated dormant species must be considered, since reactivation is crucial for the propagation rate and also the addition of R· to the Monomer is an influencing factor.^{132,131}

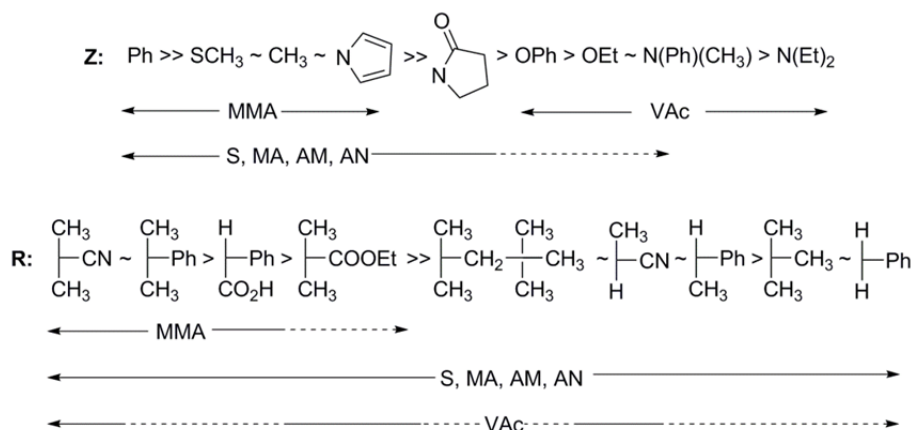


Figure 2.4. Overview for the selection of an appropriate RAFT agent. The solid line indicates full control over the polymerization, whereas the dashed line refers to only partial control of the polymerization. (MMA = methyl methacrylate, VAc = vinyl acetate, S = styrene, MA = methyl acrylate, AM = acrylamide, AN = acrylonitrile). The image was redrawn from Ref. 112. Copyright (2005) CSIRO Publishing.¹³²

As mentioned earlier, RAFT agents can further be modified with specific functional groups. In this way, the functional chain termini can be introduced into the polymer chains directly during polymerization, thus avoiding post-polymerization reactions. However, contaminations from polymer chains which were initiated via the radical starter cannot be prevented.

2.2.2.4 Macromolecular Architectures Accessible via CRPs

As previously stated, CRPs allow for the design of well-defined polymers. Features, as for example polymer functionality, composition and topology, can finally be controlled in the context of radical polymerizations. An outline of the structures which can be obtained in CRPs is given in Figure 2.5. In general, the controlling agent is incorporated into the polymer chain resulting in alkoxyamine-terminated chains for NMP, halide functional chains for ATRP and thiocarbonyl thio-functional polymer chains for RAFT. The opposing chain end bears the initiator functionality in the case of ATRP and NMP and for RAFT the functionality of the R-group. As a consequence, the easily modifiable design of the controlling species can be harnessed in order to introduce defined functionalities to the polymer chain or to produce complex architectures, e.g. stars,¹³³ brushes¹³⁴ or even cyclic structures.¹¹⁹ Furthermore, the resulting polymers are dormant species and can be reactivated for chain extensions. However, chain extension and copolymer formation is restricted to monomers with similar reactivity. Still, the versatility which was gained by means of CRP techniques led to the emerging of an entire new field of research.

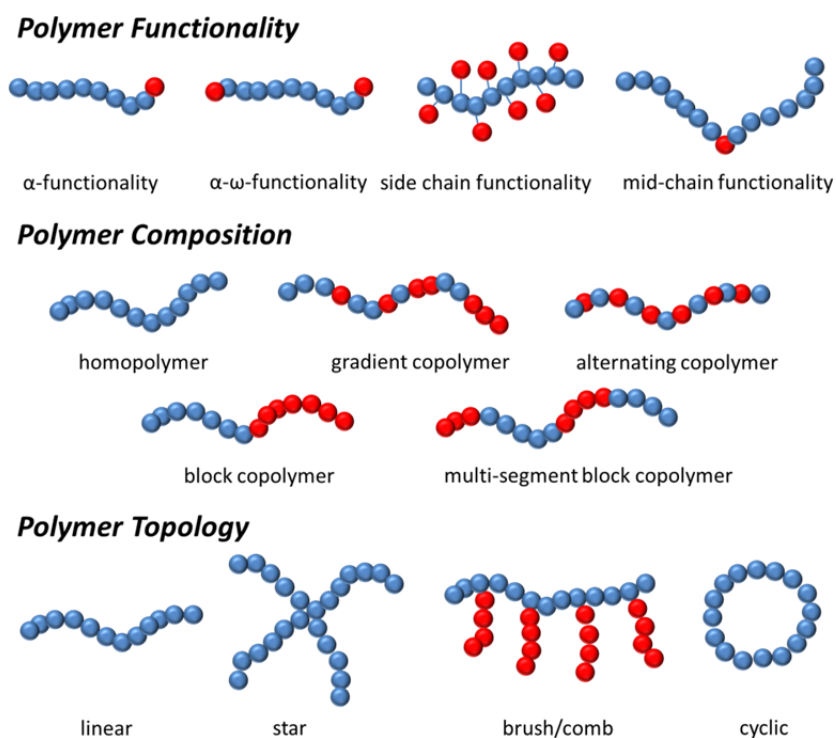


Figure 2.5. Overview of macromolecular architectures, which are accessible via CRPs.^{115,119}

2.3 Cyclodextrins

Cyclodextrins (CDs) are naturally occurring cyclic compounds which are applied in supramolecular host-guest chemistry. Due to their cheap production and biocompatibility, CDs are highly attractive for large scale industrial applications.^{135,136}

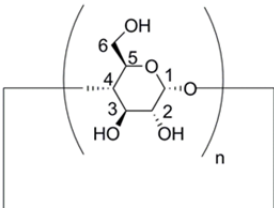
In 1891, Villiers was the first to discover cyclodextrins¹³⁷ which was followed by the isolation and detailed description by Schardinger at the beginning of the nineteenth century.^{138,135} Further, contributing to the field of molecular recognition, Emil Fisher (1894) defined the “lock and key” principle for enzyme recognition of substrates¹³⁹ and Pauling described the complementary nature of antigen and antibody structures.¹⁴⁰ Moreover, Pederson discovered crown ethers as the first artificial molecules with molecular recognition features.¹⁴¹ Subsequently, D. J. Cram applied the concept of artificial hosts to different guest molecules, thus introducing the field of host-guest chemistry.^{142,143} Finally, the term “supramolecular chemistry” was defined by Jean Marie Lehn, thus combining the chemistry of molecular recognition and molecular assembly.¹⁴⁴ According to his definition, a supramolecule is an organized complex entity created by the association of two or more chemical species, which are held together by intermolecular forces.¹⁴⁵ In 1987, Pedersen, Cram and Lehn received the Nobel Prize in chemistry "for their development and use of molecules with structure-specific interactions of high selectivity."¹⁴⁶ Compared to molecular chemistry, which is based on the formation of intramolecular covalent bonds, supramolecular chemistry forms intermolecular non-covalent bonds. Several types of non-covalent interactions are for example: hydrogen bonding, hydrophobic interactions, electrostatic interactions, dipole-dipole interactions, ionic interactions and van der Waals interactions. Furthermore, the coordinate bond between a metal atom and a ligand is assigned to the class of supramolecular chemistry.¹⁴⁵

The following paragraph focuses on the supramolecular recognition chemistry of CDs, which were employed in the course of the present thesis. In Chapter 4, the host-

guest interactions of β -CD with appropriate guest molecules are discussed in the context of complex macromolecular architectures and modular ligation.

2.3.1 The Structure of Cyclodextrins

CDs are cyclic oligosaccharides which feature a hollow truncated cone structure (Figure 2.7).¹⁴⁷ In general, CDs are obtained from starch – a polysaccharide with α -1,4-linked glucose units – via enzymatic degradation.¹⁴⁵ Usually, amylase of *Bacillus macerans* (cyclodextrinase) is added to the starch, resulting in a starch digest, which contains a mixture of CDs with varying number of glycosidic units. The mixed CDs are easily separated via selective precipitation in specific organic compounds.^{148,149} Figure 2.6 illustrates specific features of the most commonly employed CDs, which are α -CD with six glucose units, β -CD with seven glucose units and γ -CD with eight glucose units.



Type of CD	α -CD	β -CD	γ -CD
Cavity size [nm]	0.52	0.66	0.84
Cavity length [nm]	0.80	0.80	0.80
Water solubility [mol L ⁻¹] at 25 °C	0.121	0.016	0.168

α -CD: n = 6
 β -CD: n = 7
 γ -CD: n = 8

Figure 2.6. Left: Glucose units of CDs. Depending on the number of repetition units (n) CDs are categorized in α - (n = 6), β - (n = 7) and γ - CDs (n = 8). Right: Table comprising some properties of native CD, such as cavity size, cavity length and the water solubility at 25 °C.^{135, 147}

The diameter of the cavity increases according to the number of glucose units, whereas the cavity length remains constant. Furthermore, the water solubility is influenced by the agility of the glucose scaffold. For example, β -CD has a very stiff structure, compared to the relatively more flexible glucose scaffold of α - and γ -CDs. As a result, the secondary hydroxyl groups (see Figure 2.7) form intramolecular hydrogen bonds, which reduce the water solubility of β -CD.¹⁴⁵

As mentioned before, CDs have a rigid ⁴C₁-conformation of the glucose units. Therefore, the primary hydroxyl-groups (at the C⁶-atom) are located at the narrow

side of the inlet and the secondary hydroxyl-groups (at the C³-atom) are located at the reverse side of the truncated cone structure, illustrated in Figure 2.7. The C²-hydroxyl group on the wide side is turned insight into the direction of the cavity, which is lined with H₃ and H₅ protons. However, no hydroxyl groups exist on the walls of the CD structure. In summary, the exterior of CDs is hydrophilic, whereas the cavity of CDs is hydrophobic. As a result, CDs form inclusion complexes with hydrophobic guest molecules in polar solvents (most preferably water).¹⁴⁵

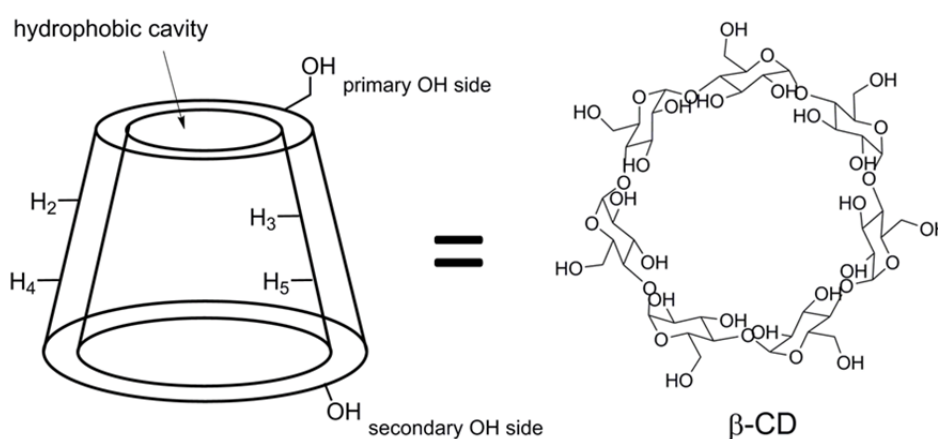
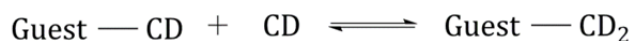


Figure 2.7. General truncated cone structure of CD and the chemical structure of a β-CD.^{145,147}

2.3.2 Complex Formation of Cyclodextrins

Host-guest complexes with CDs can be prepared in various ways, e.g. in solution,^{147,150} by co-precipitation^{150,136} or in the solid state via co-grinding or milling.^{136,147,150} More important is the selectivity with which CDs form the inclusion complexes. The molecular recognition of CDs strongly depends on the size of the cavity as well as on the size of the selected guest molecule. Figure 2.8 comprises some examples of guest molecules assigned to α- and β-CDs, along with the corresponding association constants. Furthermore, the complex formation is also influenced by the solubility of the guest molecule and sometimes requires the addition of a co-solvent to better access the guest unit.¹⁴⁷ In fact, the host-guest complex formation is a reversible process, which is based on the dynamic exchange of the compounds.

The complex formation, which is expected to follow a bimolecular process, can be summarized by the following equilibria, shown for the formation of three simple types of complexes.^{150,151}



The host-guest complexes are formed in equimolar amounts (1:1), with two guest molecules and one CD, or with two CDs and one guest molecule (1:2). The binding constants (K) of these equilibria are defined by equations 2.1 – 2.3.

$$K_{11} = \frac{[\text{Guest} - \text{CD}]}{[\text{Guest}][\text{CD}]} \quad (2.1)$$

$$K_{12} = \frac{[\text{Guest} - \text{CD}_2]}{[\text{Guest} - \text{CD}][\text{CD}]} \quad (2.2)$$

$$K_{11} = \frac{[\text{Guest}_2 - \text{CD}]}{[\text{Guest}][\text{Guest} - \text{CD}]} \quad (2.3)$$

The brackets denote molar concentrations and the binding constants (K) have the unit L mol^{-1} . The general formation of any type of host-guest complex is defined by the subsequent equilibrium (2.4):



The general equilibrium thus yields the overall association constant:

$$\beta_{mn} = \frac{[\text{Guest}_m - \text{CD}_n]}{[\text{Guest}]^m[\text{CD}]^n} \quad (2.4)$$

Furthermore, the connection between the binding constant (K) and thermodynamic parameters (Gibbs free energy (ΔG), standard enthalpy of formation (ΔH) and

standard entropy of formation (ΔS)) is given via the van't Hoff equation and the Gibbs–Helmholtz equation (2.5).

$$\Delta G = -RT \ln K = \Delta H + T\Delta S \quad (2.5)$$

In order to determine the value of K , any physical property of either host or guest molecule, which changes throughout the complex formation, can be observed. Usually, spectroscopic methods (e.g. fluorescence, UV-vis, NMR), in addition to conductivity measurements can be employed to obtain the binding constant.¹⁵¹⁻¹⁵⁴ Complex formation occurs when the system has a negative standard enthalpy of formation. Several factors exist, contributing to the driving force of the complex formation, which to the present day is still not fully understood:¹⁴⁷ i) Release of enthalpic water molecules to the surrounding water solution, thus increasing the entropy of the system. ii) Removal of the polar hydration shell from the guest molecule. iii) Hydrophobic and van der Waals interactions between host and guest molecule, as well as hydrogen bonding between the guest and the hydroxyl groups at the rim of the CD cavity. iv) Restoration of the polar hydration shell around the supramolecular complex.^{135,147} The association constant (β) strongly depends on the structure of the guest molecule and no inclusion complex is formed, if the guest exceeds the size of the CD cavity. Furthermore, β is influenced by temperature. Since the enthalpy usually has a negative value, increasing the temperature leads to dissociations of the complex.^{147,150-155} In addition, pH values and concentration of the solution can affect the complex formation.¹⁵⁰ Moreover, the guest molecule can either enter the cavity from the primary (narrow) side or from the secondary (wider) side of the truncated cone structure. The formation of the intermolecular complex, and from which side the guest molecule has entered the CD cavity can be analyzed via 2D NMR spectroscopy or X-ray crystallography.

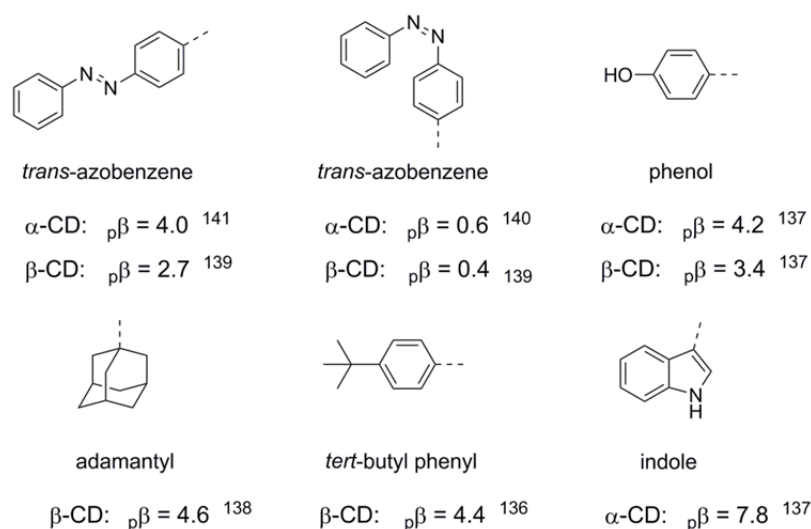


Figure 2.8. Examples of guest molecules suitable for α - and β -CDs along with the appropriate associations constants ($\rho\beta = \log(\beta \text{ mol L}^{-1})$).¹⁵⁶⁻¹⁶¹

In fact, the inclusion of the guest molecule in the CD cavity also changes several of its properties, e.g. the water solubility is enhanced, the vapor pressure decreases and the molecule is more stable against oxidation, air or light-induced degradation.¹⁵⁵ As a result, CDs are frequently employed in foods, cosmetics or toiletries in order to mask unpleasant odors.¹³⁶ Furthermore, they are utilized in drug formulations,¹⁶² catalysis¹⁶³ and as analytical separation method in chromatography.¹⁶⁴

Research on CD complex formation has increased in recent years, in particular in the field of complex macromolecular architecture formation and in the context of controlled radical polymerization techniques. In this way, several architectures were designed via supramolecular host-guest interactions. For example, Zhang and coworkers were one of the first to synthesize a supramolecular AB-diblock copolymer of poly(NiPAAm) and poly(4VP) via RAFT polymerization, which had thermoresponsive and pH responsive features, thus leading to micelle formation.¹⁶⁵ Additionally, Liu and coworkers developed a thermo- and pH-responsive supramolecular diblock copolymer via ATRP.¹⁶⁶ Furthermore, supramolecularly formed core-shell nanoparticles formed via a supramolecular AB-diblock copolymer, were reported by Stenzel and coworkers.¹⁶⁷ The formation of a supramolecular block copolymer via a di-linker molecule – equipped with α - and β -CD – was

2. Theoretical Background and Literature Overview

reported by Zhou and coworkers¹⁶⁸. Moreover, supramolecular polymer topologies, such as brushes in solution¹⁶⁹⁻¹⁷¹ and on surfaces,¹⁷²⁻¹⁷⁴ stars,¹⁷⁵⁻¹⁷⁷ cyclic structures¹⁷⁸ and branched polymer gels¹⁷⁹⁻¹⁸¹ were reported.

2.4 Spatially Resolved Surface Design

In Chapter 3, a general method for obtaining spatially resolved functionalization of polycarbonate films is introduced via a photolithographic approach, followed by the attachment of cells. The next section provides a brief overview of surface modification and patterning techniques.

The need of patterned surfaces reaches from computer technology (e.g. microchips)¹⁸² over medical technology to biological applications¹⁸³ and tissue engineering.¹⁸⁴ Especially in the context of cell culture investigations patterned surfaces are of major scientific interest.^{183,185-191} Patterned surfaces can be created on a variety of substrates, e.g. inorganic- (glass, silicon, gold), bio- (cellulose, hyaluronic acid) or polymeric devices (polystyrene, polycarbonate). The choice of modification method depends on the choice of substrate and polymer films can be attached to the surface either by deposition methods or chemical reactions. Inorganic substrates have the advantages that their smooth surfaces can readily be analyzed, and that they resist to organic solvents. Furthermore, the introduction of chemical handles is facilitated for gold and glass, since thiols are strongly attracted to gold, and silanes have an affinity to glass surfaces.¹⁹²⁻¹⁹⁵ Bio-based materials, such as cellulose or hyaluronic acid possess free hydroxyl-functionalities to which reactive species can be esterified.^{196,197} Polymer substrates can be modified via their end- or mid-chain functionalities if present in the substrate, or by directly introducing reactive moieties into the polymer backbone.^{198,199} However, if no binding sites are available on the substrate, they have to be introduced prior to further modification approaches.

For example treating the surface of a substrate with non-thermal plasma (Figure 2.9A) is a versatile technology to introduce variable functional groups to the surface.²⁰⁰ Plasma is a gaseous or fluid mixture, which is typically generated when gases are excited into energetic states (e.g. by radio frequency). The plasma mixture contains ions, free electrons, radicals and also neutral particles, thus creating a very reactive environment.²⁰⁰ The kind of functional group which is created on the

surface depends on the type of plasma gas. Argon or helium gas usually introduces free radicals, which further react with oxygen to (hydro)peroxides, whereas oxygen and nitrogen generate hydroxyl- or amino-groups. In addition, plasma polymerization is possible by converting a monomer into reactive fragments which polymerize and are further deposited on the surface.²⁰⁰ Alternatively, ozon treatment²⁰⁰ or UV-irradiation²⁰⁰ is often used to activate polymer surfaces. Another, very simple technique to apply thin polymer films onto substrates is spin coating of a polymer solutions (Figure 2.9B).²⁰¹ During spin coating a liquid is applied to a substrate which is either already spinning or is accelerated subsequent to the application of the solution.²⁰² In this way, homogenous films can be coated on substrates over a large area. The film thickness depends on rotational speed, volatility and molecular weight of the solutes.²⁰² The spin coating technique is frequently employed in the microelectronic industry, e.g. in the production of compact disks or organic solar cells.²⁰² However, the method is rather wasteful, since the majority of the applied solution is ejected.²⁰²

In order to covalently, bind polymer chains to surfaces two routes exist: the so called *grafting to* or *grafting from* approach. Each of the mentioned approaches has its benefits and drawbacks. Employing the *grafting from* approach (Figure 2.9C), initiator molecules are primarily introduced onto the surface and polymer brushes are subsequently grown from the substrate.¹³⁰ Usually, CRP protocols such as ATRP and RAFT are utilized to mediate SI polymerizations. In particular, SI-ATRP is frequently employed in surfaces modification reactions, due to the fact that the ATRP equilibrium can be easily shifted towards the inactive species (e.g. with systems with higher halide-carbon bond energy), which reduces the polymerization rate and thus solution polymerization is minimized.^{130,203} Furthermore, the *grafting from* approach yields high grafting densities, which are necessary if the grafted polymer chains serve as a passivating layer.^{130,190} In the *grafting to* approach the polymer chains are synthesized prior to attachment to the surface (Figure 2.9D), which has the advantage that the polymer chains can be fully characterized, e.g. via SEC, ESI-MS and NMR. The surfaces are generally pre-modified with a reactive moiety and the pre-synthesized polymers are attached via their functional chains ends. Attachment can occur for examples via thermally or light-induced

cycloaddition, as it was often performed by Barner-Kowollik and coworkers, e.g. on cellulose,^{58,204} gold⁵⁷ or silicon wafers.^{56,112} Yet, the drawback of the grafting to approach are the rather low grafting densities.¹³⁰

Common surface characterization techniques are for example X-ray photoelectron spectroscopy (XPS) and time of flight secondary ion mass spectrometry (ToF-SIMS), but are not further described in this context. The reader is referred to a book edited by M. Stamm which summarizes surface characterization methods.²⁰⁵

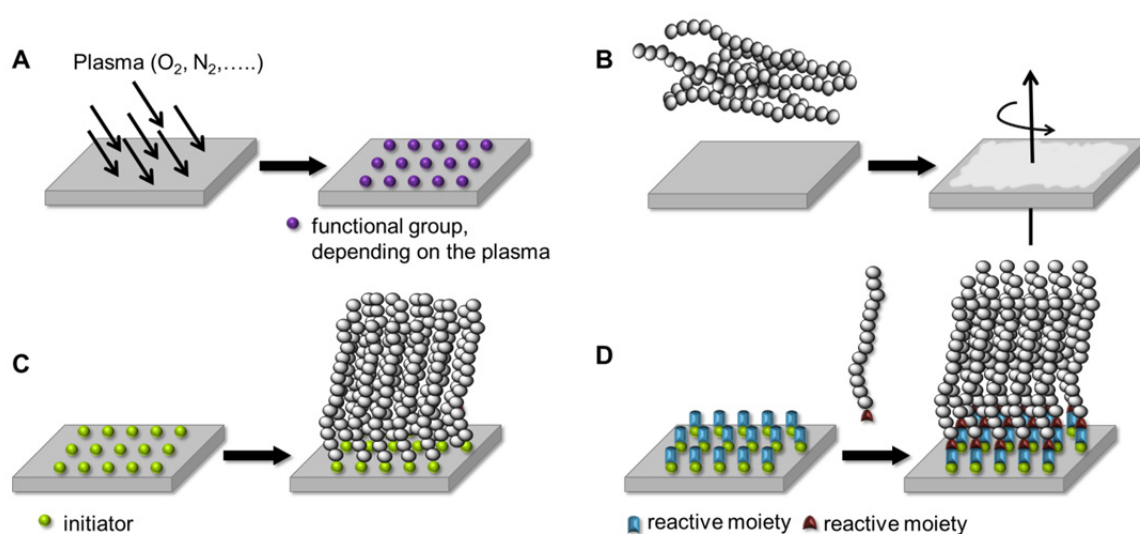


Figure 2.9. Schematic representation of substrate modification techniques. A) Plasma treatment to introduce chemical binding sites. B) Spin coating to apply a polymer layer to the surface C) Grafting from approach and D) grafting to approach to introduce polymer brushes to a surface.

In the following section three methods are introduced in order to obtain spatially resolved surfaces. Photolithography in particular is described as it was employed in Chapter 3. Furthermore, two approaches without light – microcontact printing and inkjet printing – are shortly presented to demonstrate alternative patterning techniques.

2.4.1 Photolithographic Surface Patterning

Photolithographic surface patterning is a facile and straightforward approach to introduce defined patterns on surfaces. As illustrated in Figure 2.10, patterns are

2. Theoretical Background and Literature Overview

obtained on a substrate via the exposure of a pre-coated photo-resist – e.g. light-sensitive polymers or small organic molecules – to UV light. The structure of the pattern is defined via a photomask, which protects the covered areas on the surfaces and releases the photo-resist in the exposed areas on the substrate. Subsequently, the released photo-resist is removed by washing procedures. If the photo-resist is a photoactive initiator molecule, e.g. an *o*-nitrobenzyl derivative as described in Chapter 3, polymer brushes can be grown from the surface with the remaining initiator. Thus, the generation of patterns from the macro- to the submicrometer scale is possible, but higher resolution are not accessible.¹⁸² Moreover, for a variety of structures individual masks have to be designed for each pattern. Nevertheless, photolithography is frequently used in laboratories and in the manufacturing of microelectromechanical systems.¹⁸² The method is especially suitable for sensitive substrates such as polymer films, since organic solvents can be avoided.

In the context of biomolecule and cell patterning, Welle and Gottwald utilized a photolithographic approach via simple UV irradiation of polymeric substrates through a photo-mask.^{206,207} Furthermore, the successful guiding of cells was demonstrated on a gold substrate via the removal of an ATRP initiator in defined areas on the surfaces and subsequent grafting of biorepellent polymer brushes from the non-irradiated areas by our team.²⁰⁸

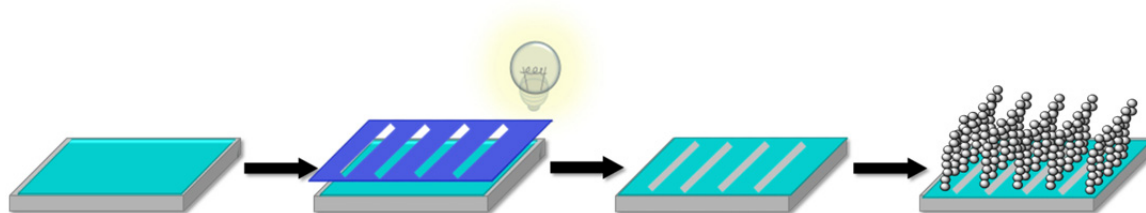


Figure 2.10. Photolithographic surface patterning. Patterns are introduced to the surface via the light-induced cleavage of a photoreactive layer, attached to the substrate, by employing a shadow mask. Subsequently, polymer chains can be *grafted from* or *to* the non-exposed surface of the substrate.

Further lithographic approaches include electron beam lithography, focused ion beam lithography, nanoimprint lithography and scanning probe lithography.¹⁸²

2.4.1.1 Microcontact Printing

The microcontact printing technique employs so-called stamps which consist of an elastomer, e.g. polydimethylsiloxane (PDMS), to introduce patterns to surfaces (Figure 2.11).²⁰⁹ The stamp is fabricated by applying a liquid polymer (PDMS) onto a master (e.g. silicon), followed by curing and the release of the stamp. Subsequently, the stamp is incubated with the desired molecule, which is then transferred to the surface upon brief contact of the stamp and the substrate.²⁰⁹ As a result, reactive moieties are introduced to the contact areas on the substrate, from which polymer chains can be grown or *grafted to*. In general, microcontact printing yields a precise and gentle method to transfer biomolecules onto substrates, without the loss of biological activity. In this way, Bernard *et al.* as well as Tolstyka *et al.* managed to pattern proteins onto a polystyrene surface.^{210,191} However, a drawback of microcontact printing is the preparation of the stamps, which can be time-consuming and the fact that the molecules are only adsorbed on the surface rather than covalently attached.

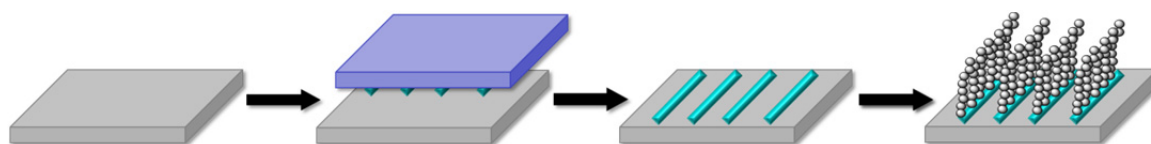


Figure 2.11. Spatially resolved surface modification via microcontact printing.

2.4.1.2 Inkjet Printing

Inkjet printing is known from the everyday life such as printing a text onto paper. The same principle as for conventional printing techniques also applies for the preparation of patterned substrates in the context of chemical surface modifications. In the inkjet printing process very small volumes (1-100 picoliters) of a so-called “ink” – which consists of solutions of either polymers or reactive molecules – are precisely positioned on a surface followed by the evaporation of the solvent (Figure 2.12).²¹¹ The droplets are directed via electrostatic forces and the resolution is defined by the spreading of the ink and the interactions of droplets on the surface.

2. Theoretical Background and Literature Overview

Thus, substrates with high surface tension are preferred in order to obtain high resolution, as well as substrates which are not affected by the solvent. Sometimes even pre-patterning of substrates is necessary for a better attachment of the ink. Additionally, dried ink can clog the tip of the nozzle, which interrupts the automatized process.^{211,212} As already mentioned, inkjet printing is mainly employed in graphics and other conventional printing, but is also employed in the production of plastic electronics²¹³ and tissue engineering.¹⁸⁷

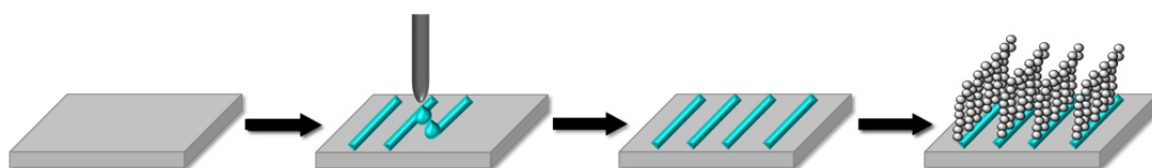


Figure 2.12. Inkjet printing technique in order to design patterned surfaces.

A variety of inorganic materials has been patterned for cell attachment in the last decades.^{208,214-216} However, amorphous polymers (e.g. poly(methyl methacrylate, polystyrene and polycarbonate) have gained great attention as attractive platforms for tissue engineering applications. The chemistry of polymer substrates is versatile and due to their flexible structure their mechanical properties can be adjusted. Moreover, polymer devices have low manufacturing costs, as well as good biocompatibility and are accessible for thermoforming processes.^{15-16,217-219}

2.5 Modular Ligation of Polymers

Modular ligation of polymers is based on the synthesis of individual functionalized polymeric building blocks which can be assembled into any desirable geometric structure via facile, orthogonal and highly efficient reactions. Modular ligation strategies were developed to design sophisticated macromolecular architectures^{220,221} as well as functional soft materials with unique physical properties.^{222,223} The advantage of the modular conjugation approach compared to the conventional sequentially controlled synthesis of macromolecular architectures – as for example via CRP protocols (see section 2.2) – is the increased number of structures which can be prepared from a single polymer chain and the possibility to combine different polymerization techniques.²²⁴ The individual building blocks can be fully characterized prior to ligation and monomers which would be incompatible in a conventional synthetic approach, due to different reactivity or solubility can be combined via modular ligation. Figure 2.13 depicts several polymer architectures which can be obtained via modular ligation approaches.

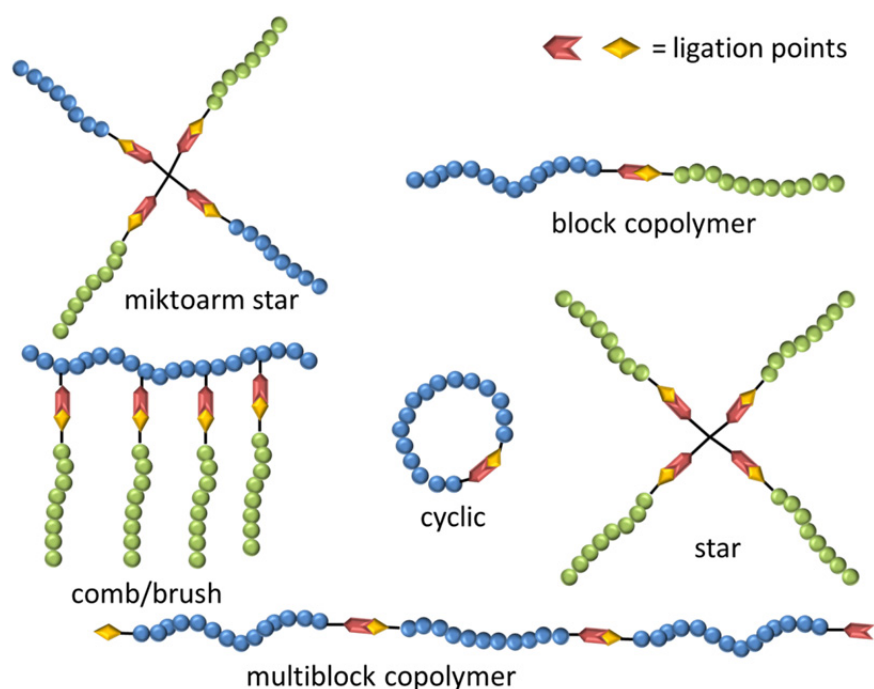


Figure 2.13. Overview of selected polymer architectures designable via modular ligation.

For example, high molecular weight block copolymers can be constructed from single polymer chains.^{224,53} Furthermore, α,ω -functionalized polymer chains can either lead to multiblock sequences at high concentrations or form cyclic structures at high dilution of the sample.¹⁷⁸ Via the incorporation of functional side chains in the polymer backbone, brush or comb polymers can be synthesized.²²⁵ Additionally, star and miktoarm star polymers are accessible via a single branching point.^{226,177} The reactions which enable the efficient formation of such large and advanced macromolecular architectures are summarized under the term *click* reactions, which are described in the following section.

2.5.1 *Click* Chemistry

The concept of *click* chemistry was introduced in 2001 by Sharpless and coworkers, and describes highly efficient reactions between so-called modular building blocks to synthesize novel molecules.²²⁷ In order to be categorized as “*click*” the reaction has to fulfill – strictly speaking – all of the following criteria:

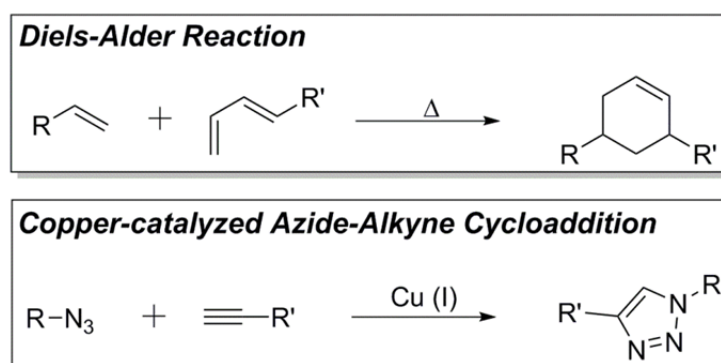
- i) Simple reaction conditions (e.g. ambient temperature, no need for exclusion of oxygen and water) with nearly quantitative yields
- ii) The reaction should be modular, wide in scope and orthogonal to other reaction steps involved
- iii) Generated byproducts should be inoffensive and the reaction should proceed in no or environmentally benign or easily removable solvents (e.g. water)
- iv) The starting materials should be readily available, the reaction products should be stable under physiological conditions and easy to purify.
- v) In addition, the reaction should be stereospecific

In general, *click* reactions have a high thermodynamic driving force which supports fast reaction rates.²²⁸ With regard to macromolecular synthesis, the term *click* reaction was adjusted by Barner-Kowollik and coauthors.²²⁹ Since the purification of polymer samples is limited to simple precipitation or dialysis – as opposed to time consuming and costly preparative size-exclusion chromatography – the *click* criteria

of high yields and simple purification in particular apply to polymer-polymer conjugation. In order to guarantee a facile purification of the polymer samples, equimolar amounts of starting materials are mandatory. Whereas stereospecificity is less relevant for polymer ligation, orthogonality is necessary to avoid undesired side products.²²⁹

Reactions which comply with *click* criteria are for example: i) The addition of carbon-carbon multiple bonds (e.g. Michael type additions, epoxidation or aziridination), ii) nucleophilic substitution (e.g. ring-opening of strained heterocycles, such as epoxides or aziridines), iii) cycloaddition reactions (see sections 2.5.2 and 2.5.3), carbonyl chemistry (e.g. formation of oxime ethers, amides or ureas).

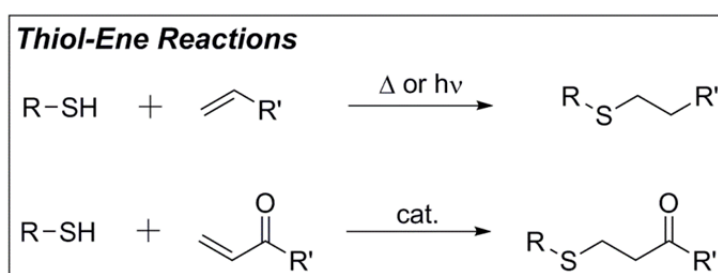
Two of the most relevant *click* type reactions in the context of polymer conjugations are depicted in Scheme 2.14: The Diels–Alder (DA) reaction^{230,231} and the copper catalyzed azide-alkyne cycloaddition (CuAAC)²³²⁻²³⁵ which are further discussed in sections 2.5.2 and 2.5.3.



Scheme 2.14. Examples of commonly employed *click* reactions for polymer conjugations.

At this point the thiol-ene reactions should be mentioned, which are also frequently employed for the conjugation of polymer chains, but in the context of polymer conjugation do not fulfill *click* criteria.²³⁶⁻²³⁸ The thiol-ene reaction denotes the addition of an alkyne and a thiol resulting in an alkyl sulfide.²³⁷ Two pathways are possible: The reaction can either proceed via free radical coupling, induced by thermal or photochemical activation of a radical starter, or via a Michael addition reaction (Scheme 2.15).^{236,239-241} The radical initiated reaction has been widely employed in polymer synthesis,^{237,242-244} but to stay within the scope of the present

dissertation, the reaction is not further discussed. Furthermore, the reader is advised to the numerous reviews on modular ligation techniques.^{18,22-24, 222-223,245-249} In fact, the thiol-ene reaction was initially believed to have *click* potential,²⁵⁰ however in the context of polymer ligation the radical initiated reaction revealed significant side reactions, e.g. disulfide formation or head to head coupling of the carbon centered radicals, wherefore the term *click* does not apply anymore.^{251,252}



Scheme 2.15. Thiol-ene reactions.

2.5.2 Diels–Alder Reaction

The concept of photo-induced DA reactions was already introduced in section 2.1.2 on the examples of photoenols (2.1.2.1), *o*-naphthoquinone methides (2.1.2.2) and thioaldehydes (2.1.2.3). In all of the aforementioned reactions, the reactive species was formed via irradiation, followed by the actual DA reaction. In the following section, an overview on DA reactions in general is given along with a short summary of the various types of DA reactions and some mechanistic background.

The DA reaction was discovered in 1928 by Otto Diels and Kurt Alder who received the Nobel Prize for their work in 1950.²⁵³ DA reactions belong to the class of pericyclic reactions, which are defined by a cyclic transition state and a concerted mechanism of bond formation or cleavage respectively, without the formation of intermediates.²⁵⁴ Generally, pericyclic reactions can be categorized into four classes: Cycloadditions, electrocyclic reactions, sigmatropic rearrangements and group transfer reactions. However, only cycloadditions – in particular [4+2] cycloadditions – will be in the focus of the following discussion. The DA reaction is classified as a

[4+2]-cycloaddition, according to the number of π -electrons participating in the ring-forming reaction. The π -orbitals are reorganized in the course of the cycloaddition resulting in the formation of two σ -bonds.^{255,256} The compounds participating in a DA reaction are a so-called diene (hydrocarbons with two carbon double bonds) and a dienophile (hydrocarbons with an isolated double or triple bond), which form a six-membered cyclic product. The stereochemistry of the diene and the dienophile is preserved during the reaction, thus the stereochemistry of the product is well predictable. This can be rationalized with the Woodward-Hoffmann rules,²⁵⁷ which are applicable for pericyclic reactions in general. As the orbital symmetry is retained, it is possible to predict whether a certain reaction can be induced by light or by thermal energy.^{258,259} According to these rules, the Diels-Alder reaction is symmetry-allowed under thermal conditions in a suprafacial* manner, but photochemically forbidden.²⁶⁰ The mechanism of the reaction can be analyzed by the orbital interactions of the reacting systems which are summarized in the frontier molecular orbital (FMO) theory, giving an explanation for the Woodward-Hoffmann rules.²⁶¹ Figure 2.14 illustrates the orbital interactions in DA reactions, also demonstrating the influence of electron-donating (EDG) and electron-withdrawing groups (EWG) on the diene or the dienophile respectively. The cycloaddition occurs through the interactions of the highest occupied molecular orbital (HOMO) and the lowest unoccupied molecular orbital (LUMO) of the diene and the dienophile. Only interactions between molecular orbitals (MOs) with the same symmetry stabilize the cyclic transition state and thus result in bonding. In general, the diene must be in cis conformation and cyclic dienes are more reactive due to their rigid cis configuration. Moreover, the FMO theory can predict the rate of DA reactions, which is influenced by electronic and structural factors lowering or increasing the HOMO-LUMO gap. The smaller the energy gap between the HOMO and the LUMO of the reacting species, the faster the reaction proceeds.²²⁸ Furthermore, the FMO can also explain the regio-selectivity that is observed for the reaction of asymmetric dienes and/or dienophiles, by taking into account the unbalanced spatial electron distribution in the frontier orbitals induced by the substituents.²⁶²

* Suprafacial means that the π -system of the diene and the dienophile interact with the same face at both ends, see also Figure 2.14.

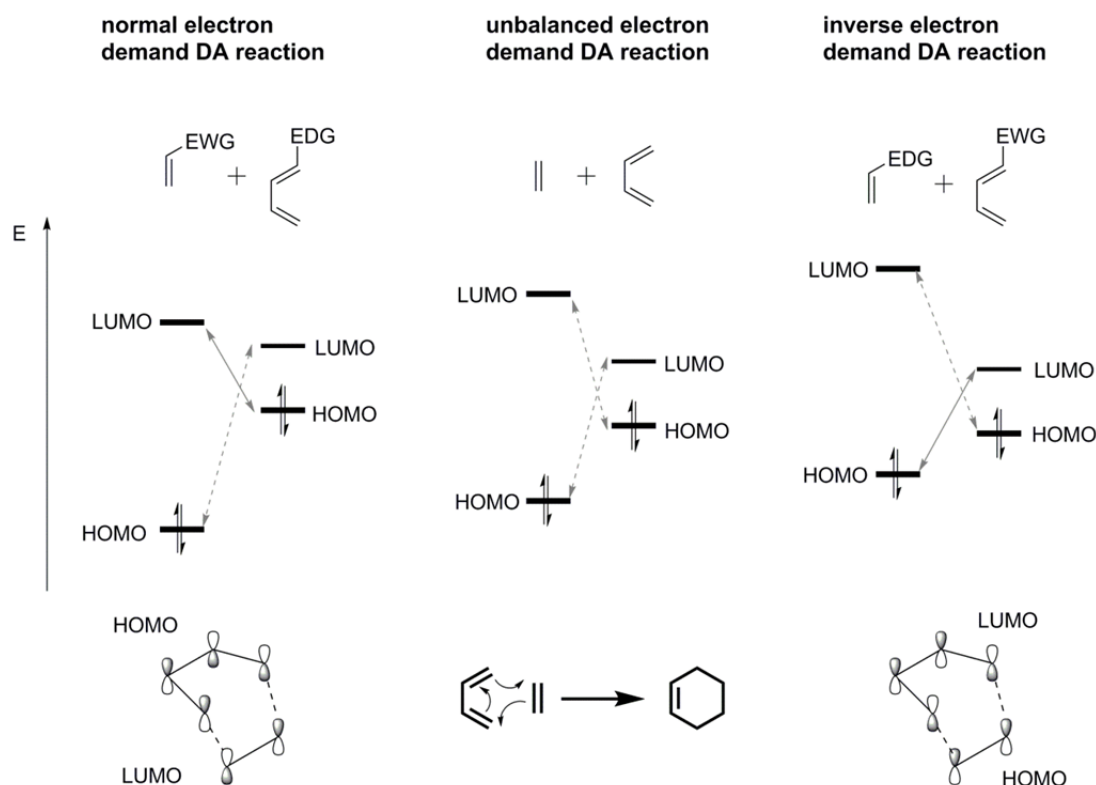


Figure 2.14. Frontier molecular orbital (FMO) theory demonstrating the orbital interaction between a diene and a dienophile in DA reactions with different electron demand (EDG = electron donating group; EWG = electron withdrawing group).^{228,263}

According to the electronic situation of the interacting species, the reaction can be categorized into three types of DA reactions, depicted in Scheme 2.16: Normal electron demand DA reactions (i), inverse electron demand DA reactions (ii) and hetero DA (HDA) reactions (iii).

In a DA reaction with normal electron demand (i) the cycloaddition occurs between an electron-rich diene, optionally substituted with an EDG (e.g. NH_2 , OR, NR_2) and an electron poor dienophile which bears an EWG (e.g. CO, COOR, CN, NO_2). The EWG lowers the HOMO as well as the LUMO of the dienophile, thus reducing the energy difference between the dienophile's LUMO and the diene's HOMO (Figure 2.14), resulting in fast reactions rates.^{228,264} With regard to a DA reaction with unbalanced electron demand – such as the reaction between butadiene and ethylene – it is obvious that this reaction is less favored than the normal electron demand DA reaction, as both conceivable HOMO-LUMO interactions exhibit a large energy gap.

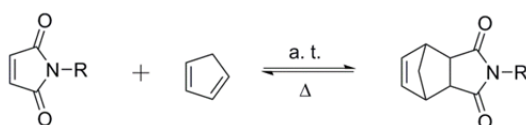
The potential of normal electron demand DA reactions for the modular construction of polymer architectures was demonstrated, for example, by Tunca and Hizal who employed a maleimide-anthracene system to synthesize block copolymers,²⁶⁵ star polymers²⁶⁶ and graft polymers.²⁶⁷ In addition, the maleimide-cyclopentadiene cycloaddition (shown in Scheme 2.16i) was successfully employed in the formation of cyclic polymers.²⁶⁸

The electronic situation in a DA reaction can also be inverted, giving rise to DA reactions with inverse electron demand (ii), in which an electron deficient diene reacts with an electron rich dienophile. The EWG in the diene lowers its HOMO and LUMO energies, whereas the EDG in the dienophile raises its HOMO and LUMO energies. Thus, the reaction proceeds via the interaction between the LUMO of the diene and the HOMO of the dienophile.²²⁸ A typical example of an inverse electron demand DA reaction is the cycloaddition of diphenylethyne to diphenyl-1,2,4,5-tetrazole to yield tetraphenylpyridazine, which is depicted in Scheme 2.16ii.^{228,269} Several inverse DA reactions have been applied in polymer chemistry by Popik and coworkers.⁶⁴⁻⁶⁶

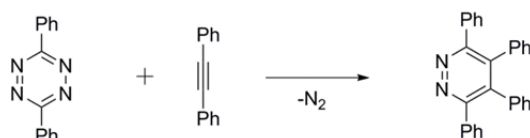
In addition, DA reactions in which a hetero atom is included in the cyclic ring are summarized under the term hetero DA reaction (HDA). The example given in Scheme 2.16iii demonstrates the HDA reaction of cyclopentadiene with an electron deficient hetero-dienophile which can additionally react as a CTA in a RAFT polymerization. In this way, RAFT polymers can be directly conjugated without the need of further end-group modifications. This atom efficient and versatile method was successfully employed and initially developed by our team for the formation of block copolymers,^{22,231,270-275} star polymer structures²²⁶ and graft polymers²²⁵ and is also referred to as RAFT-HDA reaction. Given the correct substitution on the initial RAFT agent, the HDA reaction can be completed at ambient temperature within less than one minute.

2. Theoretical Background and Literature Overview

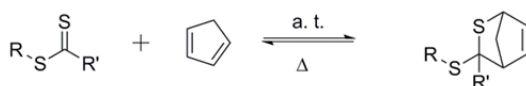
i) normal electron demand DA reaction:



ii) inverse electron demand DA reaction:



iii) HDA reaction:



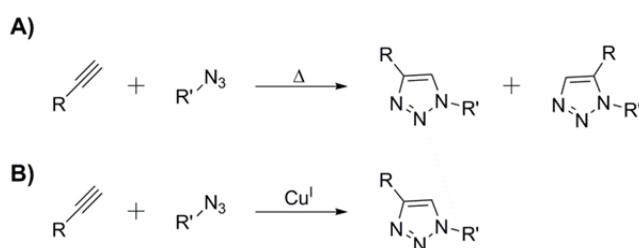
Scheme 2.16. Overview of three types of DA reactions: i) DA reaction with normal electron demand, ii) DA reaction with inverse electron demand, iii) hetero DA (HDA) reaction (a. t. = ambient temperature).

An additional important feature with respect to advanced material design is the thermally induced reversibility of some DA reactions^{276,277} which has been frequently employed in the development of self-healing materials.²⁷⁸⁻²⁸⁰

In conclusion, it can be stated that DA reactions are highly stereospecific and regioselective reactions, due to their well-defined cyclic transition state. Furthermore, the reaction is compatible with a broad variety of readily available starting materials, proceeds with fast reactions rates and without the formation of byproducts, due to its high orthogonality. Another example of a very efficient click reaction is given below with the copper catalyzed azide-alkyne cycloaddition (CuAAC).

2.5.3 Azide-Alkyne Cycloaddition

The copper catalyzed azide-alkyne cycloaddition (CuAAC) is referred to as the paramount example of *click* chemistry and is among the most powerful existing ligation methods for polymer conjugation.^{232-235, 281,282} The CuAAC reaction was first reported by Medal²⁸³ and Sharpless²⁸⁴ and is a variant of the Huisgen 1,3-dipolar cycloaddition. However, compared to the thermally induced cycloaddition which yields a mixture of regioisomers, the copper catalyzed reaction is regioselective and only produces 1,4-substituted 1,2,3-triazoles (Scheme 2.17).

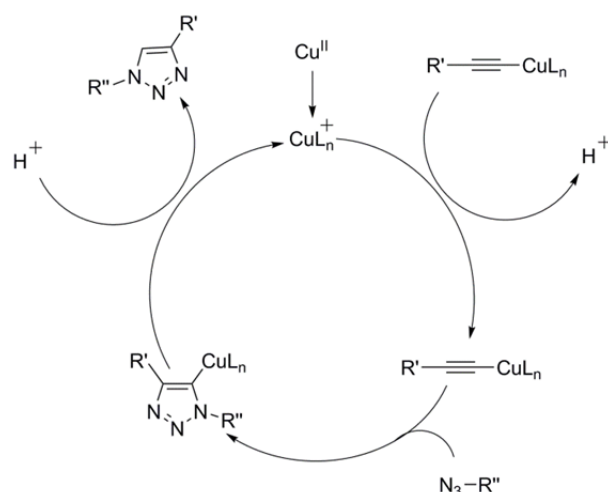


Scheme 2.17. Azide-alkyne cycloadditions. A) Thermally induced 1,3-dipolar cycloaddition yielding 1,4- and 1,5- substituted 1,2,3-triazoles. B) Copper catalyzed 1,3-dipolar azide-alkyne- cycloaddition yielding only 1,4-substituted 1,2,3-triazoles.

The catalyst system consists of a Cu(I) complex with appropriate ligands, e.g. CuBr in combination with N,N,N',N'',N''-pentamethyldiethylenetriamine (PMDETA). A less oxygen sensitive catalyst system is CuSO₄ and ascorbic acid, since Cu(I) is formed *in situ* via the reduction of Cu(II) to Cu(I).²⁸⁵

The catalytic cycle illustrated in Scheme 2.18 was proposed by Sharpless and coworkers.²⁸⁴ The mechanism proceeds via the reaction of a Cu(I) species with an alkyne under proton abstraction and the formation of a copper acetylide complex. In the subsequent step, a 1,2,3-triazole is formed in the cycloaddition reaction with an azide, followed by the release of the Cu(I) species and the regeneration of the catalyst.

2. Theoretical Background and Literature Overview



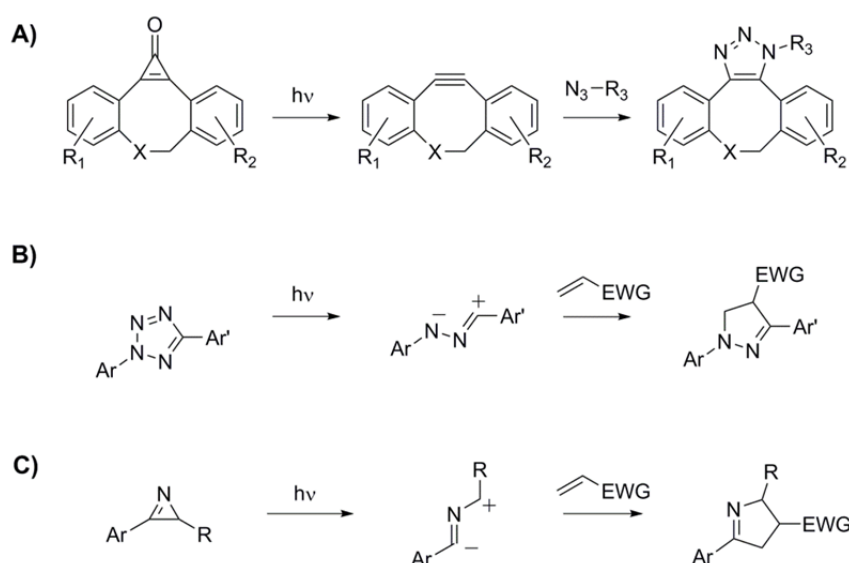
Scheme 2.18. Suggested catalytic cycle for copper catalyzed azide-alkyne cycloadditions.^{286,287}

In polymer chemistry, the CuAAC reaction was first employed in the modular synthesis of dendronized linear polymers²⁸⁸ and dendrimers.²⁸⁹ Subsequently, Opsteen and van Hest synthesized amphiphilic block copolymers via the coupling of alkyne-functionalized hydrophobic polymers with azide telechelic PEG.²⁸² Ever since, a broad variety of macromolecular architectures was obtained via CuAAC *click* conjugation of polymer building blocks, e.g. stars,^{290,291} hydrogels,²⁹² and combs,²⁹³ just to name a few. In addition, the CuAAC reaction is orthogonal to DA reactions which was employed in the sequential or one-pot synthesis of block copolymers.^{294,295}

Even though the CuAAC reactions feature many advantages, they still require a catalyst which in some applications can be unfavorable, e.g. in biological systems due to the cytotoxicity of copper.^{296,297} As an alternative, the catalyst free azide-alkyne cycloaddition in combination with the light-induced *in situ* formation of the reactive species is depicted in Scheme 2.19A. Furthermore, two examples of light-induced and highly efficient 1,3-dipolar cycloadditions are illustrated in Scheme 2.19B and C, which also allow fast ligation at ambient temperature.

The reactivity of cyclooctynes employed in the copper free reaction of azides and alkynes is attributed to a ring strain of the alkyne and thus referred to as strain promoted azide-alkyne cycloaddition (SPAAC).²⁹⁸ The reactivity of cyclooctynes can

be further enhanced via the introduction of electron withdrawing substituents, e.g. fluorine moieties in α -position of the carbon-carbon triple bond,^{299,300} or via an increase of the ring strain by merging the cyclooctynes with aryl structures as shown in Scheme 2.19A.³⁰¹ The photo-induced variant of the *in situ* formation of the cyclooctyne species from a cyclopropanone precursor (photo-SPAAC) was introduced by Popik and coworkers and employed in the selective labeling of living cells.³⁰²



Scheme 2.19. Overview of 1,3-dipolar cycloadditions. A) Light-triggered catalyst free azide-alkyne cycloaddition, B) Tetrazole chemistry (NITEC), C) Azirine photoligation (EWG = electron withdrawing group).

As a further example for a catalyst free 1,3-dipolar cycloaddition, the photo-induced nitrile imine-mediated tetrazole-ene cycloaddition (NITEC) is depicted in Scheme 2.19B. The reaction is based on the light-induced decomposition of a diaryl tetrazole via the release of nitrogen and the *in situ* formation of the nitrile imine 1,3-dipole which subsequently undergoes a cycloaddition with olefins.³⁰³ NITEC has proven to be a powerful tool by us in biorthogonal^{304,305-307} and modular polymer conjugation in solution^{308,309,310} and on surfaces.^{204,208,311}

The second example for a photo-induced 1,3-dipolar cycloaddition is the azirine photoligation (Scheme 2.19C).²⁶⁶ By a light-induced ring-opening of azirine derivatives, highly reactive nitrile ylide 1,3-dipoles are generated and form

2. Theoretical Background and Literature Overview

cycloadducts with electron deficient multiple bonds.^{312,313} Lin and coworkers employed the azirine-based cycloaddition in the fast and selective conjugation of proteins and our team recently demonstrated the visible light-triggered conjugation of pyrene-substituted azirine with functional polymeric substrates.³¹⁴

3

Light-Induced Surface Modification for Guided Cell Attachment

Cell experiments were performed in collaboration with S. Geyer and S. Scholpp (Institute of Toxicology and Genetics, KIT). ToF-SIMS measurements were performed by A. Welle (Institute of Functional Interfaces, KIT). The thermoforming of the PC film was carried out by P. Nikolov and S. Giselbrecht (Institute for Biological Interfaces, KIT; MERLN Institute for Technology-Inspired Regenerative Medicine, Maastricht University). B. Yameen (Harvard Medical School, Boston, MA, USA) and G. Delaittre (Institute of Toxicology and Genetics, KIT) are thanked for discussion. Parts of this chapter were reproduced with permission from Hirschbiel, A. F.; Geyer, S.; Yameen, B., Welle, A.; Nikolov, P.; Giselbrecht, S.; Scholpp, S.; Delaittre, G.; Barner-Kowollik, C.; *Adv. Mater.* **2015**, *27*, 2621-2626 (DOI: 10.1002/adma.201500426). Copyright 2015 Wiley.

3.1 Motivation

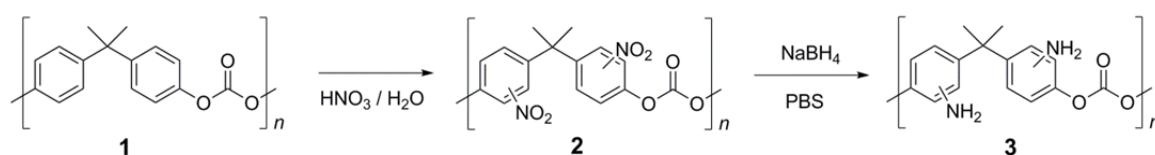
In recent years biologists have been looking for advanced substrates to mimic the *in vivo* conditions of cells for detailed cell studies as an alternative to the petri dish. Such substrates preferably possess a three-dimensional structure and boundaries in the cell culture as they naturally occur in a living system, e.g. for neural cells and networks.^{315,316} Furthermore, boundaries in a cell culture system facilitate the investigation of defined co-cultures^{12,13} as well as intercellular communication.^{317,318} UV irradiation,^{206,207} chemical^{319,320} or plasma treatment^{321,322} of a solid substrate represent effective ways to obtain spatially resolved functionalization in order to guide cells into specific areas. Especially, amorphous polymers such as polycarbonate or polystyrene are predestinated for the generation of disposable biological devices due to their low manufacturing cost and the various shapes in which they can be processed.²¹⁹

In the following chapter a facile methodology to pattern cells onto a flexible polymer substrate is introduced. By combining photolithographic cleavage of a photoactive molecule and surface initiated polymerization of a cell repellent oligo(ethylene glycol) derivative, patterned surfaces with pre-defined areas for cell guiding were obtained. The PC substrate was further shaped into a 3D microchannel generating an instructive environment for cells which resembles *in vivo* conditions.

3.2 Results and Discussion

3.2.1 Modification of Polycarbonate Surfaces

Polycarbonates are widely employed in industrial applications since they are transparent and have a high temperature and impact resistance. Furthermore, polycarbonate (PC) substrates can be easily thermoformed into any structure. Thus, a thin and precast PC film (gauge 65 μm , it4ip, Belgium) was chosen for the development of a biological platform. The purchased membrane was additionally irradiated with swift heavy ions, prior to the chemical treatment, in order to etch pores into the PC film subsequent to the thermoforming process. The pores will later serve to pervade cells on the PC surface with nutrient solution. Due to its low surface free energy, the PC surface shows a relatively low adhesiveness leading to the necessity of chemical treatment for cell attachment to the surface. In a first modification approach, a nitration of the aromatic ring of the PC was performed, which is shown in Scheme 3.1 (2). Subsequently, the nitro groups were reduced to the desired amino groups by sodium borohydride (3).³²³



Scheme 3.1. Initial approach: Amino-functionalization of the PC-film via nitration (2) and subsequent reduction (3).

Functionalization of the PC films was followed by ATR-IR measurements. A new band at 1667 cm^{-1} corresponding to the asymmetric stretching vibration of NO_2 appeared (Figure 3.1) for the treated PC surface (red trace) in comparison with the pristine PC surface (black trace), confirming the nitration of the film. After the reduction step, the mentioned band disappeared, indicating full conversion of the nitro group to the amino function (blue trace). Even though the functionalization of the PC surface with amino groups seemed to be successful, the PC membrane lost its

flexibility, which is essential for the thermoforming process even with very low concentrations of nitric acid.

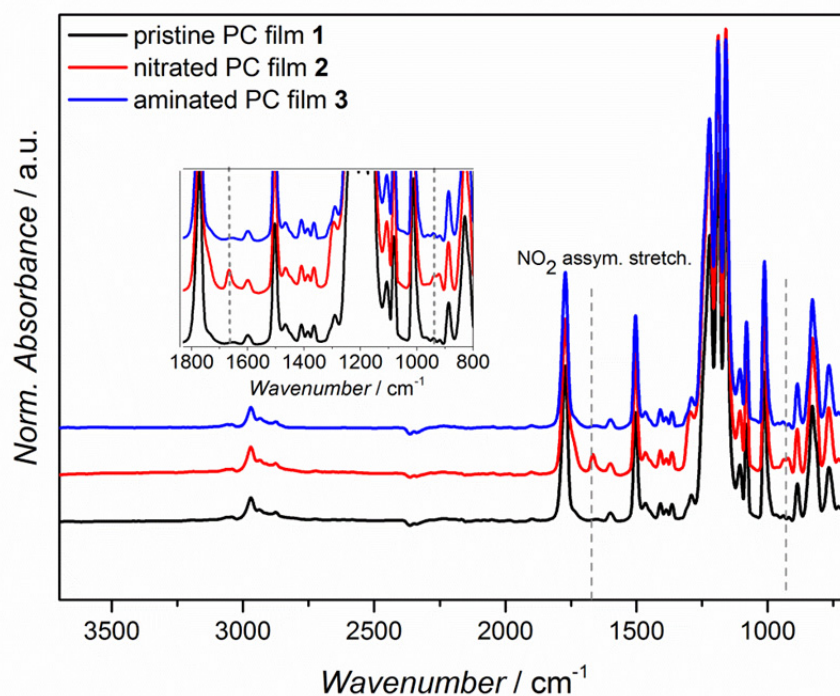
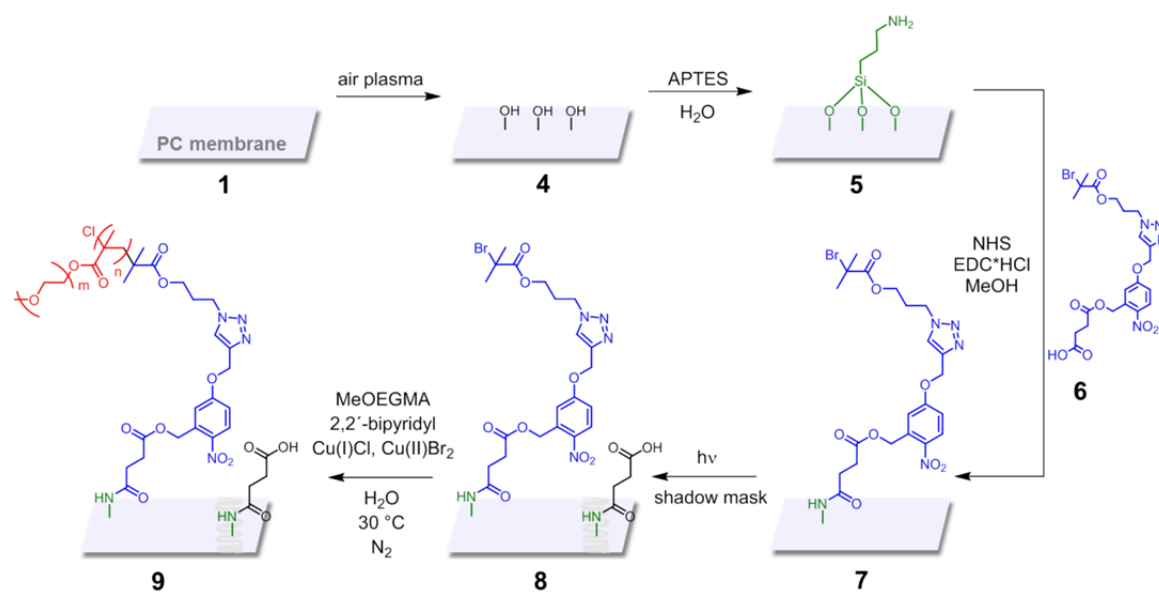


Figure 3.1. IR spectra showing the absorbance of the pristine PC film **1** (black trace), the PC film after the nitration **2**, showing the NO₂ asymmetric stretching vibration at 1667 cm⁻¹ (red trace) and the absorbance of the aminated film (blue trace). Reproduced with permission from Wiley, 2015 (DOI: 10.1002/adma.201500426).

Thus, an alternative functionalization strategy was developed, employing a milder chemical treatment to retain the flexible properties of the PC film. A further challenge of treating a very thin and non-crosslinked PC substrate was in the restricted range of suitable solvents. Only water, ethanol and methanol conserved the initial surface roughness, while other solvents such as tetrahydrofuran, dichloromethane or ethyl acetate increased it or even dissolve the entire film. Scheme 3.2 depicts the novel modification strategy for the chemical surface patterning of the PC film.

Initially, the PC films were treated with air plasma, generating hydroxyl-functionalities on the surface (**4**) which allowed the attachment of (3-

aminopropyl)triethoxysilane (APTES) via silanization (**5**). After thoroughly washing the membrane with water and ethanol, unreacted ethoxy groups of APTES were cross-linked on the surface in a subsequent annealing step. The complete functionalization of the surface with APTES was evidenced with time of flight secondary ion mass spectrometry (ToF-SIMS). ToF-SIMS is an ideal and sensitive analysis method for surfaces. During the measurement the analyzed surface is bombarded with a high energetic primarily ion beam consisting of bismuth clusters, which results in the emission of secondary ions directly from the surface. The secondary ions are then further analyzed in a time of flight mass-analyzer according to their mass to charge ratio. Figure 3.3A depicts the ToF-SIMS images of the PC film after silanization revealing the presence of NH_4^+ (18.03 u) and Si^+ (27.98 u) fragment maps of **5**.



Scheme 3.2. Synthetic route for the spatially resolved surface modification of a PC film via UV irradiation and subsequent passivation with MeOEGMA. Reproduced with permission from Wiley, 2015 (DOI: 10.1002/adma.201500426).

In order to obtain spatial resolution on the PC surface, an acid-functionalized atom transfer radical polymerization (ATRP) initiator carrying a photo-active *o*-nitrobenzylmethyl ester linker (**6**) was coupled to the aminated surface in an EDC/NHS mediated reaction to obtain **7**. Figure 3.3B shows the Br^- signal (78.92 u) stemming from the ATRP initiator and the NO_2^- fragment (45.99 u) of the *o*-nitrobenzyl unit which were detected in the ToF-SIMS analysis. The measurement

confirmed the modification of the PC film **5** with the ATRP initiator **6**. The approach was based on the photo-cleavage of *o*-nitrobenzyl derivatives which can be performed via UV irradiation around 365 nm. The advantage of this strategy is the facile synthesis of the derivatives (refer to the experimental section 3.4.3) as well as the employment of mild irradiation conditions for the photo-cleavage. The ^1H NMR spectrum of the photo-cleavable ATRP initiator **6** is shown in Appendix A, Figure A.3, revealing characteristic signals of the triazole ring at 8.30 ppm and the methylene groups of the carboxylic acid spacer at 2.53 ppm and 2.22 ppm. In the subsequent step, a metallic shadow mask was employed to generate a defined pattern on the surface via light-induced cleavage of the *o*-nitrobenzyl derivative. The photolithographic approach allows to create clearly defined patterns in the range of micrometers. Therefore, the PC film was positioned in a sample holder, covered with the shadow mask and fixed with screws (shown in Appendix A, Figure A.4). Subsequently, the samples were placed in a custom built photo-reactor (Appendix A, Figure A.5) and irradiated in the dry state with a low-pressure mercury lamp emitting at a maximum of 350 nm (36 W). The emission spectrum of the employed lamp is shown in Figure 3.2 along with the UV-vis spectrum of the *o*-nitrobenzyl ATRP initiator, measured in acetonitrile.

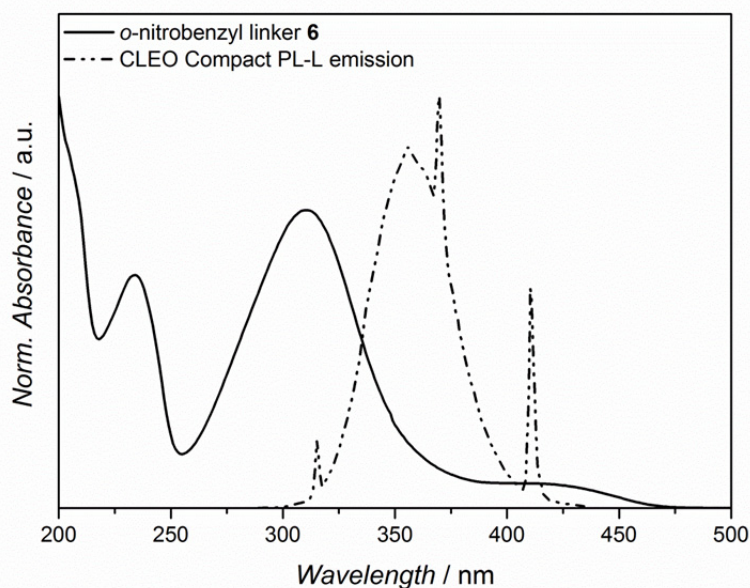


Figure 3.2. UV-vis spectrum of the *o*-nitrobenzyl linker **6** measured in acetonitrile and the emission spectrum of the employed compact low pressure fluorescent lamp (Philips CLEO Compact PL-L, 36 W). Reproduced with permission from Wiley, 2015 (DOI: 10.1002/adma.201500426).

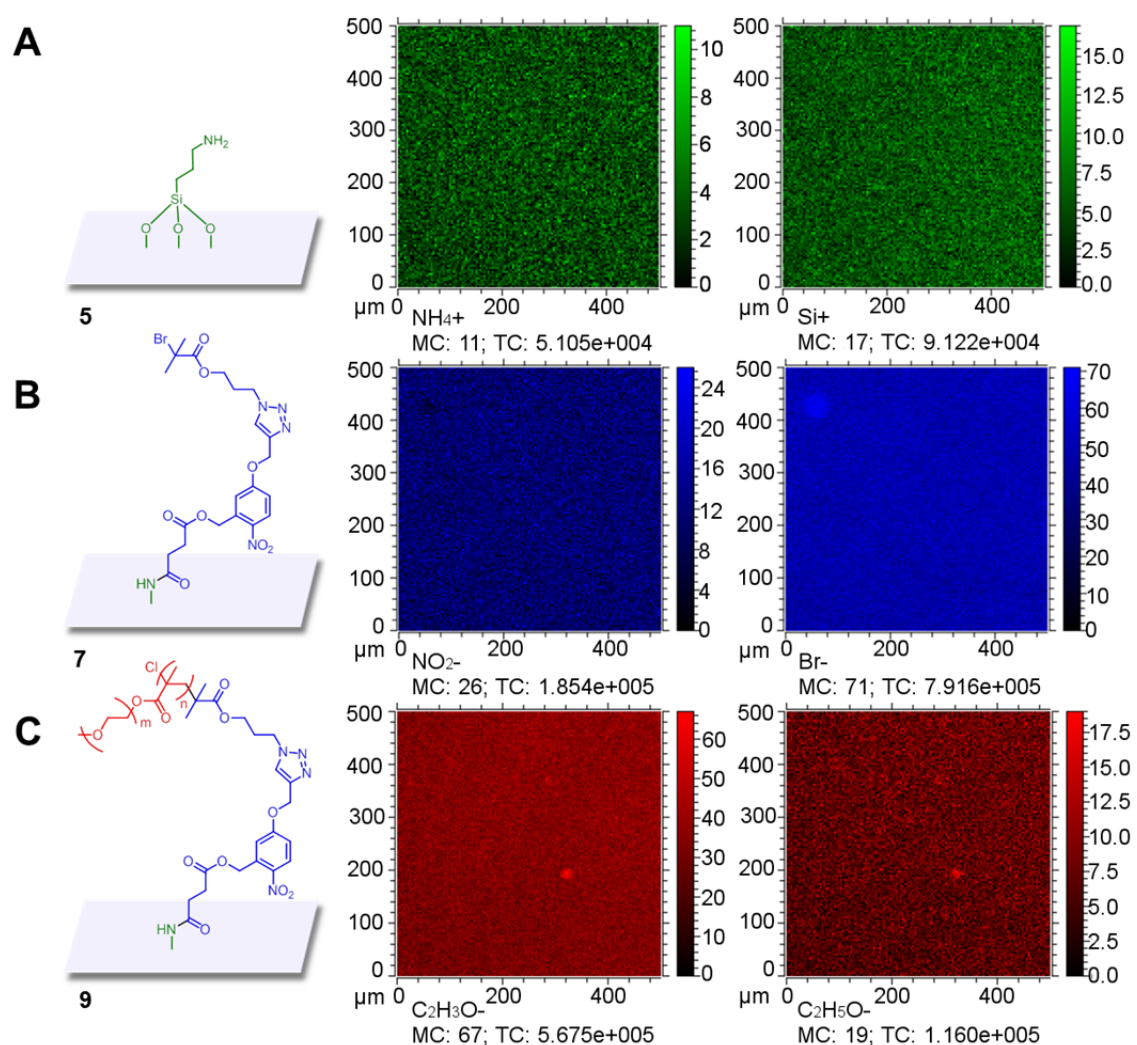


Figure 3.3. ToF-SIMS images illustrating each functionalization step of the PC surface. A) NH_4^+ and Si^+ fragment maps of **5**. B) NO_2^- and Br^- fragment maps of **7**. C) OEG fragment maps of **9**. For spectra and peak integrals refer to Appendix A, Figure A.6 and Table A.1. Reproduced with permission from Wiley, 2015 (DOI: 10.1002/adma.201500426).

After the irradiation procedure, the PC film **8** was thoroughly washed with ultrapure water (Milli Q) and distilled methanol, removing the detached initiator from the surface and leaving carboxylic acid functionalities in the irradiated areas. The carboxylic acid functionalities increase the adhesiveness of the PC surface and generate bio-friendly domains where proteins and cells can attach. The efficient removal of the ATRP initiator via irradiation is demonstrated in the ToF-SIMS image depicted in Figure 3.4. The picture reveals the wave-like pattern of the shadow mask in the irradiated areas in contrast to two Br^- typical fragments (sum of 78.92 u and 80.91 u) of the remaining ATRP initiator in the non-irradiated areas.

3. Light-Induced Surface Modification

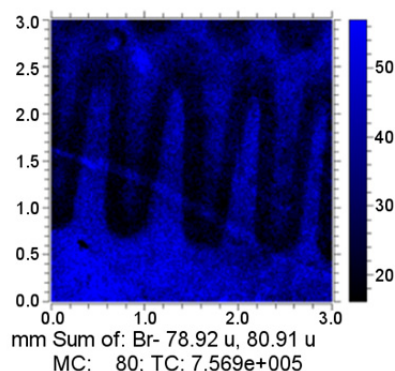


Figure 3.4. ToF-SIMS image of the PC film after irradiation with a metallic shadow mask, revealing its wave pattern in contrast to the Br⁻ signals (blue areas) stemming from the remaining initiator. The picture was modified with permission from Wiley, 2015 (DOI: 10.1002/adma.201500426).

Finally, a biorepellent layer was grafted from the non-irradiated areas on the PC film via the surface-initiated ATRP (SI-ATRP) of oligo(ethylene glycol) methyl ether methacrylate (MeOEGMA) thanks to the remaining initiator molecules on the surface. Oligo(ethylene glycol) (OEG) derivatives possess excellent antifouling properties since they are hydrophilic, electronically neutral and possesses hydrogen bond acceptors, but no hydrogen bond donors.^{324,325,326} Figure 3.3C refers to the ToF-SIMS image of the non-irradiated area, demonstrating the homogeneous coating of the film with poly(OEG). The measurement refers to the presence of the characteristic fragments of OEG: C₂H₃O⁻ (43.02 u) and C₂H₅O₂⁻ (61.03 u) among other distinctive fragments. In Figure 3.5 a photographic image of the pristine PC film is depicted, along with a picture of the film after the light-induced cleavage of the ATRP initiator and subsequent passivation with OEG, showing the wave pattern of the irradiated areas.

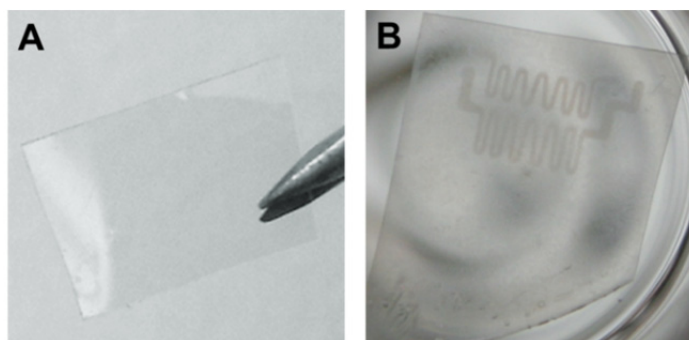


Figure 3.5. Photographic images of A) the untreated PC film and B) the PC film after photocleavage of the *o*-nitrobenzyl ATRP initiator and subsequent functionalization with poly(MeOEGMA), showing the wave pattern of the irradiated area at a certain angle of incident light. The picture was modified with permission from Wiley, 2015 (DOI: 10.1002/adma.201500426).

Apart from the observed wave pattern, the PC film remained optically unchanged when compared to the untreated film. As a result, a substrate with cell/protein adhesive areas was created on an overall biorepellent surface, which will be demonstrated in the next section.

In addition, the presence of potential copper residues after the SI-ATRP of MeOEGMA was analyzed via ToF-SIMS in order to perform cell tests on the surface, since copper is known to have cytotoxic effects.^{296,297} The extremely sensitive ToF-SIMS analysis, shown in Figure A.7, implied very small amounts of remaining copper. However, the quantities of copper were significantly low, and as shown in sections 3.2.3 the copper residues did not have cytotoxic effects on the cells.

3.2.2 Protein Adhesion on the Polycarbonate Film

In the subsequent step the patterned PC films were tested for the affinity of proteins only to the pre-defined areas on the surface. Fetal calf serum (FCS) and enhanced green fluorescent protein (eGFP) were selected as suitable proteins for the experiment.

In the first case, the PC film was treated with FCS, which is a mixture of varying proteins and frequently employed to test surface resistance to biofouling.^{204,327} The protein adsorption protocol including exact concentrations and conditions is described in the experimental section (3.4.5). ToF-SIMS analysis confirmed the attachment of FCS only to the irradiated wave-shaped pattern on the treated PC film, referring to the CN^- (26.0 u) and the CNO^- (42.0 u) fragments, which are characteristic for FCS and result from the peptide bonds of the protein, shown in Figure 3.6.³²⁸

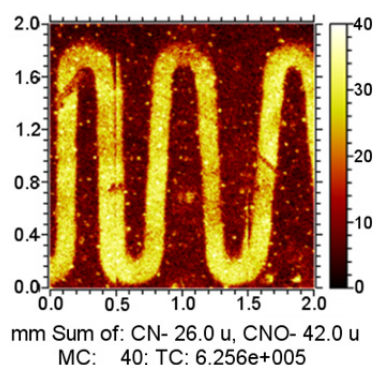


Figure 3.6. ToF-SIMS image of the CN⁻ and CNO⁻ fragments of FCS, reproducing the wave-shaped pattern of the photomask. The picture was modified with permission from Wiley, 2015 (DOI: 10.1002/adma.201500426).

Additionally, a second protein – enhanced green fluorescent protein (eGFP) – was tested for its attraction to the structured surface. Furthermore, the affinity of eGFP to the irradiated area was evaluated by measuring the fluorescence intensity inside and outside of the wave pattern and compared to the intensity of a non-patterned area on the same film. Figure 3.7A exhibits the brightfield image and the fluorescence image of a patterned surface after the treatment with eGFP solution. The white arrows in the fluorescence image indicate the measured zone about one millimeter across the partially irradiated and subsequently passivated area. Both the fluorescence microscope image and the data of the fluorescence intensity state that eGFP attaches primarily to the irradiated wave pattern and is less adsorbed on the non-irradiated areas. The quantitative evaluation of the fluorescence intensity (min = 0; max = 256), illustrated in Figure 3.7B, shows an average fluorescence value of 90.40 ± 5.61 (mean \pm standard error of the mean, SEM) in the irradiated area in comparison to an intensity of 59.80 ± 5.12 in the non-irradiated area. The promising results were an encouragement to test the patterned films in the context of cell guiding (section 3.2.3).

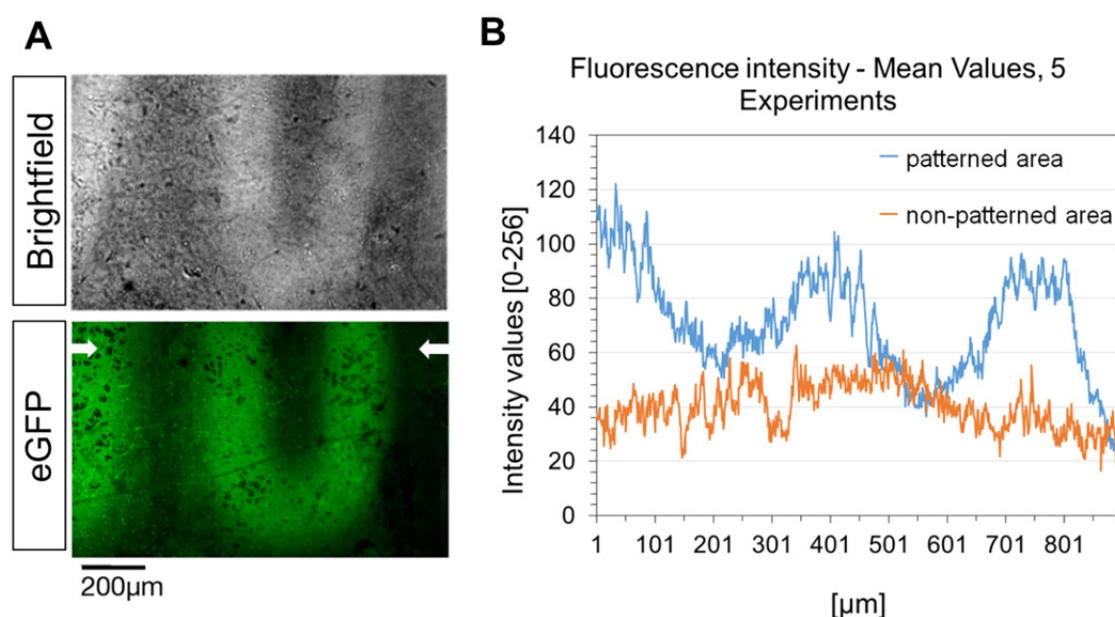


Figure 3.7. A) Attachment of eGFP to the irradiated areas on the PC surface. B) Fluorescence intensity of eGFP based on an average of 5 measurements. The intensity of eGFP inside the patterned area is compared to the intensity in the non-patterned area. The picture was modified with permission from Wiley, 2015 (DOI: 10.1002/adma.201500426).

3.2.3 Cell Guiding on the Polycarbonate Film in 2D

The successful adsorption of proteins in the irradiated areas of the patterned PC film, as described in the previous section, led to the next step to cultivate cells on the film in the context of guided cell adhesion. Cells from a robust vertebrate fibroblast line (PAC2)³²⁹ were seeded on the PC film and cultivated for 24 h in L-15 medium (containing 50 $\mu\text{g ml}^{-1}$ Gentamycin, 100 units mL^{-1} Penicillin, 100 $\mu\text{g mL}^{-1}$ Streptomycin and 15 % FCS). Subsequently, the PAC2 fibroblasts were washed with PBS^{-/‡} (2 \times 5 min) to remove non-adherent cells and fixed with 4 % paraformaldehyde (PFA) for 30 min. Afterwards, the cells were stained with markers for cell nuclei (DAPI) and actin cytoskeleton (Phalloidin). The fluorescence microscope images and the quantitative evaluation of the cell density and the surface coverage of cells on the film are illustrated in Figure 3.8. As a result, it was observed that PAC2 cells accepted the pattern, whereas they avoided the non-irradiated areas and mainly adhered to the irradiated areas on the surface

[‡] -/- indicates without MgCl_2 and CaCl_2

3. Light-Induced Surface Modification

(Figure 3.8A, B, C). Information about the density of cells on the surface was obtained from the quantification of the cell nuclei (DAPI). The cell density inside the irradiated areas is significantly higher, with $0.0004 \text{ cells } \mu\text{m}^{-2}$ (blue bar) than on the non-irradiated surface where a cell density of only $0.0001 \text{ cells } \mu\text{m}^{-2}$ (red bar) was detected. Interestingly, it was also noticed that fibroblast feature different shapes, depending on the area on the surface where they are located. The observation was highlighted by pseudo-coloring the cells in the irradiated areas in red and the cells in the non-irradiated areas in yellow (Figure 3.8C). On the non-passivated surface area cells are flatter and cover a larger area compared to the passivated surface where cells display a small, round phenotype. The actin cytoskeleton (Phalloidin) relates to the surface area covered by cells. Thus, a quantification of the surface coverage, shown in Figure 3.8E, indicates that $70.3 \pm 6.3 \%$ (mean \pm SEM) of the irradiated surface were covered with cells compared to only $15.1 \pm 4.9 \%$ on the non-irradiated surface. As a matter of fact, fibroblasts exist in a much higher density in the irradiated areas on the surface. According to the cellular shape analysis the assumption was made that fibroblast migrate from the passivated surface to the non-passivated surface. However, it was not possible to further explain the observed cellular distribution, since the cell division rate for PAC2 fibroblasts in culture is too slow.³²⁹

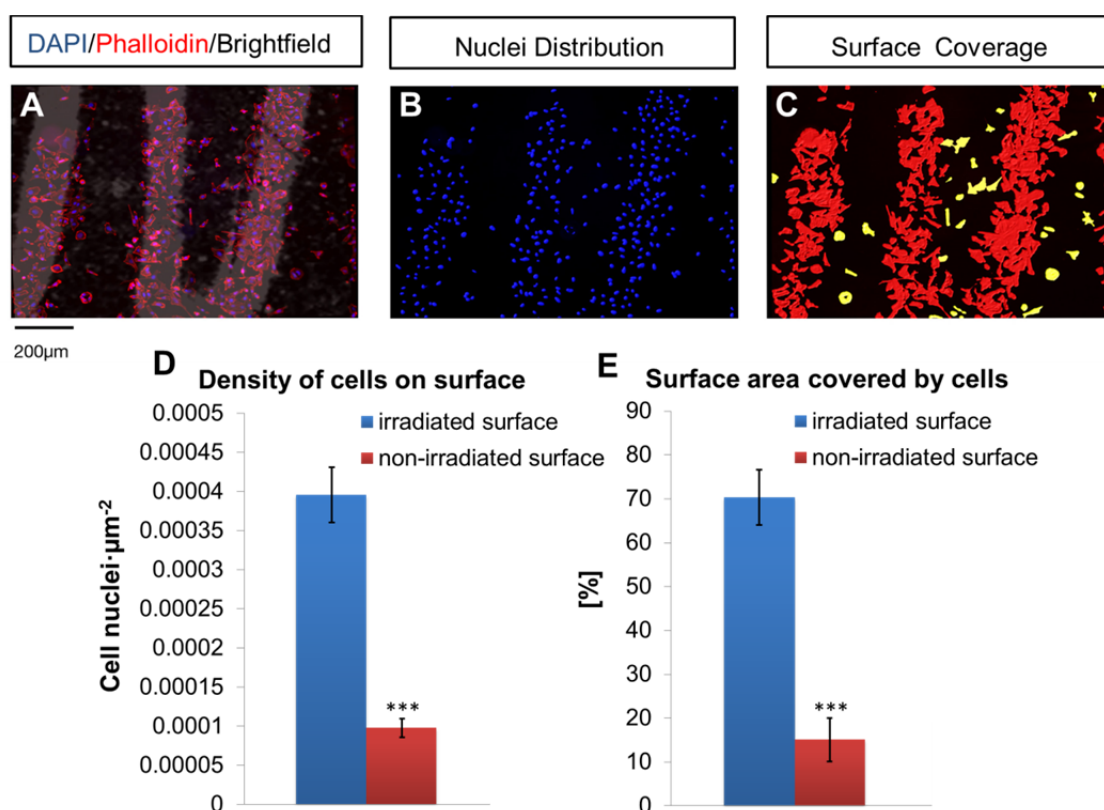


Figure 3.8. Adhesion of PAC2 fibroblast cells to the patterned PC film. A) Brightfield picture of the microscope merged with PAC2 fibroblast cells, stained with nuclei marker (DAPI) and actin cytoskeleton (Phalloidin). B) Surface rendering of the nuclear DAPI signal and localization of cell nuclei to quantify the cell distribution. C) Pseudo coloring of the cells: irradiated area (red) and non-irradiated area (yellow). D) Density of cells on the surface: irradiated area (blue) and non-irradiated area (red). E) Percentage of surface covered by cells: irradiated area (blue) and non-irradiated area (red). The cells were stained and measured after 24 h. To determine significance of difference between the data sets Student's T-Test was used and a p-value of < 0.0001 (***) was calculated. Reproduced with permission from Wiley, 2015 (DOI: 10.1002/adma.201500426).

3.2.4 Thermoforming and Cell Guiding in 3D

Finally, the cell guiding strategy was tested in a three-dimensional environment. Therefore, the pre-modified PC film **8** was shaped in a thermoforming process using the so-called SMART approach (substrate modification and replication by thermoforming).^{15,16,330} During the thermoforming process the PC film is three-dimensionally stretched under mild conditions which allows to manufacture film-based microstructures.³³⁰ In this way, a 3D microchannel was generated on a patterned PC film. Figure 3.9A depicts the film after thermoforming with the channel located in the middle of the round PC piece. The brass mold employed for SMART is

3. Light-Induced Surface Modification

shown in Figure 3.9B and Figure 3.9C illustrates a novel shadow mask in order to generate a divided channel structure on the surface. The shadow mask matching the channel was constituted from the brass mold with a narrow strip of aluminum foil placed in the middle of the slit. Exact conditions for the SMART process can be found in the experimental section (3.4.6). Following this, the thermoformed film was passivated by grafting MeOEGMA from the surface. The grafting of the biorepellent polymer was performed after the thermoforming step to prevent possible polymer degradation.

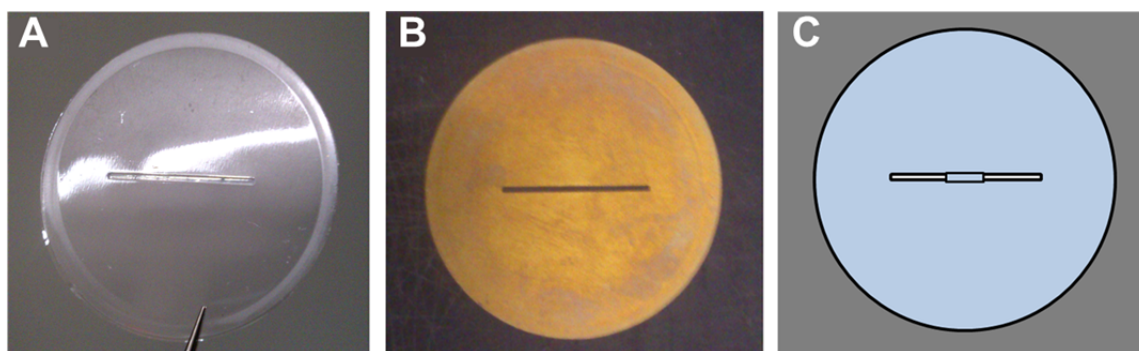


Figure 3.9. A) Photograph of a patterned PC film after thermoforming. B) Photograph of the brass mold employed for SMART. C) Schematic depiction of the homemade shadow mask employed for irradiation, consisting of the brass mold and a narrow strip of aluminum foil placed in the middle of the slit. Reproduced with permission from Wiley, 2015 (DOI: 10.1002/adma.201500426).

The channel like structure is envisaged to mimic the neural channel of a zebrafish, in order to explore the development of the thalamus. Scholpp and co-workers have investigated signaling processes between small groups of cells which are divided by naturally occurring boundaries, such as the mid-diencephalic boundary whose impact on cell signaling processes needs to be investigated.^{10,11} Via insertion of a boundary inside the microchannel the *in vivo* conditions for the *in vitro* investigation of neural zebrafish cells are partly reconstructed.

PAC2 fibroblasts were cultivated in the patterned channel for 5 days under similar conditions as described in section 3.2.3. In addition, a control experiment was performed by cultivating cells for 5 days in a pristine 3D channel. The outcome of the experiments is shown in Figure 3.10. Fibroblast in the control channel (Figure 3.10B) cover the entire area whereas cells in the patterned channel almost

exclusively attach to the irradiated areas while avoiding the passivated zone. Higher magnification images of the non-passivated zone, the border region and the passivated zone of the patterned channel are depicted in Figure 3.11.

Hence, the effectiveness of the herein described photolithographic approach is demonstrated even in combination with thermoforming, resulting in isolated cell-populated zones within a single 3D microchannel.

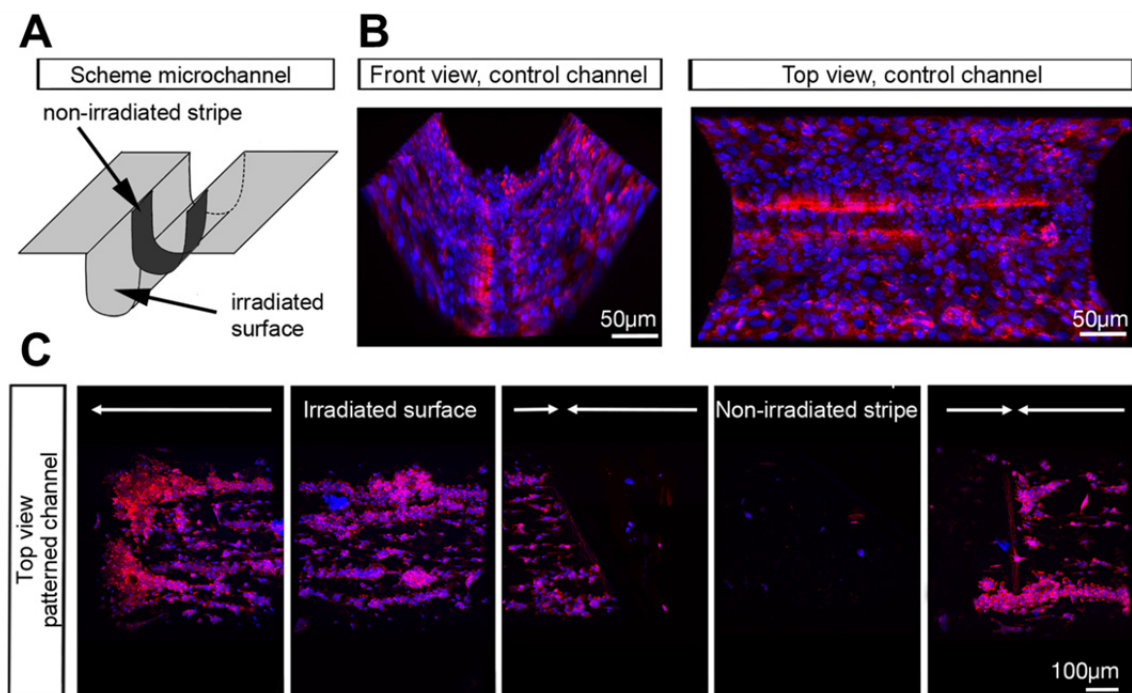


Figure 3.10. Adhesion of PAC2 fibroblast cells to a patterned 3D microchannel shaped on a pre-modified polycarbonate film. A) Outline of a thermoformed 3D microchannel with a non-irradiated zone dividing the irradiated channel. B) Frontal view and top view of an untreated microchannel (control) with PAC2 fibroblast cells stained with DAPI and Phalloidin. C) Top view of PAC2 cells in the patterned microchannel. The cells were cultivated in both cases for 5 days. Reproduced with permission from Wiley, 2015 (DOI: 10.1002/adma.201500426).

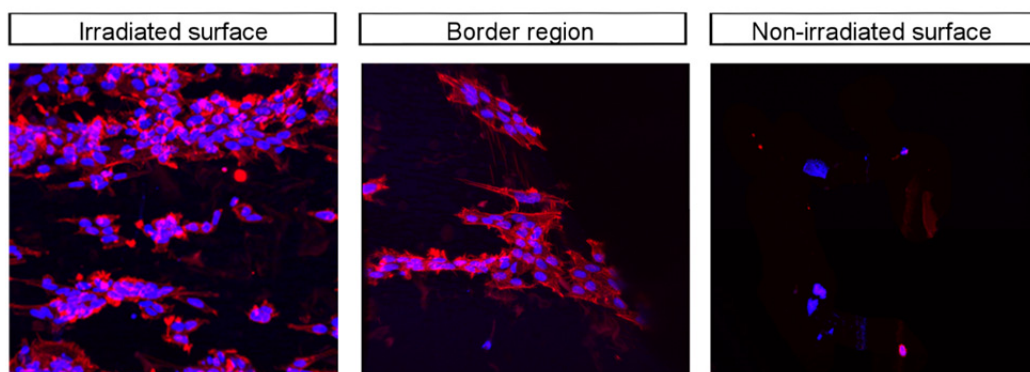


Figure 3.11. High magnification pictures of adherent fibroblast cells in the patterned microchannel. Reproduced with permission from Wiley, 2015 (DOI: 10.1002/adma.201500426).

3.3 Conclusion

A general method for the spatially resolved functionalization of polycarbonate films via a combination of photopatterning and reversible deactivation radical polymerization was described. Thus, micropatterns of an OEG derivative and carboxylic acid moieties were obtained and tested under biofouling conditions. It was observed that proteins – FCS and eGFP - which were applied to the patterned PC surface primarily attached to the non-passivated, irradiated areas whereas less or almost no protein adhesion was detected outside of the irradiated areas. Furthermore, cells of a PAC2 fibroblast line were cultivated on the modified films. Similar to the proteins, the cells preferred the carboxylic acid functionalized regions on the surface where a much higher cell density was detected compared to the passivated areas. In addition, a 3D microchannel was shaped into a pre-modified PC film in order to create a thin walled and transparent microwell for sophisticated cell studies. Thus, it was proven that the developed chemistry withstands the process and that cell patterning can be achieved inside the microchannel.

The introduced methodology paves the way for the development of patterned surfaces which can be further shaped into any desired 3D structure and thus can serve as novel and disposable devices for advanced cell culture applications.

3.4 Experimental Section

3.4.1 Materials

5-Hydroxy-2-nitrobenzyl alcohol (Aldrich), succinic anhydride (99%, Alfa Aesar), 1-(3-dimethylaminopropyl)-3-ethylcarbodiimide hydrochloride (EDC*HCl) (98+%, Alfa Aesar), 1,1,4,7,7-pentamethyldiethylenetriamine (PMDETA) (99+%, Acros), CuBr (99.9%, Sigma-Aldrich), potassium carbonate (K₂CO₃, Alfa Aesar), *N,N*-dimethylformamide extra dry (DMF) (Acros), propagyl bromide (80 wt.% in toluene, Sigma Aldrich), MgSO₄ (Roth), 4-dimethylaminopyridine (DMAP, 99%, ABCR), 3-aminopropyltriethoxysilane (APTES) (99%, Acros), *N*-hydroxysuccinimide (NHS) (98%, Aldrich), 2,2'-bipyridyl (BiPy) (99%, Sigma-Aldrich), sodium bisulfate (NaHSO₄) (Roth), CuBr₂ (99.9%, Sigma-Aldrich), CuCl (99.9%, Sigma-Aldrich), 3-azidopropyl 2-bromoisobutyrate was synthesized according to the literature and oligo(ethylene glycol) methyl ether methacrylate (MeOEGMA, Sigma-Aldrich, average Mn ~ 300 g mol⁻¹) was filtered over a column of aluminium oxide 90 active basic (Merck) before usage. Ethyl acetate, dichloromethane, cyclohexane, ethanol, and methanol were purchased as analytical grade (Aldrich) and used as received. Employed polycarbonate (PC) membranes were ion-irradiated polycarbonate films (it4ip, Belgium, fluence 106 ions cm⁻², thickness 65 μm).

3.4.2 Instrumentation

3.4.2.1 Nuclear Magnetic Resonance (NMR) Spectroscopy

The structures of the synthesized compounds were confirmed via ¹H and ¹³C NMR spectroscopy using a Bruker AM 400 MHz spectrometer for hydrogen nuclei and 100 MHz for carbon nuclei. Samples were dissolved in DMSO-*d*₆. The δ scale was referenced with tetramethylsilane (δ = 0.00) as internal standard. Abbreviations used below in the description of the synthetic steps include singlet (s), doublet (d), triplet (t), quartet (q), multiplet (m).

3.4.2.2 UV-vis Spectroscopy

UV-vis spectra were recorded on a Varian Cary 300 Bio spectrophotometer.

3.4.2.3 Time-of-Flight Secondary Ion Mass Spectrometry (ToF-SIMS)

ToF-SIMS (Time-of-Flight Secondary Ion Mass Spectrometry) was performed on a TOF.SIMS5 instrument (ION-TOF GmbH, Münster, Germany). This spectrometer is equipped with a Bi cluster primary ion source and a reflectron type time-of-flight analyzer. UHV base pressure was $< 10^{-8}$ mbar. For high mass resolution the Bi source was operated in the “high current bunched” mode providing short Bi_1^+ or Bi_3^+ primary ion pulses at 25 keV energy and a lateral resolution of approx. 4 μm . The short pulse length of 1.1 to 1.3 ns allowed for high mass resolution. The primary ion beam was rastered across a $500 \times 500 \mu\text{m}^2$ field of view on the sample, and 128×128 data points were recorded. Primary ion doses were kept below 10^{11} ions/ cm^2 (static SIMS limit). Since the PC films are good electrical insulators, charge compensation was necessary. Therefore, an electron flood gun providing electrons of 21 eV was applied and the secondary ion reflectron was tuned accordingly. Spectra were calibrated on the omnipresent C^- , C_2^- , C_3^- , or on the C^+ , CH^+ , CH_2^+ , and CH_3^+ peaks. Based on these datasets the chemical assignments for characteristic fragments were determined.

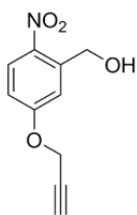
3.4.2.4 IR Spectroscopy

IR spectra were measured on a Bruker Vertex 80 FT- IR/NIR spectrometer with an InGaAs detector, CaF_2 beam splitter, as well as an ATR unit.

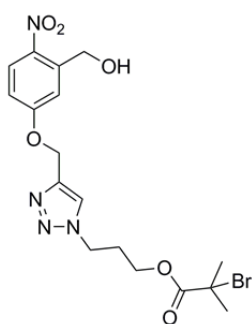
3.4.2.5 Fluorescence Microscopy

Images of cells were obtained with a Leica TCS SP5 X confocal laser-scanning microscope using 20 \times , 40 \times or 63 \times dip-in objectives. Image processing was performed with the Imaris 6.3.1 software (Bitplane AG).

3.4.3 Syntheses



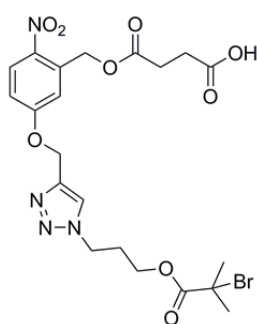
(2-nitro-5-(prop-2-yn-1-yloxy)phenyl)methanol: In a Schlenk round bottom flask under a nitrogen atmosphere, 5-hydroxy-2-nitrobenzylalcohol (1.70 g, 10.10 mmol, 1 eq.) and freshly ground K_2CO_3 (4.16 g, 12.06 mmol, 1.2 eq.) were emulsified in dry DMF and heated at 60 °C for 1 h. Subsequently, propargyl bromide (80 % in toluene, 1.30 mL, 12.06 mmol, 1.2 eq.) was slowly introduced into the reaction mixture, which was stirred for 15 h at 60 °C. The solvent was removed under reduced pressure, the residue dissolved in ethyl acetate and washed three times with distilled water. The organic phase was dried over $MgSO_4$ and the solvent was evaporated to afford a brown solid, which was recrystallized in cyclohexane/ethyl acetate (1:1). The pure product was obtained as a slightly brown solid (1.12 g, 54%). 1H NMR (500 MHz, 256 scans, $DMSO-d_6$) δ = 8.23 (dd, 1 H, $^3J_{HH}$ = 9.1 Hz, Ar-H), 7.48 (s, 1H, Ar-H), 7.17 (d, 1 H, $^3J_{HH}$ = 9.1 Hz, Ar-H), 5.69 (ds, 1 H, $^3J_{HH}$ = 3.3 Hz, CH_2-OH), 5.05 (s, 2 H, CH_2-OH), 4.93 (s, 2 H, O- $CH_2-C\equiv CH$), 3.75 (s, 1 H, $C\equiv CH$) ppm.³³¹ The 1H NMR spectrum of the structure is shown in Appendix A, Figure A.1.



3-(5-((3-(hydroxymethyl)-4-nitrophenoxy)methyl)-1H-1,2,3-triazol-1-yl)propyl 2-bromo-2-methylpropanoate: Cu(I)Br (13.85 mg, 0.10 mmol, 0.2 eq.) and PMDETA (16.73 mg, 0.10 mmol, 0.2 eq.) were placed in a Schlenk tube and stirred for 10 min. under a nitrogen atmosphere. In a second Schlenk tube under a nitrogen atmosphere, (2-nitro-5-(prop-2-yn-1-yloxy)phenyl)methanol (100.00 mg, 0.48 mmol, 1 eq.) and 3-azidopropyl 2-bromoisobutyrate (120.00 mg, 0.48 mmol, 1 eq.) were dissolved in dry DMF (3 mL). Subsequently, this solution was added to the CuBr/PMDETA mixture and the reaction was stirred overnight. The reaction mixture was then filtered over silica to remove CuBr and the solvent was evaporated under reduced pressure. The residue was dissolved in dichloromethane, washed twice with distilled water and dried over $MgSO_4$. After removal of the solvent, the pure product was obtained as a light brown solid without any further purification

3. Light-Induced Surface Modification

(142.64 mg, 65%). $^1\text{H NMR}$ (400 MHz, $\text{DMSO-}d_6$) δ = 8.30 (s, 1 H, C=CH-N), 8.14 (d, 1 H, $^3J_{\text{HH}}$ = 9.1 Hz, $\text{C}_{\text{Ar}}\text{H-C-NO}_2$), 7.42 (s, 1 H, HC_{Ar}), 7.17 (dd, 1 H, $^3J_{\text{HH}}$ = 9.1 Hz, $\text{C}_{\text{Ar}}\text{H-C-O}$), 5.57 (t, 1 H, $^3J_{\text{HH}}$ = 5.5 Hz, CH₂-OH), 5.31 (s, 2 H, O-CH₂-C), 4.85 (d, 2 H, $^3J_{\text{HH}}$ = 5.5 Hz, $\text{C}_{\text{Ar}}\text{-CH}_2\text{-OH}$), 4.49 (t, 2H, $^3J_{\text{HH}}$ = 6.9 Hz, N-CH₂-CH₂), 4.14 (t, 1 H, $^3J_{\text{HH}}$ = 6.1 Hz, O-CH₂-CH₂), 1.77 (quin., 2 H, $^3J_{\text{HH}}$ = 6.5 Hz, OCH₂-CH₂-CH₂) ppm. MS (ESI) m/z calculated for $\text{C}_{17}\text{H}_{21}\text{BrN}_4\text{O}_6$ $[\text{M}+\text{Na}]^+$: m/z theo: 479.05, m/z exp: 479.12. The $^1\text{H NMR}$ spectrum of the structure is shown in Appendix A, Figure A.2.



4-((5-((1-(3-((2-bromo-2-methylpropanoyl)oxy)propyl)-1H-1,2,3-triazol-5-yl)methoxy)-2-nitrobenzyl)oxy)-4-oxobutanoic acid (6): 3-(5-((3-(hydroxymethyl)-4-nitrophenoxy)-methyl)-1H-1,2,3-triazol-1-yl)propyl 2-bromo-2-methylpropanoate (100.00 mg, 0.22 mmol, 1 eq.), DMAP (6.66 mg, 0.07 mmol, 0.3 eq.), and succinic anhydride (30.76 mg,

0.31 mmol, 1.4 eq.) were dissolved in dichloromethane (5 mL) and left to react overnight. The solution was then extracted four times with NaHSO_4 (10 %). The organic phase was subsequently dried with MgSO_4 , filtered, and concentrated. The product was obtained as brown oil which crystallized to a light brown solid (106 mg, 87% yield). $^1\text{H NMR}$ (400 MHz, $\text{DMSO-}d_6$) δ = 8.30 (s, 1 H, C=CH-N=N), 8.19 (d, 1 H, $^3J_{\text{HH}}$ = 9.4 Hz, $\text{HC}_{\text{Ar}}\text{-CNO}_2$), 7.24 (m, 2 H, $\text{HC}_{\text{Ar}}\text{-C-O}$, HC_{Ar}), 5.46 (s, 2 H, Ar-CH₂-CO₂), 5.34 (s, 2 H, Ar-O-CH₂-C), 4.49 (t, 2 H, $^3J_{\text{HH}}$ = 6.9 Hz, N-CH₂-CH₂), 4.14 (t, 2 H, $^3J_{\text{HH}}$ = 6.2 Hz, CH₂-CH₂-O), 2.68 (m, 2 H, CO-CH₂-CH₂), 2.53 (m, 2 H, CO-CH₂-CH₂-COOH), 2.22 (quin., 2 H, $^3J_{\text{HH}}$ = 6.6 Hz, CH₂-CH₂-CH₂), 1.88 (s, 6 H, CO₂-C-C₂H₆-Br) ppm. MS (ESI) m/z calculated for $\text{C}_{21}\text{H}_{25}\text{BrN}_4\text{O}_9$ $[\text{M}+\text{Na}]^+$: m/z theo: 579.07, m/z exp: 579.08. The $^1\text{H NMR}$ spectrum of the structure is shown in Appendix A, Figure A.3.

3.4.4 Surface Reactions

Treatment of the PC film with air plasma (4) and functionalization with 3-aminopropyltriethoxysilane (APTES) (5)

A round piece of polycarbonate film (\varnothing 4 cm) (1) was treated with air plasma (power: 100 W) for 5 minutes. Subsequently, the film was immersed in an aqueous solution of APTES (6 % v/v) at 90 °C for 4 h. The film was removed from the solution and thoroughly washed with Milli Q water and distilled ethanol in an ultrasonic bath as well as rinsing the sample by using a pipette. The sample was finally dried under a stream of nitrogen gas and placed in a drying oven at 90 °C for 15 h to anneal the APTES bonds on the surface.

Functionalization of the PC film with 4-((5-((1-(3-((2-bromo-2-methylpropanoyl)oxy)propyl)-1H-1,2,3-triazol-5-yl)methoxy)-2-nitrobenzyl)oxy)-4-oxobutanoic acid (6)

Compound **6** (78 mg, 0.25 mmol, 1.00 eq.) was dissolved in distilled methanol (5.5 mL) and N-hydroxysuccinimide (25 mg, 0.22 mmol, 1.57 eq.) was added. The solution was stirred and deoxygenated by purging with nitrogen for 5 min at ambient temperature. Subsequently, the solution was added to a flask containing a piece of APTES functionalized film (4.5 cm²) (5) under nitrogen atmosphere. To this solution, EDC·HCl (30.58 mg, 0.16 mmol, 1.14 eq.) dissolved in methanol (1 mL) was added. The reaction mixture was shaken overnight at ambient temperature in the dark. Subsequently, the film was extensively rinsed with distilled methanol and distilled water and additionally ultrasonicated for 2 min (3 times) in the same solvents. Finally, the film was dried in a stream of nitrogen gas and stored in the dark.

Irradiation of the PC film

The PC film functionalized with the *o*-nitrobenzyl ATRP initiator (7) was placed on a silicon wafer for fixation purposes. The wafer and the film were subsequently positioned in a sample holder and covered with a shadow mask, which was then

3. Light-Induced Surface Modification

secured with screws (Figure A.4). The complete assembly was positioned in a glass vial, placed in the UV photoreactor (Figure A.5), and irradiated for 12 h in the dry state. Subsequently, the film was removed from the sample holder and thoroughly washed with Milli Q water and methanol, by rinsing and ultrasonic treatment (6 times). Finally, the patterned film (**8**) was dried under a stream of nitrogen gas.

Functionalization of the PC film with poly(MeOEGMA) (9)

In a Schlenk tube, MeOEGMA (3.99 g, 3.70 ml, 13.32 mmol, 1.00 eq.) was dissolved in Milli Q water (3.7 mL) at 30 °C. To this solution, 2,2'-bipyridyl (53.25 mg, 0.34 mmol, 0.03 eq.) and Cu(II)Br₂ (3 mg, 0.01 mmol, 0.001 eq.) were added. The mixture was stirred and degassed by purging with nitrogen for 1 h before Cu(I)Cl (13.17 mg, 0.13 mmol, 0.01 eq.) was added. The mixture was subsequently deoxygenated for an additional 15 min. A piece of the ATRP initiator functionalized film (1 cm²) (**8**) was sealed in a Schlenk tube and deoxygenated by four high-vacuum pump/nitrogen refill cycles. The reaction mixture was transferred by a degassed syringe into the film containing Schlenk tube, adding enough to cover the film completely. The polymerization was allowed to proceed at 30 °C for 1 h. Subsequently, the film was removed and thoroughly rinsed with deionized water and ultrasonicated for 2 min several times to remove any physically adsorbed materials to yield film **9**.

3.4.5 Protein adhesion studies

Fouling studies with fetal calf serum (FCS)

Fouling resistance of the pre-treated PC film was assessed by challenging the surfaces with fetal calf serum (FCS). After irradiation with a shadow mask and subsequent passivation with poly(MeOEGMA), the PC films (**9**) (1 cm²) were immersed in vials containing 2 mL of phosphate buffered saline (PBS, pH 7.4). Subsequently, FCS was added (1 mL). The sample was gently shaken for 15 min. The surface was rinsed by addition of copious amounts of PBS and subsequent removal of 75% of the volume. This operation was repeated five times with special care to prevent any solid-air interface which would induce additional protein adsorption.

Finally, the surface was rinsed with Milli Q water and dried at reduced pressure for 5 h.

Enhanced Green Fluorescent Protein (GFP) affinity assay

The polycarbonate film (**9**) was incubated for 15 min in a solution containing a 1 μM concentration of enhanced green fluorescence protein (eGFP) in PBS. 1.93 μL were taken from a stock solution of eGFP in PBS (154 μM , 100 μL) and diluted in 3 mL PBS. After incubation, the polycarbonate film was washed 3×5 min in PBS^{-/-§} and finally 2×15 min washing steps in PBS. The fluorescence intensity was measured on an Olympus SZX16 microscope. In this context, five linear scans passing non-irradiated and irradiated areas were carried out across the polycarbonate film and compared with the fluorescence intensity measured in a non-irradiated zone on the same film.

3.4.6 Thermoforming

Microthermoforming of the patterned PC film

For the thermoforming process a round piece of PC film with a diameter of 40 mm was functionalized with the *o*-nitrobenzyl ATRP initiator **6** as previously described. Subsequently, the film was irradiated in the presence a homemade shadow mask, consisting of the brass mold for thermoforming and aluminum foil, in the same conditions as stated above (shown in Figure 3.9C). Thereafter, the microchannels were formed on an in-house developed thermoforming device with lockable brass tool.¹⁶ The brass mold with an outer diameter of 40 mm and dimensions of mold 20 mm \times 0.8 mm \times 0.3 mm ($l \times w \times d$) was mounted within the brass tool, connected to a vacuum pump. The irradiated area of the PC film with a thickness of 65 μm was oriented to match the channel of the brass mold and the lockable tool was evacuated and heated up to 157 $^{\circ}\text{C}$. Upon reaching the forming temperature, gas pressure of 1.3 MPa was applied, resulting in forming of microchannels. Afterwards, the tool was cooled down and the microchannels with an average depth of 200 μm were carefully

§ -/-: indicates without MgCl_2 and CaCl_2

removed from the mold. Finally, MeOEGMA was graft-polymerized from the ATRP initiator present in the previously non-irradiated zones on the thermoformed film. The polymer passivation was performed after the thermoforming process to avoid possible polymer degradation.

3.4.7 Cell Guiding Experiments

Cell guiding experiment in 2D

In the 2D cell guiding experiment PAC2 fibroblasts were seeded on a patterned polycarbonate film (9) and cultivated in L-15 medium containing 50 $\mu\text{g mL}^{-1}$ Gentamycin, 100 units mL^{-1} Penicillin, 100 $\mu\text{g mL}^{-1}$ Streptomycin and 15% FCS (thermo cabinet Lovibond) at 28 °C – the optimum temperature for PAC2 cells – for 24 h. Afterwards, the cells were washed in PBS^{-/-} (2 × 5 min) to remove non-adherent cells. Next, the cells were fixed with 4 % paraformaldehyde (PFA) for 30 min and stained with the nuclei marker DAPI and the actin cytoskeleton marker Phalloidin.

Cell guiding experiment in a thermoformed 3D microchannel

The microchannels were coated with a Laminin-1/fibronectin mix (0.02 mg mL^{-1} , 0.02 mg mL^{-1} , respectively) for 2 h at 31 °C. Afterwards the coating solution was removed and unbound proteins were washed out by incubation with PBS^{-/-} (3 × 5 min). Cells were seeded in the microchannel and incubated in L-15 medium (ingredients as described) at 28 °C for 5 days. Subsequently, the cells were washed, fixed and stained as mentioned above.

4

Complex Macromolecular Architectures via Supramolecular Chemistry and Photochemical Ligation

NOESY NMR measurements were performed in collaboration with D. Schulze-Sünninghausen and B. Luy (Institute for Organic Chemistry, KIT). AFM measurements were performed by P. Krolla-Sidenstein (Institute of Functional Interfaces, KIT). W. Konrad (Institute for Chemical Technology and Polymer Chemistry (ITCP), KIT) is thanked for the synthesis of the *t*BuBn-trithiocarbonate during his advanced lab-course under the author's supervision. J. Blinco (Queensland University of Technology) and S. Wiedmann (ITCP) are thanked for discussions. Parts of this chapter were reproduced with permission from Hirschbiel, A. F.; Schmidt, B. V. K. J.; Krolla-Sidenstein, P.; Blinco, J. P.; Barner-Kowollik, C.; *Macromolecules* **2015**, *48*, 4410-4420 (DOI: 10.1021/acs.macromol.5b00923) and from Hirschbiel, A. F.; Konrad, W.; Schulze-Sünninghausen, D.; Wiedmann, S.; Luy, B.; Schmidt, B. V. K. J., Barner-Kowollik, C.; *ACS Macro Lett.* **2015**, *4*, 1062-1066 (DOI: 10.1021/acsmacrolett.5b00485). Copyright 2015 American Chemical Society.

4.1 Motivation

In order to design innovative and advanced materials, one approach is the combination of polymeric materials via efficient and facile ligation methods. The modular ligation of polymer chains with varying properties, e.g. crystallinity, flexibility or even stimuli responsive qualities is an effective tool to generate complex macromolecular architectures which are further employed in the development of functional soft materials.^{332,333} Such polymer architectures such as multiblock copolymers,^{334,224} polymer stars^{335,336} or networks^{337,310} can be obtained via the incorporation of active moieties in the side chain of the polymer or the functionalization of the polymer termini with reactive groups.^{338,339,247} Organic chemistry concepts in combination with macromolecular design have led to a multiplicity of mild and rapid polymer conjugation techniques.^{22,18} In particular, click chemistry is employed as a mild, efficient and fast coupling strategy and has found broad application in the synthesis of tailor-made polymer structures.^{24,23} Furthermore, controlled radical polymerization techniques result in well-defined polymer chains with narrow molecular weight distributions. Among atom-transfer radical polymerization (ATRP) and nitroxide mediated polymerization (NMP), reversible addition-fragmentation chain transfer (RAFT) polymerization is a powerful tool to polymerize a multitude of monomers and to introduce functional chain termini to a polymer, depending upon the choice of chain transfer agent (CTA).^{21,123,340}

In the present chapter, the supramolecular host-guest interaction of β -cyclodextrin (CD)^{341,342,343} is combined with light-induced Diels-Alder reactions of 2-methoxy-6-methylbenzaldehyde (photoenol, PE)^{55,60,6} for the preparation of block copolymers. RAFT polymerization is employed to synthesize polymer chains with supramolecular recognition units, as well as photo-active moieties and reactive double bonds. Both β -CD host-guest interactions and photoenol chemistry are mutually orthogonal ligation methods and highly appealing, since no coupling agents or initiators are necessary and the polymeric building blocks are simply added in stoichiometric amounts. Furthermore, it is demonstrated that the thus obtained

block copolymers can be employed for the synthesis of thermoresponsive nanoparticles.

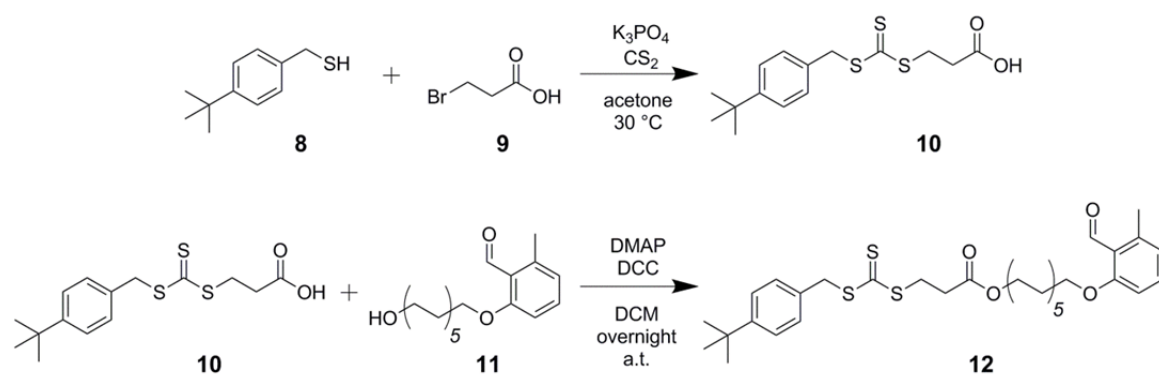
4.2 Results and Discussion

4.2.1 Synthesis of Chain Transfer Agents

CTAs or so-called RAFT agents are, for example, trithiocarbonates or dithioesters which transfer their R- and Z- groups to the α - and ω - chain ends of the polymer during the polymerization process (see section 2.2.2.3). In order to obtain polymers with defined chain termini, a range of RAFT agents were synthesized with corresponding functionalities, e.g. guest molecules for β -CD or photoenol units. The trithiocarbonates were prepared as reported by Skey and O'Reilly via a facile synthetic strategy.³⁴⁴

4.2.1.1 Synthesis of the Bifunctional CTA *t*BuBnPE-Trithiocarbonate

The aim was to develop block copolymers via the combination of the supramolecular assembly of β -CD with a guest-molecule and the light-induced reaction of PE with a maleimide. Thus, a bifunctional RAFT agent – equipped with a *tert*-butyl phenyl guest and a PE – was synthesized for the preparation of an α,ω -functional polymer center block (Scheme 4.1). *tert*-Butyl phenyl was chosen since it is an ideal guest molecule for the inclusion in β -CD with high complexation constants ($K \sim 18000 - 25000 \text{ L}\cdot\text{mol}^{-1}$).³⁴⁵



Scheme 4.1. Synthetic route for the bifunctional RAFT agent 11-(2-formyl-3-methylphenoxy)undecyl 3-(((4-(*tert*-butyl)benzyl)thio) carbonothioyl)thio) propanoate (*t*BuBnPE-trithiocarbonate) **12**.

The trithiocarbonate precursor for the bifunctional RAFT agent **10** was synthesized with the mercaptan of the *tert*-butyl phenyl guest molecule **8** and 3-bromopropanoic acid **9** together with carbon disulfide (CS₂) and tripotassium phosphate (K₃PO₄) in acetone. During the reaction the thiol is deprotonated by the K₃PO₄ and performs a nucleophilic attack on the carbon disulfide. The resulting trithiocarbonate salt then again attacks on the bromo-compound. The crude product **10** was purified via column chromatography (Appendix B, Figure B.1: ¹H NMR spectrum) and subsequently used in the following step. A PE derivative, 2-((11-hydroxyundecyl)oxy)-6-methylbenzaldehyde **11**, was synthesized according to the literature⁵⁵ and esterified under Steglich conditions with *N,N'*-dicyclohexylcarbodiimide (DCC) and 4-(dimethylamino)-pyridine (DMAP). After purification, the product **12** was obtained as a yellow oil with yields up to 88 %. The ¹H NMR spectrum of 3-(((4-(*tert*-butyl)benzyl)thio) carbonothioyl)thio)propanoate (*t*BuBnPE-trithiocarbonate) **12** is illustrated in Figure 4.1, revealing the proton resonances of the highly pure product.

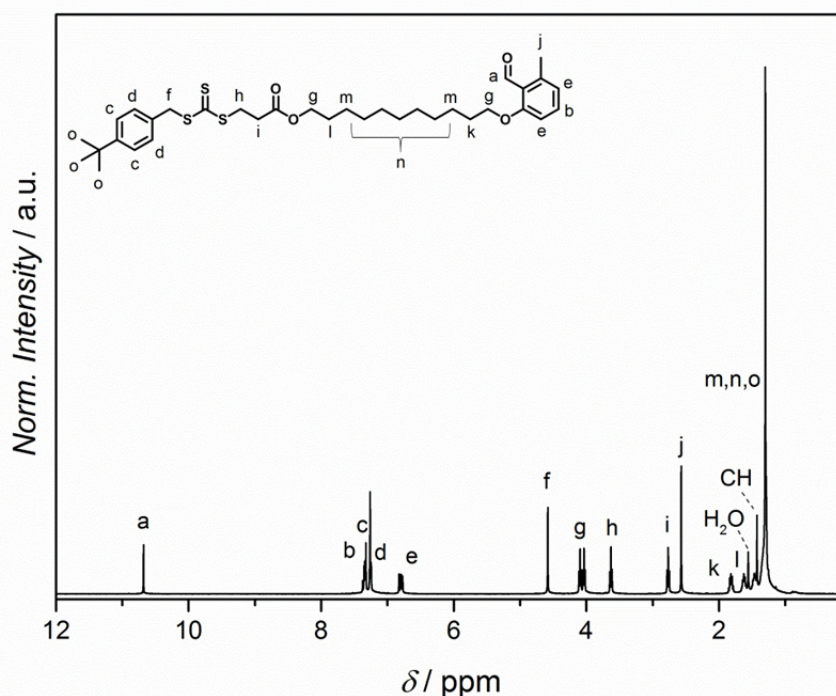
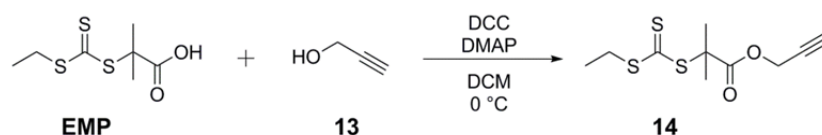


Figure 4.1. ¹H NMR (400 MHz, CDCl₃, 25 °C) spectrum of 11-(2-formyl-3-methylphenoxy)-undecyl 3-(((4-(*tert*-butyl)benzyl)thio)carbonothioyl)thio)propanoate (*t*BuBnPE-trithiocarbonate) **12**. Reproduced with permission from the American Chemical Society, 2015 (DOI: 10.1021/acsmacrolett.5b00485).

4.2.1.2 Synthesis of an Alkyne-Terminated CTA

Furthermore, a second RAFT agent with an alkyne function (alkyne-trithio-carbonate) at the R-group **14** was employed in the present work for the introduction of a β -CD host molecule to several chain termini after polymerization. 2-(((ethylthio))thioxomethyl)thio)-2-methyl-propionic acid (EMP) was synthesized following a literature procedure³⁴⁶ in the same fashion as described for *t*BuBnPE-trithiocarbonate **12** and esterified with propargyl alcohol **13**, shown in Scheme 4.2. The alkyne-trithiocarbonate **14** was received from B. Schmidt (KIT).^{347,177} For the analytic data and experimental procedure please refer to “*Novel Macromolecular Architectures via a Combination of Cyclodextrin Host/Guest Complexation and RAFT Polymerization*” Schmidt, B. V. K. J, *Dissertation 2013*, KIT.



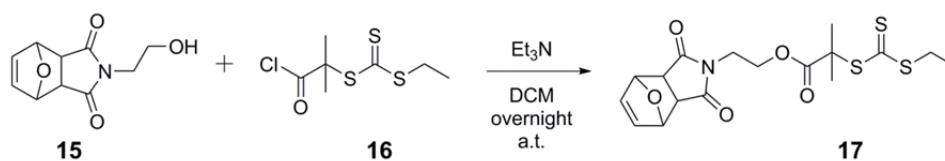
Scheme 4.2. Synthesis of prop-2-yn-1-yl 2-(((ethylthio)carbonothioyl)thio)-2-methyl-propanoate (alkyne-trithiocarbonate) **14**.^{177,347}

4.2.1.3 Synthesis of a Maleimide-Functionalized CTA

As counterpart for the light-induced PE Diels-Alder reaction, a maleimide-functionalized RAFT agent (Mal-trithiocarbonate) **17** was prepared (Scheme 4.3).^{††} The above synthesized EMP was transformed to the acid chloride **16**, employing oxalyl chloride and was subsequently esterified with the protected maleimide compound **15** without further purification. The synthesis of the protected maleimide-compound 2-(2-hydroxyethyl)-3a,4,7,7a-tetrahydro-1H-4,7-epoxyiso-indole-1,3(2H)-dione **15** was performed as described in the literature.³⁴⁸

^{††} The Mal-trithiocarbonate RAFT agent **17** was synthesized by T. Claus during her advanced lab-course under the supervision of B. Schmidt (Claus, T.; *Advance Lab-Course Report 2012*, KIT).

4. Complex Macromolecular Architectures



Scheme 4.3. Esterification reaction of a protected maleimide compound with a trithiocarbonate to obtain 2-(1,3-dioxo-1,3,3a,4,7,7a-hexahydro-2H-4,7-epoxyisoindol-2-yl)ethyl 2-(((ethylthio)carbonothioyl)thio)-2-methylpropanoate (Mal-trithiocarbonate) **17**.^{349,350,351}

The crude product **17** was purified via column chromatography and analyzed via ¹H NMR spectroscopy, shown in Figure 4.2. The spectrum shows the proton resonances of the furan protecting group (a, b), along with the resonances of the methylene spacer (c, d) and the ethyl resonances next to the trithiocarbonate (e, h).

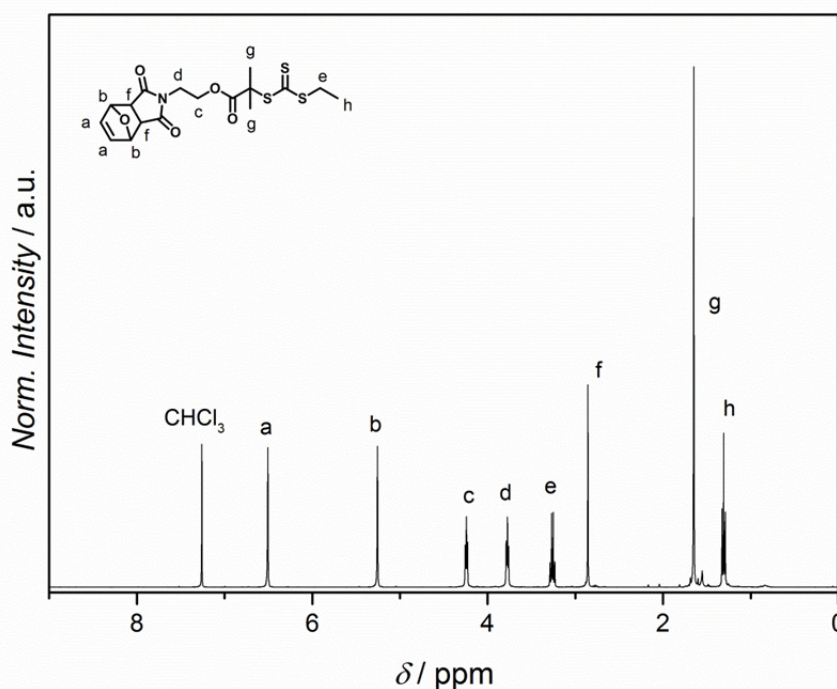
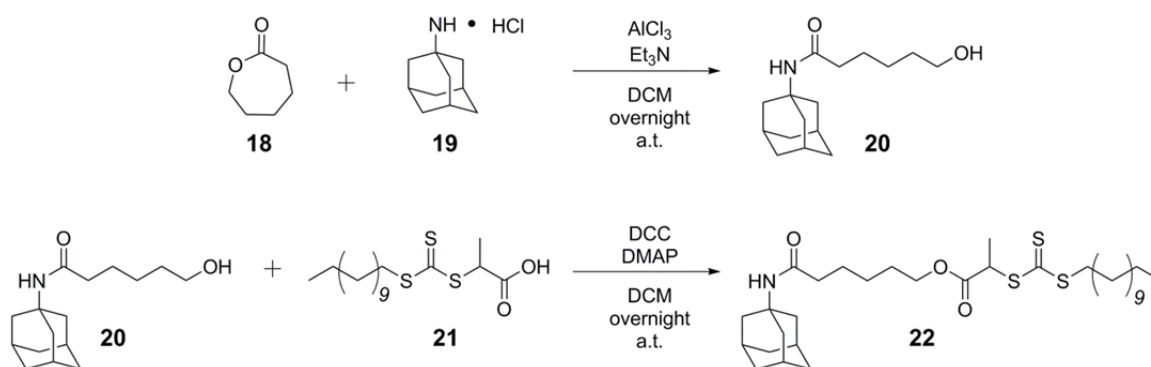


Figure 4.2. ¹H NMR (400 MHz, CDCl₃, 25 °C) spectrum of 2-(1,3-dioxo-1,3,3a,4,7,7a-hexahydro-2H-4,7-epoxyisoindol-2-yl)ethyl 2-(((ethylthio)carbonothioyl)thio)-2-methyl propanoate (Mal-trithiocarbonate) **17**. Reproduced with permission from the American Chemical Society, 2015 (DOI: 10.1021/acsmacrolett.5b00485).

4.2.1.4 Synthesis of an Adamantyl-Carrying CTA

In addition, a RAFT agent bearing an adamantyl molecule as an alternative guest for β -CD was synthesized. Hence, commercially available 2-(dodecylthiocarbonylthio)-propionic acid (DoPAT) (**21**) was coupled with the adamantane derivative **20**, employing DCC and DMAP. N-((3s,5s,7s)-adamantan-1-yl)-6-hydroxyhexanamide **20** was obtained in a ring opening amidation reaction with ϵ -caprolactone and 2-adamantylamine hydrochloride **19**.³⁵² A spacer was introduced to the adamantyl amine **19** to improve the accessibility of the adamantyl guest molecule for β -CD.



Scheme 4.4. Synthesis of the adamantyl-functionalized RAFT agent DoPAT-Ada **22**.

Figure 4.3 depicts the ^1H NMR spectrum of 6-(((3s,5s,7s)-adamantan-1-yl) amino)-6-oxohexyl 2-(((dodecylthio) carbonothioyl) thio) propanoate (DoPAT-Ada) **22** which was received as a yellow oil with yields of 70 % after purification via column chromatography. The proton resonances corresponding to the adamantyl unit are detected between 1.5 ppm - 2.0 ppm (f, g, h).

Consequently, a toolbox of CTAs was established for the development of multifunctional polymer blocks via RAFT-polymerization.

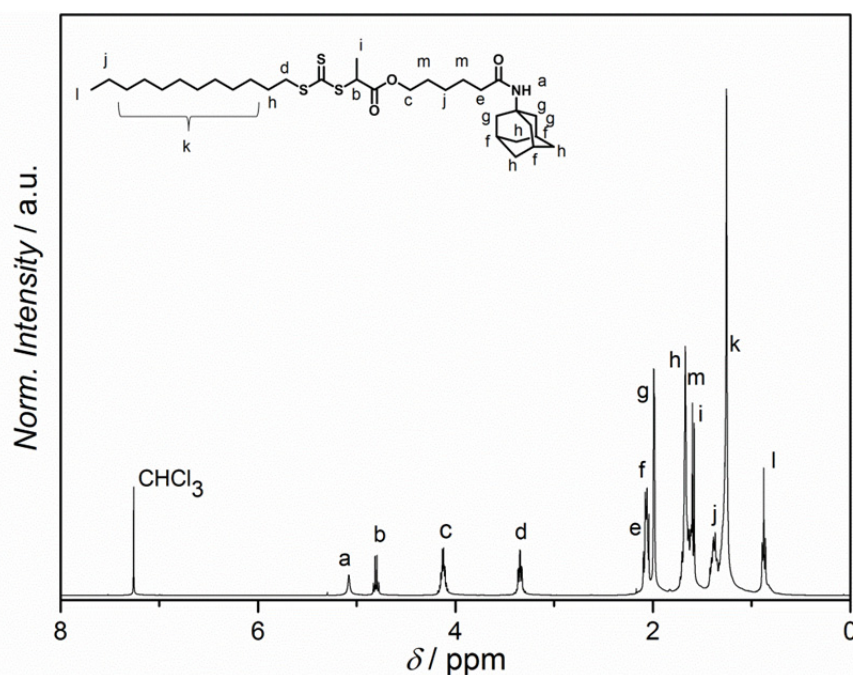


Figure 4.3. ^1H NMR (400 MHz, CDCl_3 , 25 $^\circ\text{C}$) spectrum of 6-(((3s,5s,7s)-adamantan-1-yl) amino)-6-oxohexyl 2-(((dodecylthio) carbonothioyl) thio) propanoate (DoPAT-Ada) (**22**). Reproduced with permission from the American Chemical Society, 2015 (DOI: 10.1021/acs.macromol.5b00923).

4.2.2 Generation of Multifunctional Polymeric Building Blocks

Concerning the development of multifunctional block copolymers, individual polymeric building blocks with functional chain-termini were prepared via RAFT polymerization, employing the RAFT agents described in section 4.2.1 (Figure 4.4).

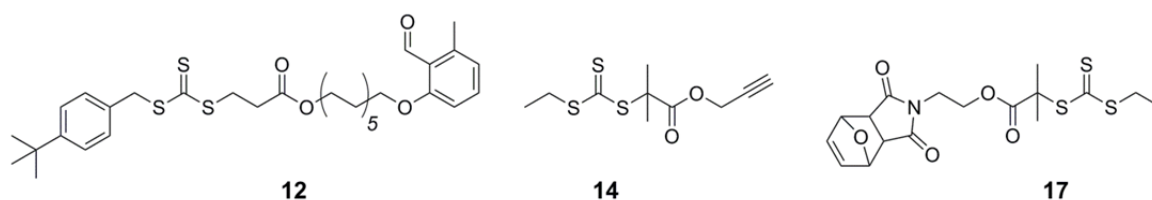
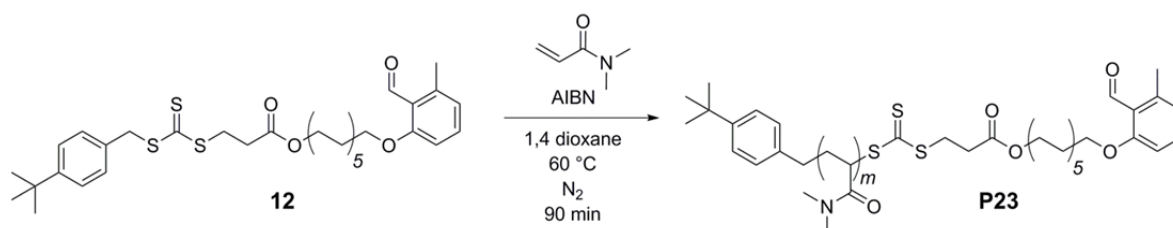


Figure 4.4. RAFT agents for the polymerization of multifunctional polymer blocks.

Water soluble acrylamide monomers were employed for the synthesis of the polymer blocks, since supramolecular host-guest interactions of β -CD are performed in aqueous solution.

4.2.2.1 α -*t*BuBn- ω -PE-Functionalized Polymer Center Block

Initially, an α,ω -functionalized polymeric center block was prepared in a RAFT polymerization of *N,N'*-dimethylacrylamide (DMAAm) with the *t*BuBnPE-trithiocarbonate **12** (Scheme 4.5).



Scheme 4.5. Synthetic route for poly(DMAAm)-*t*BuBnPE **P23**. Reproduced with permission from the American Chemical Society, 2015 (DOI: 10.1021/acsmacrolett.5b00485).

The polymerization was performed in 1,4-dioxane at 60 °C, with a ratio of *t*BuBnPE-trithiocarbonate **12** to the initiator (AIBN) of 10:1. After 90 min, the reaction mixture was quenched by cooling with liquid nitrogen, dialyzed against deionized water and lyophilized. Poly(DMAAm)-*t*BuBnPE **P23** was obtained as a yellowish solid and analyzed via SEC, ¹H NMR and ESI-MS. The ¹H NMR spectrum illustrated in Figure 4.5 (left) reveals the typical proton resonances ascribed to the poly(DMAAm) backbone between 1.2 ppm – 3.3 ppm together with the resonances of the chain termini, *tert*-butyl phenyl (7.31 ppm – 7.27 ppm) and PE (6.74 ppm – 6.69 ppm).

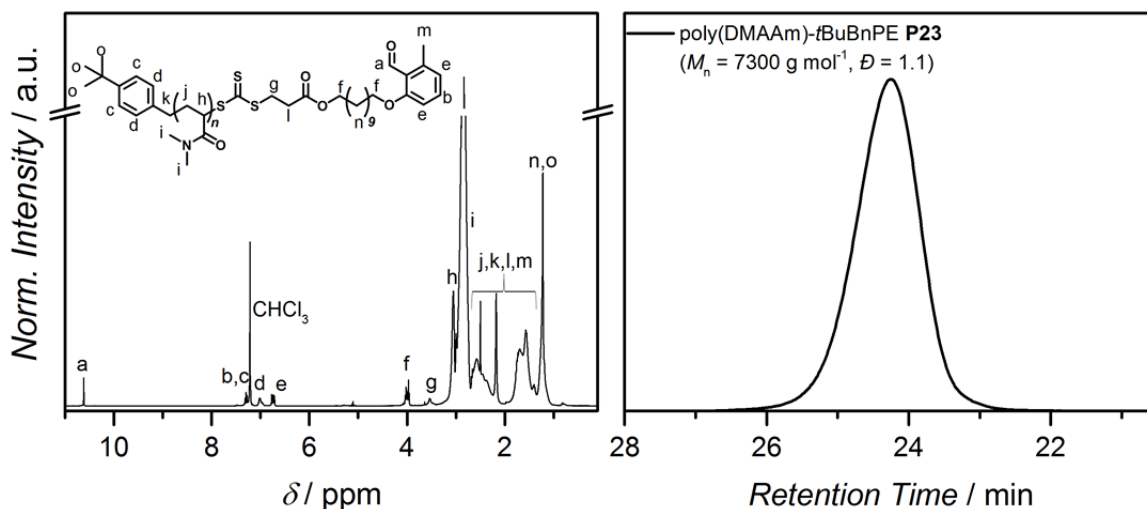


Figure 4.5. ¹H NMR (400 MHz, CDCl₃, 25 °C) spectrum and SEC trace of poly(DMAAm)-*t*BuBnPE (**P23**) measured in DMAC at 50 °C. The picture was modified with permission from the American Chemical Society, 2015 (DOI: 10.1021/acsmacrolett.5b00485).

The molecular weight distribution of poly(DMAAm)-*t*BuBnPE **P23** was determined via SEC (Figure 4.5, right) with an average M_n of 7300 g mol⁻¹ and \mathcal{D} of 1.1. The narrow size distribution and the low \mathcal{D} indicated the controlled character of the polymerization. In addition, a mass spectrum of **P23** was recorded which is shown in Figure 4.6. The spectrum displays the single, double and triple charged polymer chains of poly(DMAAm)-*t*BuBnPE. No side products could be detected in the mass spectrum, thus further confirming the successful polymerization with the *t*BuBnPE—trithiocarbonate **12**. Furthermore, Table 1 collates the exact masses of all assigned peaks in the mass range between 2200 – 2270 Da in excellent accordance with the calculated theoretical masses for **P23**.

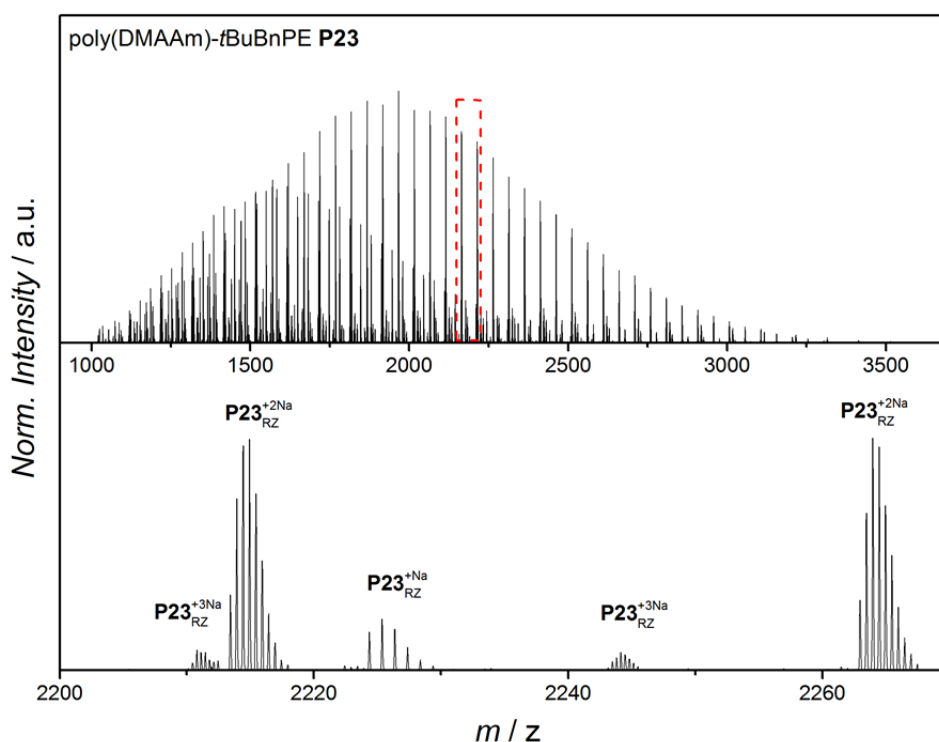


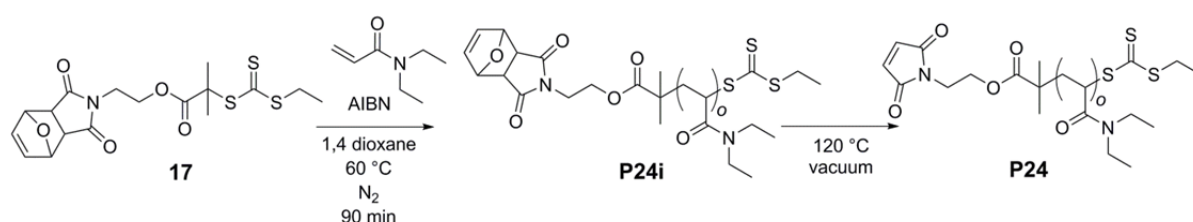
Figure 4.6. ESI-MS spectrum of poly(DMAAm)-*t*BuBnPE **P23** (above) and a magnification of the spectrum (below). The spectrum shows the single, double and triple charged polymer chains of the polymer **P23**, ionized with Na⁺. Reproduced with permission from the American Chemical Society, 2015 (DOI: 10.1021/acsmacrolett.5b00485).

Table 1. Mass peak assignment for poly(DMAAm)-*t*BuBnPE **P23**. Experimental and theoretical m/z values for the labelled peaks shown in Figure 4.6. Reproduced with permission from the American Chemical Society, 2015 (DOI: 10.1021/acsmacrolett.5b00485).

m/z_{exp}	assignment	chemical formula	m/z_{theo}	$\Delta m/z$
2211.129	p(DMAAm)- <i>t</i> BuBnPE + Na ₃	[C ₃₃₄ H ₅₈₈ N ₆₀ Na ₃ O ₆₄ S ₃] ³⁺	2211.119	0.01
2214.437	p(DMAAm)- <i>t</i> BuBnPE + Na ₂	[C ₂₂₄ H ₃₉₀ N ₃₈ Na ₂ O ₄₂ S ₃] ²⁺	2214.428	0.009
2225.365	p(DMAAm)- <i>t</i> BuBnPE + Na	[C ₁₁₄ H ₁₉₂ N ₁₆ NaO ₂₀ S ₃] ⁺	2225.358	0.007
2244.152	p(DMAAm)- <i>t</i> BuBnPE + Na ₃	[C ₃₃₉ H ₅₉₇ N ₆₁ Na ₃ O ₆₅ S ₃] ³⁺	2244.142	0.01
2263.970	p(DMAAm)- <i>t</i> BuBnPE + Na ₂	[C ₂₂₉ H ₃₉₉ N ₃₉ Na ₂ O ₄₃ S ₃] ²⁺	2263.962	0.008

4.2.2.2 Maleimide End-Functionalized Polymer Block

Next, a polymer block carrying a maleimide at the chain-terminus was synthesized (Scheme 4.6). Thus, *N,N'*-diethylacrylamide (DEAAm) was polymerized in the presence of the protected Mal-trithiocarbonate CTA **17** and AIBN (ratio 10:1) in 1,4 dioxane. The polymerization was quenched after 90 min and dialyzed against deionized water. In the subsequent step, the furan protecting group was removed from the maleimide by heating poly(DEAAm)-Mal-protc. **P24i** at 120 °C *in vacuo* overnight. The residue was dissolved in water, dialyzed once again and freeze-dried.



Scheme 4.6. Mal-trithiocarbonate **17** mediated RAFT-polymerization and subsequent removal of the furan protecting group in order to obtain poly(DEAAm)-Mal **P24**. The scheme was modified with permission from the American Chemical Society, 2015 (DOI: 10.1021/acsmacrolett.5b00485).

Figure 4.7 displays the ¹H NMR spectra (left) along with the SEC analyses (right) of poly(DEAAm)-Mal **P24** before and after the deprotection reaction. In comparison, the two proton NMR spectra evidenced the successful deprotection of the maleimide

via the disappearance of the furan protection group resonances at 6.51 ppm (a) and 5.26 ppm (b) in the spectrum of poly(DEAAm)-Mal-protc. **P24i** (above). In addition, the appearance of the maleimide double bond resonances at 6.71 ppm (a) in the spectrum of poly(DEAAm)-Mal **P24** (below) further proved the efficient deprotection of **P24i**. The SEC traces (Figure 4.7, right) of poly(DEAAm)-Mal-protc. **P24i** (red) ($M_{n,SEC} = 5400 \text{ g mol}^{-1}$, $\mathcal{D} = 1.2$) and poly(DEAAm)-Mal **P24** (black) ($M_{n,SEC} = 5600 \text{ g mol}^{-1}$, $\mathcal{D} = 1.2$) exhibit narrow size distributions referring to the controlled nature of the polymerization. Moreover, the traces are almost identical, showing no side- or coupling-products. The data corroborates the mild nature of the deprotection reaction, which was also confirmed via ESI-mass spectrometry.

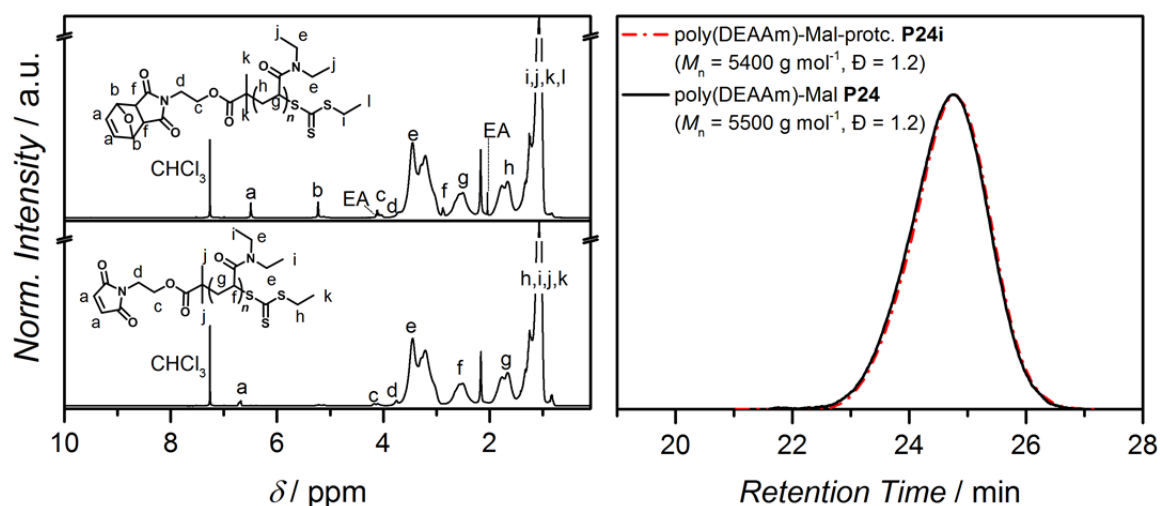


Figure 4.7. Right: ^1H NMR (400 MHz, CDCl_3 , 25 $^\circ\text{C}$) spectra of poly(DEAAm)-Mal-protc. **P24i** (above) and poly(DEAAm)-Mal **P24** (below). Left: The corresponding SEC traces measured in DMAC at 50 $^\circ\text{C}$. The picture was modified with permission from the American Chemical Society, 2015 (DOI: 10.1021/acsmacrolett.5b00485).

The ESI-MS spectrum of poly(DEAAm)-Mal **P24** is illustrated in Figure 4.8, revealing the single and doubled charged polymer chains of **P24**. As compared to the mass spectrum of the protected species **P24i** (shown in Appendix B, Figure B.2 and Table B.1), a clear shift of the mass peaks **P24** is observed. No remaining protected polymer chains were found in the spectrum of **P24** as well as no side-products. The assignment of the mass peaks shown in the magnification of the mass spectrum (Figure 4.8, below) are listed in Table 2. Here, as well as for poly(DMAAm)-*t*BuBnPE center block polymer (described in section 4.2.2.1), the experimentally found mass peaks were in very good agreement with the theoretical mass values.

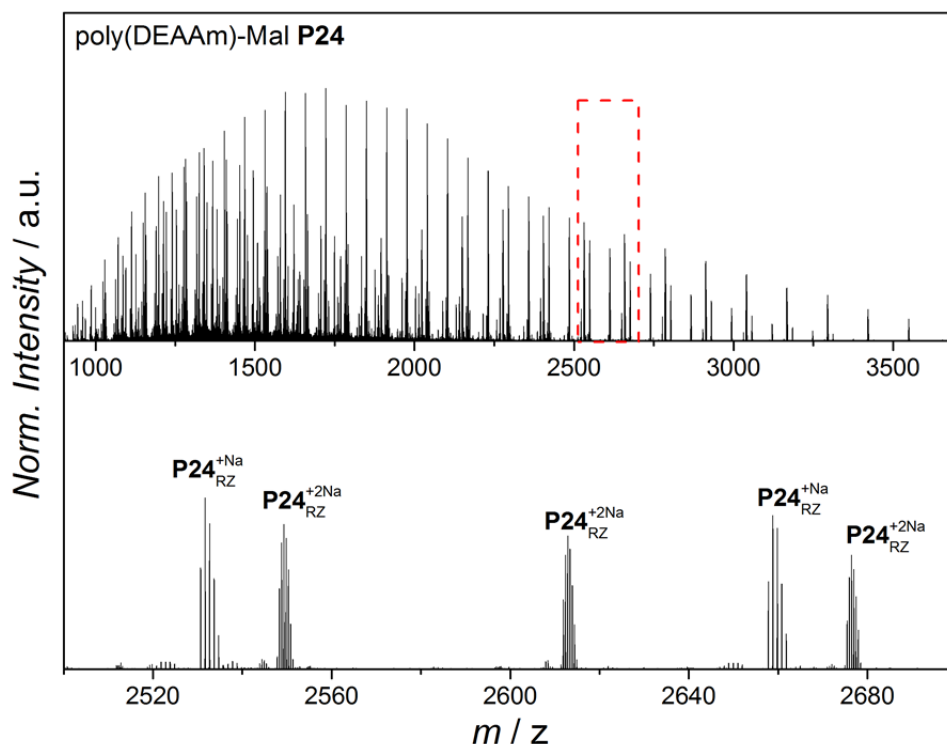


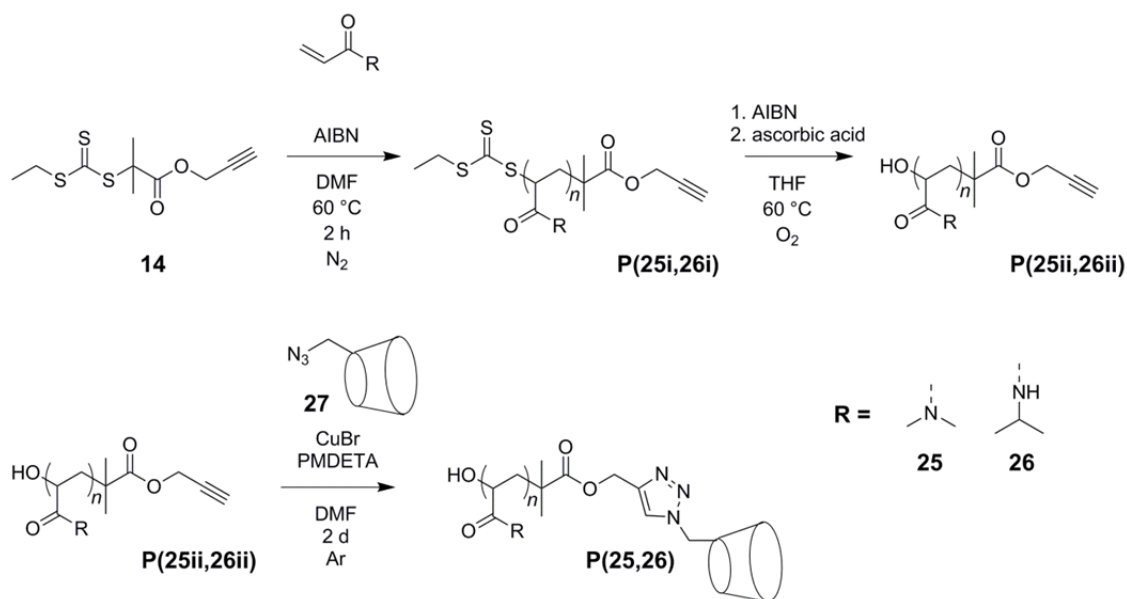
Figure 4.8. ESI-MS spectrum of poly(DEAAm)-Mal **P24** and a magnification of the spectrum (below). The spectrum shows the single and double charged polymer chains of **P24** ionized with Na^+ . Reproduced with permission from the American Chemical Society, 2015 (DOI: 10.1021/acsmacrolett.5b00485).

Table 2. Mass peak assignment for poly(DEAAm)-Mal **P24**. Experimental and theoretical m/z values for the labelled peaks shown in Figure 4.8. Reproduced with permission from the American Chemical Society, 2015 (DOI: 10.1021/acsmacrolett.5b00485).

m/z_{exp}	assignment	chemical formula	m/z_{theo}	$\Delta m/z$
2531.732	p(DEAAm)-Mal + Na	$[\text{C}_{132}\text{H}_{238}\text{N}_{18}\text{NaO}_{21}\text{S}_3]^+$	2531.719	0.013
2549.365	p(DEAAm)-Mal + Na_2	$[\text{C}_{272}\text{H}_{498}\text{N}_{38}\text{Na}_2\text{O}_{41}\text{S}_3]^{2+}$	2549.355	0.01
2612.915	p(DEAAm)-Mal + Na_2	$[\text{C}_{279}\text{H}_{511}\text{N}_{39}\text{Na}_2\text{O}_{42}\text{S}_3]^{2+}$	2612.905	0.01
2658.832	p(DEAAm)-Mal + Na	$[\text{C}_{139}\text{H}_{251}\text{N}_{19}\text{NaO}_{22}\text{S}_3]^+$	2658.819	0.013
2676.467	p(DEAAm)-Mal + Na_2	$[\text{C}_{286}\text{H}_{524}\text{N}_{40}\text{Na}_2\text{O}_{43}\text{S}_3]^{2+}$	2676.454	0.013

4.2.2.3 β -Cyclodextrin Functionalized Polymer Blocks

In addition, polymer blocks of poly(DMAAm) and poly(*N*-isopropylacrylamide) (poly(NiPAAm)) were prepared and equipped with a β -CD host molecule. The overall synthetic strategy is shown in Scheme 4.7.



Scheme 4.7. Synthetic strategy for the preparation of β -CD equipped polymer blocks.##

In general, the alkyne-trithiocarbonate **14** was employed in the controlled polymerization of DMAAm and NiPAAm. Both polymerization reactions proceeded in DMF at 60 °C. The exact reaction conditions are summarized in the experimental section (4.4.4). Thus, alkyne end-functionalized poly(DMAAm) **P25i** ($M_{n,SEC} = 10100 \text{ g mol}^{-1}$, $D = 1.1$) and poly(NiPAAm) **P26i** ($M_{n,SEC} = 8800 \text{ g mol}^{-1}$, $D = 1.1$) were obtained and analyzed via SEC and NMR (Appendix B, Figure B.3 and Figure B.4: 1H NMR and Figure B.5: SEC traces). The alkyne end-group of the thus generated polymers can be further modified via the conjugation of any desired functionality. Subsequent to the polymerization, the trithiocarbonate was cleaved from the polymer chains and transformed into a hydroxyl function. Therefore, poly(DMAAm)-alkyne **P25i** and poly(NiPAAm)-alkyne **P26i** respectively were dissolved in THF at 60 °C and AIBN was added. Under vigorous stirring in the

The β -CD functionalized polymer blocks were provided by B. Schmidt.

presence of ambient oxygen the reaction continued until complete discoloration of the slightly yellow solution, which indicated full conversion. Via the addition of ascorbic acid the generated hydroperoxide-functional polymers were reduced to the hydroxyl-functionalized polymers **P25ii** and **P26ii**. The NMR spectrum and the SEC traces for alkyne-poly(DMAAm)-OH **P25ii** are depicted in Figure 4.9 and Figure 4.10 the analytical data for **P26ii** is comprised in Appendix B, Figure B.4 and Figure B.5. After the transformation mechanism – which was described in detail by Dietrich *et al.*³⁴⁰ – the SEC traces of the hydroxyl terminated polymers revealed shoulders in the higher molecular weight region, exemplarily shown in Figure 4.10 for poly(DMAAm).

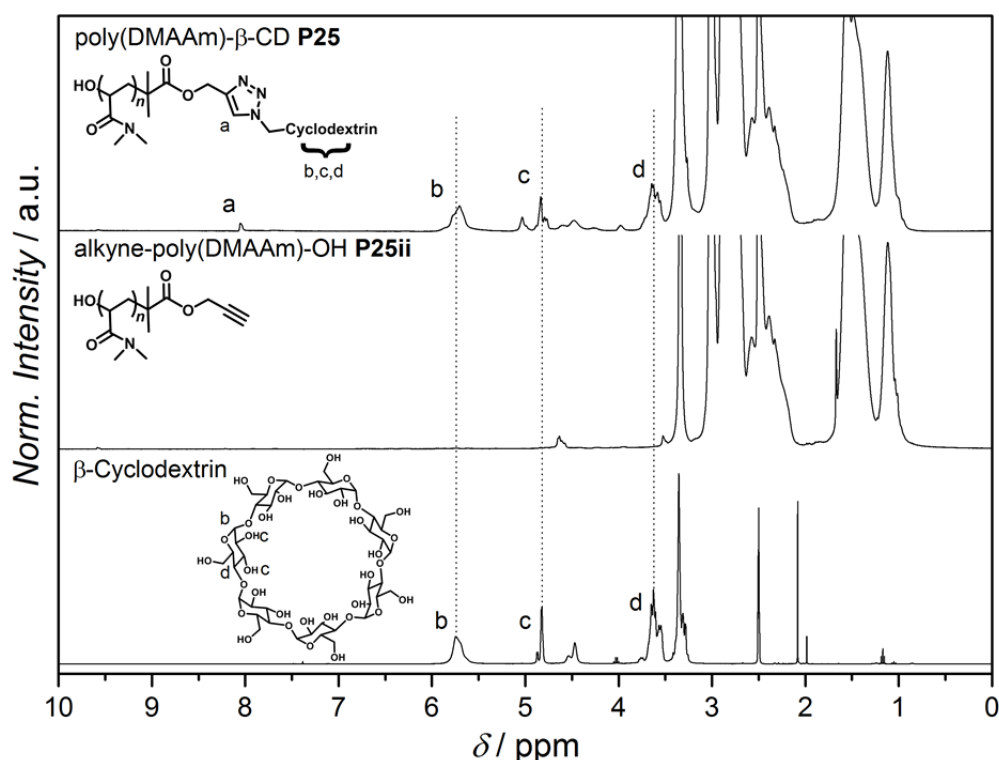


Figure 4.9. ¹H NMR (400 MHz, DMSO-*d*₆, 25 °C) spectra collection of pure β-CD (bottom), alkyne-poly(DMAAm)-OH **P25ii** (center) and poly(DMAAm)-β-CD **P25** (top), showing the successful end-group modification sequence. Reproduced with permission from the American Chemical Society, 2015 (DOI: 10.1021/acs.macromol.5b00923).

The shoulder likely resulted from heating the alkyne polymer in the presence of AIBN, which led to small amounts of coupling products. The transformation of the trithiocarbonate was performed in order to introduce the β-CD host molecule via copper catalyzed azide alkyne cycloaddition (CuAAC). It was previously noted that the CuAAC reactions proceed in a more effective manner without the RAFT

groups.³⁵³ Finally, the azide-functionalized β -CD host molecule **27** was *clicked* to the alkyne chain-termini of alkyne-poly(DMAAm)-OH **P25ii** and alkyne-poly(NiPAAm)-OH **P26ii** with CuBr and PMDETA, resulting in poly(DMAAm)- β -CD **P25** ($M_{n,sec} = 10700 \text{ g mol}^{-1}$, $\mathcal{D} = 1.3$) and poly(NiPAAm)- β -CD **P26** ($M_{n,sec} = 8800 \text{ g mol}^{-1}$, $\mathcal{D} = 1.2$). An overview following the end-group modification with β -CD is depicted in the NMR spectra collection in Figure 4.9. The NMR spectra are shown for poly(DMAAm) and the corresponding spectra and SEC traces for poly(NiPAAM) can be found in Appendix B (Figure B.4 and Figure B.5). The spectra illustrated in Figure 4.9 of pure β -CD (bottom), alkyne-poly(DMAAm)-OH **P25ii** (center) and poly(DMAAm)- β -CD **P25** (top) confirmed the successful synthetic sequence by the appearance of the proton resonances of the triazole-*click* product at 8.05 ppm (a) in the spectrum of **P25**. Furthermore, the inner and outer proton resonances of the β -CD guest group at 5.71, 4.83 and 3.64 ppm (b,c,d) were detected in the ^1H NMR spectrum of poly(DMAAm)- β -CD **P25**. The corresponding SEC trace of poly(DMAAm)- β -CD is illustrated in Figure 4.10.

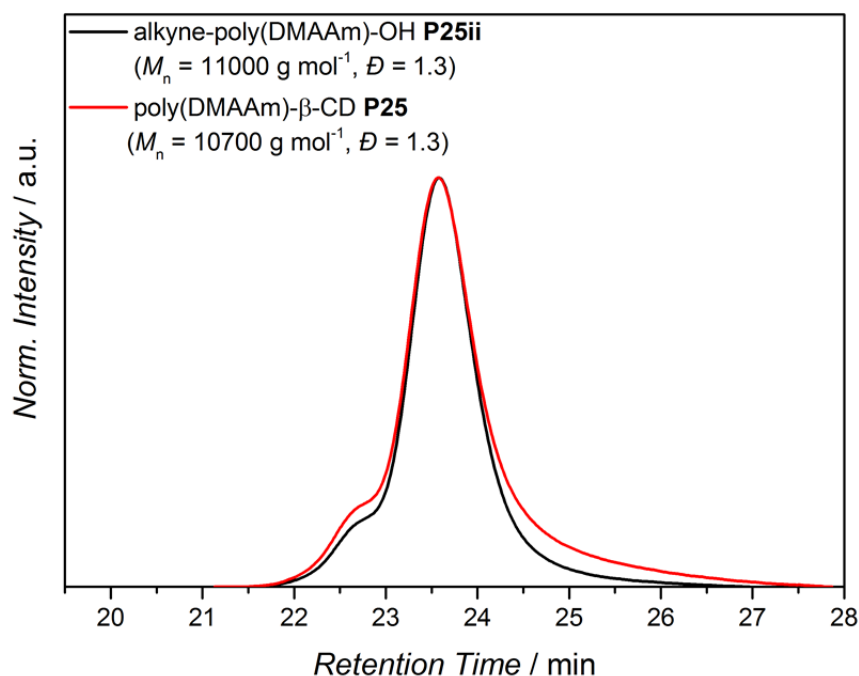
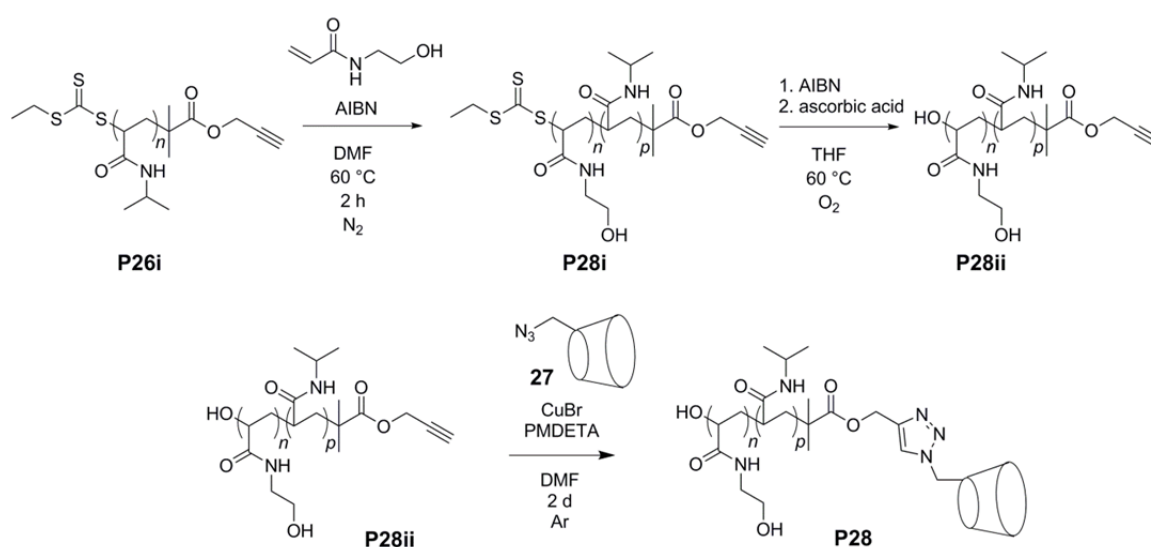


Figure 4.10. SEC trace of alkyne-poly(DMAAm)-OH **P25ii** and poly(DMAAm)- β -CD **P25** measured in DMAC at 50 °C. The picture was modified with permission from the American Chemical Society, 2015 (DOI: 10.1021/acsmacrolett.5b00485).

Furthermore, a polymer chain extension of poly(NiPAAm)-alkyne **P26i** with *N*-hydroxyethylacrylamide (HOEAAM) was performed, resulting in an alkyne

functionalized diblock copolymer poly(NiPAAm)-*b*-poly(HOEAAM)-alkyne **P28i** (Scheme 4.8). The diblock copolymer **P28i** was further transformed in the hydroxyl-functionalized alkyne-poly(NiPAAm)-*b*-poly(HOEAAM)-OH **P28ii** which was then conjugated with β -CD-azide **27** as previously described for **P25** and **P26**. The ^1H NMR spectra and the SEC traces before and after the chain extension of poly(NiPAAm)-alkyne **P26i** are shown in Figure 4.11. The analytical data of the final β -CD polymer **P28** and the precursor polymer **P28ii** are collected in Appendix B, Figure B.6.



Scheme 4.8. Chain extension of poly(NiPAAm)-alkyne **P26i** with HOEAAM, hydroxyl transformation of the trithiocarbonate of the diblock copolymer **P28i** and further conjugation with β -CD azide **27**.

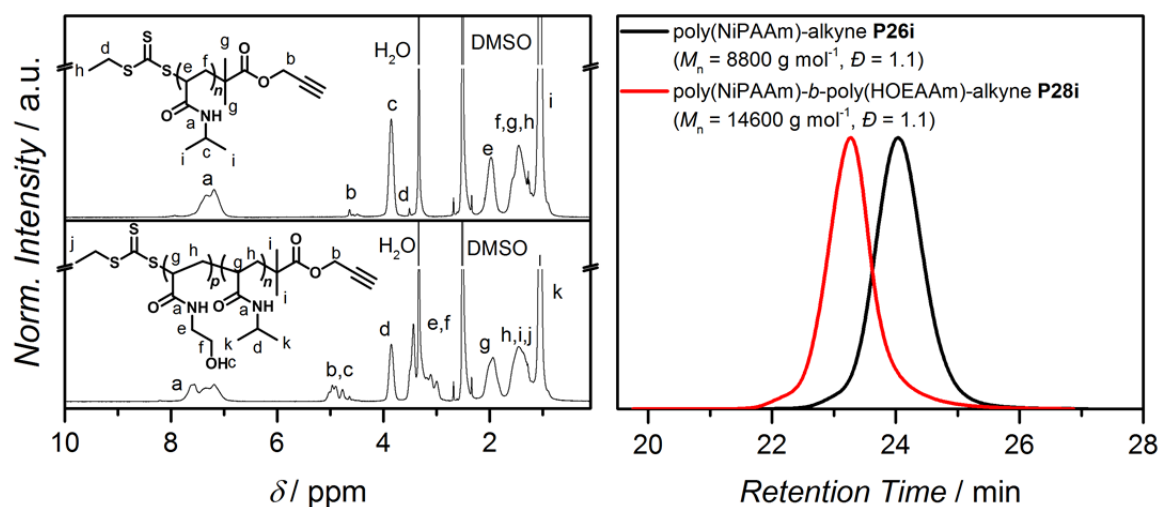
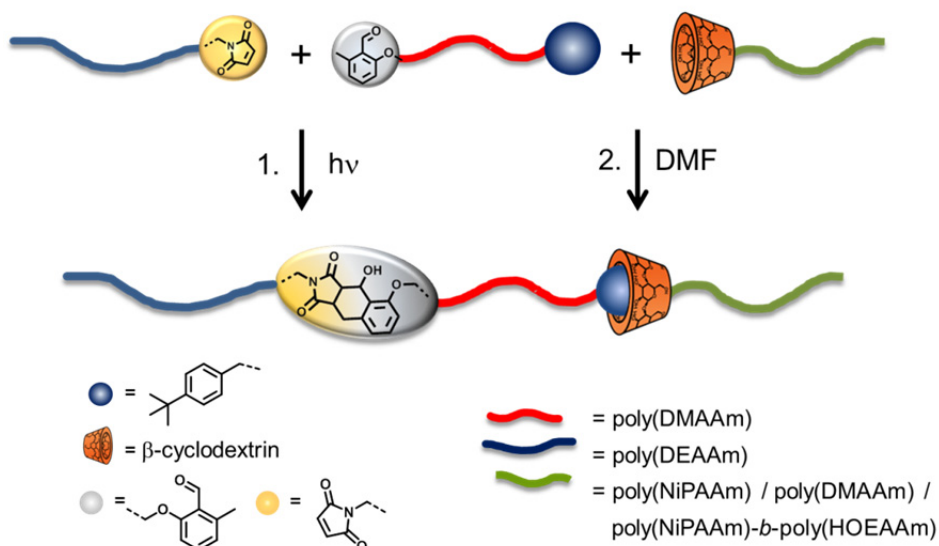


Figure 4.11. ^1H NMR (400 MHz, $\text{DMSO}-d_6$, 25 °C) spectra (left) of poly(NiPAAm)-alkyne **P26i** (top) and poly(NiPAAm)-*b*-poly(HOEAAM)-alkyne **P28i** (bottom). SEC traces (right) of **P26i** (black) and **P28i** (red) measured in DMAC at 50 °C. The picture was modified with permission from the American Chemical Society, 2015 (DOI: 10.1021/acsmacrolett.5b00485).

4.2.3 Modular Ligation of Polymer Chains to Multiblock Copolymers

In section 4.2.2 the syntheses of various polymer blocks with individual functional chain-termini was described. In the following, the assembly of the single polymer chains to di-, tri- and tetrablock copolymers is outlined, along with a detailed characterization. Scheme 4.9 illustrates the overall strategy for the orthogonal formation of multiblock copolymers.

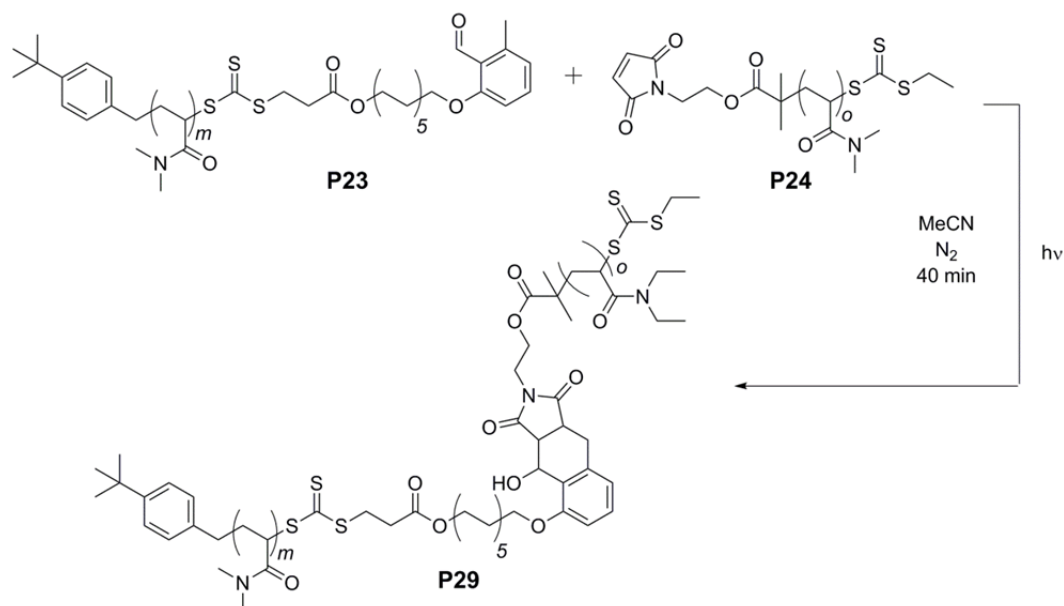


Scheme 4.9. Outline of the multiblock copolymer formation approach followed in the current section. Reproduced with permission from the American Chemical Society, 2015 (DOI: 10.1021/acsmacrolett.5b00485).

At first a diblock is formed via the light-induced reaction of the PE chain-terminus of an α,ω -functionalized center block with the maleimide end-group of a second polymer block. Subsequently, the freshly formed diblock copolymer is employed in the supramolecular self-assembly of the remaining guest molecule at its α -chain-end with the β -CD host unit of a third polymer block. For both ligation reactions no additives such as coupling compounds or initiators were necessary, which is the reason they are highly attractive conjugation techniques.

4.2.3.1 Light-Induced Diblock Copolymer Formation

By means of the photo-induced Diels–Alder reaction, the α -*t*BuBn- ω -PE-functionalized poly(DMAAm) center block **P23** was conjugated with poly(DEAAm)-Mal **P24**. Therefore, the polymer blocks were dissolved in acetonitrile (MeCN) in stoichiometric amounts at a low concentration (5 mg mL^{-1}). Then, the solution was filled into headspace vials, crimped airtight with a SBR seal with PTFE inlet and placed into the photoreactor (Figure A5). The mixture was purged with nitrogen for 15 min to remove the oxygen. Following this, the sample was irradiated with a compact low-pressure fluorescent lamp (Arimed B6, 36 W) at 320 nm for 40 min. Figure B.7 in Appendix B depicts the UV-vis spectrum of the *t*BuBnPE-trithiocarbonate **12** in MeCN and the emission spectrum of the employed lamp. During irradiation the PE forms a reactive diene, which undergoes a DA reaction with the maleimide, as already described in the theoretical background in section 2.1.2.



Scheme 4.10. Light-induced diblock copolymer formation. Reproduced with permission from the American Chemical Society, 2015 (DOI: 10.1021/acsmacrolett.5b00485).

Afterwards, the sample was immediately analyzed via NMR spectroscopy (Figure B.8, Appendix B), SEC and ESI-MS (Figure 4.12). The SEC traces of poly(DEAAm)-Mal **P24** (black trace), poly(DMAAm)-*t*BuBnPE **P23** (red trace) and poly(DMAAm)-*b*-poly(DEAAm) **P29** revealed a shift to lower retention time after the diblock

copolymer formation, indicating the success of the ligation reaction. The diblock formation was further confirmed by the disappearance of the SEC traces of **P23** and **P24**. However, due to the loss of end-group fidelity during the RAFT polymerization, a slight shoulder remained in the SEC trace of the diblock copolymer **P29**. The reduced end-group fidelity of the RAFT polymerization results from the rather slow decomposition of the AIBN initiator, which can replace the RAFT end-group of some polymer chains.^{354,355} Additionally, the ESI-MS spectra (Figure 4.12 left) of the three polymer compounds **P24** (black), **P23** (red) and **P29** (blue) indicate a clear shift to higher m/z for the diblock copolymer **P29**, confirming the effective ligation. In analogy with the SEC measurement, the mass spectrum of poly(DMAAm)-*b*-poly(DEAAm) **P29** shows small traces of the starting materials **P24** and **P23**. The specific mass peak assignments of poly(DMAAm)-*t*BuBnPE **P23** (Figure 4.6 Table 1) and poly(DEAAm)-Mal **P24** (Figure 4.8 Table 2) were already depicted in Section 4.2.2. The assignment for the mass spectrum of the diblock copolymer can be found in Appendix B, Figure B.9 and Table B.2. Moreover, DLS measurements of the water soluble polymer chains were performed, which are shown in Figure B.10 and additionally confirm the photo-induced ligation reaction via the shift to higher hydrodynamic radii for the diblock copolymer **P29**.

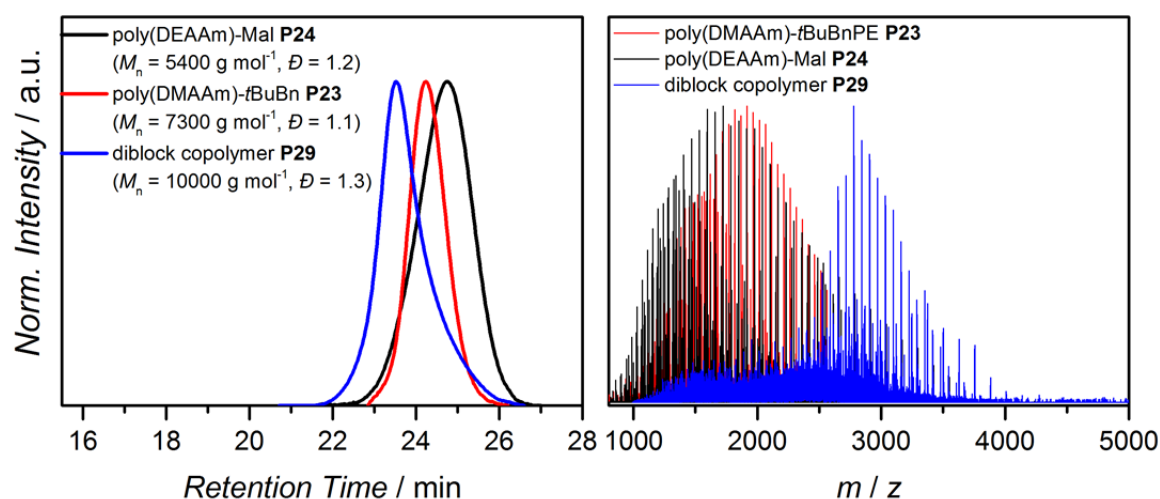
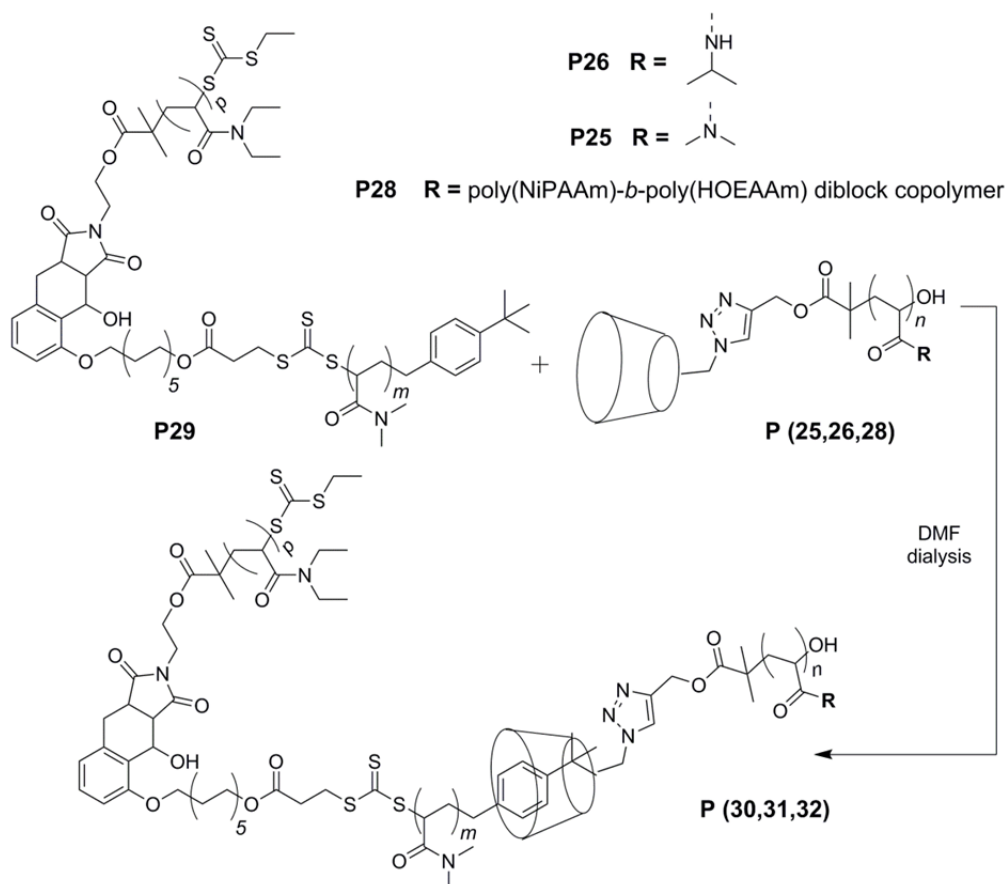


Figure 4.12. Left: SEC traces of poly(DEAAm)-Mal **P24** (black), poly(DMAAm)-*t*BuBnPE **P23** (red) and the diblock copolymer **P29** (blue) recorded in DMAC at 50 °C. Right: ESI-MS spectra of poly(DEAAm)-Mal **P24** (black), poly(DMAAm)-*t*BuBnPE **P23** (red) and the diblock copolymer **P29** (blue). The picture was modified with permission from the American Chemical Society, 2015 (DOI: 10.1021/acsmacrolett.5b00485).

4.2.3.2 Supramolecular Tri- and Tetrablock Copolymer Formation

Supramolecular host-guest interactions of β -CD with corresponding guest molecules, e.g. *tert*-butyl phenyl or adamantane, have been widely employed for the construction of complex polymer architectures with non-covalent conjunctions.^{343,341,356} Due to the dynamic nature of the supramolecularly formed bond, the linkage is responsive to external triggers such as pH,³⁵⁷ light,^{334,358} redox³⁵⁹ or temperature.^{334,360} In this way, supramolecularly bonded polymers can either be exchanged or completely removed, which results in a multitude of possible applications for the development of smart materials.

Scheme 4.11 displays the formation of supramolecularly connected tri- and tetrablock copolymers with the Diels-Alder product **P29**, utilizing the β -CD equipped polymers poly(NiPAAm)- β -CD **P26**, poly(DMAAm)- β -CD **P25** and the diblock copolymer poly(NiPAAm)-*b*-poly(HOEAAM)- β -CD **P28**, which were described in section 4.2.2.



Scheme 4.11. Supramolecular tri- and tetrablock copolymer formation with poly(NiPAAm)- β -CD **P26**, poly(DMAAm)- β -CD **P25** and poly(NiPAAm)-*b*-poly(HOEAAM)- β -CD **P28**. Reproduced with permission from the American Chemical Society, 2015 (DOI: 10.1021/acsmacrolett.5b00485).

In order to form the supramolecular complex between the remaining *tert*-butyl benzyl guest molecule at the α -chain end of poly(DMAAm)-*b*-poly(DEAAm) **P29**, the diblock was dissolved in DMF and mixed with equimolar solutions of the β -CD-functionalized polymers in separate vials. The mixtures were stirred at ambient temperature for 30 min and subsequently dialyzed against deionized water. Since DMF is a non-selective solvent for all employed polymer blocks, the guest molecule is better accessible in DMF than in water. Via the slow exchange of the solvent the supramolecular inclusion complex is formed. After lyophilization the supramolecular multiblock copolymers **P30**, **P31** and **P32** were analyzed via DLS and nuclear Overhauser effect spectroscopy (NOESY). Figure 4.13 outlines the analytical data of the ABC triblock copolymer poly(NiPAAm)-*b*-poly(DMAAm)-*b*-poly(DEAAm) **P30** (top), the AAB triblock copolymer poly(DMAAm)-*b*-poly(DMAAm)-*b*-poly(DEAAm) **P31** (center) and the ABCD tetrablock copolymer poly(NiPAAm)-*b*-poly(HOEAAm)-*b*-poly(DMAAm)-*b*-poly(DEAAm) **P32** (bottom). All DLS measurements showed a shift to higher hydrodynamic radii after the addition of the β -CD blocks (**P25**, **P26**, **P28**) to the diblock copolymer **P29**, which indicated the formation of the supramolecular bond. Furthermore, the NOESY measurements of the three compounds (**P30**, **P31**, **P32**) revealed cross correlation peaks between the inner protons of β -CD at 3.10 ppm, 3.34 ppm and 3.60 ppm and the protons of the *tert*-butyl phenyl guest unit at 6.90 ppm and 7.10 ppm. NOESY records the homo nuclear correlation of protons in close proximity and thus provides evidence for the host-guest interactions. In addition, correlation between the phenyl ring (6.90 ppm and 7.10 ppm) and the methyl protons of the *tert*-butyl group (1.86 ppm) were detected as well.

According to all analytical evidence the successful formation of partly covalent and partly supramolecularly connected multiblock copolymers via the modular ligation of functionalized polymer blocks was demonstrated. The following presents the construction of even more complex architectures via the combination of photo-induced Diels-Alder reactions and the supramolecular host-guest interactions of β -CD.

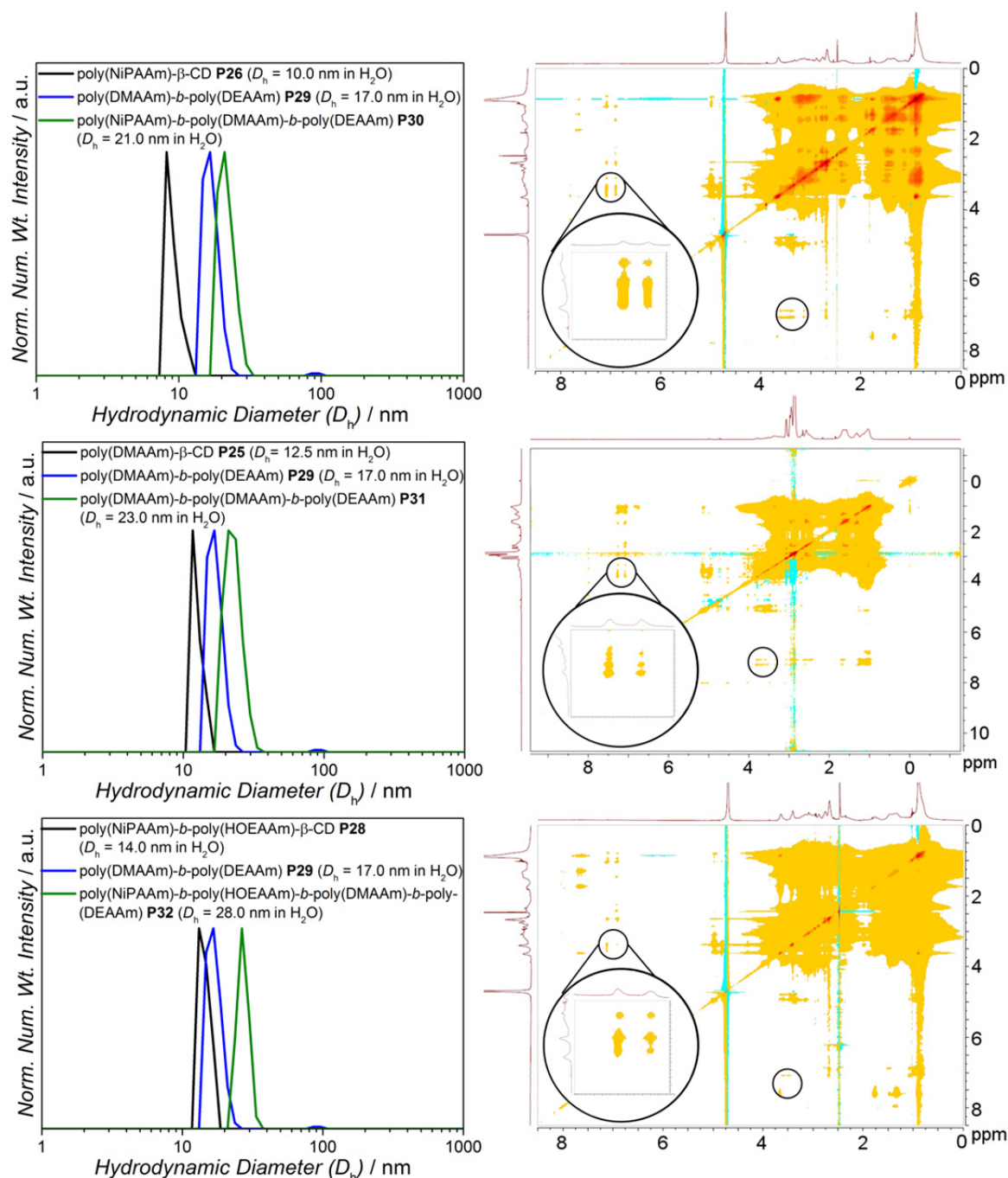
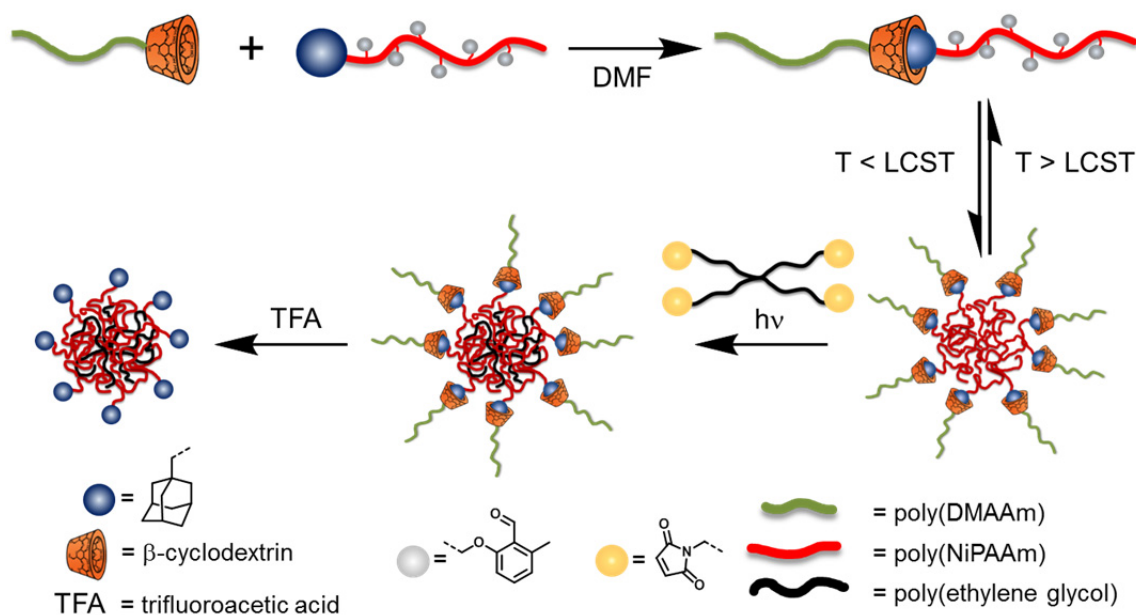


Figure 4.13. NOESY and DLS measurements of the supramolecularly formed ABC, AAB and ABCD block copolymers. Top) ABC triblock copolymer poly(NiPAAm)-*b*-poly(DMAAm)-*b*-poly(DEAAm) P30. Center) AAB triblock copolymer poly(DMAAm)-*b*-poly(DMAAm)-*b*-poly(DEAAm) P31. Bottom) ABCD tetrablock copolymer poly(NiPAAm)-*b*-poly(HOEAAm)-*b*-poly(DMAAm)-*b*-poly(DEAAm) P32. The NOESY spectra reveal cross-correlations peaks of the inner protons of β -CD (3.10 ppm, 3.34 ppm and 3.60 ppm) with the aromatic protons of the *tert*-butyl phenyl guest unit (6.90 ppm and 7.10 ppm). DLS measurements were performed in water with a concentration of 0.06 mmol L⁻¹. The picture was modified with permission from the American Chemical Society, 2015 (DOI: 10.1021/acsmacrolett.5b00485).

4.2.4 Development of Thermoresponsive Nanoparticles from Complex Macromolecular Architectures

Modular ligated di- and triblock copolymers often find application for the generation of micelles and nanoparticles.^{361,362} Such micelles and nanoparticles can serve as nanoreactors,^{363,364} microelectronic sensors,^{365,366,367} drug delivery systems,^{368,369,370} or molecular imaging agents.^{371,372,373} Especially, nanoparticles, which react to an external stimulus, e.g. temperature,^{374,335,375} light,^{335,376,377} pH^{378,379} or voltage,³⁶² are of great scientific interest.

Thus, the efficiency of supramolecular host-guest interaction in combination with light-induced chemistry was examined in the context of thermoresponsive nanoparticle formation. Scheme 4.12 outlines the overall strategy for the development of thermoresponsive nanoparticles.



Scheme 4.12. Outline of the thermoresponsive nanoparticle formation via a sacrificial micellization approach. The picture was modified with permission from the American Chemical Society, 2015 (DOI: 10.1021/acs.macromol.5b00923).

To begin with, a supramolecular diblock copolymer is formed via the complexation of the β -CD-host molecule attached to a polymer chain with an adamantyl-guest group of a second polymer chain. The adamantyl-functionalized polymer block has

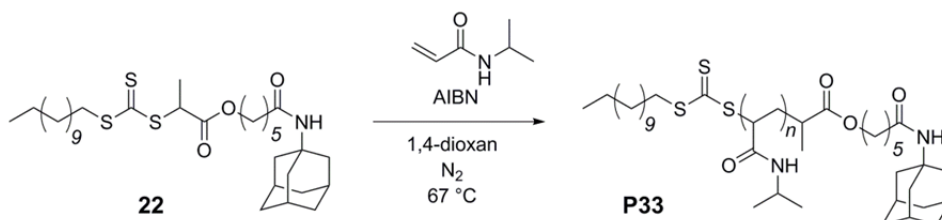
thermoresponsive features and additional photoactive PE units incorporated in its side chain. After the supramolecular copolymer formation, the diblock undergoes micellization when heated above the lower critical solution temperature (LCST) of the thermoresponsive block. Subsequently, the micelle is cross-linked in its core via the addition of a linking molecule, which reacts with the PE units under the irradiation with UV light. Finally, the nanoparticle is released from the micellar scaffold by the removal of the β -CD-functionalized arms.

4.2.4.1 Preparation of the Thermoresponsive Guest-Bearing Polymer Block

For the preparation of the thermoresponsive guest-bearing polymer block, the DoPAT-Ada CTA **22**, which was described in section 4.2.1 was employed for the RAFT polymerization of NiPAAm. Similar to *tert*-butyl phenyl, adamantane forms strong inclusion complexes with β -CD. With complexing constants up to 10^5 M^{-1} ,³⁸⁰ the adamantyl/ β -CD complex is even stronger than the *t*BuPh/ β -CD complex, which makes it more robust for the several reaction steps in the development of the nanoparticles. NiPAAm is well known for its thermoresponsive features^{381,382} and frequently employed in the generation of stimuli responsive materials.^{383,384,385} Moreover, the LCST of NiPAAm can be fine-tuned via its chain length or the copolymerization with other water soluble monomers (e.g. DMAAm or DEAAm). In order to adjust the thermoresponsive polymer block to a certain chain length, a kinetic investigation of the RAFT polymerization with DoPAT-Ada **22** was performed.

Kinetic Study of the DoPAT-Ada Mediated RAFT Polymerisation of NiPAAM

The kinetic study of the DoPAT-Ada **22** mediated RAFT polymerization of NiPAAm (Scheme 4.13) was carried out in 1,4-dioxane at a reaction temperature of 67 °C. Oxygen was removed from the reaction mixture via three freeze-pump-thaw cycles, prior to the polymerization. During a total polymerization time of 220 min, samples were drawn at preset time intervals via a degassed syringe. Exact concentrations of the polymerization solution are collated in Table 3.



Scheme 4.13. Kinetic investigation of the DoPAT-Ada **22** mediated polymerization of NiPAAm.

Subsequently, the samples were analyzed by ^1H NMR spectroscopy to deduce the conversion of poly(NiPAAm) via the integration of the vinyl proton resonances against the backbone resonances of the polymer, which decrease with increasing conversion. SEC measurements of the samples provided the experimental molecular weight distribution ($M_{n \text{ exp}}$), which were plotted against conversion, shown in Figure 4.14A. The plot $M_{n \text{ exp}}$ versus conversion showed linear behavior, thus confirming the living character of the polymerization. In addition, ESI-MS was recorded of selected polymer samples after precipitation (Figure 4.14C,D). The mass spectra featured a clean RAFT-controlled polymer distribution without further side products. The assignments of the mass peaks shown in Figure 4.14D are listed in Table 4.

Table 3 Reaction conditions for the DoPAT-Ada **22** mediated polymerization of NiPAAm in 1,4-dioxane as well as the calculated number average molecular weight based on 100% conversion ($M_{n \text{ theo}}$). c_{Mon}^0 is the concentration of the monomer, c_{CTA}^0 is the concentration of DoPAT-Ada and c_{AIBN}^0 is the initial AIBN concentration. Reproduced with permission from the American Chemical Society, 2015 (DOI: 10.1021/acs.macromol.5b00923).

c_{Mon}^0 [mmol L $^{-1}$]	c_{CTA}^0 [mmol L $^{-1}$]	c_{AIBN}^0 [mmol L $^{-1}$]	T [°C]	$M_{n \text{ theo}}$ [g mol $^{-1}$]
1841.05	86.73	8.67	67	3000

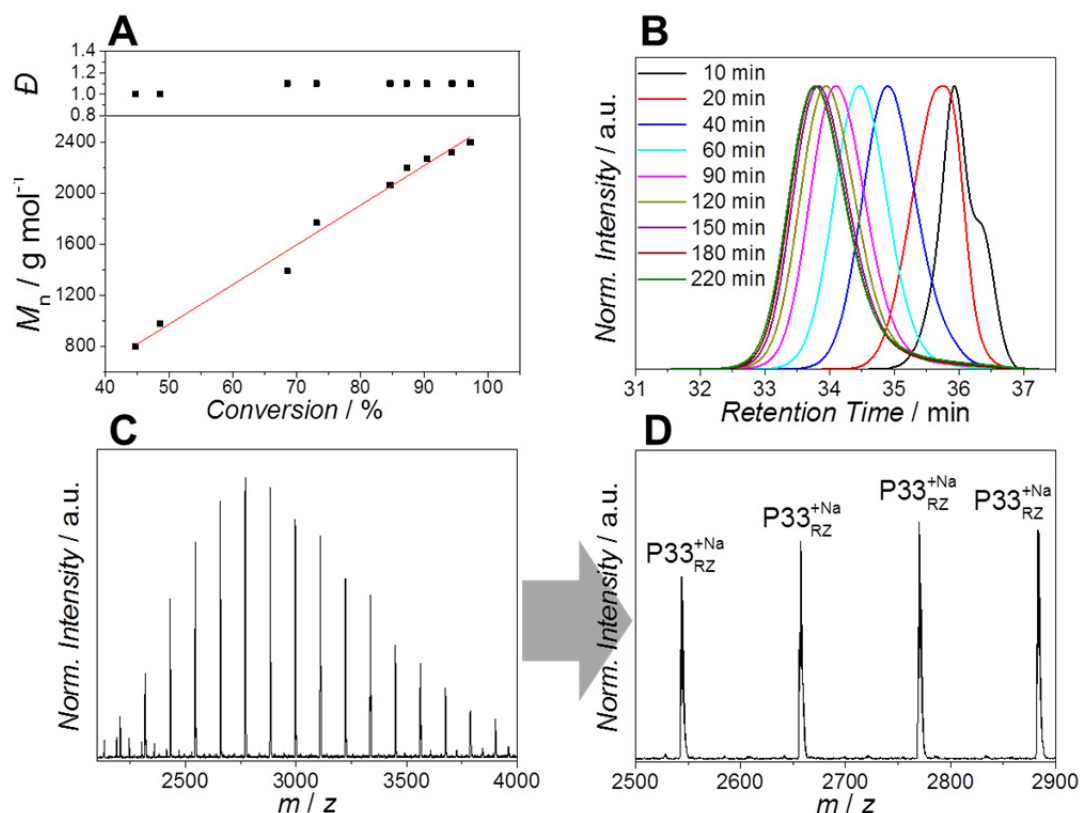


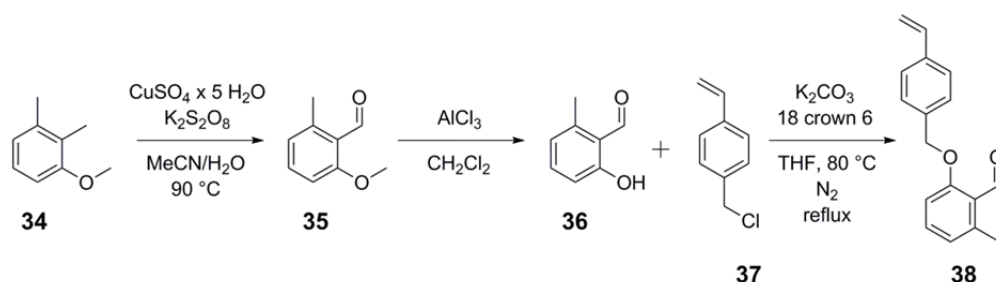
Figure 4.14. Kinetic study of the DoPAT-Ada **22** mediated RAFT polymerization with NiPAAm ($DP_n = 27$). A) M_n (relative to PS standards with the Mark Houwink parameters of poly(NiPAAm)) and \bar{D} versus conversion. B) SEC traces in THF at 35 °C. C) ESI-MS spectrum. D) Magnification of the ESI-MS spectrum. Reproduced with permission from the American Chemical Society, 2015 (DOI: 10.1021/acs.macromol.5b00923).

Table 4. Mass peak assignment for poly(NiPAAm)-Ada **P33**. Experimental and theoretical m/z values for the labelled peaks shown in Figure 4.14D.

m/z_{exp}	assignment	chemical formula	m/z_{theo}	$\Delta m/z$
2544.000	p(NiPAAm)-Ada + Na	$[\text{C}_{134}\text{H}_{242}\text{N}_{18}\text{NaO}_{20}\text{S}_3]^+$	2543.757	0.24
2657.091	p(NiPAAm)-Ada + Na	$[\text{C}_{140}\text{H}_{253}\text{N}_{19}\text{NaO}_{21}\text{S}_3]^+$	2656.841	0.25
2770.000	p(NiPAAm)-Ada + Na	$[\text{C}_{149}\text{H}_{264}\text{N}_{20}\text{NaO}_{22}\text{S}_3]^+$	2769.924	0.08
2883.273	p(NiPAAm)-Ada + Na	$[\text{C}_{152}\text{H}_{275}\text{N}_{21}\text{NaO}_{23}\text{S}_3]^+$	2883.008	0.27

Synthesis of 2-methyl-6-((4-vinylbenzyl)oxy)benzaldehyde (PE-Monomer)

Furthermore, a PE monomer was synthesized to introduce PE cross-linking units into the side chain of the thermoresponsive block. The overall synthesis of 2-methyl-6-((4-vinylbenzyl)oxy)benzaldehyde (PE monomer) **38** is depicted in Scheme 4.14. At first an aldehyde was introduced to commercially available 2,3-dimethylanisole **34** through an oxidation pathway with potassium persulfate and copper sulfate pentahydrate. Furthermore, the methyl group of the methoxy aldehyde intermediate **35** was cleaved via the oxidation of the methyl group with aluminum chloride (AlCl_3) in dichloromethane (CH_2Cl_2). Both intermediate products **35** and **36** were purified by simple flash chromatography. Subsequently, the PE product **36** was etherified with vinylbenzyl chloride **37**, resulting in the styrene derivative 2-methyl-6-((4-vinylbenzyl)oxy)benzaldehyde (PE monomer) **38**. After purification via column chromatography, the pure product was obtained as a white solid with a yield of 47 %. The ^1H NMR spectrum of the pure compound is illustrated in Figure 4.15, showing the characteristic vinyl resonances at 6.73, 5.77 and 5.28 ppm.



Scheme 4.14. Syntheses of 2-methyl-6-((4-vinylbenzyl)oxy)benzaldehyde (PE monomer) **38**.

Next, the ether group of the methoxy aldehyde intermediate **35** was cleaved via the oxidation of the methyl group with aluminum chloride (AlCl_3). Both intermediate products **35** and **36** were purified by simple flash chromatography. Subsequently, the PE product **36** was etherified with vinylbenzyl chloride **37**, resulting in the styrene derivative 2-methyl-6-((4-vinylbenzyl)oxy)benzaldehyde (PE monomer) **38**. After purification via column chromatography, the pure product was obtained as a white solid with a yield of 47 %. The ^1H NMR spectrum of the pure compound is illustrated in Figure 4.15, showing the characteristic vinyl resonances at 6.73, 5.77 and 5.28 ppm.

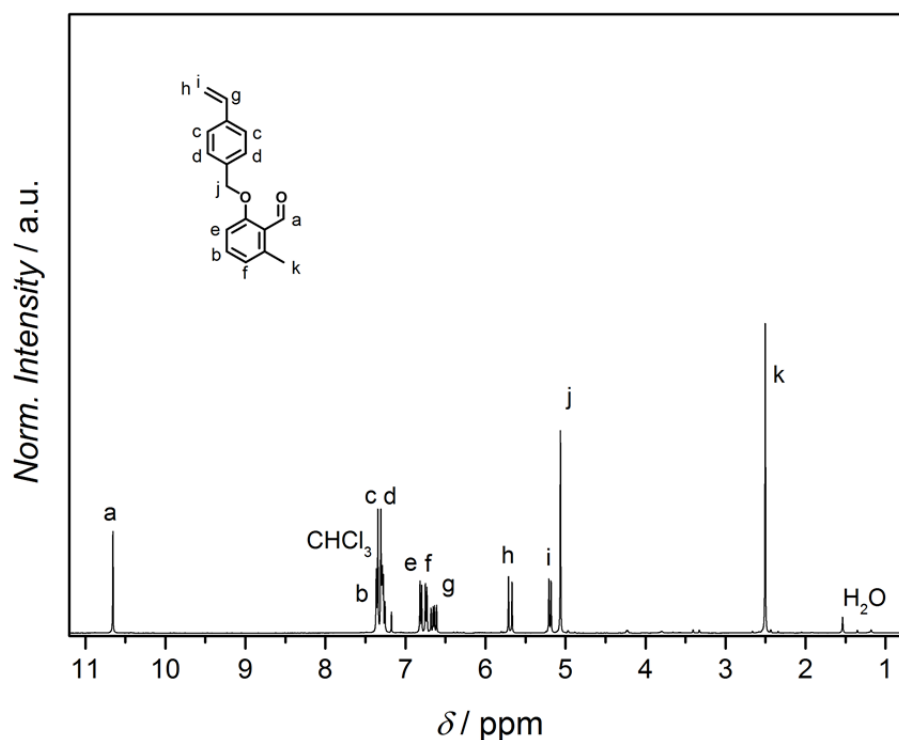
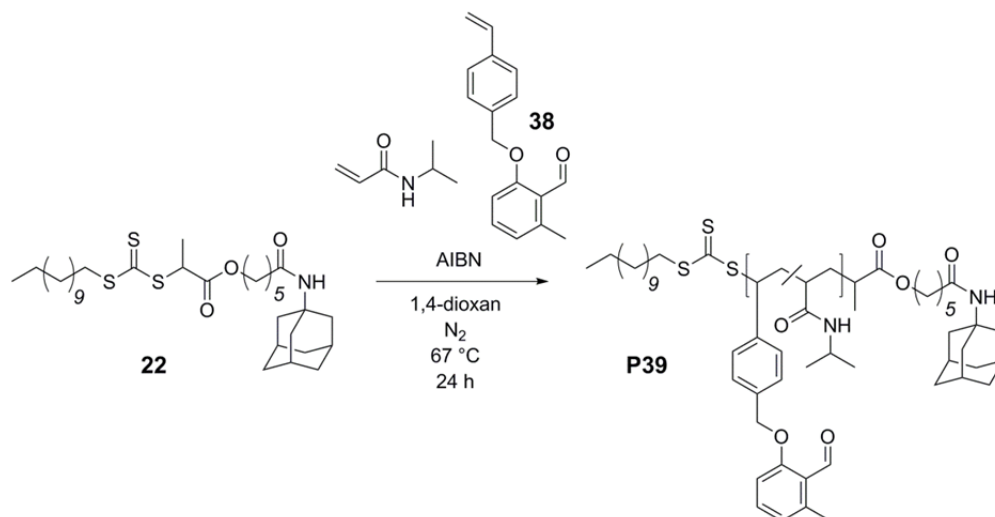


Figure 4.15. ^1H NMR (400 MHz, CDCl_3) spectrum of 2-methyl-6-((4-vinylbenzyl)oxy)benzaldehyde **38**. Reproduced with permission from the American Chemical Society, 2015 (DOI: 10.1021/acs.macromol.5b00923).

Copolymerization of NiPAAm with PE-Monomer

Finally, in order to obtain the thermoresponsive block for the supramolecular diblock formation, the PE-monomer **38** was copolymerized with NiPAAm. Thus, NiPAAm and the PE-monomer **38** were dissolved in 1,4 dioxane with DoPAT-Ada **22** and AIBN in a ratio 10:1 (Scheme 4.15). Prior to polymerization, the mixture was degassed by three freeze-pump-thaw cycles. After 24 h the reaction was quenched by cooling the mixture with liquid nitrogen and the polymer was precipitated in cold diethyl ether. A styrene derivative was chosen for the copolymerization, as this has been studied in detail by Nichifor and Zhu.³⁸⁶ According to their publication, the resulting copolymer is of a statistical nature and the styrene content was controlled by the added mol% of the monomer to the polymerization mixture. Poly(NiPAAm/PE)-Ada was analyzed via SEC and NMR measurements, which are depicted in Figure 4.16. The SEC trace showed a monomodal and narrow size distribution with $M_{n\text{ SEC}} = 39100 \text{ g mol}^{-1}$ and $\mathcal{D} = 1.2$. Furthermore, the ratio of PE to

NiPAAm units was calculated from ^1H NMR (Figure 4.16C) to be 30:1 (NiPAAm/PE), which results in approx. seven PE-monomer (**38**) units (3 %) and approx. 200 NiPAAm units. The amount was calculated via the evaluation of the aldehyde proton (10.69 ppm, a) and the methylene protons of the PE-monomer (5.12 ppm, h) against the single proton resonance of the isopropyl group of NiPAAM at 4.02 ppm (i).



Scheme 4.15. Copolymerization of NiPAAm and the PE-monomer **38**, resulting in the thermoresponsive, adamantyl-functionalized copolymer poly(NiPAAm/PE)-Ada **P39**. The picture was modified with permission from the American Chemical Society, 2015 (DOI: 10.1021/acs.macromol.5b00923).

In addition, the molecular weight of poly(NiPAAm/PE)-Ada **P39** was calculated from the NMR spectrum as well with the aforementioned proton resonances, which were integrated against the proton signals stemming from the polymer backbone ($M_n^{\text{NMR}} = 24100 \text{ g mol}^{-1}$). For further calculations the M_n values resulting from the NMR calculations were considered. The SEC traces reflect relative molecular weight information only, since they are calibrated relative to PS standards, thus the M_n values obtained from the NMR were more accurate for the copolymer **P39**. The LCST of poly(NiPAAm/PE)-Ada **P39** (approx.. 20 °C) was determined via UV-vis turbidity measurements in Milli Q water in the temperature range from 5 – 40 °C, with a polymer concentration of 0.06 mmol L⁻¹. The UV-vis traces, illustrated in Figure 4.16B show hysteresis of the LCST between heating and cooling of **P39**, which is due to the amide-functionality of poly(NiPAAm). Above the LCST of poly(NiPAAm/PE)-Ada **P39**, the amide-functions lead to additional inter- and intramolecular

interactions, which hinder the rehydration of the polymer and thus lead to the observed behavior.³⁸⁷

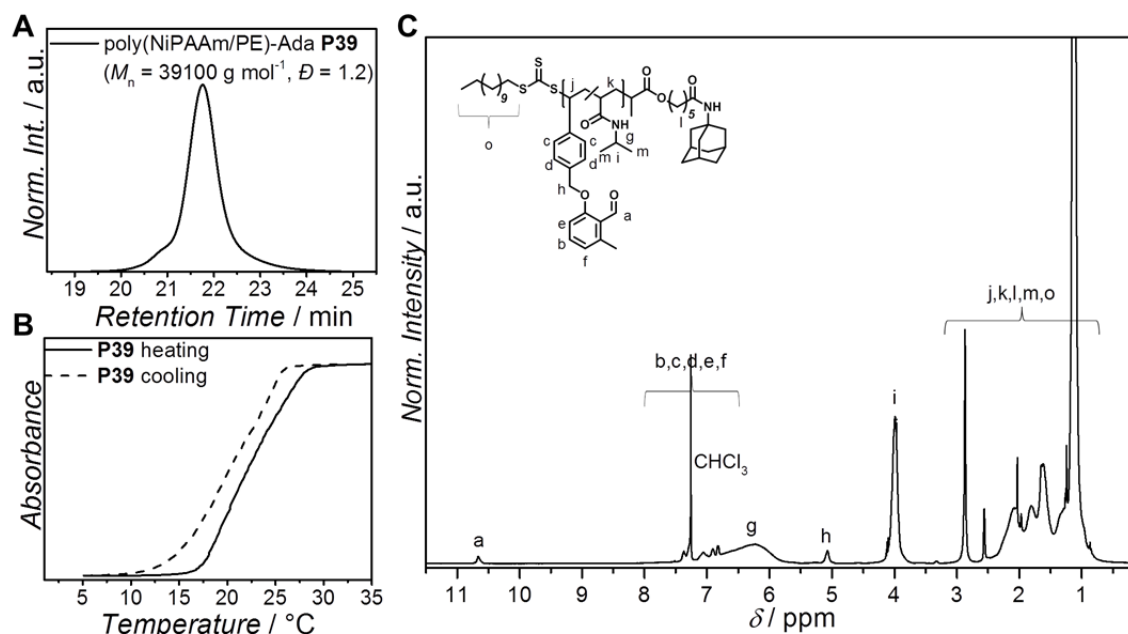
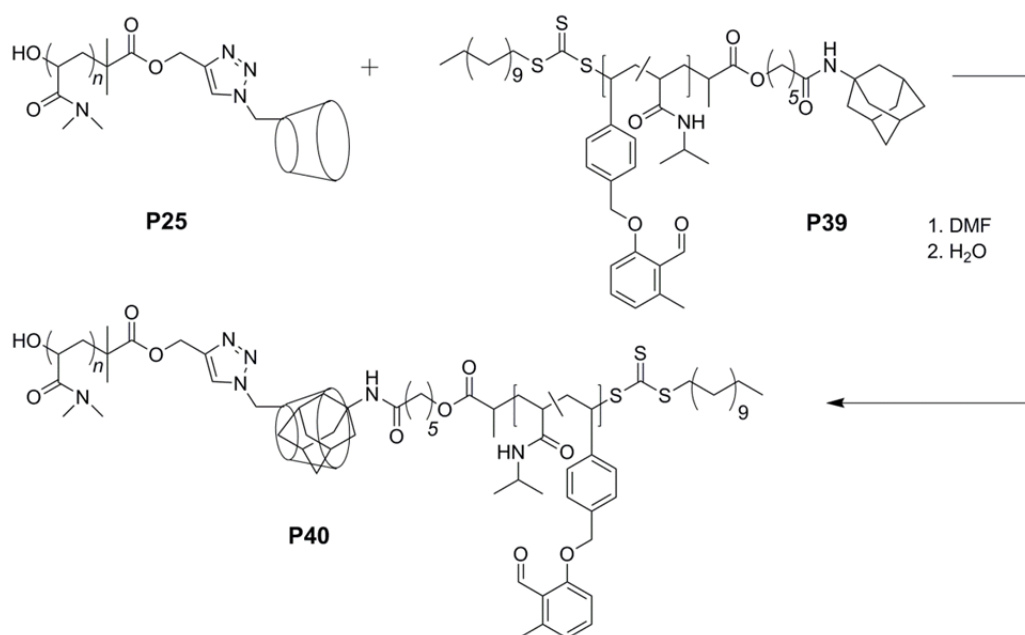


Figure 4.16. Characterization of poly(NiPAAm/PE)-Ada **P39**. A) SEC traces of the thermoresponsive polymer **P39** recorded in DMAC at 50 °C. B) LCST measurements of **P39** in water with a concentration of 0.06 mmol L⁻¹. C) ¹H NMR (400 MHz, CDCl₃, 25 °C) spectrum of **P39** (M_n NMR = 24100 g mol⁻¹) with 3 % PE units incorporated in the side chain. Reproduced with permission from the American Chemical Society, 2015 (DOI: 10.1021/acs.macromol.5b00923).

4.2.4.2 Formation of the supramolecular diblock copolymer

Poly(DMAAm)-β-CD, which was already described in section 4.2.2 and utilized in the formation of a the block copolymer formation in section 4.2.3, was employed for the supramolecular diblock formation with poly(NiPAAm/PE)-Ada **P39**. As already stated previously, the supramolecular interactions of β-CD with suitable guest molecules form dynamic bonds in aqueous solutions. Especially adamantane and β-CD are known to form strong inclusion complexes. Thus, the two building blocks – poly(DMAAm)-β-CD **P25** and poly(NiPAAm/PE)-Ada **P39** – were added in equimolar amounts, dissolved in DMF and stirred for 30 min. Subsequently, the mixture was dialyzed against deionized water. DMF was again chosen for the supramolecular diblock formation. Because DMF is a non-selective solvent for the polymer blocks, the hydrophobic guest molecule is better accessible.



Scheme 4.16. Formation of the supramolecular diblock copolymer: poly(DMAAm)-*b*-poly-(NiPAAm/PE) **P40**.

Here, as well as for poly(NiPAAm/PE)-Ada **P39**, the M_n values obtained from the NMR measurement were applied for the stoichiometric calculations of poly(DMAAm)- β -CD **P25** ($M_{n, \text{NMR}} = 10050 \text{ g mol}^{-1}$). The molecular weight calculated via NMR spectroscopy was derived from the integration of the triazole proton resonances of the click product against the polymer backbone (see Figure 4.9). To analyze the supramolecular diblock copolymer **P40**, DLS was performed in water with a polymer concentration of 0.06 mmol L^{-1} . The graph depicted in Figure 4.17 (left) illustrates the number weighted distribution of the adamantyl-functional poly(NiPAAm/PE) **P39** ($D_h = 9.0 \text{ nm}$, black trace), poly(DMAAm)- β -CD **P25** ($D_h = 12.5 \text{ nm}$, green trace) and the distribution of the resulting diblock copolymer poly(DMAAm)-*b*-poly(NiPAAm/PE) **P40** ($D_h = 19.0 \text{ nm}$, orange trace). The shift to higher hydrodynamic radii of the diblock copolymer **P40** indicated the block formation. In addition, LCST measurements of the supramolecular diblock copolymer **P40** were performed in comparison to the single thermoresponsive block **P39**, which is shown in Figure 4.17 (right). The LCST of poly(DMAAm)-*b*-poly(NiPAAm/PE) **P40** shows a shift to higher temperatures, due to the encapsulation of the hydrophobic adamantyl molecule in β -CD, confirming the DLS measurements.³⁸⁸

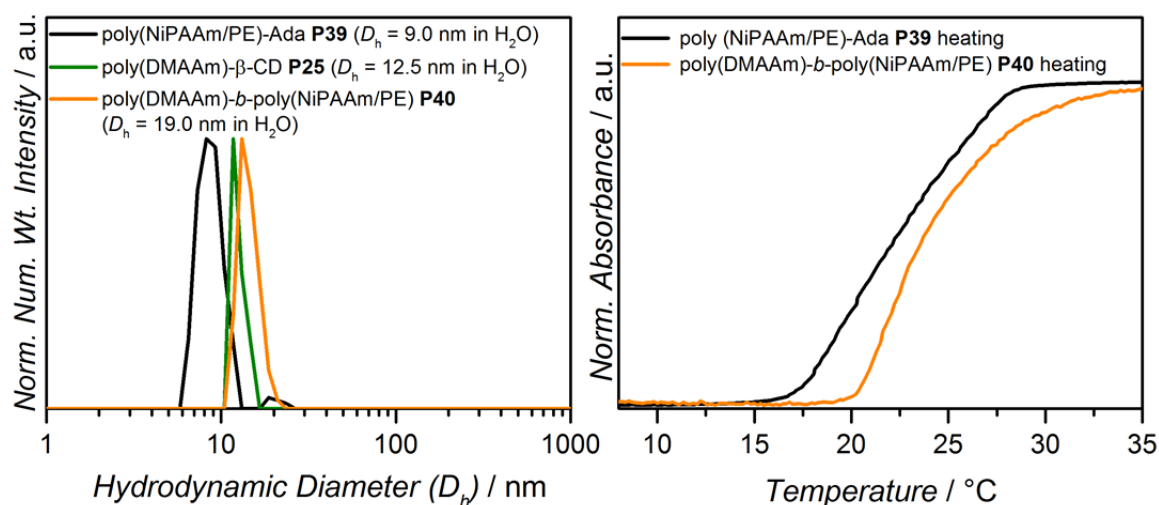


Figure 4.17. Left) DLS measurements in Milli Q water at 10 °C, depicting the number weighted size distribution of poly(NiPAAm/PE)-Ada **P39** ($D_h = 9.0$ nm in H_2O), poly(DMAAm)- β -CD **P25** ($D_h = 12.5$ nm in H_2O) and the supramolecular diblock copolymer **P40** with a polymer concentration of 0.06 mmol L^{-1} . Right) LCST measurement of poly(DMAAm)-*b*-poly(NiPAAm) **P40** in comparison with the LCST before the diblock formation of poly(NiPAAm/PE)-Ada **P39**. Reproduced with permission from the American Chemical Society, 2015 (DOI: 10.1021/acs.macromol.5b00923).

Moreover, the connection of β -CD with the adamantyl guest was analyzed via NOESY. The NOESY spectrum shown in Figure 4.18 revealed cross-correlation peaks of the inner protons of β -CD at 3.64 ppm with the peaks of the adamantyl unit at 1.73 ppm, 1.99 ppm and 2.05 ppm, which results from their close proximity. The structure of the adamantyl/ β -CD inclusion complex is illustrated in Figure 4.18B. However, additional cross-correlation peaks were detected at 0.88 ppm and 1.31 ppm with the inner protons of β -CD (3.64 ppm). These additional cross-correlation peaks result from the enclosure of the alkyl portion of DoPAT, attached to the other chain end of poly(NiPAAm/PE)-Ada **P39** in some β -CD units (Figure 4.18A). Bertrand *et al.* already observed the inclusion of the $C_{12}H_{25}$ chain in β -CD by employing a similar DoPAT derivative for the synthesis of an adamantane end-capped poly(acrylic acid) chain, which further assembled to supramolecular comb shaped polymers.¹⁶⁹ Nonetheless, the study pointed out that the association constant of the alkyl/ β -CD complex ($K_{assoc} \approx 10^2$ M^{-1}) is two orders of magnitude weaker than for the adamantyl/ β -CD complex ($K_{assoc} \approx 10^4$ M^{-1}), which means that the alkyl complex is clearly less abundant.¹⁶⁹ In general, for the temperature-induced formation of the micelle, it was irrelevant from which side of poly(NiPAAm/PE)-Ada

P39 the β -CD-functionalized chain attached. Thus, the supramolecular diblock copolymer was employed without further optimization in the nanoparticle design.

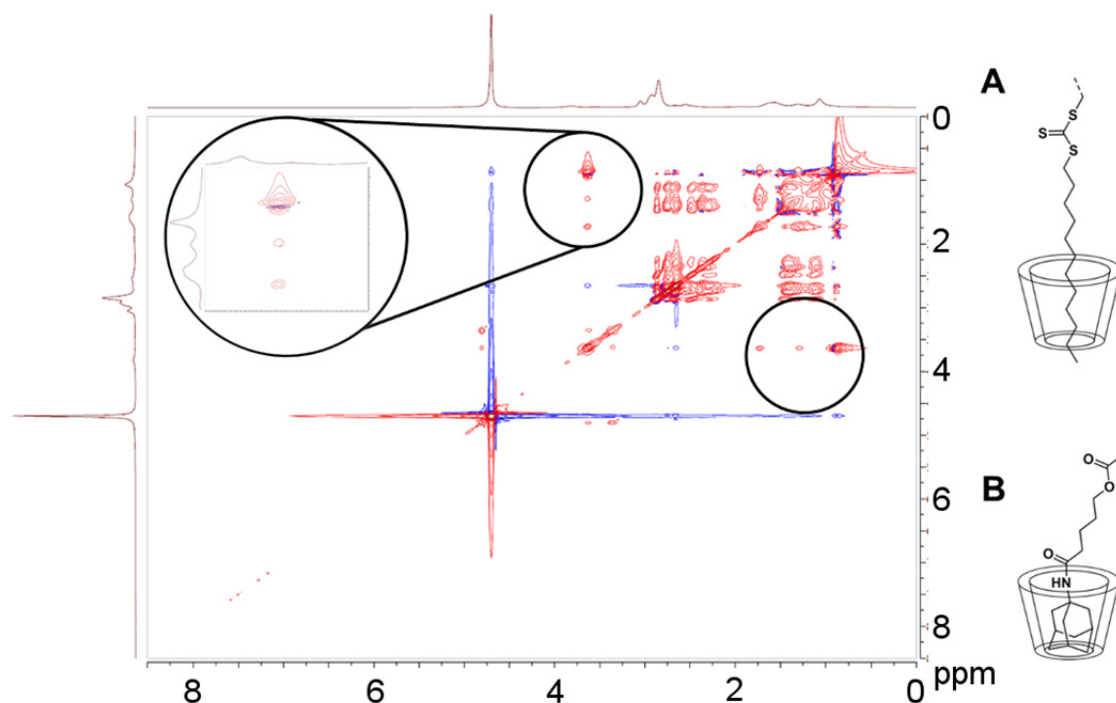
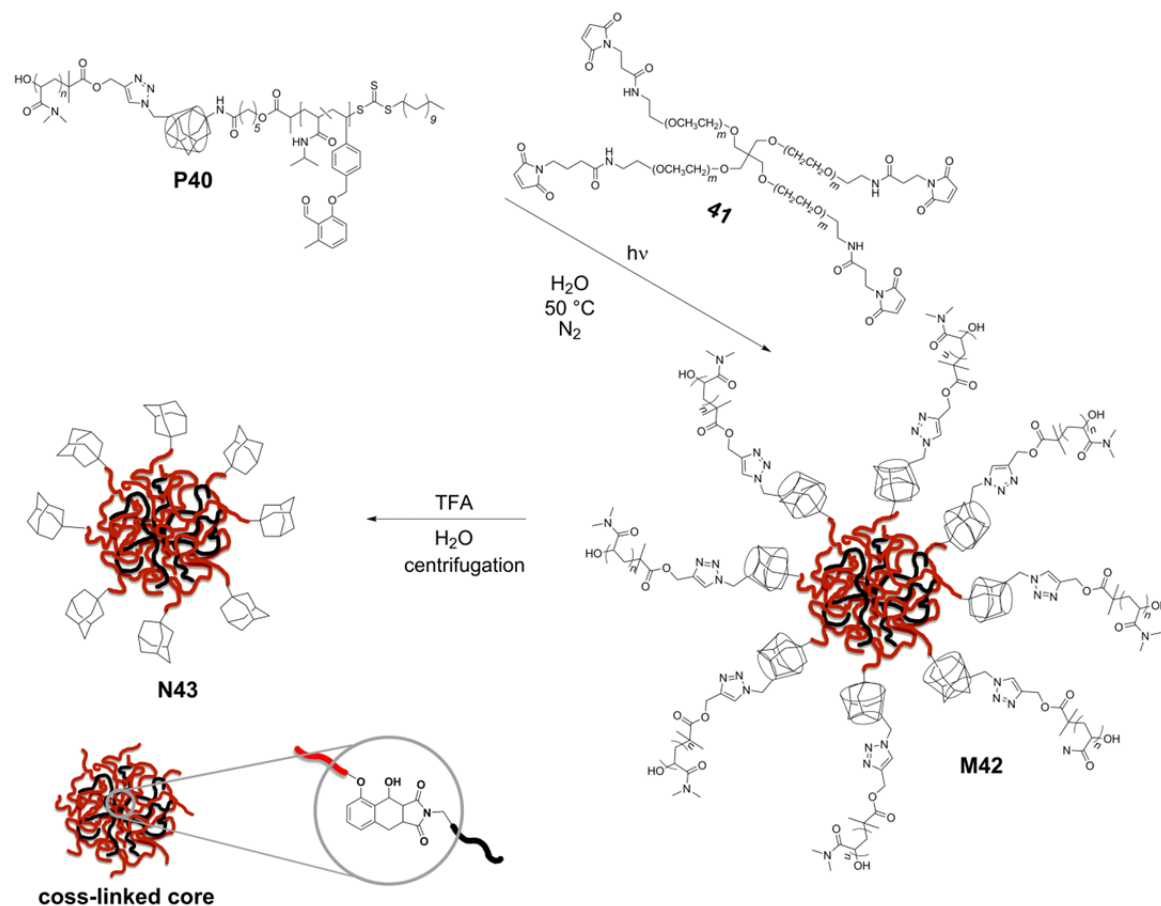


Figure 4.18. 2D NOESY NMR spectrum of the supramolecular diblock copolymer poly(DMAAm)-*b*-poly(NiPAAm/PE) **P40** in D_2O at $10\text{ }^\circ\text{C}$. The cross-correlation of β -CD (3.64 ppm) and the adamantyl protons (1.73 ppm, 1.99 ppm and 2.05 ppm) are circled in the spectrum. A) Structure of the inclusion complex of β -CD and the alkyne chain of the DoPAT unit, whose cross-correlation peaks also appear in the circled area. B) Structure of the inclusion complex of β -CD and the adamantyl unit of poly(NiPAAm/PE). Reproduced with permission from the American Chemical Society, 2015 (DOI: 10.1021/acs.macromol.5b00923).

4.2.4.3 Nanoparticle Design via Sacrificial Micellization

The successfully formed supramolecular diblock copolymer **P40** was subsequently applied in the design of thermoresponsive nanoparticles via a micellar scaffold. Scheme 4.17 illustrates the synthetic strategy for the nanoparticle formation. For micellization and simultaneous cross-linking, the diblock copolymer **P40** was dissolved in Milli Q water at low concentrations (0.06 mmol L^{-1}). Subsequently, the 4-arm maleimide cross-linker **41** was added to the solution, which was cooled on ice water while being purged with nitrogen for 1 h. In the meantime, the photoreactor (Figure A.5) was equipped with five compact low pressure mercury lamps with an emission maximum at $\lambda = 320\text{ nm}$ (36 W). The emission spectrum of the utilized

lamps and the UV spectrum of the PE-monomer **38** are illustrated in Appendix B, Figure A.5. The reactor was heated to an inside temperature of 50 °C by switching on the lamps one hour prior to use, with the ventilation turned off. Next, the sample was heated above its LCST and placed in the photoreactor for irradiation.



Scheme 4.17. Synthetic route for the formation of thermoresponsive nanoparticles. Reproduced with permission from the American Chemical Society, 2015 (DOI: 10.1021/acs.macromol.5b00923).

During the micellization process, the maleimide cross-linker was encapsulated in the hydrophobic core of the micelle. Upon irradiation with UV light, the PE units in the side chain of the thermoresponsive block formed reactive dienes. The PE dienes further reacted with the maleimide cross-linker in a Diels-Alder reaction, thus linking the core of the micelle. It must be mentioned that the equilibrium constant of the adamantyl/ β -CD inclusion complex is reduced at elevated temperatures.¹⁶⁷ For example, Schmidt *et al.* degraded a supramolecular three-armed star polymer at 70 °C.³⁸⁹ Nevertheless, the temperature inside the photoreactor might weaken the

supramolecular bond, but is not sufficiently high to destroy the structure completely. After an irradiation time of six hours, the cross-linked micelles **M42** were obtained. Prior experiments showed that the light-induced DA reaction in water proceeds rather slowly, therefore longer irradiation times were necessary. Atomic force microscopy (AFM) (Figure 4.22) and DLS measurements (Figure 4.20) were performed to characterize the micelles. To compare the data of the micelles with the data of the nanoparticle, the results of the analyses are discussed later in this chapter.

Finally, the nanoparticles were released from the micellar scaffold via the addition of trifluoroacetic acid (TFA) to the aqueous mixture of the cross-linked micelles. TFA destroys the β -CD structure by hydrolyzing the α -1,4 glucose units, resulting in a seven membered linear glucose chain.³⁹⁰ Furthermore, to separate the schismatic micelle arms from the released nanoparticles, the mixture was centrifuged at 40 °C. The centrifugation was performed at elevated temperature with low rotation, so the non-responsive poly(DMAAm)-arms stayed in solution and the thermoresponsive nanoparticles would agglomerate. The experimental section (4.4.6) comprises a detailed description of the centrifugation process. NMR analyses, shown in Figure 4.19, were employed to evidence the successful separation of nanoparticles and micelle arms via the disappearance of the proton resonances between 2.75 ppm – 3.08 ppm, originating from poly(DMAAm). Alternative ways exist to separate the β -CD units and the guest molecules. For example the enzyme α -amylase also cleaves the glucose units of β -CD, similar to TFA. However, TFA was preferred to α -amylase, since it is a small molecule and thus more suitable to obtain pure nanoparticles via centrifugation. Moreover, the addition of either an excess of β -CD or an excess of adamantane guest molecule to the aqueous suspension of the micelles can suppress the diblock formation. Following this, the mixture can be purified via dialysis. Yet, the acidic cleavage of the arms and the subsequent purification via centrifugation was an efficient and fast way to separate arms and nanoparticles. Figure 4.20 illustrates the DLS measurements to give information about the size of the micelles and nanoparticles.

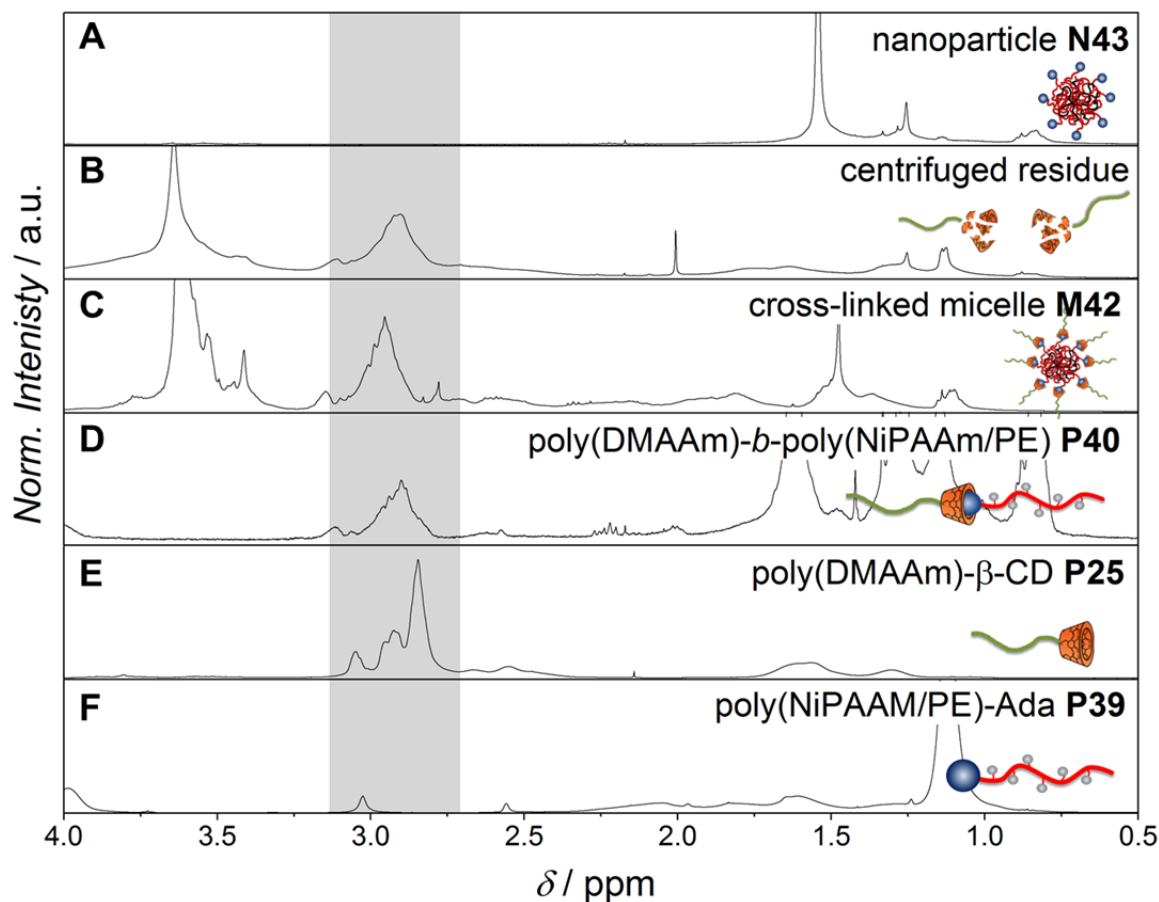


Figure 4.19. ^1H NMR (400 MHz, CDCl_3 , 25 $^\circ\text{C}$). spectra collection. A) Nanoparticles **N43** obtained after centrifugation, without remaining poly(DMAAm) proton resonances in the spectrum. B) Isolated substance received from the supernatant fluid after centrifugation. C) Cross-linked micelle **M42**. D) poly(DMAAm)-*b*-poly(NiPAAm/PE) **P40**. E) Poly(DMAAm)- β -CD **P25**. F) Poly(NiPAAm/PE)-Ada **P39**. The picture was modified with permission from the American Chemical Society, 2015 (DOI: 10.1021/acs.macromol.5b00923).

By way of comparison, the distribution of the supramolecular diblock copolymer poly(DMAAm)-*b*-poly(NiPAAm/PE) **P40** ($D_h = 19.0$ nm) is depicted together with the number weighted distribution of the cross-linked micelles **M43** with a hydrodynamic diameter of 48 nm and the nanoparticles **N43** with a size of 34.0 nm. The shift from 19 nm of the diblock copolymer **P40** to approximately 50 nm for the micelles after the photo-induced cross-linking was a strong indication for the successful formation of the micelles. After the cleavage of the micelle arms and further purification via centrifugation the hydrodynamic diameter decreased to 34 nm.

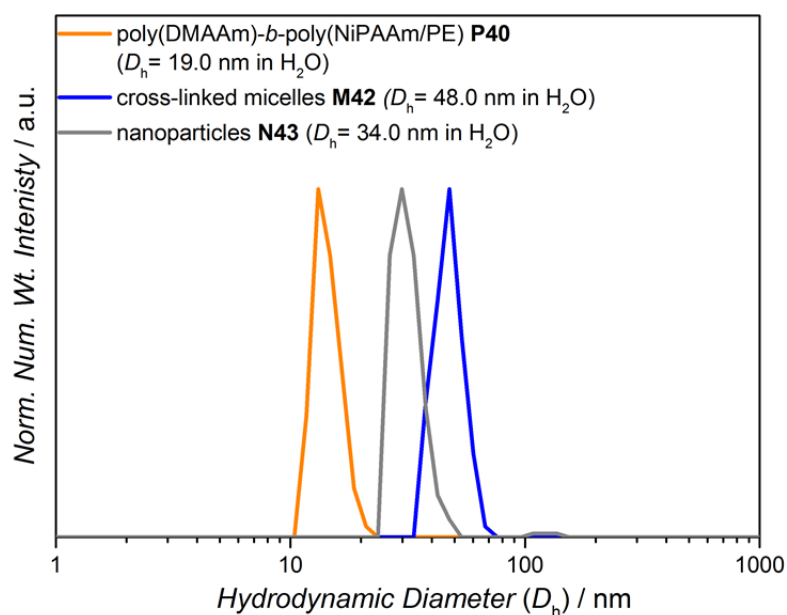


Figure 4.20. DLS measurements in Milli Q water at 10 °C, illustrating the number weighted size distributions of the supramolecular diblock copolymer **P40** (0.06 mmol L⁻¹), the micelles **M42** and the nanoparticles **N43** at a concentration of 1 mg mL⁻¹. The nanoparticles were sonicated for several minutes before the DLS measurement to avoid agglomeration of the particles, due to their hydrophobic shell. Reproduced with permission from the American Chemical Society, 2015 (DOI: 10.1021/acs.macromol.5b00923).

The shift to lower D_h for the nanoparticles is in accordance with the NMR spectra in Figure 4.19, also confirming the release of the nanoparticles.

Furthermore, DLS was employed to investigate the thermoresponsive behavior of micelles and nanoparticles, as presented in Figure 4.21. For both, micelles as well as nanoparticles, a change in D_h is observed with changing temperature, which refers to the temperature induced contraction and relaxation of the thermoresponsive species and shows the same hysteresis as the UV-vis turbidity measurement. The trigger temperature of micelles as well as nanoparticles was close to 30 °C.

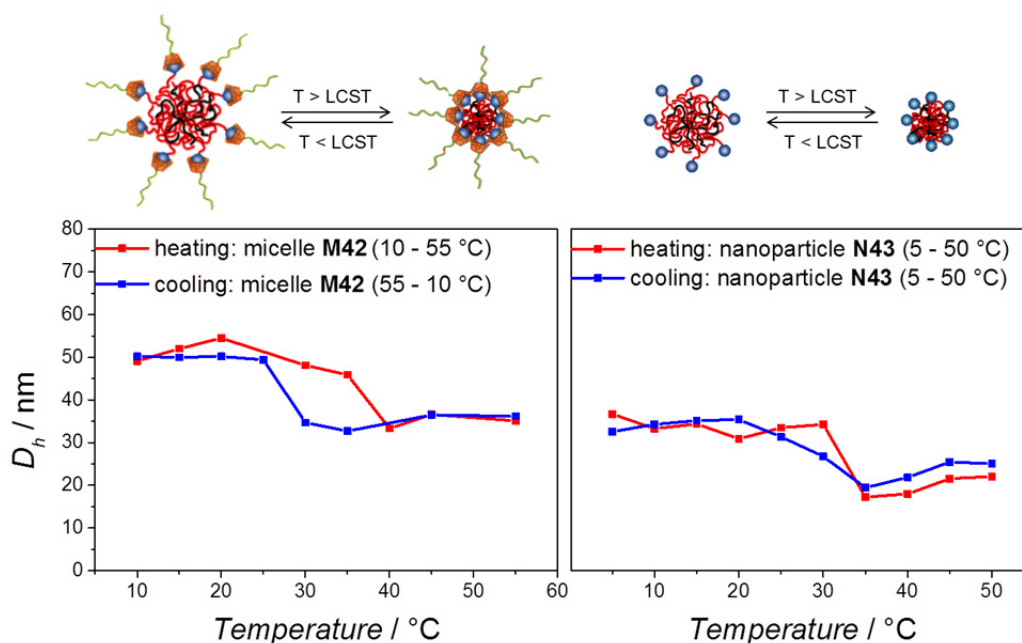


Figure 4.21. Contraction and relaxation of the stimuli responsive species during temperature sequenced DLS measurements. Left) Cross-linked micelles **M42**. Right) Nanoparticles **N43**. Reproduced with permission from the American Chemical Society, 2015 (DOI: 10.1021/acs.macromol.5b00923).

In addition, the expected size differences of micelles and nanoparticles were imaged and characterized via AFM. For the measurement, diluted solutions of the samples in Milli Q water ($0.1 \mu\text{g mL}^{-1}$) were adsorbed on freshly cleaved mica surfaces, dried and measured with a scan size of $1 \times 1 \mu\text{m}$.³²³ Figure 4.22 depicts the two- and three-dimensional topographic maps of the micelles **M42** (A) and the nanoparticle **N43** (B). Higher magnification images of the AFM measurement are shown in Appendix B, Figure B.13. In the AFM images, both samples show dispersity in particle size, which is due to the inherently disperse nature of the polymer samples **P25** and **P39**. Moreover, particle analysis for each sample was performed with a NanoScope Analysis tool and is illustrated in Figure B.11 and Figure B.12. The particle analysis revealed a decrease in diameter – on average – when going from micelles to nanoparticles (compare to the values in the tables of Figure B.11 and Figure B.12). Thus, the AFM data was in accordance with the disappearance of the proton signals of poly(DMAAm) in the NMR spectrum after centrifugation and the decrease in D_h in the DLS measurement of the nanoparticles. Hence, AFM additionally confirmed the degradation of the micelles to the nanoparticles. Due to tip-convolution effects, the

diameter values measured via AFM contained uncertainties. Furthermore, the particle size data obtained from AFM and DLS were not directly comparable. In the AFM measurement the particles were air dried on a mica surface, which could result in particle shrinking effects,³⁸⁷ compared to the particles in the DLS measurement which are swollen in solution. Thus, AFM rather served to visualize micelles and nanoparticles.

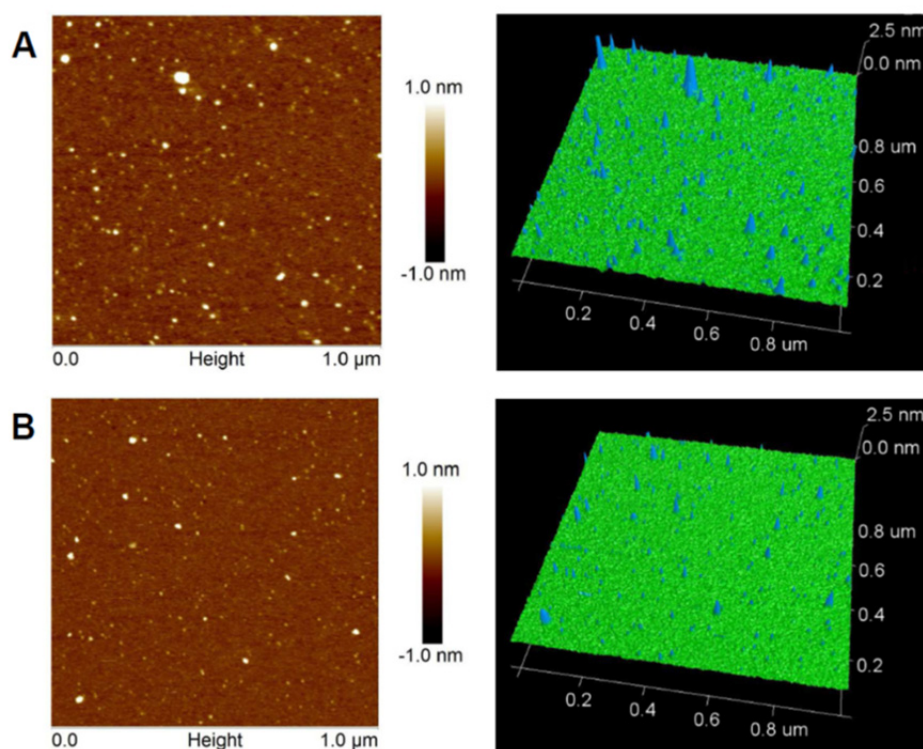


Figure 4.22. 2D and 3D AFM topography images of A) micelles and B) nanoparticles. The samples were measured on freshly cleaved mica-surfaces and cast from a $0.1 \mu\text{g mL}^{-1}$ solution in Milli Q water. The picture was modified with permission from the American Chemical Society, 2015 (DOI: 10.1021/acs.macromol.5b00923).

In future applications the remaining adamantyl units at the corona of the nanoparticles could be re-functionalized with β -CD bearing moieties. Thus, varying polymer chains or proteins can be attached to the nanoparticles influencing their availability.

4.3 Conclusion

In the course of Chapter 4, several RAFT agents, equipped with defined functional molecules were designed and employed for the controlled polymerizations of water soluble acrylamides. In this way several polymer chains with reactive termini, defined chain lengths and narrow size distributions were developed and applied in the construction of complex polymer structures. It was demonstrated that the host-guest complexations of β -CD and light-induced photoenol chemistry are highly efficient and orthogonal conjugation techniques to form multiblock copolymers, without the addition of coupling agents or initiators. The di-, tri- and tetrablock copolymers were precisely analyzed via NMR spectroscopy, SEC, ESI-MS, DLS and NOESY, which verified the successful formation of the multiblock copolymers. Furthermore, even more sophisticated structures, such as micelles were generated by means of photochemical cross-linking and supramolecular self-assembly, evidencing the efficiency of the combination of both techniques. In this context, a facile synthetic approach was introduced to design thermoresponsive nanoparticles via a sacrificial micellar scaffold. A partly thermoresponsive and partly non-responsive supramolecularly connected diblock copolymer self-assembled into a micellar structure at elevated temperatures in aqueous solution. The micelle was further cross-linked in its core upon UV irradiation and the addition of a linker molecule. In a final step the β -CD units were hydrolyzed to cleave the micelle arms and to release the nanoparticles. Micelles and nanoparticles were analyzed via ^1H NMR spectroscopy, AFM and DLS. The successful transformation of the micelle to the nanoparticle was evidenced as well as its thermoresponsive contractions. In conclusion, the combination of supramolecular host-guest interactions with light-induced chemistry yields new possibilities in the design of complex macromolecular architectures, which can be employed in the development of advanced functional materials.

4.4 Experimental Section

4.4.1 Materials

Cs₂CO₃ (≥ 99.9%, Roth), 11-bromoundecanol (97%, ABCR), MgSO₄ (≥ 99%, Roth), 4-*tert*-butylbenzyl mercaptan (97%, Aldrich), K₃PO₄ (Roth), carbon disulfide (CS₂, >99.9%, VWR), 3-bromopropionic acid (97%, ABCR), HCl (37%, Roth), 4-(dimethylamino)-pyridine (DMAP, 99%, Acros), *N,N'*-dicyclohexylcarbodiimide (DCC, 99%, Acros), NaHCO₃ (≥ 99%, Roth), MgSO₄ (≥ 99%, Roth), ascorbic acid (99%, Acros), Quantofix 100 peroxide dipsticks (1 - 100 mg L⁻¹ H₂O₂, Roth), CuBr (99.9%, Acros), *N,N,N',N',N''*-pentamethyldiethylenetriamine (PMDETA, 99.9%, Merck), 2-(dodecylthiocarbonothioylthio) propionic acid (DoPAT, Orica), 18-crown-6 (99%, Acros), K₂CO₃ (VWR), 4-arm PEG-Maleimide (2 k, Creative PEGWorks), trifluoroacetic acid (TFA, 99%, ABCR) were used as received. *N,N*-Diethylacrylamide (DEAAm, 98%, TCI), *N,N*-dimethylacrylamide (DMAAm, 99%, TCI), *N*-hydroxyethyl acrylamide (HOEAAM, 97%, Aldrich) and 4-vinylbenzyl chloride (90%, Sigma) were filtered over basic aluminum oxide and subsequently stored at -19 °C. *N*-Isopropylacrylamide (NiPAAm, 98%, TCI) was recrystallized in hexane prior to use and stored at -19 °C. Azobisisobutyronitrile (AIBN, 99%, Fluka) was recrystallized twice in methanol and stored at -19 °C. Milli-Q water was obtained from a purification system by VWR (TKA Micro-Pure; 0.055 μS cm⁻¹), *N,N*-dimethylformamide extra dry (DMF, 99.8%, Acros), 1,4-dioxane (Sigma Aldrich), dichloromethane extra dry (DCM, 99.8% Acros) tetrahydrofuran (THF) dichloromethane (DCM), acetone, ethyl acetate (EA), cyclohexane, diethyl ether (Et₂O) and acetonitrile (MeCN) were purchased as analytical grade (VWR) and used as received.

4.4.2 Instrumentation

4.4.2.1 Size Exclusion Chromatography (SEC)

SEC measurements were performed with *N,N*-dimethylacetamide (DMAC) as eluent containing 0.03 wt% LiBr on a Polymer Laboratories PL-GPC 50 Plus Integrated System, comprising an autosampler, a PLgel 5 μm bead-size guard column (50 \times 7.5 mm) followed by three PLgel 5 μm MixedC columns (300 \times 7.5 mm), and a differential refractive index detector at 50 $^{\circ}\text{C}$ with a flow rate of 1.0 mL min^{-1} . The SEC system was calibrated against linear poly(styrene) standards with molecular weights ranging from 160 to 6 \cdot 10⁶ g mol^{-1} . Calculations for the molecular weight of poly(DMAAm) and poly(NiPAAm/PE) were carried out according to a poly(styrene) calibration, i.e. $K = 14.1 \cdot 10^{-5}$ dL g^{-1} , $\alpha = 0.70$ (PS).⁶² The molecular weight dispersity is abbreviated as \bar{D} .

4.4.2.2 Electrospray Ionization-Mass Spectrometry (ESI-MS)

Mass spectra were recorded on a Q Exactive (Orbitrap) mass spectrometer (Thermo Fisher Scientific, San Jose, CA, USA) equipped with an HESI II probe. The instrument was calibrated in the m/z range 74-1822 using premixed calibration solutions (Thermo Scientific). A constant spray voltage of 4.7 kV and a dimensionless sheath gas flow of 5 were applied. The capillary temperature and the S-lens RF level were set to 320 $^{\circ}\text{C}$ and 62.0, respectively. The samples were dissolved with a concentration of 0.05 $\text{mg}\cdot\text{mL}^{-1}$ in a mixture of THF and MeOH (3:2) containing 100 μmol of sodium trifluoroacetate (NaTFA) and infused with a flow of 5 $\mu\text{L}\cdot\text{min}^{-1}$.

The mass spectra depicted in Figure 25 were recorded on an LXQ mass spectrometer (ThermoFisher Scientific, San Jose, CA, USA) equipped with an atmospheric pressure ionization source operating in the nebulizer assisted electrospray mode. The instrument was calibrated in the m/z range 195-1822 using a standard containing caffeine, Met-Arg-Phe-Ala acetate (MRFA) and a mixture of fluorinated phosphazenes (Ultramark 1621) (all from Aldrich). A constant spray voltage of 3.5 kV, a dimensionless sheath gas of 8 and a sweep gas flow rate of 2 were applied.

The capillary voltage, the tube lens offset voltage, and the capillary temperature, were set to 60 V, 120 V and 300 °C, respectively.

4.4.2.3 UV-Vis Spectrometer

UV-vis spectra were measured on a Cary 300 Bio UV-Vis spectrophotometer (Varian) at either 25 °C or 10 °C, depending on the sample. Cloud points were measured on the same instrument at 600 nm. The heating rate was set to 0.32 °C min⁻¹ and the concentration at 0.06 mmol L⁻¹. For the determination of the cloud point the point of inflection of the transmittance vs temperature plot was used.

4.4.2.4 Nuclear Magnetic Resonance (NMR) Spectroscopy

NMR measurements for structure confirmation were carried out on a Bruker Ascend 400 spectrometer with 400 MHz for hydrogen nuclei and 100 MHz for carbon nuclei. Samples were dissolved in CDCl₃, DMSO-*d*₆ or D₂O. The δ -scale was referenced with tetramethylsilane ($\delta = 0.00$) as internal standard. Abbreviations used below in the description of the materials syntheses include singlet (s), broad singlet (bs), doublet (d), triplet (t), quartet (q), broad multiplet (bm), and unresolved multiplet (m).

The 2D NOESY (nuclear Overhauser enhancement spectroscopy) spectra were measured on a 600 MHz Bruker Avance III spectrometer equipped with a ¹H, ¹³C, ¹⁵N – TCI inversely detecting cryoprobe at 10 °C (283 K) for samples containing poly(NiPAAm) and 25 °C for all other samples. The mixing time was set to 300 μ s and the concentration of the sample was 50 mg mL⁻¹ in D₂O.

4.4.2.5 Dynamic Light Scattering (DLS)

Samples were prepared by dissolving the samples in Milli Q water at a constant concentration of 0.06 mmol L⁻¹. The concentration for the micelles and the nanoparticles were at 1 mg mL⁻¹. The solutions were filtered via a 0.2 μ m syringe filter to remove dust particles. Before the measurement the solution of the diblock was left for 30 min, so the equilibrium between β -CD and adamantyl units could re-establish. Hydrodynamic diameters were determined with dynamic light scattering (Nicomp 380 DLS spectrometer from Particle Sizing Systems, Santa Barbara, USA, laser diode: 90 mW, 658 nm). Measurements were performed in automatic mode

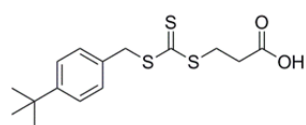
and evaluated with a standard Gaussian and an advanced evaluation method, the latter proceeding via an inverse Laplace algorithm to analyze for multimodal distributions. The values provided in study are the number-weighted average values as calculated in the NICOMP evaluation. All measurements were determined at an angle of 90° to the incident beam. The associated auto-correlation functions can be found in the Supporting Information section.

4.4.2.6 Atomic Force Microscopy (AFM)

Sample Preparation: Freshly prepared and dried micelles as well as nanoparticles (~1 mg) were dissolved in Milli Q water (1 mL). 10 µL of 1:10000 stock solutions (stepwise diluted with Milli Q water) were pipetted onto freshly cleaved mica discs of 12 mm diameter. The samples were covered and spread-dried at elevated temperature (hot plate being hand warm). Sample measurements: AFM analysis was performed on a NanoScope IIIa controlled MultiMode 2 AFM (Bruker) equipped with a scanner type “E” at a scan size of 1 × 1 µm, at a scan speed of 0.5 Hz, with a resolution of 512 lines and points and a scan angle of 0°. A Silicon nitrate cantilever was used with a typical resonant frequency of 75 kHz and force constant of approximately 0.2 N/m (MikroMasch, HQ: NSC18/No Al). The image data were processed with the NanoScope Analysis 1.40 software (Bruker).

4.4.3 Small Molecule Syntheses

2-(((ethylthio)carbonothioyl)thio)-2-methylpropanoic acid (**EMP**),³⁹¹ prop-2-yn-1-yl 2-(((ethylthio)carbonothioyl)thio)-2-methylpropanoate (**14**),¹⁷⁷ 2-(2-hydroxyethyl)-3a,4,7,7a-tetrahydro-1H-4,7-epoxyisoindole-1,3(2H)-dione (**15**),³⁴⁸ *N*-((3s,5s,7s)-adamantan-1-yl)-6-hydroxyhexanamide (**20**)¹⁷⁷ and mono-(6-azido-6-desoxy)-β-cyclodextrin (β-CD-N₃) (**27**)³⁹² were synthesized according to literature procedures.

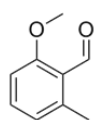


3-(((4-(tert-butyl)benzyl)thio)carbonothioyl)thio)propanoic acid (10): 4-*tert*-butylbenzyl mercaptan **8** (5.50 g,

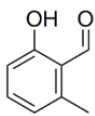
30.50 mmol, 1.10 eq.) was added to a suspension of K₃PO₄

(8.25 g, 38.80 mmol, 1.40 eq.) in acetone (150 mL) and stirred for 20 min at ambient

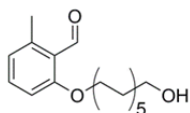
temperature. Subsequently CS₂ (6.54 g, 86.00 mmol, 3.10 eq.) was added to the reaction mixture, which turned yellow. After another 20 min of stirring 3-bromopropanoic acid **9** (4.25 g, 27.70 mmol, 1.00 eq.), dissolved in acetone (10 mL) was added to the suspension and the reaction was stirred at 40 °C overnight. HCl (1 M, 100 mL) was added to the reaction mixture and the aqueous solution was extracted with DCM (2 × 150 mL). The combined organic extracts were washed with deionized water (150 mL) and brine (150 mL) and dried over MgSO₄. After evaporation of the solvent the yellow oil was purified via column chromatography on silica gel in a mixture of cyclohexane and ethyl acetate which was gradually changed from 3:1 to 1:1 to result in a yellow oil which solidified in the freezer (8.62 g, 94%). ¹H NMR (400 MHz, DMSO-*d*₆): δ = 12.51 (bs, 1 H, COOH); 7.36 – 7.29 (m, 4 H, Ar-H); 4.64 (s, 2 H, Ar-CH₂-S); 3.54 (t, 2 H, ³J_{HH} = 6.9 Hz, S-CH₂-CH₂); 2.68 (t, 2 H, ³J_{HH} = 6.9 Hz, CH₂-CO); 1.26 (s, 9 H, C-C₃H₉) ppm. ¹³C NMR (400 MHz, DMSO-*d*₆): δ = 223.92 (C=S), 172.91 (O-C-OH), 130.68 (C_{Ar}-C₄H₉), 132.41 (C_{Ar}-CH₂), 129.28 (C_{Ar}), 125.90 (C_{Ar}), 34.72 (C_{Ar}-CH₂-S), 32.83 (CH₂, C-C₃H₉), 32.14 (S-CH₂), 31.32 (C-C₃H₉) ppm.



2-Methoxy-6-methylbenzaldehyde(35): 2,3-Dimethyl anisole **34** (7.03 g, 51.6 mmol, 1.00 eq), copper sulfate pentahydrate (13.11 g, 52.5 mmol, 1.02 eq) and potassium peroxodisulfate (41.85 g, 154.8 mmol, 3.00 eq) were added to a mixture of acetonitrile/water (1:1, 500 mL). The vigorously stirred suspension was placed in a thermostatted oil bath kept at 90°C until the TLC showed no remaining starting material. After 45 min the mixture was cooled to ambient temperature and the undissolved copper salt was removed by filtration. Dichloromethane (150 mL) was added and the phases were separated. The aqueous phase was extracted two times with dichloromethane (100 mL) and the combined organic layers were dried over magnesium sulfate. After removal of the solvent under reduced pressure, the crude product was purified by flash chromatography (silica gel, hexane/ethyl acetate, 4:1), yielding 5.2 g (68%) of a yellow solid. ¹H-NMR (400 MHz, CHCl₃) δ = 10.64 (s, 1H, CHO), 7.38 (t, ³J_{HH} = 7.97 Hz, 1H, ArH), 6.81 (t, ³J_{HH} = 7.97 Hz, 2H, ArH), 3.89 (s, 3H, OCH₃), 2.57 (s, 3H, CH₃) ppm.⁵⁵



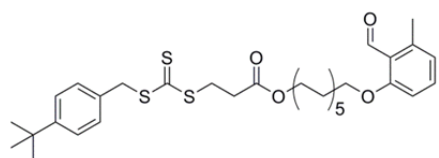
2-Hydroxy-6-methylbenzaldehyde (36): 2-Methoxy-6-methylbenzaldehyde **35** (5.20 g, 34.6 mmol, 1.00 eq) was dissolved in dry dichloromethane (75 mL) and cooled to 0°C. AlCl₃ (13.9 g, 103.9 mmol, 3.00 eq) was added and the mixture was stirred at ambient temperature overnight. The reaction was quenched with H₂O (100 mL) and the phases were separated. The aqueous layer was extracted three times with dichloromethane (100 mL). The combined organic layers were dried over magnesium sulfate and the solvent was evaporated. The final purification was carried out by flash chromatography (silica gel, cyclohexane/ethyl acetate, 2:1) yielding 3.9 g (82%) of a yellow solid. ¹H-NMR (400 MHz, CHCl₃) δ = 11.91 (s, 1H, OH), 10.32 (s, 1H, CHO), 7.38 (t, ³J_{HH} = 7.9 Hz, 1H, ArH), 6.76 (dd, J_{HH} = 25.3, 7.9 Hz, 2H, ArH), 2.61 (s, 3H, CH₃) ppm.⁵⁵



2-((11-Hydroxyundecyl)oxy)-6-methylbenzaldehyde (11): Cs₂CO₃ (3.25 g, 9.97 mmol, 1.67 eq.) was suspended in dry DMF (20 mL). 2-Hydroxy-6-methyl benzaldehyde (1.02 g, 7.46 mmol, 1.25 eq.) was added and the mixture was stirred for 20 min at ambient temperature. Subsequently, a solution of 1-bromoundecanol (1.50 g, 5.97 mmol, 1.00 eq.) in dry DMF (5 mL) was added dropwise to the suspension and the reaction proceeded at 50 °C overnight. The solvent was evaporated under reduced pressure. Afterwards, the residue was dissolved in diethyl ether and washed three times with brine (50 mL). The organic phase was dried over MgSO₄ and the solvent was evaporated. The crude product was purified via column chromatography with a mixture of cyclohexane/ethyl acetate (2:1). The product was obtained as a slightly yellow solid (1.66 g, 90% yield). ¹H NMR (400 MHz, CDCl₃): δ = 10.63 (s, 1 H, CHO), 7.35 (t, 1 H, ³J_{HH} = 7.9 Hz, Ar-H), 6.82-6.77 (m, 2 H, Ar-H), 4.04 (t, 2 H, ³J_{HH} = 6.3 Hz, O-CH₂), 3.64 (t, 2 H, ³J_{HH} = 6.6 Hz, CH₂-OH), 2.57 (s, 3 H, Ar-CH₃), 1.82 (quin., 2 H, ³J_{HH} = 6.5 Hz, OCH₂-CH₂), 1.58-1.57 (m, 2 H, CH₂), 1.49-1.43 (m, 2 H, C₅H₁₀-CH₂), 1.38-1.28 (m, 12 H, CH₂) ppm. ¹³C NMR (400 MHz, CHCl₃): δ = 192.57 (CHO), 162.90 (HC_{Ar}-C_{Ar}-O), 141.98 (C_{Ar}-CH₃), 134.43 (C_{Ar}-CH-C_{Ar}), 123.85 (C_{Ar}-CHO), 123.39 (C_{Ar}-C_{Ar}-CH₃), 109.90 (C_{Ar}-C_{Ar}-O), 68.67 (O-CH₂-CH₂), 63.09 (CH₂-OH), 32.81 (CH₂-CH₂-OH), 29.49 (CH₂-C₅H₁₀-CH₂), 29.15 (O-CH₂-CH₂), 26.10 (O-C₂H₄-CH₂), 25.72 (CH₂-C₂H₄-OH),

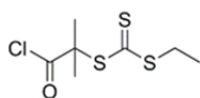
4. Complex Macromolecular Architectures

21.54 (Ar-CH₃) ppm. MS: (ESI) m/z calculated for C₁₉H₃₀O₃ [M+Na]⁺: m/z _{theo}: 329.21, m/z _{exp}: 329.28.⁵⁵



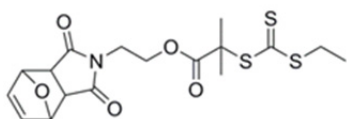
11-(2-formyl-3-methylphenoxy)-undecyl 3-(((4-(tert-butyl)benzyl)thio)carbonothioyl)thio propanoate (tBuBnPE-trithiocarbonate)

(12): 3-(((4-(tert-butyl)benzyl)thio)carbonothioyl)thio)propanoic acid **10** (787.89 mg, 2.39 mmol, 1.5 eq.) 2-((11-hydroxyundecyl)oxy)-6-methylbenzaldehyde **11** (490.00 mg, 1.59 mmol, 1.0 eq.) and DMAP (3.91 mg, 0.03 mmol, 0.02 eq.) were dissolved in dry DCM (10 mL). Subsequently, a solution of DCC (494.87 mg, 2.39 mmol, 1.5 eq.) in dry DCM (5 mL) was added dropwise to the reaction mixture at 0 °C. The reaction was covered with aluminum foil and the mixture was stirred overnight at ambient temperature. The suspension was filtered, washed with aqueous HCl (5%), NaHCO₃ solution and deionized water. The organic phase was dried over MgSO₄ and the solvent was removed under reduced pressure. The crude product was purified via column chromatography in cyclohexane/ethyl acetate (5:1) to give a yellow oil (868.10 mg, 88%). ¹H NMR (400 MHz, CHCl₃): δ = 10.68 (s, 1 H, CHO), 7.29-7.29 (m, 3 H, Ar-H), 7.17 (d, 2 H, ³J_{HH} = 8.2 Hz, Ar-H), 6.74-6.69 (m, 2 H, Ar-H), 4.74 (q, 1 H, ³J_{HH} = 7.4 Hz, S-CH-CH₃), 4.49 (s, 2 H, Ar-CH₂-S), 4.09-4.03 (m, 2 H, O-CH₂-CH₂), 3.95 (t, 2 H, ³J_{HH} = 6.4 Hz, CH₂-CH₂-O), 2.49 (s, 3 H, Ar-CH₃), 1.77-1.71 (m, 2 H, H₁₄C₇-CH₂-CH₂O), 1.58- 1.52 (m, 3 H, CH₃-C-S), 1.49-1.45 (m, 2 H, O-CH₂-CH₂-C₇H₁₁), 1.30-1.26 (m, 23 H, C₇H₁₁, C₃H₉) ppm. ¹³C NMR (400 MHz, CHCl₃) δ = 223.23 (C=S), 192.53 (H-C=O), 171.50 (O-C=O), 162.89 (O-C_{Ar}), 150.88 (C_{Ar}-C₄H₉), 141.96 (C_{Ar}-CH₃), 134.43 (C_{Ar}), 131.68 (C_{Ar}-CH₂), 128.97 (C_{Ar}), 125.69 (C_{Ar}-CHO), 123.85 (C_{Ar}), 123.40 (C_{Ar}), 109.91 (C_{Ar}), 68.67 (CH₂-CH₂-O), 65.15 (O-CH₂-CH₂), 41.26 (C_{Ar}-CH₂-S), 34.57 (CH₂-CH₂-CO), 33.21 (C-C₃H₉), 31.40 (C₃H₉), 29.47 (CH₂-CH₂-CH₂), 29.33 (CH₂-C₅H₁₀-CH₂), 28.55 (CH₂-CH₂-CH₂), 26.11 (CH₂-CH₂-CH₂), 25.89 (S-CH₂-CH₂), 21.55 (CH₃-C_{Ar}) ppm. MS (ESI) m/z calculated for C₃₂H₄₈O₄S₃ [M+Na]⁺: m/z _{theo} 639.26, m/z _{exp}: 639.28.



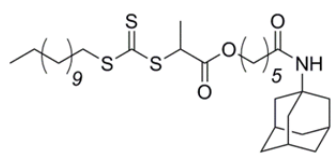
Synthesis of 1-chloro-2-methyl-1-oxopropan-2-yl ethyl carbonotrithioate (16):

2-(((ethylthio)carbonothioyl)thio)-2-methylpropanoic acid (**EMP**) (3.00 g, 13.30 mmol, 1.0 eq) was placed in a round bottom Schlenk-flask, evacuated and flooded with nitrogen. The substance was dissolved in dry DCM (90 mL) with the addition of 0.5 mL DMF. At 0 °C oxalyl chloride (3.50 mL, 18.6 mmol, 1.4 eq.) was slowly added to the solution. The reaction was allowed to reach ambient temperature and stirred overnight. The solvent was removed in vacuo and the obtained product (3.25 g, 99%) was used directly for the synthesis of 2-(1,3-dioxo-1,3,3a,4,7,7a-hexahydro-2H-4,7-epoxyisoindol-2-yl)ethyl 2-(((ethylthio)carbonothioyl)thio)-2-methylpropanoate.³⁴⁹



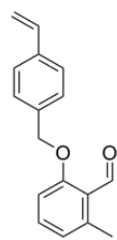
Synthesis of 2-(1,3-dioxo-1,3,3a,4,7,7a-hexahydro-2H-4,7-epoxyisoindol-2-yl)ethyl 2-(((ethylthio)carbonothioyl)thio)-2-methylpropanoate (Mal-trithio-carbonate (17):

In a round bottom Schlenk-flask under a nitrogen atmosphere, 2-(2-hydroxyethyl)-3a,4,7,7a-tetrahydro-1H-4,7-epoxyisoindole-1,3(2H)-dione **15** (2.78 g, 13.3 mmol, 1.1 eq.) was dissolved in dry DCM (30 mL), cooled to 0 °C in an ice bath and triethylamine (3.72 mL, 13.17 mmol, 1.0 eq) was added dropwise to the solution. Subsequently, 1-chloro-2-methyl-1-oxopropan-2-yl ethyl carbonotrithioate **16** (3.25 g, 13.17 mmol, 1.0 eq.) dissolved in dry DCM (40 mL) was added dropwise to the mixture, which was stirred overnight at ambient temperature. DCM (50 mL) was added to the reaction and the mixture was washed with NaHCO₃ solution, deionized water and brine and dried over MgSO₄. The solvent was removed under reduced pressure and the crude product was purified via column chromatography in a mixture of n-hexane/ ethyl acetate (1:1). The pure product was obtained as yellow solid (2.33 g, 49%). ¹H NMR (400 MHz, CDCl₃) δ = 6.51 (s, 2 H, **HC=CH**), 5.26 (s, 2 H, **HC-O-CH**), 4.26 (t, 2 H, ³J_{HH} = 5.3 Hz, CH₂-CH₂-O), 3.78 (t, 2 H, ³J_{HH} = 5.4 Hz, N-CH₂-CH₂), 3.26 (q, 2 H, ³J_{HH} = 7.4 Hz, S-CH₂-CH₃), 2.86 (s, 2 H, **HC-CH**), 1.65 (s, 6 H, C₂H₆), 1.31 (t, 3 H, ³J_{HH} = 7.4 Hz, CH₂-CH₃) ppm. ¹³C NMR (400 MHz, CDCl₃) δ = 221.51 (**C=S**), 175.82 (N-**C=O**), 172.70 (O-**C=O**), 136.56 (**C=C**), 80.87 (**C-O-C**), 62.17 (CH₂-CH₂-O), 55.95 (**HC-CH**), 47.54 (C₂H₉-**C-S**), 37.57 (N-CH₂), 31.25 (S-CH₂-CH₃), 25.13 (C-C₂H₆), 12.88 (CH₂-CH₃) ppm.³⁴⁹



Synthesis of 6-(((3*s*,5*s*,7*s*)-adamantan-1-yl) amino)-6-oxohexyl 2-(((dodecylthio) carbonothioyl) thio) propanoate (DoPAT-Ada) (22):

DoPAT **21** (1.00 g, 2.85 mmol, 1.00 eq.), *N*-((3*s*,5*s*,7*s*)-adamantan-1-yl)-6-hydroxyhexanamide **20** (0.72 g, 2.85 mmol, 1.00 eq.) and DMAP (0.07 g, 0.06 mmol, 0.02 eq.) were dissolved in 25 mL of dry DCM. The solution was cooled to 0 °C in an ice bath and DCC (0.88 g, 4.27 mmol, 1.50 eq.), dissolved in 5 mL dry DMF, was added drop wise to the mixture. After one hour, the ice bath was removed and the reaction stirred over night at ambient temperature. The solvent was removed under reduced pressure and the residue dissolved in diethyl ether. After filtration, the organic layer was washed with 5% HCl, saturated NaHCO₃ solution and deionized H₂O and dried over MgSO₄. Subsequently, the solvent was removed on a rotary evaporator and the crude product was purified via column chromatography (silica gel, cyclohexane/ethyl acetate 5:1, *R_f* = 0.31) to give a yellow oil, which was stored in the fridge (1.19 g, 70%). ¹H NMR (400 MHz, CDCl₃) δ = 5.08 (s, 1 H, NH), 4.81 (q, 1 H, ^{HH}*J*³ = 7.4 Hz, S-CH-CH₃-CO), 4.18-4.08 (m, 2 H, CO₂-CH₂-CH₂), 3.35 (dt, 2 H, ^{HH}*J*³ = 7.3 Hz, CH₂-CH₂-S), 2.10-2.06 (m, 5 H, CH₂-CH₂-CO, Ad-H), 1.99 (s, 6 H, Ad-H), 1.73-1.59 (m, 9H, CH₂-CH₂-S, OC₂H₂-CH₂-CH₂-CH₂-CH₂CO), 1.43-1.35 (m, 2 H, OC₂H₂-CH₂-CH₂-CH₂-CH₂CO), 1.26 (s, 18 H, CH₃-C₉H₁₈-CH₂), 0.88 (t, 3 H, ^{HH}*J*³ = 6.7 Hz, CH₃-C₉H₁₈.) ppm. ¹³C NMR (400 MHz, CDCl₃) δ = 171.87 (OCH-NH), 171.21 (CH₃-CH-CO), 65.75 (O-CH₂-CH₂), 51.86 (NH-C_{Ada}), 48.07 (S-CH-CH₃), 41.77 (C_{Ada}), 37.60 (C_{AD}), 37.30 (CH₂-CO-NH), 36.42 (CH₂-S₃), 31.96 (CH₃-CH₂-CH₂), 29.60 (O-CH₂-CH₂), 29.50 (CH₃-C₂H₄-CH₂), 29.38 (C₆H₁₂-C₂H₄S), 27.94 (C_{Ada}), 25.49 (OC₂H₂-CH₂-C₃H₅ONH), 25.32 (CH₂-C₂HONH), 22.73 (CH₃-CH₂), 16.96 (S-CH-CH₃), 14.17 (CH₃-C₉H₁₈) ppm. MS (ESI) *m/z* calculated for C₃₂H₅₅NO₃S₃ [M+Na]⁺: *m/z*_{theo}: 620.32, *m/z*_{exp}: 620.44.



Synthesis of 2-methyl-6-((4-vinylbenzyl)oxy)benzaldehyde (PE-monomer) (38):

In a three necked round bottom flask, equipped with a reflux condenser 2-hydroxy-6-methylbenzaldehyde **36** (500.00 mg, 3.67 mmol, 1.00 eq.), K₂CO₃ (761.29 mg, 5.51 mmol, 1.5 eq.) and 18-crown-6 (14.55 mg, 0.06 mmol, 0.015 eq.) were evacuated with subsequent addition of nitrogen. The reagents were emulsified in dry THF (10 mL)

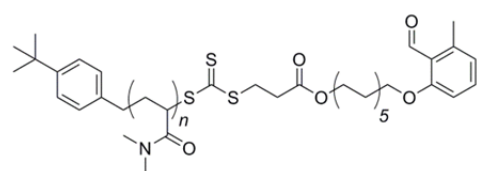
and stirred for 4 h at 80 °C. The slightly yellow reaction mixture turned light green. Subsequently, 4-vinyl benzyl chloride **37** (616.53 mg, 4.04 mmol, 1.10 eq.) was slowly added to the reaction and stirring was continued at 80 °C for another 17 h. The solvent was evaporated under reduced pressure and the residue was dissolved in DCM, washed with deionized H₂O (4 × 100 mL) and dried over MgSO₄. After evaporation of the solvent, the crude product was purified via column chromatography (cyclohexane/ethyl acetate, 10:1, *R_f* = 0.41) to yield a white solid (877.20 mg, 47%). ¹H NMR (400 MHz, CHCl₃): δ = 10.74 (s, 1 H, CHO), 7.38-7.27 (m, 5 H, CH_{Ar}), 6.89 (d, 1 H, ^{HH}J³ = 8.4 Hz, HC_{Ar}-CO), 6.83 (d, 1 H, ^{HH}J³ = 7.6 Hz, HC_{Ar}-C-CH₃), 6.77-6.69 (m, 1 H, CH=CH₂), 5.77 (d, 1 H, ^{HH}J³ = 16.9 Hz, CH_{cis}H_{trans}), 5.28 (d, 1 H, = 11.6 Hz, CH_{cis}H_{trans}), 5.15 (s, 2 H, Ar-CH-O), 2.59 (s, 3 H, Ar-CH₃) ppm. ¹³C NMR (400 MHz, CHCl₃): δ = 192.29 (CHO), 162.30 (C_{Ar}-O), 142.16 (C_{Ar}-CH₃), 137.59 (C_{Ar}-CH=CH₂), 136.32 (C_{Ar}-CH₂-O), 135.73 (CH=CH₂), 134.39 (HC_{Ar}), 127.52 (HC_{Ar}-C_{Ar}-C_{Ar}H), 126.52 (HC_{Ar}-C_{Ar}-C_{Ar}H), 124.45 (C_{Ar}-CHO), 123.69 (C_{Ar}-C_{Ar}-CH₃), 114.37 (CH=CH₂), 110.46 (C_{Ar}-C_{Ar}-O), 70.40 (C_{Ar}-CH₂-O), 21.53 (C_{Ar}-CH₃) ppm.

4.4.4 Polymer Syntheses

Theoretical molecular weight calculations

Theoretical molecular weights were calculated with the equation below:

$$M_{n \text{ theo}} = \left(\frac{[\text{monomer}]}{[\text{CTA}]_0} \times M_{\text{monomer}} \times U \right) + M_{\text{CTA}}$$

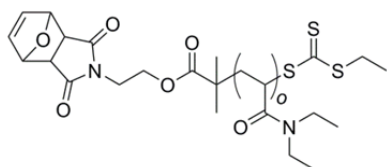


Poly(DMAAm)-tBuBnPE (P23): tBuBnPE-trithiocarbonate **12** (74.04 mg, 0.12 mmol, 1.00 eq.), AIBN (1.90 mg, 11.93 μmol, 0.10 eq.) and DMAAm (1.00 g, 10.09 mmol, 84.62 eq.)

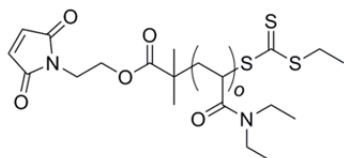
were dissolved in 1,4-dioxane (1.10 mL). The yellow solution was added to a Schlenk-tube and oxygen was removed from the mixture via three consecutive freeze pump thaw cycles. Subsequently, the sample was placed in a preheated oil

4. Complex Macromolecular Architectures

bath at 60 °C for 90 min. The reaction was quenched by cooling on ice and subsequently dialyzed against deionized water with a SpectraPor3 membrane (MWCO = 1000 Da) for three days at ambient temperature. After lyophilization of the aqueous solution, the pure product was obtained as yellowish powder (745.00 mg, $M_{n,theo} = 9000 \text{ g mol}^{-1}$, $M_{n,SEC}(\text{DMAC}) = 7300 \text{ g mol}^{-1}$).

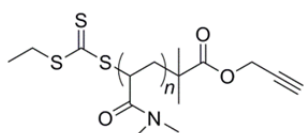


Poly(DEAAm)-Mal-protc. (P24i): DEAAm (1.00 g, 7.862 mmol, 114.67 eq.), Mal-trithiocarbonate **17** (28.49 mg, 0.068 mmol, 1 eq.) and AIBN (1.13 mg, 0.006 mmol, 0.1 eq.) were placed in a Schlenk-tube and dissolved in 1,4-dioxane (1.10 mL). Oxygen was removed from the solution via three freeze pump thaw cycles. The mixture was placed in a preheated oil bath, stirred for 20 min at 60 °C and quenched by cooling on ice. The solution was dialyzed against deionized water with a SpectraPor3 membrane (MWCO = 1000 Da) for three days at 4 °C in the fridge and subsequently lyophilized. The product was obtained as slightly yellow powder (197.40 mg, $M_{n,theo} = 15000 \text{ g mol}^{-1}$, $M_{n,SEC}(\text{DMAC}) = 5400 \text{ g mol}^{-1}$).



Poly(DEAAm)-Mal (P24): poly(DEAAm)-Mal-protc. **P24i** was placed in a round bottom Schlenk-flask. The flask was heated to 120 °C in an oil bath overnight, while being evacuated under high vacuum. Subsequently, the solid was dissolved in deionized water and lyophilized to result in slightly orange powder (169.00 mg, $M_{n,theo} = 15000 \text{ g mol}^{-1}$, $M_{n,SEC}(\text{DMAC}) = 5600 \text{ g mol}^{-1}$).

Exemplary reaction procedures for the β -CD-functionalized polymer blocks:

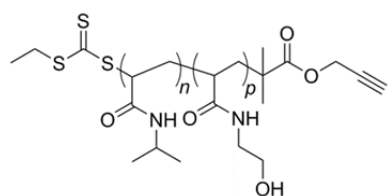


Synthesis of alkyne functionalized poly(DMAAm) (P25): Prop-2-yn-1-yl 2-(((ethylthio)carbonothioyl)thio)-2-methylpropanoate **14** (0.21 g, 0.79 mmol, 1.0 eq., 21.94 mmol L⁻¹), DMAAm (12.00 g, 121.05 mmol, 152.71 eq., 3362.50 mmol L⁻¹) and AIBN (0.012 g, 0.07 mmol, 0.01 eq., 2.19 mmol L⁻¹) were added into a Schlenk-tube,

equipped with a stirring bar and dissolved in DMF (36.0 mL). Oxygen was removed from the reaction mixture via three consecutive freeze-pump-thaw cycles. Subsequently, the tube was placed in an oil bath at 60 °C and the reaction was quenched after 2 h by cooling with liquid nitrogen. The mixture was dialyzed against deionized water with a SpectraPor3 membrane (MWCO = 1000 Da) for three days at ambient temperature. The water was removed by lyophilization and the polymer was obtained as a yellow solid (5.40 g, $M_{n \text{ theo}} = 15400 \text{ g mol}^{-1}$, $M_{n \text{ SEC}} \text{ (DMAC)} = 10100 \text{ g mol}^{-1}$, $\bar{D} = 1.1$, $M_{n \text{ NMR}} = 10050 \text{ g mol}^{-1}$).

Table 5. Reaction conditions for the alkyne-trithiocarbonate **14** mediated polymerization of NiPAAm. The same synthesis procedures applies as it was described for poly(DMAAm)-alkyne **P25i** above. The reaction proceeded at 60 °C for 2.5 h. c_{Mon}^0 is the concentration of the monomer, c_{CTA}^0 is the concentration of CTA **14** and c_{AIBN}^0 is the initial AIBN concentration. $M_{n \text{ theo}}$ refers to the calculated number average molecular weight based on 100% conversion.

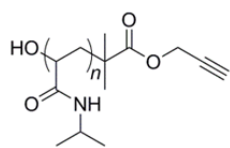
Polymer	c_{Mon}^0 [mmol L ⁻¹]	c_{CTA}^0 [mmol L ⁻¹]	c_{AIBN}^0 [mmol L ⁻¹]	$M_{n \text{ theo}}$ [g mol ⁻¹]	$M_{n \text{ SEC}}$ [g mol ⁻¹]	\bar{D}
p(NiPAAm) P26i	1921.10	22.08	2.11	10500	8800	1.1



Chain extension poly(NiPAAm)-alkyne (P28i):

Poly(NiPAAm)-alkyne **P26i** ($M_{n \text{ SEC}} \text{ (DMAC)} = 8800 \text{ g mol}^{-1}$, 1.00 g, 0.11 mmol, 1.0 eq, 2.84 mmol L⁻¹), AIBN (0.004 g, 0.02 mmol, 0.21 eq., 0.61 mmol L⁻¹) and HOEAAM (2.00 g, 17.37 mmol, 152.87 eq., 434.29 mmol L⁻¹) were placed in a Schlenk-tube and dissolved in DMF (40 mL). Oxygen was removed from the reaction mixture via three consecutive freeze-pump-thaw cycles and the tube was subsequently placed in an oil bath at 60 °C. The solution was stirred at 60 °C for 2.5 h and quenched by cooling with liquid nitrogen. The mixture was dialyzed against deionized water for three days with a SpectraPor3 membrane (MWCO = 1000 Da). After lyophilization the product was obtained as yellow powder (1.03 g, $M_{n \text{ SEC}} \text{ (DMAC)} = 14600 \text{ g mol}^{-1}$, $\bar{D} = 1.1$).

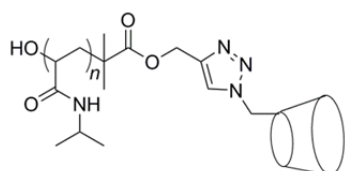
4. Complex Macromolecular Architectures



Alkyne-poly(NiPAAm)-OH (P26ii): In a round bottom flask freshly distilled THF (52 mL) was heated to 60 °C in an oil bath. Under vigorous stirring AIBN (340 mg, 2.07 mmol, 36.00 eq., 39.81 mmol L⁻¹) was added to the flask and stirred for 5 min. Subsequently, poly(NiPAAm)-alkyne **P26i** (M_n (DMAC) = 8800 g mol⁻¹, 500 mg, 0.06 mmol, 1.00 eq., 1.96 mmol L⁻¹) was added to the mixture which turned light yellow. The solution was stirred until complete discoloration (indication of full conversion) under ambient oxygen. To quench the generated peroxides the temperature was reduced to 40 °C and ascorbic acid (108 mg, 0.61 mmol, 6.0 eq., 5.68 mmol L⁻¹) was added. Peroxide dipsticks (Quantofix Peroxid 100, 1 – 100 mg L⁻¹ H₂O₂) were employed to check for the presence of peroxides. The solvent was reduced in vacuo after the removal of the peroxides and the residue was dialyzed against deionized water for three days, employing a SpectraPor3 membrane (MWCO = 1000 Da). The product was obtained as white powder (414.00 mg, $M_{n,SEC}$ (DMAC) = 8900 g mol⁻¹, \bar{D} = 1.1).

Table 6. Reaction conditions for the radical transformation reactions of the trithiocarbonate into a hydroxyl function for poly(DMAAm)-alkyne **P25ii** and poly(NiPAAm)-*b*-(HOEAAm)-alkyne **P28ii**. The same synthetic procedure applies as for poly(NiPAAm)-alkyne **P26ii** above. c^0_{Polymer} is the concentration of the polymer, c^0_{AIBN} is the initial AIBN concentration and $c^0_{\text{ascorbic acid}}$ is the concentration of the radical quencher (ascorbic acid).

Polymer	M_n [g mol ⁻¹]	c^0_{Polymer} [mmol L ⁻¹]	c^0_{AIBN} [mmol L ⁻¹]	$c^0_{\text{ascorbic acid}}$ [mmol L ⁻¹]	$M_{n,SEC}$ [g mol ⁻¹]	\bar{D}
p(DMAAm) P25ii	10100	1.99	39.60	11.80	11700	1.3
p(NiPAAm)- <i>b</i> - p(HOEAAm) P28ii	14600	1.04	39.31	11.87	15500	1.3

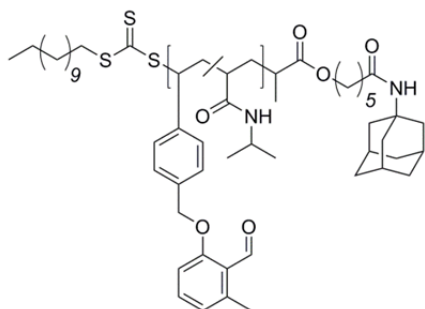


Poly(NiPAAm)- β -CD (P26): In a Schlenk-tube *N,N,N',N',N''*-pentamethyldiethylenetriamine (PMDETA) (100 mg, 0.61 mmol, 14.90 eq., 26.45 mmol L⁻¹), alkyne-poly(NiPAAm)-OH **P26ii** ($M_{n,SEC}$ = 8900 g mol⁻¹, 200 mg, 0.06 mmol, 1.00 eq., 1.77 mmol L⁻¹) and β -CD-N₃ **15** (485 mg, 0.42 mmol, 10.00 eq., 18.23 mmol L⁻¹) were dissolved in DMF (23 mL). Oxygen was removed from the reaction mixture via three consecutive freeze pump thaw cycles and CuBr (77 mg, 0.54 mmol, 13.15 eq.,

23.34 mmol L⁻¹) was added under a stream of argon. The mixture was stirred for two days at ambient temperature und dialyzed against deionized water (SpectraPor3 membrane (MWCO = 1000 Da)) for three days. After lyophilization, the product was obtained as white solid (189 mg, $M_{n, SEC}$ (DMAC) = 8800 g mol⁻¹, \bar{D} = 1.2).

Table 7. Reaction conditions for the CuAAC-click reactions of an azide-functionalized β -CD **15** to alkyne terminated polymers as was described above for poly(NiPAAm)- β -CD **P26**. c^0_{Polymer} is the concentration of the polymer, $c^0_{\beta\text{-CD-azide}}$ is the concentration of the azide-functionalized β -CD **15**, c^0_{CuBr} is the concentration of CuBr and c^0_{PMDETA} the concentration of the ligand.

	M_n [g mol ⁻¹]	c^0_{Polymer} [mmol L ⁻¹]	$c^0_{\beta\text{-CD-azide}}$ [mmol L ⁻¹]	c^0_{CuBr} [mmol L ⁻¹]	c^0_{PMDETA} [mmol L ⁻¹]	$M_{n, SEC}$ [g mol ⁻¹]	\bar{D}
P25	11700	1.25	37.29	26.04	23.96	10700	1.3
P28	15500	0.86	17.75	22.77	25.86	16400	1.3



Synthesis of adamantyl functionalized poly(NIPAAm/Photoenol) (poly(NiPAAM/PE)-Ada) (P39): 6-(((3s,5s,7s)-adamantan-1-yl) amino)-6-oxohexyl 2-(((dodecylthio) carbonothioyl) thio) propanoate **22** (20.34 mg, 0.034 mmol, 1.00 eq.), NIPAAm (1.00 g, 8.837 mmol, 259.82 eq.), 2-methyl-6-((4-vinylbenzyl)oxy)benzaldehyde **38** (66.89 mg, 0.265 mmol, 7.79 eq.) and AIBN (0.55 mg, 0.003 mmol, 0.10 eq.) were added to a Schlenk-tube and dissolved in 1,4-dioxane (4 mL). Oxygen was removed from the mixture via four freeze pump thaw cycles. Subsequently, the tube was placed in an oil bath at 67 °C for 24 h. The mixture was dialyzed against deionized water with a SpectraPor3 membrane (MWCO = 1000 Da) for three days at 4 °C. The solvent was removed by lyophilization and the residue was precipitated in cold diethyl ether from a THF solution. After filtration the polymer was obtained as white powder (633 mg, $M_{n, theo}$ = 30000 g mol⁻¹, SEC(DMAC): $M_{n, SEC}$ = 39700 g mol⁻¹, \bar{D} = 1.2, $M_{n, NMR}$ = 24100 g mol⁻¹, calc. (NMR): 3% photoenol units incorporated).

6-(((3s,5s,7s)-adamantan-1-yl) amino)-6-oxohexyl 2-(((dodecylthio) carbonothioyl) thio) propanoate **22** (20.34 mg, 0.034 mmol, 1.00 eq.), NIPAAm (1.00 g, 8.837 mmol, 259.82 eq.), 2-methyl-6-((4-vinylbenzyl)oxy)benzaldehyde **38** (66.89 mg, 0.265 mmol, 7.79 eq.) and AIBN (0.55 mg, 0.003 mmol, 0.10 eq.) were added to a Schlenk-tube and dissolved in 1,4-dioxane (4 mL). Oxygen was removed from the mixture via four freeze pump thaw cycles. Subsequently, the tube was placed in an oil bath at 67 °C for 24 h. The mixture was dialyzed against deionized water with a SpectraPor3 membrane (MWCO = 1000 Da) for three days at 4 °C. The solvent was removed by lyophilization and the residue was precipitated in cold diethyl ether from a THF solution. After filtration the polymer was obtained as white powder (633 mg, $M_{n, theo}$ = 30000 g mol⁻¹, SEC(DMAC): $M_{n, SEC}$ = 39700 g mol⁻¹, \bar{D} = 1.2, $M_{n, NMR}$ = 24100 g mol⁻¹, calc. (NMR): 3% photoenol units incorporated).

4.4.5 Multiblock Copolymer Formation

Formation of the diblock copolymer via the photo-induced Diels-Alder reaction (P29)

poly(DEAAm)-Mal **P24** (20.00 mg, 0.0014 mmol, 1.0 eq. based on $M_{n\text{ SEC}} = 5600\text{ g mol}^{-1}$) and poly(DMAAm)-*t*BuBnPE **P23** (10.43 mg, 0.0035 mmol, 0.4 eq. based on $M_{n\text{ SEC}} = 7300\text{ g mol}^{-1}$) were dissolved in MeCN (6 mL) and aliquoted into headspace vials. The vials were crimped airtight with SBR seals with PTFE inlet and oxygen was removed from the solution by purging with nitrogen for 15 min. Subsequently, the vial was placed in a custom-built photoreactor and irradiated at a wavelength of 320 nm for 40 min. The solvent was removed in vacuo and the residue measured directly in the SEC (30.00 mg, $M_{n\text{ SEC}}$ (DMAC) = 10000 g mol⁻¹).

Exemplary procedure for the formation of the supramolecular triblock copolymer (P30)

The diblock copolymer **P29** (30.00 mg, 0.003 mmol, 1.00 eq., 1.00 mmol L⁻¹, based on $M_n = 10000\text{ g mol}^{-1}$) was dissolved in 2.0 mL DMF. In a separate vial poly(NiPAAm)- β -CD **P26** (26.40 mg, 0.003 mmol, 1.00 eq., 1.00 mmol L⁻¹, based on $M_n = 8800\text{ g mol}^{-1}$) was dissolved in DMF (1.0 mL) as well. The solution of **7** was slowly added to the solution of **6** and was stirred at ambient temperature for 30 min. Subsequently, the mixture was dialyzed against a gradient of deionized H₂O/DMF (70:30, 80:20, 90:10 and finally 100% H₂O) in a SpectraPor3 membrane (MWCO = 1000 Da). The inclusion complex of β -CD and the *tert*-butyl phenyl moiety was evidenced via 2D NOESY NMR in D₂O and DLS measurements in Milli-Q water with a concentration of 0.06 mmol L⁻¹ ($D_h \approx 23.0\text{ nm}$).

Table 8. Reaction conditions for supramolecular self-assembly of the β -CD-polymers with the covalently bound diblock copolymer **P29**. The same reaction conditions apply as stated for the formation of poly(DEAAm)-*b*-poly(DMAAm)-*b*-poly(NiPAAm) **P30**.

supramolecular block	M_n β -CD polymer [g mol ⁻¹]	C^0 Polymer [mmol L ⁻¹]	C^0 diblock copolymer 6 [mmol L ⁻¹]
P31	10700	0.47	0.47
P32	16400	1.00	1.00

4.4.6 Nanoparticle Design

Formation of the supramolecular diblock copolymer (P40)

Poly(NIPAAm/PE)-Ada **P39** (M_n NMR = 24100 g mol⁻¹, 100.00 mg, 1.00 eq.) was placed into a vial and dissolved in DMF (10 mL). In a second vial poly(DMAAm)- β -CD **P25** (M_n NMR = 11000 g mol⁻¹, 65.56 mg, 1.00 eq.) was also dissolved in DMF (5 mL). Subsequently, the solution of the poly(DMAAm)- β -CD **P25** was added to the DMF solution of poly(NIPAAm/PE)-Ada **P39** and stirred at ambient temperature for 30 min. Afterwards, the mixture was dialyzed with a SpectraPor3 membrane (MWCO = 1000 Da) against a gradient of deionized H₂O/DMF (70:30, 80:20, 90:10 and finally 100% H₂O). The formed complex was analyzed via 2D NOESY NMR in D₂O and DLS measurements in Milli-Q water with a concentration of 0.06 mmol L⁻¹ ($D_h \approx 19$ nm). Spectra and graphs are shown in the results and discussion section. For later stoichiometric calculation, the sum of the molecular weight distributions of poly(NiPAAm/PE)-Ada and poly(DMAAm)- β -CD is employed for the M_n of the diblock copolymer.

Formation of the cross-linked micelle (M42)

The supramolecular diblock copolymer **P40** (M_n = 39900 g mol⁻¹, 10.60 mg, 0.0003 mmol, 0.006 mmol L⁻¹, 1.00 eq.) and 4-arm PEG-maleimide **41** (M_n = 2090 g mol⁻¹, 3.04 mg, 0.0012 mmol, 0.025 mmol L⁻¹, 4.00 eq.) were added into a headspace vial, dissolved in Milli-Q water (4.5 mL) and sealed. The vial was placed in an ice bath and the mixture was purged with nitrogen for 1 h. Meanwhile, a photo-

reactor was equipped with five Arimed B6 low pressure mercury lamps (320 nm, 36 W) and turned on for 1 h before adding the sample, so a reactor temperature close to 50 °C was established. Prior to irradiation of the sample, the solution was heated above the LCST of the diblock copolymer, resulting in a slightly turbid emulsion. Subsequently, the vial was positioned in the photo-reactor and irradiated at 50 °C for 6 h. The sample was filtered through a 0.45 µm syringe filter and freeze dried. The cross-linked micelles were analyzed via DLS ($D_h \approx 50$ nm) and AFM. The data is discussed in the results and discussion section.

Release of the nanoparticles (N43)

Trifluoroacetic acid (TFA) (0.20 mL) was added to a dispersion of the crosslinked micelle **M42** (5.64 mg) at a concentration of 1 mg mL⁻¹ in Milli-Q water (5.64 mL), stirred for 1 h at ambient temperature and stored in the fridge for two days. To remove the cleaved micelle arms the sample was centrifuged stepwise. Therefore, the solution was distributed into four Eppendorf Safe-Lock Tubes (500 µL) and placed in a preheated centrifuge (40 °C) for 5 min. Subsequently, the samples were centrifuged at 40 °C for 4 min with 3000 rpm. Subsequently, 400 µL of the supernatant fluid were withdrawn from the Safe-Lock Tubes and collected in a vial. Then, another 500 µL of the nanoparticle solution was added to the same tube and centrifuged at 40 °C for 4 min at 5000 rpm. Following the removal of the supernatant fluid, the sample was washed by the addition of 400 µL Milli-Q water and subsequent centrifugation. The washing was repeated two times. The last centrifugation step was carried out at 40 °C with 13000 rpm for 4 min. The nanoparticle was analyzed via NMR, DLS ($D_h \approx 35$ nm) and AFM, please refer to the results and discussion section.

5

Conclusion and Outlook

Light-induced reactions have inspired scientists since the beginning of the last century. As a consequence, research in the field of photochemistry is constantly evolving, allowing for precise control over spatial and temporal resolution offered by such techniques. Furthermore, light-induced reactions are independent of catalytic systems and usually proceed without the formation of interfering side products. Within the scope of the current thesis, the efficiency of light induced reactions was exploited in the context of macromolecular design in solution and on surfaces.

In Chapter 3, the spatially resolved deprotection of a photolabile protecting group, functionalized with an ATRP initiator and covalently attached onto a polycarbonate film, was demonstrated. The mild and efficient photolithographic approach allowed for the generation of defined patterns of hydrophilic moieties on the micrometer

scale. Moreover, a biorepellent polymer was grafted from the surface with the remaining initiator molecules, thus creating boundaries for guided protein and cell attachment. The patterned surface was successfully shaped into a three-dimensional microchannel to provide a biomimetic polymeric environment to investigate cell cultures. In addition, cells were successfully seeded on the surface, and the evaluations showed that they primarily attached to the pre-defined hydrophobic areas on the surfaces of the 2D substrate and inside the 3D microchannel. In view of the successful thermoforming process that did not compromise the preceding chemical surface modification, a promising method was introduced for the development of disposable biologic platforms for e.g. artificial neurochannel design. Prospectively, there is a strong motivation to test a broad variety of hollow structures on patterned surfaces, thus investigating not only one set of cells, but also co-cultures on a single substrate. In addition, more intensive studies to demonstrate active guiding via visualized cell migration experiments should be performed, by labelling the cells prior to planting. At a certain stage of the work, the route employed herein appeared to be the most convenient, due to the restricted range of solvents applicable to the PC film. Nevertheless, it would be interesting to explore alternative grafting strategies onto the surface and to exploit the amenability of polycarbonate to thermoforming in other scientific fields as well.

In Chapter 4, versatile macromolecular architectures were successfully designed via a modular approach, combining photo-initiated Diels–Alder reactions with supramolecular host-guest interactions of cyclodextrins. For the first time, the two very efficient, orthogonal and facile conjugation methods were employed in combination, yielding multiblock copolymers as well as stimuli responsive micelles and nanoparticles. It was demonstrated that both reactions can be readily performed in stoichiometric amounts and without the addition of further reagents. The polymeric building blocks were prepared via RAFT polymerization, thus directly introducing the desired functionalities into the polymer chains via the RAFT agent or by post-polymerization modification. Even though the RAFT process is a versatile polymerization method for the synthesis of well-defined polymer chains with respect to molecular weight and size distribution, the end-group fidelity of RAFT

polymerization still has its limitations. As a consequence, non-functionalized polymer chains remained in the sample after the light-induced formation of the covalently bound diblock copolymer, which might affect future applications, e.g. as a self-healing material supported by the dynamic supramolecular interactions. Thus, further research should be performed to determine the quantity of non-reacted chains in the sample and to further minimize them, if necessary.

Importantly, thermoresponsive nanoparticles were designed via the micellar assembly of a supramolecularly formed diblock copolymer which was photochemically cross-linked in its core. By the destruction of the host unit of the supramolecular inclusion complex, the sacrificial micellar arms were removed from the core and the nanoparticles were released. The nanoparticles and micelles were probed for their thermoresponsive contraction and relaxation, which was evidenced by the temperature-induced change of the hydrodynamic radii in DLS measurements. The synthetic approach to construct nanoparticles via a micellar scaffold is promising, since the system can either be applied as a thermoresponsive micelle or as a plain nanoparticle. In addition, the removal of the micelle arms leaves the nanoparticle covered by guest moieties which still serve as active ligations points. In this context, further studies should be undertaken to re-functionalize the nanoparticles, e.g. with host-functionalized proteins to be employed as drug delivery systems. For the purpose of utilizing the nanoparticles as a delivery system, their potential to encapsulate hydrophobic substances should be explored, e.g. via fluorescent dye release experiments.³⁹³ In the long term, the nanostructures could be reversibly attached to solid substrates modified with receptor host molecules, so-called molecular printboards.³⁹⁴⁻³⁹⁶

In summary, the work performed in the course of the present dissertation contributed to the broad field of applications of photochemically induced reactions. By means of a photolithographic approach, a simple polymer substrate was transformed into an innovative biological platform with cell-guiding attributes. Furthermore, light induced reactions in conjunction with other ligation techniques, such as supramolecular host-guest interactions, was a fundamental step towards

5. Conclusion and Outlook

advanced functional materials which may find their way into application oriented research and development.

References

1. Ciamician, G. *Science* **1912**, 36, 385-394.
2. Heindel, N. D.; Pfau, M. A. *J. Chem. Educ.* **1965**, 42, 383-386.
3. Büchi, G.; Inman, C. G.; Lipinsky, E. S. *J. Am. Chem. Soc.* **1954**, 76, 4327-4331.
4. Hoffmann, N. *Chem. Rev.* **2008**, 108, 1052-1103.
5. Tasdelen, M. A.; Yagci, Y. *Angew. Chem. Int. Ed.* **2013**, 52, (23), 5930-5938.
6. Hiltebrandt, K.; Pauloehrl, T.; Blinco, J. P.; Linkert, K.; Börner, H. G.; Barner-Kowollik, C. *Angew. Chem. Int. Ed.* **2015**, 54, 2838-2843.
7. Yamaguchi, S.; Chen, Y.; Nakajima, S.; Furuta, T.; Nagamune, T. *Chem. Commun.* **2010**, 46, 2244-2246.
8. Dormán, G.; Prestwich, G. D. *Trends Biotechnol.* **2000**, 18, 64-77.
9. Ellis-Davies, G. C. R. *Nat. Meth.* **2007**, 4, 619-628.
10. Scholpp, S.; Shimogori, T. *Front. Neurosci.* **2013**, 7, 1-2.
11. Scholpp, S.; Wolf, O.; Brand, M.; Lumsden, A. *Development* **2006**, 133, 855-864.
12. Bhatia, S. N.; Balis, U. J.; Yarmush, M. L.; Toner, M. *J. Biomater. Sci., Polym. Ed.* **1998**, 9, 1137-1160.
13. Bhatia, S. N.; Balis, U. J.; Yarmush, M. L.; Toner, M. *Biotechnol. Prog.* **1998**, 14, 378-387.
14. Bhatia, S. N.; Chen, C. S. *Biomed. Microdevices* **1999**, 2, 131-144.
15. Truckenmuller, R.; Giselbrecht, S. *IEE. Proc. Nanobiotechnol.*, **2004**, 163-166.
16. Truckenmüller, R.; Giselbrecht, S.; Rivron, N.; Gottwald, E.; Saile, V.; van den Berg, A.; Wessling, M.; van Blitterswijk, C. *Adv. Mater.* **2011**, 23, 1311-29.
17. Truckenmüller, R.; Giselbrecht, S.; van Blitterswijk, C.; Dambrowsky, N.; Gottwald, E.; Mappes, T.; Rolletschek, A.; Saile, V.; Trautmann, C.; Weibezahn, K. F.; Welle, A. *Lab Chip* **2008**, 8, 1570-9.
18. Hawker, C. J.; Wooley, K. L. *Science* **2005**, 309, 1200-1205.
19. Hadjichristidis, N.; Hiraio, A.; Tezuka, Y.; Du Prez, F., *Complex macromolecular architectures: synthesis, characterization, and self-assembly*. John Wiley & Sons: **2011**.
20. Gregory, A.; Stenzel, M. H. *Prog. Polym. Sci.* **2012**, 37, 38-105.
21. Chong, Y. K.; Le, T. P. T.; Moad, G.; Rizzardo, E.; Thang, S. H. *Macromolecules* **1999**, 32, 2071-2074.

22. Inglis, A. J.; Barner-Kowollik, C. *Macromol. Rapid Commun.* **2010**, 31, 1247-1266.
23. Kempe, K.; Krieg, A.; Becer, C. R.; Schubert, U. S. *Chem. Soc. Rev.* **2012**, 41, 176-191.
24. Sumerlin, B. S.; Vogt, A. P. *Macromolecules* **2010**, 43, 1-13.
25. Zhou, J.; Ritter, H. *Polym. Chem.* **2010**, 1, 1552-1559.
26. Nakahata, M.; Takashima, Y.; Yamaguchi, H.; Harada, A. *Nat. Commun.* **2011**, 2, 511.
27. Trommsdorff, H. *Ann. der Pharm.* **1834**, 11, 190-207.
28. Einstein, A. *Ann. Phys.* **1905**, 164-181.
29. Bodenstein, M.; Weigert, F.; Luther, R.; Franck, J.; Ornstein, L. S.; Lindemann, F. A.; Rice, J.; Christiansen, J. A.; Baly, E. C. C.; Rice; Rideal, E. K.; Allmand, A. J.; von Halban, H.; Lasareff, P.; Bowen, E. J.; Taylor, H. S.; Chapman, D. L.; Roy, S. C.; Langedyk, S. L.; Padoa, M.; Rawlins, F. I. G. *Trans. Faraday Soc.* **1926**, 21, 515-524.
30. Bodenstein, M. *Z. Phys. Chem* **1913**, 85, 329-421.
31. Ciamician, G.; Silber, P. *Ber. Dtsch. Chem. Ges* **1901**, 34, 2040-2046.
32. Ciamician, G.; Silber, P. *Ber. Dtsch. Chem. Ges* **1907**, 40, 2415-2424.
33. Ciamician, G.; Silber, P. *Ber. Dtsch. Chem. Ges* **1908**, 41, 1928-1935.
34. Albini, A.; Fagnoni, M., *Handbook of synthetic photochemistry*. John Wiley & Sons: **2009**.
35. Bamford, C. H.; Norrish, R. G. W. *J. Chem. Soc. (Resumed)* **1938**, 1544-1554.
36. Norrish, R.; Bamford, C. *Nature* **1936**, 138, 1016-1016.
37. Norrish, R.; Bamford, C. *Nature* **1937**, 140, (3535), 195-196.
38. Norrish, R. G. W.; Appleyard, M. E. S. *J. Chem. Soc. (Resumed)* **1934**, 874-880.
39. Jabłoński, A. *Z. Phys.* **1935**, 94, 38-46.
40. Atkins, P. W., *Physikalische Chemie*. **2001**; 3. Edition.
41. Cowan, D., *Elements of organic photochemistry*. Springer Science & Business Media: **2012**.
42. Frick, E.; Ernst, H. A.; Voll, D.; Wolf, T. J. A.; Unterreiner, A.-N.; Barner-Kowollik, C. *Polym. Chem.* **2014**, 5, 5053-5068.
43. Marciniak, B. *J. Chem. Educ.* **1988**, 65, 832-834.
44. Griesbeck, A. G.; Mattay, J., *Synthetic organic photochemistry*. CRC Press: **2004**.
45. Yang, N. C.; Rivas, C. *J. Am. Chem. Soc.* **1961**, 83, 2213-2213.
46. Yang, N. C.; Yang, D.-D. H. *J. Am. Chem. Soc.* **1958**, 80, 2913-2914.
47. Porter, G.; Tchir, M. F. *J. Chem. Soc. D Chem. Commun.* **1970**, 1372-1373.
48. Porter, G.; Tchir, M. F. *J. Chem. Soc. A* **1971**, 3772-3777.

-
49. Small, R. D.; Scaiano, J. C. *J. Am. Chem. Soc.* **1977**, 99, 7713-7714.
 50. Small, R. D.; Scaiano, J. C. *J. Phys. Chem.* **1978**, 82, 2662-2664.
 51. Wagner, P. J.; Kelso, P. A.; Zepp, R. G. *J. Am. Chem. Soc.* **1972**, 94, 7480-7488.
 52. Wagner, P. J.; Sedon, J. H. *Tetrahedron Lett.* **1978**, 19, 1927-1930.
 53. Gruending, T.; Oehlenschlaeger, K. K.; Frick, E.; Glassner, M.; Schmid, C.; Barner-Kowollik, C. *Macromol. Rapid Commun.* **2011**, 32, 807-812.
 54. Glassner, M.; Oehlenschlaeger, K. K.; Gruending, T.; Barner-Kowollik, C. *Macromolecules* **2011**, 44, 4681-4689.
 55. Oehlenschlaeger, K. K.; Mueller, J. O.; Heine, N. B.; Glassner, M.; Guimard, N. K.; Delaittre, G.; Schmidt, F. G.; Barner-Kowollik, C. *Angew. Chem. Int. Ed.* **2013**, 52, 762-766.
 56. Pauloehrl, T.; Delaittre, G.; Winkler, V.; Welle, A.; Bruns, M.; Börner, H. G.; Greiner, A. M.; Bastmeyer, M.; Barner-Kowollik, C. *Angew. Chem. Int. Ed.* **2012**, 51, 1071-1074.
 57. Preuss, C. M.; Tischer, T.; Rodriguez-Emmenegger, C.; Zieger, M. M.; Bruns, M.; Goldmann, A. S.; Barner-Kowollik, C. *J. Mater. Chem. B* **2014**, 2, 36-40.
 58. Tischer, T.; Claus, T. K.; Oehlenschlaeger, K. K.; Trouillet, V.; Bruns, M.; Welle, A.; Linkert, K.; Goldmann, A. S.; Börner, H. G.; Barner-Kowollik, C. *Macromol. Rapid Commun.* **2014**, 35, 1121-1127.
 59. Altintas, O.; Willenbacher, J.; Wuest, K. N. R.; Oehlenschlaeger, K. K.; Krolla-Sidenstein, P.; Gliemann, H.; Barner-Kowollik, C. *Macromolecules* **2013**, 46, 8092-8101.
 60. Kaupp, M.; Tischer, T.; Hirschbiel, A. F.; Vogt, A. P.; Geckle, U.; Trouillet, V.; Hofe, T.; Stenzel, M. H.; Barner-Kowollik, C. *Macromolecules* **2013**, 46, 6858-6872.
 61. Ashram, M.; Miller, D. O.; Georghiou, P. E. *J. Chem. Soc. Perkin Trans. 1* **2002**, 1470-1476.
 62. Arumugam, S.; Popik, V. V. *J. Am. Chem. Soc.* **2011**, 133, 5573-5579.
 63. Arumugam, S.; Guo, J.; Mbua, N. E.; Friscourt, F.; Lin, N.; Nekongo, E.; Boons, G.-J.; Popik, V. V. *Chem. Sci.* **2014**, 5, 1591-1598.
 64. Arumugam, S.; Orski, S. V.; Locklin, J.; Popik, V. V. *J. Am. Chem. Soc.* **2012**, 134, 179-182.
 65. Arumugam, S.; Popik, V. V. *J. Am. Chem. Soc.* **2011**, 133, 15730-15736.
 66. Arumugam, S.; Popik, V. V. *J. Am. Chem. Soc.* **2012**, 134, 8408-8411.
 67. Klán, P.; Šolomek, T.; Bochet, C. G.; Blanc, A.; Givens, R.; Rubina, M.; Popik, V.; Kostikov, A.; Wirz, J. *Chem. Rev.* **2013**, 113, 119-191.
 68. Kulikov, A.; Arumugam, S.; Popik, V. V. *J. Org. Chem.* **2008**, 73, 7611-7615.
 69. McNitt, C. D.; Popik, V. V. *Org. Biomol. Chem.* **2012**, 10, 8200-8202.

References

70. Orski, S. V.; Poloukhine, A. A.; Arumugam, S.; Mao, L.; Popik, V. V.; Locklin, J. *J. Am. Chem. Soc.* **2010**, 132, 11024-11026.
71. Nekongo, E. E.; Popik, V. V. *J. Org. Chem.* **2014**, 79, 7665-7671.
72. Vedejs, E.; Eberlein, T. H.; Mazur, D. J.; McClure, C. K.; Perry, D. A.; Ruggeri, R.; Schwartz, E.; Stults, J. S.; Varie, D. L. *J. Org. Chem.* **1986**, 51, 1556-1562.
73. Vedejs, E.; Eberlein, T. H.; Wilde, R. G. *J. Org. Chem.* **1988**, 53, 2220-2226.
74. Glassner, M.; Oehlenschlaeger, K. K.; Welle, A.; Bruns, M.; Barner-Kowollik, C. *Chem. Commun.* **2013**, 49, 633-635.
75. Pauloehrl, T.; Welle, A.; Oehlenschlaeger, K. K.; Barner-Kowollik, C. *Chem. Sci.* **2013**, 4, 3503-3507.
76. del Campo, A.; Boos, D.; Spiess, H. W.; Jonas, U. *Angew. Chem. Int. Ed.* **2005**, 44, 4707-4712.
77. Cui, J.; Miguel, V. S.; del Campo, A. *Macromol. Rapid Commun.* **2013**, 34, 310-329.
78. Bochet, C. G. *J. Chem. Soc. Perkin Trans. 1* **2002**, 125-142.
79. Kessler, M.; Glatthar, R.; Giese, B.; Bochet, C. G. *Org. Lett.* **2003**, 5, 1179-1181.
80. Pelliccioli, A. P.; Wirz, J. *Photochem. Photobiol. Sci.* **2002**, 1, 441-458.
81. Delaittre, G.; Greiner, A. M.; Pauloehrl, T.; Bastmeyer, M.; Barner-Kowollik, C. *Soft Matter* **2012**, 8, 7323-7347.
82. Pauloehrl, T.; Delaittre, G.; Bruns, M.; Meißler, M.; Börner, H. G.; Bastmeyer, M.; Barner-Kowollik, C. *Angew. Chem. Int. Ed.* **2012**, 51, 9181-9184.
83. Fehrentz, T.; Schönberger, M.; Trauner, D. *Angew. Chem. Int. Ed.* **2011**, 50, 12156-12182.
84. Kramer, R. H.; Chambers, J. J.; Trauner, D. *Nat. Chem. Biol.* **2005**, 1, 360-365.
85. Lovell, J. F.; Liu, T. W. B.; Chen, J.; Zheng, G. *Chem. Rev.* **2010**, 110, 2839-2857.
86. Barltrop, J.; Schofield, P. *J. Chem. Soc. (Resumed)* **1965**, 4758-4765.
87. Barltrop, J. A.; Schofield, P. *Tetrahedron Lett.* **1962**, 3, 697-699.
88. Hoffmann, N. *Photochem. Photobiol. Sci.* **2012**, 11, 1613-1641.
89. Mayer, G.; Heckel, A. *Angew. Chem.* **2006**, 118, 5020-5042.
90. Patchornik, A.; Amit, B.; Woodward, R. B. *J. Am. Chem. Soc.* **1970**, 92, 6333-6335.
91. Rajasekharan Pillai, V. *Synthesis* **1980**, 1, 1-26.
92. Suyama, K.; Shirai, M. *Prog. Polym. Sci.* **2009**, 34, 194-209.
93. Yu, H.; Li, J.; Wu, D.; Qiu, Z.; Zhang, Y. *Chem. Soc. Rev.* **2010**, 39, 464-473.
94. Zhao, H.; Sterner, E. S.; Coughlin, E. B.; Theato, P. *Macromolecules* **2012**, 45, 1723-1736.
95. Corrie, J. E. T.; Barth, A.; Munasinghe, V. R. N.; Trentham, D. R.; Hutter, M. C. *J. Am. Chem. Soc.* **2003**, 125, 8546-8554.

-
96. Holmes, C. P. *J. Org. Chem.* **1997**, 62, 2370-2380.
 97. Petropoulos, C. C. *J. Polym. Sci. A Polym. Chem.* **1977**, 15, 1637-1644.
 98. Johnson, J. A.; Finn, M. G.; Koberstein, J. T.; Turro, N. J. *Macromolecules* **2007**, 40, 3589-3598.
 99. Johnson, J. A.; Turro, N. J.; Koberstein, J. T.; Mark, J. E. *Prog. Polym. Sci.* **2010**, 35, 332-337.
 100. Kloxin, A. M.; Kasko, A. M.; Salinas, C. N.; Anseth, K. S. *Science* **2009**, 324, 59-63.
 101. Jiang, J.; Tong, X.; Morris, D.; Zhao, Y. *Macromolecules* **2006**, 39, 4633-4640.
 102. Jiang, X.; Jin, S.; Zhong, Q.; Dadmun, M. D.; Zhao, B. *Macromolecules* **2009**, 42, 8468-8476.
 103. Schumers, J. M.; Bertrand, O.; Fustin, C. A.; Gohy, J. F. *J. Polym. Sci. A Polym. Chem.* **2012**, 50, 599-608.
 104. Handwerger, R. G.; Diamond, S. L. *Bioconjug. Chem.* **2007**, 18, 717-723.
 105. Piggott, A. M.; Karuso, P. *Tetrahedron Lett.* **2005**, 46, 8241-8244.
 106. Goldbach, J. T.; Lavery, K. A.; Penelle, J.; Russell, T. P. *Macromolecules* **2004**, 37, 9639-9645.
 107. Goldbach, J. T.; Russell, T. P.; Penelle, J. *Macromolecules* **2002**, 35, 4271-4276.
 108. Kang, M.; Moon, B. *Macromolecules* **2008**, 42, 455-458.
 109. Bhatnagar, P.; Malliaras, G. G.; Kim, I.; Batt, C. A. *Adv. Mater.* **2010**, 22, 1242-1246.
 110. Doh, J.; Irvine, D. J. *J. Am. Chem. Soc.* **2004**, 126, 9170-9171.
 111. Kim, M.; Choi, J.-C.; Jung, H.-R.; Katz, J. S.; Kim, M.-G.; Doh, J. *Langmuir* **2010**, 26, 12112-12118.
 112. Pauloehrl, T.; Delaittre, G.; Bruns, M.; Meißler, M.; Börner, H. G.; Bastmeyer, M.; Barner-Kowollik, C. *Angew. Chem. Int. Ed.* **2012**, 51, 9181-9184.
 113. Matyjaszewski, K. *Macromolecules* **2012**, 45, 4015-4039.
 114. Matyjaszewski, K.; Davis, T. P., *Handbook of Radical Polymerization*. John Wiley & Sons: Hoboken, NJ, **2002**.
 115. Matyjaszewski, K.; Müller, A. H., *Controlled and Living Polymerizations: From Mechanisms to Applications*. John Wiley & Sons: **2009**.
 116. Hadjichristidis, N.; Pitsikalis, M.; Pispas, S.; Iatrou, H. *Chem. Rev.* **2001**, 101, 3747-3792.
 117. Szwarc, M. *Nature* **1956**, 178, 1168-1169.
 118. Hawker, C. J.; Bosman, A. W.; Harth, E. *Chem. Rev.* **2001**, 101, 3661-3688.
 119. Braunecker, W. A.; Matyjaszewski, K. *Prog. Polym. Sci.* **2008**, 33, 165.
 120. Ouchi, M.; Terashima, T.; Sawamoto, M. *Chem. Rev.* **2009**, 109, 4963-5050.
 121. Wang, J.-S.; Matyjaszewski, K. *J. Am. Chem. Soc.* **1995**, 117, 5614-5615.

122. Fischer, H. *Chem. Rev.* **2001**, 101, 3581-610.
123. Moad, G.; Chong, Y. K.; Postma, A.; Rizzardo, E.; Thang, S. H. *Polymer* **2005**, 46, 8458-8468.
124. Moad, G.; Rizzardo, E.; Thang, S. H. *Acc. Chem. Res.* **2008**, 41, 1133-1142.
125. Moad, G.; Rizzardo, E.; Thang, S. H. *Aust. J. Chem.* **2009**, 62, 1402-1472.
126. Fukuda, T.; Terauchi, T.; Goto, A.; Ohno, K.; Tsujii, Y.; Miyamoto, T.; Kobatake, S.; Yamada, B. *Macromolecules* **1996**, 29, 6393-6398.
127. Georges, M. K.; Veregin, R. P. N.; Kazmaier, P. M.; Hamer, G. K. *Macromolecules* **1993**, 26, 2987-2988.
128. Kato, M.; Kamigaito, M.; Sawamoto, M.; Higashimura, T. *Macromolecules* **1995**, 28, 1721-1723.
129. Matyjaszewski, K.; Xia, J. *Chem. Rev.* **2001**, 101, 2921-2990.
130. Barbey, R.; Lavanant, L.; Paripovic, D.; Schüwer, N.; Sugnaux, C.; Tugulu, S.; Klok, H.-A. *Chem. Rev.* **2009**, 109, 5437-5527.
131. Barner-Kowollik, C., *Handbook of RAFT-Polymerization*. **2008**.
132. Moad, G.; Rizzardo, E.; Thang, S. H. *Aust. J. Chem.* **2005**, 58, 379-410.
133. Mayadunne, R. T. A.; Jeffery, J.; Moad, G.; Rizzardo, E. *Macromolecules* **2003**, 36, 1505-1513.
134. Stenzel, M. H.; Zhang, L.; Huck, W. T. *Macromol. Rapid Commun.* **2006**, 27, 1121-1126.
135. Bender, M. L.; Komiyama, M., *Cyclodextrin chemistry*. Springer Science & Business Media: **2012**.
136. Hedges, A. R. *Chem. Rev.* **1998**, 98, 2035-2044.
137. Villiers, A. *Compt. Rend. Acad. Sci.* **1891**, 112, 536.
138. Schardinger, F. *Z. Lebensm. Unters. Forsch. A* **1903**, 6, 865-880.
139. Lichtenthaler, F. W. *Angew. Chem. Int. Ed.* **1995**, 33, 2364-2374.
140. Koshland, D. E. *Angew. Chem. Int. Ed.* **1995**, 33, 2375-2378.
141. Pedersen, C. J. *Science* **1988**, 241, 536-540.
142. Cram, D. J.; Cram, J. M. *Science* **1974**, 183, 803-809.
143. Cram, D. J. *Inclusion Phenom.* **1988**, 6, 397-413.
144. Lehn, J.-M. *J. Inclusion Phenom.* **1988**, 6, 351-396.
145. Ariga, K.; Kunitake, T., *Supramolecular Chemistry-Fundamentals and Applications: Advanced Textbook*. Springer Science & Business Media: **2006**.
146. Release, P. "The 1987 Nobel Prize in Chemistry". Nobelprize.org. Nobel Media AB 2014. Web. 22 Aug **2015**.
147. Dodziuk, H., *Cyclodextrins and their Complexes: Chemistry, Analytical Methods, Applications*. John Wiley & Sons: **2006**.
148. Cramer, F.; Henglein, F.-M. *Chem. Ber.* **1958**, 91, 308-310.

-
149. Freudenberg, K.; Jacobi, R. *Liebigs Ann.* **1935**, 518, 102-108.
 150. Martin Del Valle, E. M. *Process Biochem.* **2004**, 39, 1033-1046.
 151. Connors, K. A. *Chem. Rev.* **1997**, 97, 1325-1358.
 152. Broser, W.; Lautsch, W. *Z. Naturforsch. B* **1953**, 8, 711-722.
 153. Cramer, F.; Saenger, W.; Spatz, H. C. *J. Am. Chem. Soc.* **1967**, 89, 14-20.
 154. Schneider, H.-J. *Angew. Chem. Int. Ed.* **1991**, 30, 1417-1436.
 155. Saenger, W. *Angew. Chem.* **1980**, 92, 343-361.
 156. Höfler, T.; Wenz, G. *J. Inclusion Phenom.* **1996**, 25, 81-84.
 157. Lewis, E. A.; Hansen, L. D. *J. Chem. Soc., Perkin Trans. 2* **1973**, 2081-2085.
 158. Miyaji, T.; Kuroono, Y.; Uekama, K.; Ikeda, K. E. N. *Chem. Pharm. Bull.* **1976**, 24, 1155-1159.
 159. Takashima, Y.; Nakayama, T.; Miyauchi, M.; Kawaguchi, Y.; Yamaguchi, H.; Harada, A. *Chem. Lett.* **2004**, 33, 890-891.
 160. Tamesue, S.; Takashima, Y.; Yamaguchi, H.; Shinkai, S.; Harada, A. *Angew. Chem. Int. Ed.* **2010**, 49, 7461-7464.
 161. Tomatsu, I.; Hashidzume, A.; Harada, A. *Macromolecules* **2005**, 38, 5223-5227.
 162. Loftsson, T.; Jarho, P.; Másson, M.; Järvinen, T. *Expert Opin. Drug Deliv.* **2005**, 2, 335-351.
 163. Szejtli, J. *J. Mater. Chem.* **1997**, 7, 575-587.
 164. Nishi, H.; Fukuyama, T.; Terabe, S. *J. Chromatogr. A* **1991**, 553, 503-516.
 165. Zeng, J.; Shi, K.; Zhang, Y.; Sun, X.; Zhang, B. *Chem. Commun.* **2008**, 3753-3755.
 166. Liu, H.; Zhang, Y.; Hu, J.; Li, C.; Liu, S. *Macromol. Chem. Phys.* **2009**, 210, 2125-2137.
 167. Yhaya, F.; Binauld, S.; Callari, M.; Stenzel, M. H. *Aust. J. Chem.* **2012**, 65, 1095-1103.
 168. Quan, C.-Y.; Chen, J.-X.; Wang, H.-Y.; Li, C.; Chang, C.; Zhang, X.-Z.; Zhuo, R.-X. *ACS Nano* **2010**, 4, 4211-9.
 169. Bertrand, A.; Stenzel, M.; Fleury, E.; Bernard, J. *Polym. Chem.* **2012**, 3, 377-383.
 170. Ren, S.; Chen, D.; Jiang, M. *J. Polym. Sci. A Polym. Chem.* **2009**, 47, 4267-4278.
 171. Yan, J.; Zhang, X.; Li, W.; Zhang, X.; Liu, K.; Wu, P.; Zhang, A. *Soft Matter* **2012**, 8, 6371-6377.
 172. Zhao, Q.; Wang, S.; Cheng, X.; Yam, R. C.; Kong, D.; Li, R. K. *Biomacromolecules* **2010**, 11, 1364-1369.
 173. Nijhuis, C. A.; Huskens, J.; Reinhoudt, D. N. *J. Am. Chem. Soc.* **2004**, 126, 12266-12267.
 174. Auletta, T.; Dordi, B.; Mulder, A.; Sartori, A.; Onclin, S.; Bruinink, C. M.; Péter, M.; Nijhuis, C. A.; Beijleveld, H.; Schönherr, H. *Angew. Chem.* **2004**, 116, 373-377.

175. Ohno, K.; Wong, B.; Haddleton, D. M. *J. Polym. Sci. A Polym. Chem.* **2001**, 39, 2206-2214.
176. Stenzel, M. H.; Davis, T. P. *J. Polym. Sci. A Polym. Chem.* **2002**, 40, 4498-4512.
177. Schmidt, B. V. K. J.; Hetzer, M.; Ritter, H.; Barner-Kowollik, C. *Polym. Chem.* **2012**, 3, 3064-3064.
178. Willenbacher, J.; Schmidt, B. V. K. J.; Schulze-Suenninghausen, D.; Altintas, O.; Luy, B.; Delaittre, G.; Barner-Kowollik, C. *Chem. Commun.* **2014**, 50, 7056-7059.
179. Ren, L.; He, L.; Sun, T.; Dong, X.; Chen, Y.; Huang, J.; Wang, C. *Macromol. Biosci.* **2009**, 9, 902-910.
180. Sui, K.; Shan, X.; Gao, S.; Xia, Y.; Zheng, Q.; Xie, D. *J. Polym. Sci. A Polym. Chem.* **2010**, 48, 2143-2153.
181. He, L.; Huang, J.; Chen, Y.; Xu, X.; Liu, L. *Macromolecules* **2005**, 38, 3845-3851.
182. Pimpin, A.; Srituravanich, W. *Engineering Journal* **2011**, 16, 37-56.
183. Kaji, H.; Camci-Unal, G.; Langer, R.; Khademhosseini, A. *Biochim. Biophys. Acta Gen. Subj.* **2011**, 1810, 239-250.
184. Stratakis, E.; Ranella, A.; Fotakis, C. *Biomicrofluidics* **2011**, 5, 013411.
185. Ferris, C. J.; Gilmore, K. G.; Wallace, G. G. *Appl. Microbiol. Biotechnol.* **2013**, 97, 4243-4258.
186. Martin, T. A.; Caliarì, S. R.; Williford, P. D.; Harley, B. A.; Bailey, R. C. *Biomaterials* **2011**, 32, 3949-3957.
187. Nakamura, M.; Kobayashi, A.; Takagi, F.; Watanabe, A.; Hiruma, Y.; Ohuchi, K.; Iwasaki, Y.; Horie, M.; Morita, I.; Takatani, S. *J. Tissue Eng.* **2005**, 11, 1658-1666.
188. Park, T. J.; Lee, K.-B.; Lee, S. J.; Park, J. P.; Lee, Z.-W.; Lee, S. Y.; Choi, I. S. *J. Am. Chem. Soc.* **2004**, 126, 10512-10513.
189. Park, T. J.; Lee, S. Y.; Lee, S. J.; Park, J. P.; Yang, K. S.; Lee, K.-B.; Ko, S.; Park, J. B.; Kim, T.; Kim, S. K.; Shin, Y. B.; Chung, B. H.; Ku, S.-J.; Kim, D. H.; Choi, I. S. *Anal. Chem.* **2006**, 78, 7197-7205.
190. Rodriguez-Emmenegger, C.; Kylián, O.; Houska, M.; Brynda, E.; Artemenko, A.; Kousal, J.; Alles, A. B.; Biederman, H. *Biomacromolecules* **2011**, 12, 1058-1066.
191. Tolstyka, Z. P.; Richardson, W.; Bat, E.; Stevens, C. J.; Parra, D. P.; Dozier, J. K.; Distefano, M. D.; Dunn, B.; Maynard, H. D. *ChemBioChem* **2013**, 14, 2464-2471.
192. Chan, E. W. L.; Yu, L. *Langmuir* **2002**, 18, 311-313.
193. El Zubir, O.; Barlow, I.; Ul-Haq, E.; Tajuddin, H. A.; Williams, N. H.; Leggett, G. J. *Langmuir* **2013**, 29, 1083-1092.
194. Herne, T. M.; Tarlov, M. J. *J. Am. Chem. Soc.* **1997**, 119, 8916-8920.

-
195. Salierno, M. J.; García, A. J.; del Campo, A. *Adv. Funct. Mater.* **2013**, *23*, 5974-5980.
 196. Tischer, T.; Claus, T. K.; Bruns, M.; Trouillet, V.; Linkert, K.; Rodriguez-Emmenegger, C.; Goldmann, A. S.; Perrier, S.; Börner, H. G.; Barner-Kowollik, C. *Biomacromolecules* **2013**, *14*, 4340-4350.
 197. Hansson, S.; Trouillet, V.; Tischer, T.; Goldmann, A. S.; Carlmark, A.; Barner-Kowollik, C.; Malmström, E. *Biomacromolecules* **2013**, *14*, 64-74.
 198. Hu, Y.; Li, J. S.; Yang, W. T.; Xu, F. J. *Thin Solid Films* **2013**, *534*, 325-333.
 199. Chen, R. T.; Marchesan, S.; Evans, R. A.; Styan, K. E.; Such, G. K.; Postma, A.; McLean, K. M.; Muir, B. W.; Caruso, F. *Biomacromolecules* **2012**, *13*, 889-895.
 200. Desmet, T.; Morent, R.; Geyter, N. D.; Leys, C.; Schacht, E.; Dubruel, P. *Biomacromolecules* **2009**, *10*, 2351-2378.
 201. Sahu, N.; Parija, B.; Panigrahi, S. *Indian J. Phys.* **2009**, *83*, 493-502.
 202. Krebs, F. C. *Sol. Energy Mater. Sol. Cells* **2009**, *93*, 394-412.
 203. Rodriguez-Emmenegger, C.; Hasan, E.; Pop-Georgievski, O.; Houska, M.; Brynda, E.; Alles Bologna, A. *Macromol. Biosci.* **2012**, *12*, 525-532.
 204. Tischer, T.; Rodriguez-Emmenegger, C.; Trouillet, V.; Welle, A.; Schueler, V.; Mueller, J. O.; Goldmann, A. S.; Brynda, E.; Barner-Kowollik, C. *Adv. Mater.* **2014**, *26*, 4087-4092.
 205. Stamm, M., *Polymer surfaces and interfaces*. Springer Berlin Heidelberg: **2008**.
 206. Welle, A.; Gottwald, E. *Biomed. Microdevices* **2002**, *4*, 33-41.
 207. Welle, A.; Gottwald, E.; Weibezahn, K. *Biomed. Tech.* **2002**, *47*, 401-403.
 208. Rodriguez-Emmenegger, C.; Preuss, C. M.; Yameen, B.; Pop-Georgievski, O.; Bachmann, M.; Mueller, J. O.; Bruns, M.; Goldmann, A. S.; Bastmeyer, M.; Barner-Kowollik, C. *Adv. Mater.* **2013**, *25*, 6123-6127.
 209. Alom Ruiz, S.; Chen, C. S. *Soft Matter* **2007**, *3*, 168-177.
 210. Bernard, A.; Renault, J. P.; Michel, B.; Bosshard, H. R.; Delamarche, E. *Adv. Mater.* **2000**, *12*, 1067-1070.
 211. Derby, B. *Annu. Rev. Mater. Res.* **2010**, *40*, 395-414.
 212. Calvert, P. *Chem. Mater.* **2001**, *13*, 3299-3305.
 213. Siringhaus, H.; Kawase, T.; Friend, R. H.; Shimoda, T.; Inbasekaran, M.; Wu, W.; Woo, E. P. *Science* **2000**, *290*, 2123-2126.
 214. Dalsin, J. L.; Messersmith, P. B. *Mater. Today* **2005**, *8*, 38-46.
 215. Nan Cheng, X. C. *J. Colloid Interface Sci.* **2010**, *348*, 71-79.
 216. Wischerhoff, E.; Uhlig, K.; Lanckenau, A.; Börner, H. G.; Laschewsky, A.; Duschl, C.; Lutz, J. F. *Angew. Chem. Int. Ed.* **2008**, *47*, 5666-5668.
 217. Atala, A.; Kasper, F. K.; Mikos, A. G. *Sci. Transl. Med.* **2012**, *4*, 160RV112.
 218. El-Ali, J.; Sorger, P. K.; Jensen, K. F. *Nature* **2006**, *442*, 403-411.

219. Neuži, P.; Giselbrecht, S.; Länge, K.; Huang, T. J.; Manz, A. *Nat. Rev. Drug Discov.* **2012**, *11*, 620-32.
220. Fournier, D.; Hoogenboom, R.; Schubert, U. S. *Chem. Soc. Rev.* **2007**, *36*, 1369-1380.
221. Golas, P. L.; Matyjaszewski, K. *Chem. Soc. Rev.* **2010**, *39*, 1338-1354.
222. Iha, R. K.; Wooley, K. L.; Nyström, A. M.; Burke, D. J.; Kade, M. J.; Hawker, C. J. *Chem. Rev.* **2009**, *109*, 5620-5686.
223. Nandivada, H.; Jiang, X.; Lahann, J. *Adv. Mater.* **2007**, *19*, 2197-2208.
224. Durmaz, H.; Dag, A.; Altintas, O.; Erdogan, T.; Hizal, G.; Tunca, U. *Macromolecules* **2007**, *40*, 191-198.
225. Bousquet, A.; Barner-Kowollik, C.; Stenzel, M. H. *J. Polym. Sci. A Polym. Chem.* **2010**, *48*, 1773-1781.
226. Inglis, A. J.; Sinnwell, S.; Davis, T. P.; Barner-Kowollik, C.; Stenzel, M. H. *Macromolecules* **2008**, *41*, 4120-4126.
227. Kolb, H. C.; Finn, M. G.; Sharpless, K. B. *Angew. Chem. Int. Ed.* **2001**, *40*, 2004-2021.
228. Sankararaman, S., *Pericyclic Reactions: A Textbook: Reactions, Applications and Theory*. Wiley-VCH: **2005**.
229. Barner-Kowollik, C.; Du Prez, F. E.; Espeel, P.; Hawker, C. J.; Junkers, T.; Schlaad, H.; Van Camp, W. *Angew. Chem. Int. Ed.* **2011**, *50*, 60-62.
230. Hizal, G.; Tunca, U.; Sanyal, A. *J. Polym. Sci. A Polym. Chem.* **2011**, *49*, 4103-4120.
231. Tasdelen, M. A. *Polym. Chem.* **2011**, *2*, 2133-2145.
232. Binder, W. H.; Sachsenhofer, R. *Macromol. Rapid Commun.* **2008**, *29*, 952-981.
233. Evans, R. A. *Aust. J. Chem.* **2007**, *60*, 384-395.
234. Lutz, J. F. *Angew. Chem. Int. Ed.* **2007**, *46*, 1018-1025.
235. Meldal, M. *Macromol. Rapid Commun.* **2008**, *29*, 1016-1051.
236. Hoyle, C. E.; Bowman, C. N. *Angew. Chem. Int. Ed.* **2010**, *49*, 1540-1573.
237. Hoyle, C. E.; Lowe, A. B.; Bowman, C. N. *Chem. Soc. Rev.* **2010**, *39*, 1355-1387.
238. Lowe, A. B. *Polym. Chem.* **2010**, *1*, 17-36.
239. Campos, L. M.; Killops, K. L.; Sakai, R.; Paulusse, J. M. J.; Damiron, D.; Drockenmuller, E.; Messmore, B. W.; Hawker, C. J. *Macromolecules* **2008**, *41*, 7063-7070.
240. Gress, A.; Völkel, A.; Schlaad, H. *Macromolecules* **2007**, *40*, 7928-7933.
241. Ten Brummelhuis, N.; Diehl, C.; Schlaad, H. *Macromolecules* **2008**, *41*, 9946-9947.
242. Delaittre, G.; Pauloehrl, T.; Bastmeyer, M.; Barner-Kowollik, C. *Macromolecules* **2012**, *45*, 1792-1802.

-
243. Pauloehrl, T.; Delaittre, G.; Bastmeyer, M.; Barner-Kowollik, C. *Polym. Chem.* **2012**, 3, 1740-1749.
244. Quick, A. S.; Fischer, J.; Richter, B.; Pauloehrl, T.; Trouillet, V.; Wegener, M.; Barner-Kowollik, C. *Macromol. Rapid Commun.* **2013**, 34, 335-340.
245. Barner-Kowollik, C.; Inglis, A. J. *Macromol. Chem. Phys.* **2009**, 210, 987-992.
246. Becer, C. R.; Hoogenboom, R.; Schubert, U. S. *Angew. Chem. Int. Ed.* **2009**, 48, 4900-4908.
247. Goldmann, A. S.; Glassner, M.; Inglis, A. J.; Barner-Kowollik, C. *Macromol. Rapid Commun.* **2013**, 34, 810-849.
248. Lutz, J.-F.; Schlaad, H. *Polymer* **2008**, 49, 817-824.
249. Mansfeld, U.; Pietsch, C.; Hoogenboom, R.; Becer, C. R.; Schubert, U. S. *Polym. Chem.* **2010**, 1, 1560-1560.
250. Dondoni, A. *Angew. Chem. Int. Ed.* **2008**, 47, 8995-8997.
251. Derboven, P.; D'hooge, D. R.; Stamenovic, M. M.; Espeel, P.; Marin, G. B.; Du Prez, F. E.; Reyniers, M.-F. *Macromolecules* **2013**, 46, 1732-1742.
252. Koo, S. P. S.; Stamenović, M. M.; Prasath, R. A.; Inglis, A. J.; Du Prez, F. E.; Barner-Kowollik, C.; Van Camp, W.; Junkers, T. J. *Polym. Sci. A Polym. Chem.* **2010**, 48, 1699-1713.
253. Diels, O.; Alder, K. *Liebigs Ann.* **1928**, 460, 98-122.
254. Fleming, I., *Pericyclic Reactions 2nd Edition*. Oxford University Press: **2015**.
255. Nicolaou, K. C.; Snyder, S. A.; Montagnon, T.; Vassilikogiannakis, G. *Angew. Chem. Int. Ed.* **2002**, 41, 1668-1698.
256. Oliver Kappe, C.; Shaun Murphree, S.; Padwa, A. *Tetrahedron* **1997**, 53, 14179-14233.
257. Woodward, R. B.; Hoffmann, R. *J. Am. Chem. Soc.* **1965**, 87, 395-397.
258. Martin, J. G.; Hill, R. K. *Chem. Rev.* **1961**, 61, 537-562.
259. Woodward, R. B.; Hoffmann, R. *Angew. Chem. Int. Ed.* **1969**, 8, 781-853.
260. Gill, G. *Quart. Rev. Chem. Soc.* **1968**, 22, 338-389.
261. Fukui, K. *Angew. Chem. Int. Ed.* **1982**, 21, 801-809.
262. Houk, K. N. *J. Am. Chem. Soc.* **1973**, 95, 4092-4094.
263. Brückner, R., *Reaktionsmechanismen*, Spektrum Akademischer Verlag, Heidelberg, Berlin: **2008**.
264. Sakai, S. *J. Phys. Chem. A* **2000**, 104, 922-927.
265. Durmaz, H.; Colakoglu, B.; Tunca, U.; Hizal, G. *J. Polym. Sci. A Polym. Chem.* **2006**, 44, 1667-1675.
266. Dag, A.; Durmaz, H.; Hizal, G.; Tunca, U. *J. Polym. Sci. A Polym. Chem.* **2008**, 46, 302-313.

267. Gacal, B.; Durmaz, H.; Tasdelen, M. A.; Hizal, G.; Tunca, U.; Yagci, Y.; Demirel, A. L. *Macromolecules* **2006**, 39, 5330-5336.
268. Glassner, M.; Blinco, J. P.; Barner-Kowollik, C. *Macromol. Rapid Commun.* **2011**, 32, 724-8.
269. Afarinkia, K.; Vinader, V.; Nelson, T. D.; Posner, G. H. *Tetrahedron* **1992**, 48, 9111-9171.
270. Winkler, M.; Mueller, J. O.; Oehlenschlaeger, K. K.; Montero de Espinosa, L.; Meier, M. A. R.; Barner-Kowollik, C. *Macromolecules* **2012**, 45, 5012-5019.
271. Espinosa, E.; Glassner, M.; Boisson, C.; Barner-Kowollik, C.; D'Agosto, F. *Macromol. Rapid Commun.* **2011**, 32, 1447-1453.
272. Glassner, M.; Delaittre, G.; Kaupp, M.; Blinco, J. P.; Barner-Kowollik, C. *J. Am. Chem. Soc.* **2012**, 134, 7274-7277.
273. Inglis, A. J.; Sinnwell, S.; Stenzel, M. H.; Barner-Kowollik, C. *Angew. Chem. Int. Ed.* **2009**, 48, 2411-2414.
274. Inglis, A. J.; Stenzel, M. H.; Barner-Kowollik, C. *Macromol. Rapid Commun.* **2009**, 30, 1792-1798.
275. Quemener, D.; Davis, T. P.; Barner-Kowollik, C.; Stenzel, M. H. *Chem. Commun.* **2006**, 5051-5053.
276. Sanyal, A. *Macromol. Chem. Phys.* **2010**, 211, 1417-1425.
277. Chen, X.; Dam, M. A.; Ono, K.; Mal, A.; Shen, H.; Nutt, S. R.; Sheran, K.; Wudl, F. *Science* **2002**, 295, 1698-1702.
278. Oehlenschlaeger, K. K.; Mueller, J. O.; Brandt, J.; Hilf, S.; Lederer, A.; Wilhelm, M.; Graf, R.; Coote, M. L.; Schmidt, F. G.; Barner-Kowollik, C. *Adv. Mater.* **2014**, 26, 3561-3566.
279. Guimard, N. K.; Oehlenschlaeger, K. K.; Zhou, J.; Hilf, S.; Schmidt, F. G.; Barner-Kowollik, C. *Macromol. Chem. Phys.* **2012**, 213, 131-143.
280. Barner-Kowollik, C.; Georg Schmidt, F. *Macromol. Chem. Phys.* **2012**, 213, 129-130.
281. Díaz, D. D.; Punna, S.; Holzer, P.; McPherson, A. K.; Sharpless, K. B.; Fokin, V. V.; Finn, M. J. *Polym. Sci. A Polym. Chem.* **2004**, 42, 4392-4403.
282. Opsteen, J. A.; van Hest, J. C. *Chem. Commun.* **2005**, 57-59.
283. Tornøe, C. W.; Christensen, C.; Meldal, M. *J. Org. Chem.* **2002**, 67, 3057-3064.
284. Rostovtsev, V. V.; Green, L. G.; Fokin, V. V.; Sharpless, K. B. *Angew. Chem.* **2002**, 114, 2708-2711.
285. Kuijpers, B. H. M.; Groothuys, S.; Keereweer, A. R.; Quaedflieg, P. J. L. M.; Blaauw, R. H.; van Delft, F. L.; Rutjes, F. P. J. T. *Org. Lett.* **2004**, 6, 3123-3126.
286. Rostovtsev, V. V.; Green, L. G.; Fokin, V. V.; Sharpless, K. B. *Angew. Chem. Int. Ed.* **2002**, 41, 2596-9.

-
287. Bräse, S.; Gil, C.; Knepper, K.; Zimmermann, V. *Angew. Chem. Int. Ed.* **2005**, *44*, 5188-5240.
288. Helms, B.; Mynar, J. L.; Hawker, C. J.; Fréchet, J. M. J. *J. Am. Chem. Soc.* **2004**, *126*, 15020-15021.
289. Wu, P.; Feldman, A. K.; Nugent, A. K.; Hawker, C. J.; Scheel, A.; Voit, B.; Pyun, J.; Fréchet, J. M.; Sharpless, K. B.; Fokin, V. V. *Angew. Chem. Int. Ed.* **2004**, *43*, 3928-3932.
290. Hoogenboom, R.; Moore, B. C.; Schubert, U. S. *Chem. Commun.* **2006**, 4010-4012.
291. Whittaker, M. R.; Urbani, C. N.; Monteiro, M. J. *J. Am. Chem. Soc.* **2006**, *128*, 11360-11361.
292. Malkoch, M.; Vestberg, R.; Gupta, N.; Mespouille, L.; Dubois, P.; Mason, A. F.; Hedrick, J. L.; Liao, Q.; Frank, C. W.; Kingsbury, K. *Chem. Commun.* **2006**, 2774-2776.
293. Vogt, A. P.; Sumerlin, B. S. *Macromolecules* **2008**, *41*, 7368-7373.
294. Durmaz, H.; Sanyal, A.; Hizal, G.; Tunca, U. *Polym. Chem.* **2012**, *3*, 825-835.
295. Sinnwell, S.; Inglis, A. J.; Stenzel, M. H.; Barner-Kowollik, C. *Macromol. Rapid Commun.* **2008**, *29*, 1090-1096.
296. Luza, S. C.; Speisky, H. C. *Am. J. Clin. Nutr.* **1996**, *63*, 812S-820S.
297. Wolbers, F.; ter Braak, P.; Le Gac, S.; Luttge, R.; Andersson, H.; Vermes, I.; van den Berg, A. *Electrophoresis* **2006**, *27*, 5073-5080.
298. Dommerholt, J.; Schmidt, S.; Temming, R.; Hendriks, L. J. A.; Rutjes, F. P. J. T.; van Hest, J. C. M.; Lefeber, D. J.; Friedl, P.; van Delft, F. L. *Angew. Chem. Int. Ed.* **2010**, *49*, 9422-9425.
299. Gold, B.; Shevchenko, N. E.; Bonus, N.; Dudley, G. B.; Alabugin, I. V. *J. Org. Chem.* **2012**, *77*, 75-89.
300. Gold, B.; Dudley, G. B.; Alabugin, I. V. *J. Am. Chem. Soc.* **2013**, *135*, 1558-1569.
301. Varga, B. R.; Kállay, M.; Hegyi, K.; Béni, S.; Kele, P. *Chemistry-A European Journal* **2012**, *18*, 822-828.
302. Poloukhine, A. A.; Mbua, N. E.; Wolfert, M. A.; Boons, G.-J.; Popik, V. V. *J. Am. Chem. Soc.* **2009**, *131*, 15769-15776.
303. Clovis, J. S.; Eckell, A.; Huisgen, R.; Sustmann, R. *Chem. Ber.* **1967**, *100*, 60-70.
304. Song, W.; Wang, Y.; Yu, Z.; Vera, C. I. R.; Qu, J.; Lin, Q. *ACS Chem. Biol.* **2010**, *5*, 875-885.
305. Song, W.; Wang, Y.; Qu, J.; Lin, Q. *J. Am. Chem. Soc.* **2008**, *130*, 9654-9655.
306. Song, W.; Wang, Y.; Qu, J.; Madden, M. M.; Lin, Q. *Angew. Chem.* **2008**, *120*, 2874-2877.
307. Wang, Y.; Hu, W. J.; Song, W.; Lim, R. K.; Lin, Q. *Org. Lett.* **2008**, *10*, 3725-3728.

308. Dürr, C. J.; Lederhose, P.; Hlalele, L.; Abt, D.; Kaiser, A.; Brandau, S.; Barner-Kowollik, C. *Macromolecules* **2013**, 46, 5915-5923.
309. Mueller, J. O.; Voll, D.; Schmidt, F. G.; Delaittre, G.; Barner-Kowollik, C. *Chem. Commun.* **2014**, 50, 15681-15684.
310. Mueller, J. O.; Guimard, N. K.; Oehlenschlaeger, K. K.; Schmidt, F. G.; Barner-Kowollik, C. *Polym. Chem.* **2014**, 5, (4), 1447-1456.
311. Dietrich, M.; Delaittre, G.; Blinco, J. P.; Inglis, A. J.; Bruns, M.; Barner-Kowollik, C. *Adv. Funct. Mater.* **2012**, 22, 304-312.
312. Padwa, A. *Acc. Chem. Res.* **1976**, 9, 371-378.
313. Padwa, A.; Dharan, M.; Smolanoff, J.; Wetmore, S. I. *J. Am. Chem. Soc.* **1973**, 95, 1945-1954.
314. Mueller, J. O.; Schmidt, F. G.; Blinco, J. P.; Barner-Kowollik, C. *Angew. Chem. Int. Ed.* **2015**, 54, 10284-10288.
315. Kleinfeld, D.; Kahler, K.; Hockberger, P. *J. Neurosci.* **1988**, 8, 4098-4120.
316. Valentini, R.; Vargo, T.; Gardella, J.; Aebischer, P. *J. Biomater. Sci., Polym. Ed.* **1994**, 5, 13-36.
317. Wu, F. J.; Friend, J. R.; Rimmel, R. P.; Cerra, F. B.; Hu, W. S. *Cell Transplant* **1999**, 8, 233-46.
318. Lazar, A.; Peshwa, M. V.; Wu, F. J.; Chi, C. M.; Cerra, F. B.; Hu, W. S. *Cell Transplant* **1995**, 4, 259-68.
319. Yeow, B.; Coffey, J. W.; Muller, D. A.; Grøndahl, L.; Kendall, M. A.; Corrie, S. R. *Anal. Chem.* **2013**, 85, 10196-10204.
320. Bañuls, M.-J.; García-Piñón, F.; Puchades, R.; Maquieira, Á. *Bioconjug. Chem.* **2008**, 19, 665-672.
321. Qureshi, A.; Shah, S.; Pelagade, S.; Singh, N.; Mukherjee, S.; Tripathi, A.; Despande, U.; Shripathi, T. *JPCS* **2010**, 208, 012108.
322. Yameen, B.; Khan, H. U.; Knoll, W.; Förch, R.; Jonas, U. *Macromol. Rapid Commun.* **2011**, 32, 1735-1740.
323. Hirschbiel, A. F.; Schmidt, B. V. K. J.; Krolla-Sidenstein, P.; Blinco, J. P.; Barner-Kowollik, C. *Macromolecules* **2015**, 48, 4410-4420.
324. Jeffrey L. Dalsin, P. B. M. *Mater. Today* **2005**, 8, 38-46.
325. Konradi, R.; Acikgoz, C.; Textor, M. *Macromol. Rapid Commun.* **2012**, 33, 1663-1676.
326. Merrill, E. W. *Ann. N. Y. Acad. Sci.* **1987**, 516, 196-203.
327. Cesar Rodriguez-Emmenegger, M. H., Aldo Bologna Alles, Eduard Brynda. *Macromol. Biosci.* **2012**, 12, 1413-1422.
328. Wagner, M.; Castner, D. G. *Langmuir* **2001**, 17, 4649-4660.
329. Senghaas, N.; Köster, R. W. *Cold. Spring. Harb. Protoc.* **2009**, pdb.prot5235.

-
330. Giselbrecht, S.; Gietzelt, T.; Gottwald, E.; Trautmann, C.; Truckenmüller, R.; Weibezahn, K. F.; Welle, a. *Biomed. Microdevices* **2006**, 8, 191-199.
331. Schumers, J.-M.; Gohy, J.-F.; Fustin, C.-A. *Polym. Chem.* **2010**, 1, 161-163.
332. Bosman, A. W.; Vestberg, R.; Heumann, A.; Fréchet, J. M. J.; Hawker, C. J. *J. Am. Chem. Soc.* **2003**, 125, 715-728.
333. Schacher, F. H.; Rugar, P. A.; Manners, I. *Angew. Chem. Int. Ed.* **2012**, 51, 7898-7921.
334. Schmidt, B. V. K. J.; Hetzer, M.; Ritter, H.; Barner-Kowollik, C. *Macromolecules* **2013**, 46, 1054-1065.
335. Blasco, E.; Schmidt, B. V. K. J.; Barner-Kowollik, C.; Pinol, M.; Oriol, L. *Polym. Chem.* **2013**, 4, 4506-4514.
336. Altintas, O.; Schulze-Suenninghausen, D.; Luy, B.; Barner-Kowollik, C. *Eur. Polym. J.* **2015**, 62, 409-417.
337. Johnson, J. A.; Finn, M. G.; Koberstein, J. T.; Turro, N. J. *Macromol. Rapid Commun.* **2008**, 29, 1052-1072.
338. Glassner, M.; Oehlenschlaeger, K. K.; Gruending, T.; Barner-Kowollik, C. *Macromolecules* **2011**, 44, 4681-4689.
339. Bapat, A. P.; Ray, J. G.; Savin, D. A.; Hoff, E. A.; Patton, D. L.; Sumerlin, B. S. *Polym. Chem.* **2012**, 3, 3112-3120.
340. Dietrich, M.; Glassner, M.; Gruending, T.; Schmid, C.; Falkenhagen, J.; Barner-Kowollik, C. *Polym. Chem.* **2010**, 1, 634-634.
341. Harada, A.; Takashima, Y.; Nakahata, M. *Acc. Chem. Res.* **2014**, 47, 2128-2140.
342. Stadermann, J.; Komber, H.; Erber, M.; Däbritz, F.; Ritter, H.; Voit, B. *Macromolecules* **2011**, 44, 3250-3259.
343. Schmidt, B. V. K. J.; Hetzer, M.; Ritter, H.; Barner-Kowollik, C. *Prog. Polym. Sci.* **2014**, 39, 235-249.
344. Skey, J.; O'Reilly, R. K. *Chem. Commun.* **2008**, 4183-4185.
345. Weickenmeier, M.; Wenz, G.; Huff, J. *Macromol. Rapid Commun.* **1997**, 18, 1117-1123.
346. Convertine, A. J.; Lokitz, B. S.; Vasileva, Y.; Myrick, L. J.; Scales, C. W.; Lowe, A. B.; McCormick, C. L. *Macromolecules* **2006**, 39, 1724-1730.
347. Schmidt, B. V. K. J. *Dissertation* **2013**, KIT.
348. Gramlich, W. M.; Robertson, M. L.; Hillmyer, M. A. *Macromolecules* **2010**, 43, 2313-2321.
349. Claus, T. *Advanced Lab-Course Report* **2012**, KIT.
350. Bays, E.; Tao, L.; Chang, C.-W.; Maynard, H. D. *Biomacromolecules* **2009**, 10, 1777-1781.

351. Li, X.; Prukop, S. L.; Biswal, S. L.; Verduzco, R. *Macromolecules* **2012**, *45*, 7118-7127.
352. Yu, Z.; Sawkar, A. R.; Whalen, L. J.; Wong, C.-H.; Kelly, J. W. *J. Med. Chem.* **2007**, *50*, 94-100.
353. Schmidt, B. V. K. J.; Barner-Kowollik, C. *Polym. Chem.* **2014**, *5*, 2461-2472.
354. Nyström, F.; Soeriyadi, A. H.; Boyer, C.; Zetterlund, P. B.; Whittaker, M. R. *J. Polym. Sci. A Polym. Chem.* **2011**, *49*, 5313-5321.
355. Schmidt, B. V. K. J.; Barner-Kowollik, C. *ChemCatChem* **2014**, *6*, 3060-3062.
356. Harada, A.; Takashima, Y.; Yamaguchi, H. *Chem. Soc. Rev.* **2009**, *38*, 875-882.
357. Zhang, Z.; Lv, Q.; Gao, X.; Chen, L.; Cao, Y.; Yu, S.; He, C.; Chen, X. *ACS Appl. Mater. Interfaces* **2015**, *7*, 8404-8411.
358. Yan, Q.; Xin, Y.; Zhou, R.; Yin, Y.; Yuan, J. *Chem. Commun.* **2011**, *47*, 9594-9596.
359. Szillat, F.; Schmidt, B. V. K. J.; Hubert, A.; Barner-Kowollik, C.; Ritter, H. *Macromol. Rapid Commun.* **2014**, *35*, 1293-1300.
360. Yan, Q.; Zhang, H.; Zhao, Y. *ACS Macro Lett.* **2014**, *3*, 472-476.
361. van Nostrum, C. F. *Soft Matter* **2011**, *7*, 3246-3259.
362. Peng, L.; Feng, A.; Zhang, H.; Wang, H.; Jian, C.; Liu, B.; Gao, W.; Yuan, J. *Polym. Chem.* **2014**, *5*, 1751-1759.
363. Vriezema, D. M.; Comellas Aragonès, M.; Elemans, J. A. A. W.; Cornelissen, J. J. L. M.; Rowan, A. E.; Nolte, R. J. M. *Chem. Rev.* **2005**, *105*, 1445-1490.
364. Liu, S.; Weaver, J. V. M.; Save, M.; Armes, S. P. *Langmuir* **2002**, *18*, 8350-8357.
365. Mubeen, S.; Zhang, T.; Yoo, B.; Deshusses, M. A.; Myung, N. V. *J. Phys. Chem. C* **2007**, *111*, 6321-6327.
366. Soulantica, K.; Erades, L.; Sauvan, M.; Senocq, F.; Maisonnat, A.; Chaudret, B. *Adv. Funct. Mater.* **2003**, *13*, 553-557.
367. Yang, Y.; Jiang, Y.; Xu, J.; Yu, J. *Polymer* **2007**, *48*, 4459-4465.
368. Du, A. W.; Stenzel, M. H. *Biomacromolecules* **2014**, *15*, 1097-1114.
369. Farokhzad, O. C.; Langer, R. *ACS Nano* **2009**, *3*, 16-20.
370. Ding, J.; Chen, L.; Xiao, C.; Chen, L.; Zhuang, X.; Chen, X. *Chem. Commun.* **2014**, *50*, 11274-11290.
371. Lee, J.-H.; Huh, Y.-M.; Jun, Y.-w.; Seo, J.-w.; Jang, J.-t.; Song, H.-T.; Kim, S.; Cho, E.-J.; Yoon, H.-G.; Suh, J.-S.; Cheon, J. *Nat. Med.* **2007**, *13*, 95-99.
372. Yezhelyev, M. V.; Gao, X.; Xing, Y.; Al-Hajj, A.; Nie, S.; O'Regan, R. M. *Lancet Oncol.* **2006**, *7*, 657-667.
373. Mulder, W. J. M.; Strijkers, G. J.; van Tilborg, G. A. F.; Griffioen, A. W.; Nicolay, K. *NMR Biomed.* **2006**, *19*, 142-164.
374. Zhang, J.; Jiang, X.; Zhang, Y.; Li, Y.; Liu, S. *Macromolecules* **2007**, *40*, 9125-9132.

-
375. Zou, H.; Schlaad, H. *J. Polym. Sci. A Polym. Chem.* **2015**, *53*, 1260-1267.
376. Hu, X.; Tian, J.; Liu, T.; Zhang, G.; Liu, S. *Macromolecules* **2013**, *46*, 6243-6256.
377. Sun, L.; Zhu, B.; Su, Y.; Dong, C.-M. *Polym. Chem.* **2014**, *5*, 1605-1613.
378. Binauld, S.; Stenzel, M. H. *Chem. Commun.* **2013**, *49*, 2082-2102.
379. Gaitzsch, J.; Appelhans, D.; Grafe, D.; Schwille, P.; Voit, B. *Chem. Commun.* **2011**, *47*, 3466-3468.
380. Rekharsky, M. V.; Inoue, Y. *Chem. Rev.* **1998**, *98*, 1875-1918.
381. Heskins, M.; Guillet, J. E. *J. Macromol. Sci. Chem.* **1968**, *2*, 1441-1455.
382. Afroze, F.; Nies, E.; Berghmans, H. *J. Mol. Struct.* **2000**, *554*, 55-68.
383. Lokitz, B. S.; Convertine, A. J.; Ezell, R. G.; Heidenreich, A.; Li, Y.; McCormick, C. L. *Macromolecules* **2006**, *39*, 8594-8602.
384. Wei, H.; Zhang, X.-Z.; Zhou, Y.; Cheng, S.-X.; Zhuo, R.-X. *Biomaterials* **2006**, *27*, 2028-2034.
385. FitzGerald, P. A.; Gupta, S.; Wood, K.; Perrier, S.; Warr, G. G. *Langmuir* **2014**, *30*, 7986-7992.
386. Nichifor, M.; Zhu, X. X. *Polymer* **2003**, *44*, 3053-3060.
387. Hocine, S.; Li, M.-H. *Soft Matter* **2013**, *9*, 5839-5861.
388. Schmidt, B. V. K. J.; Hetzer, M.; Ritter, H.; Barner-Kowollik, C. *Macromol. Rapid Commun.* **2013**, *34*, 1306-1311.
389. Schmidt, B. V. K. J.; Rudolph, T.; Hetzer, M.; Ritter, H.; Schacher, F. H.; Barner-Kowollik, C. *Polym. Chem.* **2012**, *3*, 3139-3145.
390. Swanson, M. A.; Cori, C. F. *J. Biol. Chem.* **1948**, *172*, 797-804.
391. Schmidt, B. V. K. J.; Hetzer, M.; Ritter, H.; Barner-Kowollik, C. *Macromolecules* **2011**, *44*, 7220-7232.
392. Amajjahe, S.; Choi, S.; Munteanu, M.; Ritter, H. *Angew. Chem. Int. Ed.* **2008**, *47*, 3435-3437.
393. Motornov, M.; Roiter, Y.; Tokarev, I.; Minko, S. *Prog. Polym. Sci.* **2010**, *35*, 174-211.
394. Abt, D.; Schmidt, B. V. K. J.; Pop-Georgievski, O.; Quick, A. S.; Danilov, D.; Kostina, N. Y.; Bruns, M.; Wenzel, W.; Wegener, M.; Rodriguez-Emmenegger, C.; Barner-Kowollik, C. *Chem. Eur. J.* **2015**, *21*, 13186-13190.
395. Ling, X. Y.; Reinhoudt, D. N.; Huskens, J. *Chem. Mater.* **2008**, *20*, 3574-3578.
396. Ludden, M. J.; Reinhoudt, D. N.; Huskens, J. *Chem. Soc. Rev.* **2006**, *35*, 1122-1134.

List of Abbreviations

a.t.	ambient temperature
Ada	adamantyl
AFM	atomic force microscopy
AIBN	azobisisobutyronitrile
AM	acrylamide
AN	acrylonitrile
APTES	(3-aminopropyl)triethoxysilane
ATR-IR	attenuated total reflectance infrared spectroscopy
ATRP	atom-transfer radical polymerization
CD	cyclodextrin
CNS	central nervous system
CRP	controlled radical polymerization
CTA	chain transfer agent
CuAAC	copper catalyzed azide alkyne cycloaddition
\mathcal{D}	polydispersity index
Da	Dalton
DA	Diels-Alder
DBPO	dibenzoyl peroxide
DCC	<i>N,N'</i> -dicyclohexylcarbodiimide
DCM	dichloromethane
DEAAm	<i>N,N'</i> -diethylacrylamide
D_h	hydrodynamic radius
DLS	dynamic light scattering
DMAAm	<i>N,N'</i> -dimethylacrylamide
DoPAT	2-(dodecylthiocarbonothioylthio) propionic acid
EDC	1-(3-dimethylaminopropyl)-3-ethylcarbodiimide
EDG	electron donating group
eGFP	enhanced green fluorescent protein
EMP	2-(((ethylthio)carbonothioyl)thio)-2-methylpropanoic acid
ESI-MS	Electrospray Ionization-Mass Spectrometry
EWG	electron withdrawing group

List of Abbreviations

FCS	fetal calf serum
FRP	free radical polymerization
HDA	hetero Diels-Alder
HOEAAM	<i>N</i> -hydroxyethylacrylamide
HOMO	highest occupied molecular orbital
IC	internal conversion
ISC	inter system crossing
LCST	lower critical solution temperature
LUMO	lowest unoccupied molecular orbital
MA	methyl acrylate
Mal	maleimide
MeCN	acetonitrile
MeOEGMA	oligo(ethylene glycol) methyl ether methacrylate
MMA	methyl methacrylate
M_n	molecular weight
NHS	<i>N</i> -hydroxysuccinimide
NiPAAM	<i>N</i> -isopropylacrylamide
NITEC	nitrile imine-mediated tetrazole-ene cycloaddition
NMP	nitroxide mediated polymerization
NMR	nuclear magnetic resonance
NOESY	nuclear Overhauser effect spectroscopy
OEG	oligo(ethylen glycol)
<i>o</i> NB	<i>o</i> -nitrobenzyl
<i>o</i> NQM	<i>o</i> -naphthoquinone methides
PC	polycarbonate
PDMS	polydimethylsiloxane
PE	photoenol
PEG	poly(ethylen glycol)
PMDETA	<i>N,N,N',N'',N'''</i> -pentamethyldiethylenetriamine
PPGs	photolabile protecting groups
PS	polystyrene
PVC	poly(vinyl chloride)
RAFT	reversible addition-fragmentation

RDRP	reversible deactivation radical polymerization
SEC	size exclusion chromatography
SI-ATRP	surface-initiated atom-transfer radical polymerization
SMART	substrate modification and replication by thermoforming
SPAAC	strain promoted azide-alkyne cycloaddition
TEMPO	2,2,6,6-tetramethyl-1-piperidinyloxy
TFA	trifluoroacetic acid
ToF-SIMS	time of flight secondary ion mass spectrometry
UV	ultra violet
VAc	vinyl acetate
XPS	X-ray photoelectron spectroscopy

Appendix A

Light-Induced Surface Modification for Guided Cell Attachment (Appendix to Chapter 3)

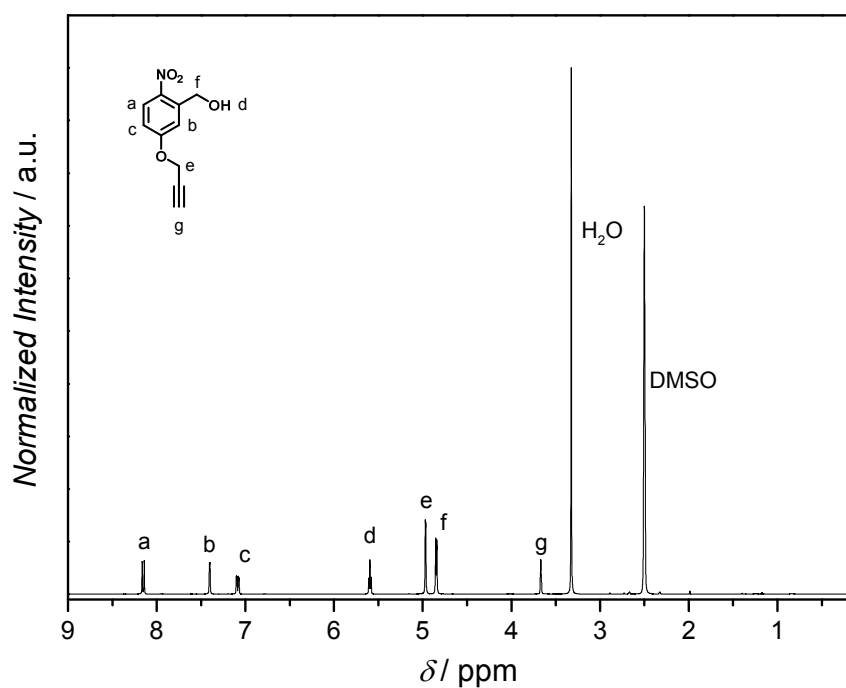


Figure A.1. ^1H NMR (500 MHz, 256 scans, DMSO- d_6) spectrum of (2-nitro-5-(prop-2-yn-1-yloxy)phenyl)methanol. Reproduced with permission from Wiley, 2015 (DOI: 10.1002/adma.201500426).

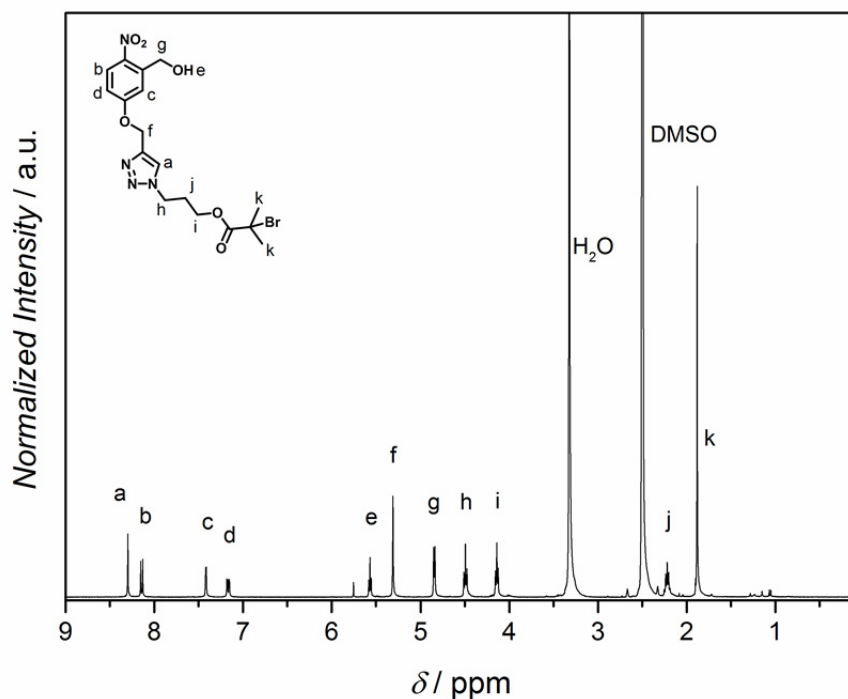


Figure A.2. ¹H NMR (400 MHz, DMSO-*d*₆) of 3-(5-((3-(hydroxymethyl)-4-nitro-phenoxy)methyl)-1H-1,2,3-triazol-1-yl)propyl 2-bromo-2-methylpropanoate. Reproduced with permission from Wiley, 2015 (DOI: 10.1002/adma.201500426).

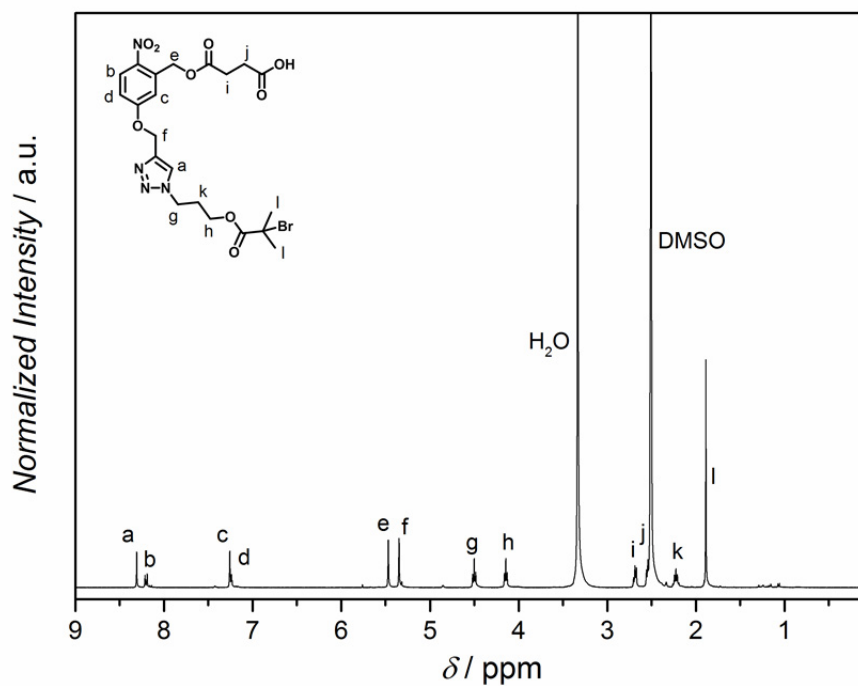


Figure A.3. ¹H NMR (400 MHz, DMSO-*d*₆) of 4-((5-((1-(3-((2-bromo-2-methylpropanoyl)oxy)propyl)-1H-1,2,3-triazol-5-yl)methoxy)-2-nitrobenzyl)oxy)-4-oxobutanoic acid (6). Reproduced with permission from Wiley, 2015 (DOI: 10.1002/adma.201500426).



Figure A.4. Sample holder made of stainless steel with the shadow mask utilized for photopatterning. The film is placed on a silicon wafer in the sample holder. Then the shadow mask is placed on top and secured with screws. Reproduced with permission from Wiley, 2015 (DOI: 10.1002/adma.201500426).

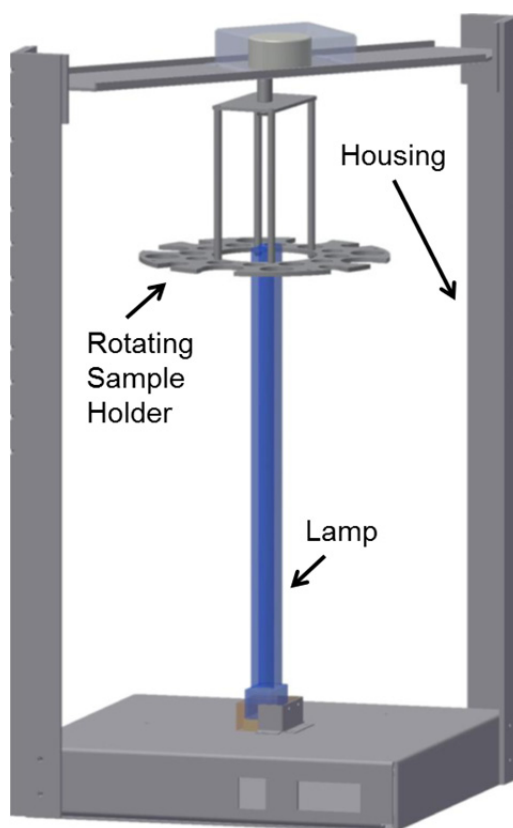


Figure A.5. Illustration of the custom-built photoreactor employed in the current study.

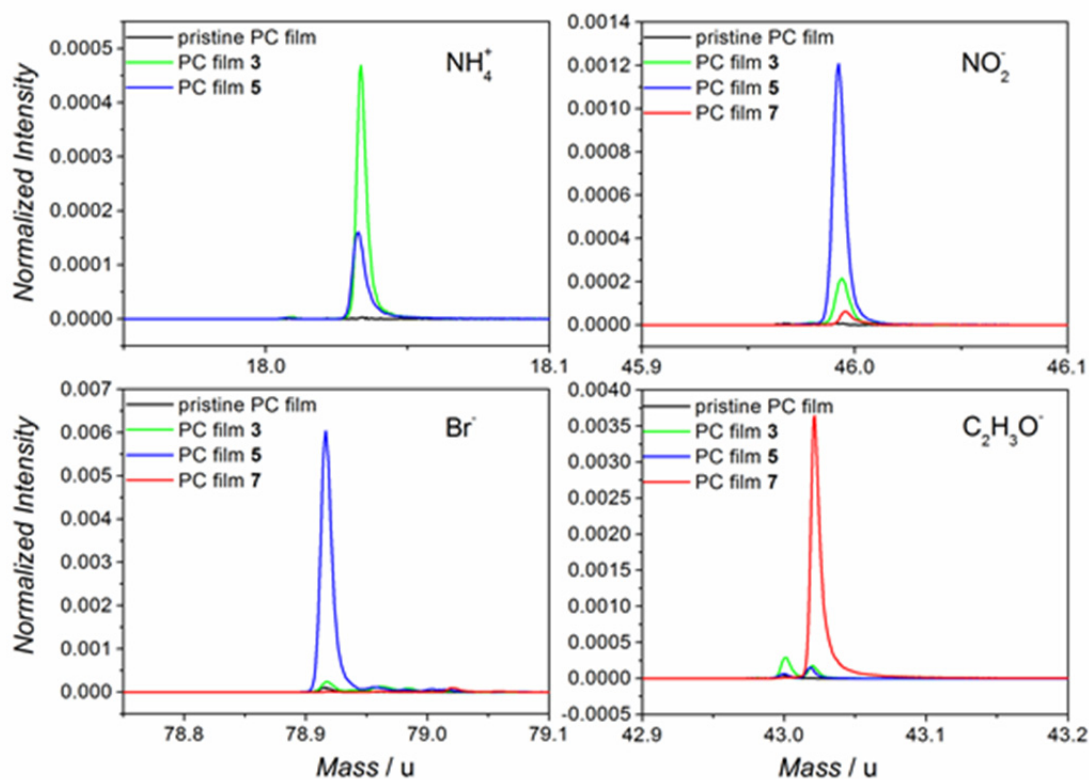


Figure A.6. ToF-SIMS spectra of important secondary ions which were imaged in Figure 3.3, Section 3.2.1. Reproduced with permission from Wiley, 2015 (DOI: 10.1002/adma.201500426).

Table A.1. ToF-SIMS analysis. Peak areas of the secondary ions shown in Figure A.6, normalized to total counts. Reproduced with permission from Wiley, 2015 (DOI: 10.1002/adma.201500426).

	NH_4^+	NO_2^-	Br^-	$\text{C}_2\text{H}_3\text{O}^-$
Pristine PC film	not detectable	not detectable	not detectable	not detectable
PC film 3	4.2×10^{-3}	2.2×10^{-3}	3.2×10^{-3}	2.3×10^{-3}
PC film 5	1.9×10^{-3}	1.1×10^{-2}	6.6×10^{-2}	2.5×10^{-3}
PC film 7	-	6.5×10^{-4}	1.2×10^{-4}	2.9×10^{-2}

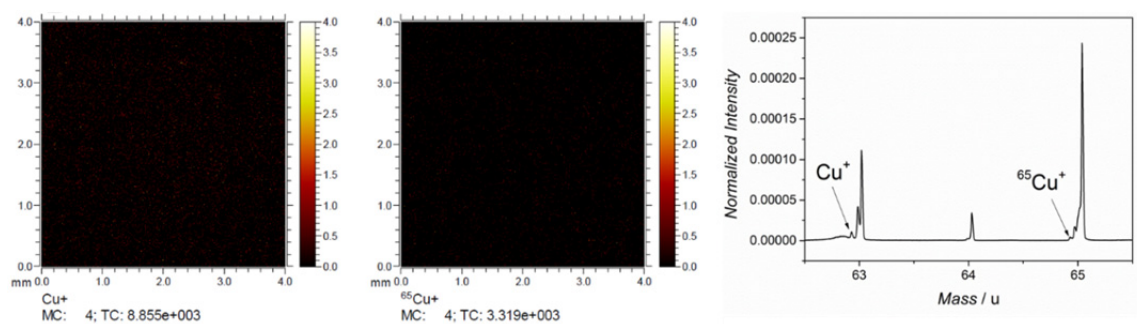


Figure A.7. ToF-SIMS maps for Cu^+ and $^{65}\text{Cu}^+$ ions and corresponding mass spectra normalized to total counts are depicted for the PC surface after SI-ATRP of MeOEGMA (9). Reproduced with permission from Wiley, 2015 (DOI: 10.1002/adma.201500426).

Appendix B

Complex Macromolecular Architectures via Supramolecular Chemistry and Photochemical Ligation (Appendix to Chapter 4)

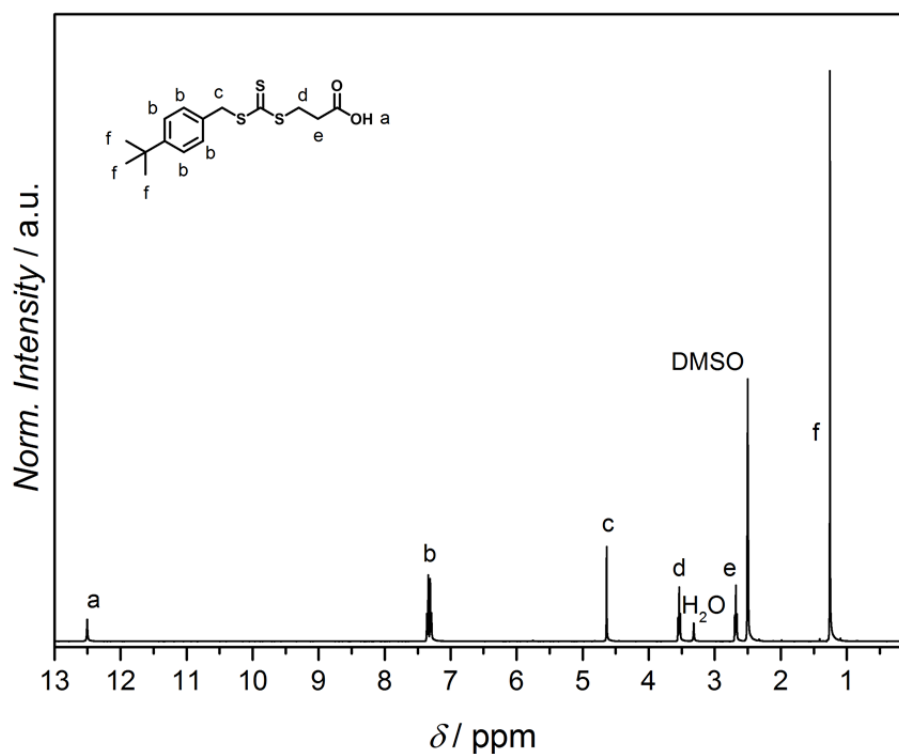


Figure B.1. ^1H NMR (400 MHz, $\text{DMSO-}d_6$, 25 $^\circ\text{C}$) spectrum of 3-(((4-(*tert*-butyl)benzyl)thio)carbonothioyl)thio)propanoic acid (**10**). Reproduced with permission from the American Chemical Society, 2015 (DOI: 10.1021/acsmacrolett.5b00485).

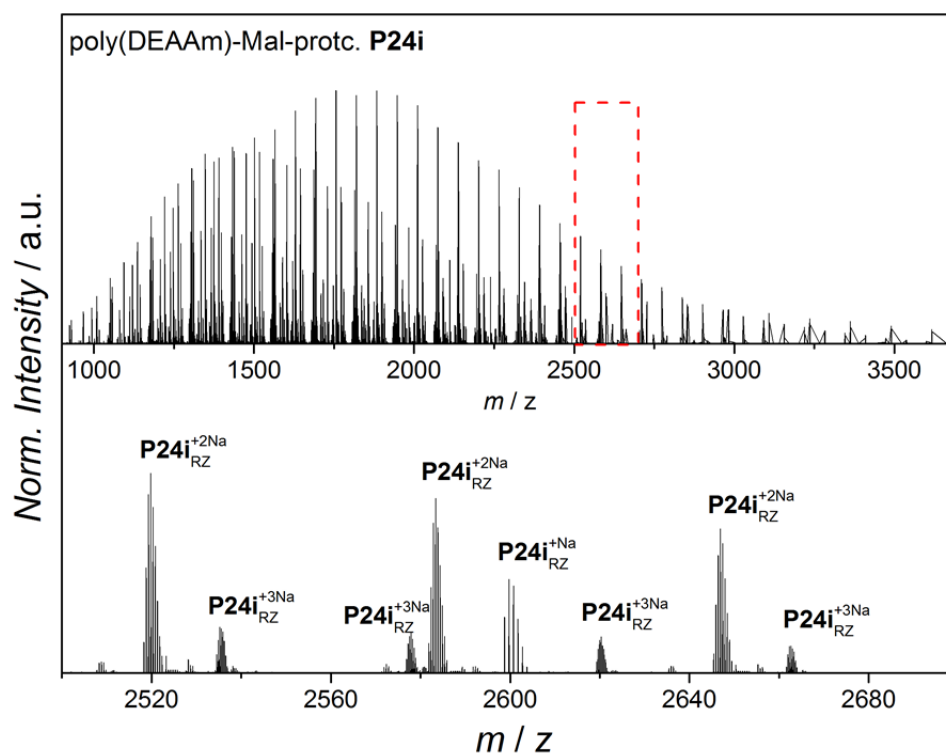


Figure B.2. ESI-MS spectrum of poly(DEAAm)-Mal-protc. **P24i** and a magnification of the spectrum (below). The spectrum shows the single, double and triple charged polymer chains of **P24i** ionized with Na⁺. Reproduced with permission from the American Chemical Society, 2015 (DOI: 10.1021/acsmacrolett.5b00485).

Table B.1. Mass peak assignment for poly(DEAAm)-Mal-protc. **P24i**. Experimental and theoretical m/z values for the labelled peaks shown in Figure B.2. Reproduced with permission from the American Chemical Society, 2015 (DOI: 10.1021/acsmacrolett.5b00485).

m/z_{exp}	assignment	chemical formula	m/z_{theo}	$\Delta m/z$
2519.346	p(DEAAm)-Mal-protc. + Na ₂	[C ₂₆₉ H ₄₈₉ N ₃₇ Na ₂ O ₄₁ S ₃] ²⁺	2519.316	0.030
2535.566	p(DEAAm)-Mal-protc. + Na ₃	[C ₄₀₉ H ₇₄₉ N ₅₇ Na ₃ O ₆₁ S ₃] ³⁺	2535.542	0.024
2577.938	p(DEAAm)-Mal-protc. + Na ₃	[C ₄₁₆ H ₇₆₂ N ₅₈ Na ₃ O ₆₂ S ₃] ³⁺	2577.909	0.029
2583.399	p(DEAAm)-Mal-protc. + Na ₂	[C ₂₇₆ H ₅₀₂ N ₃₈ Na ₂ O ₄₂ S ₃] ²⁺	2583.368	0.031
2599.776	p(DEAAm)-Mal-protc. + Na	[C ₁₃₆ H ₂₄₂ N ₁₈ NaO ₂₂ S ₃] ⁺	2599.745	0.031
2619.973	p(DEAAm)-Mal-protc. + Na ₃	[C ₄₂₃ H ₇₇₅ N ₅₉ Na ₃ O ₆₃ S ₃] ³⁺	2619.941	0.032
2646.950	p(DEAAm)-Mal-protc. + Na ₂	[C ₂₈₃ H ₅₁₅ N ₃₉ Na ₂ O ₄₃ S ₃] ²⁺	2646.918	0.032
2662.672	p(DEAAm)-Mal-protc. + Na ₃	[C ₄₃₀ H ₇₈₈ N ₆₀ Na ₃ O ₆₄ S ₃] ³⁺	2662.642	0.030

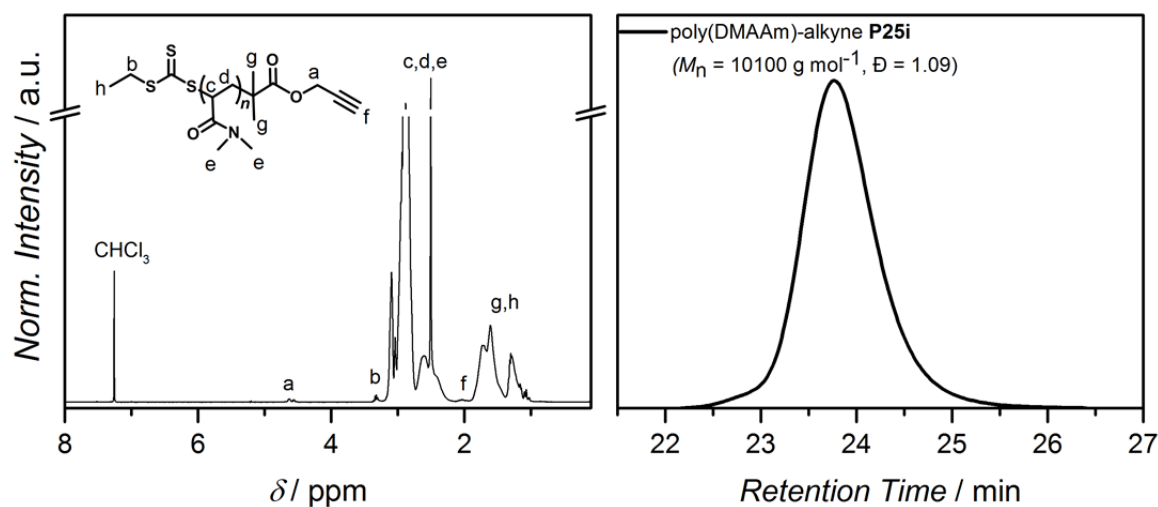


Figure B.3. ^1H NMR (400 MHz, CDCl_3) spectrum (left) and SEC trace (right) of poly(DMAAm)-alkyne (P25i). The picture was modified with permission from the American Chemical Society, 2015 (DOI: 10.1021/acsmacrolett.5b00485).

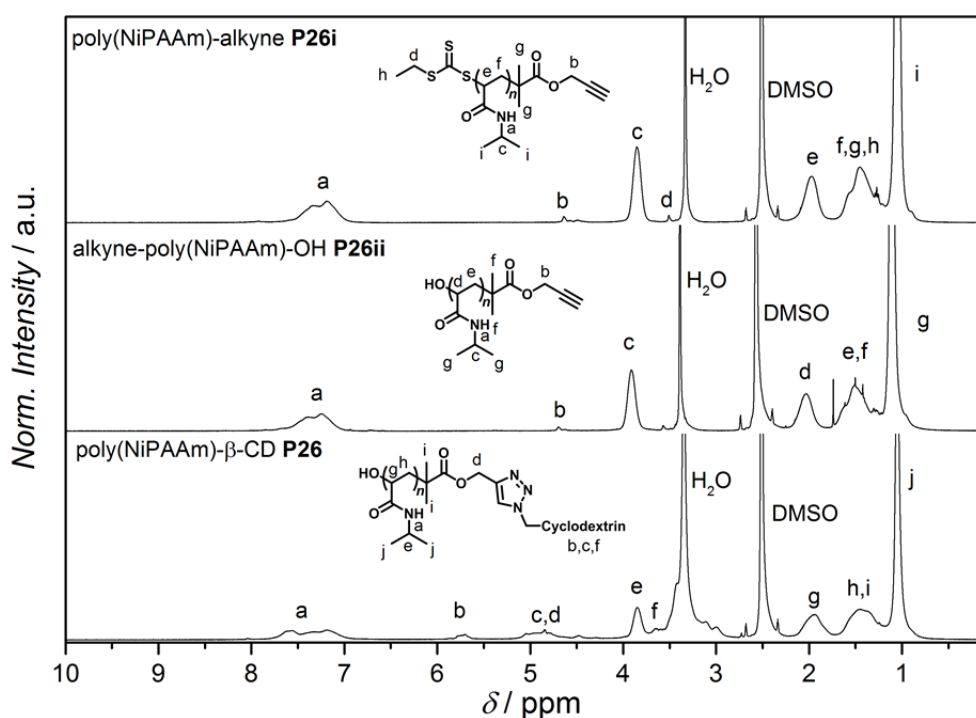


Figure B.4. ^1H NMR (400 MHz, DMSO-d_6 , $25\text{ }^\circ\text{C}$) spectrum of poly(NiPAAm)-alkyne **P26i** (top), alkyne-poly(NiPAAm)-OH **P26ii** and the final β -CD functionalized poly(NiPAAm)- β -CD **P26**, clearly showing the proton resonance signals of β -CD. Reproduced with permission from the American Chemical Society, 2015 (DOI: 10.1021/acsmacrolett.5b00485).

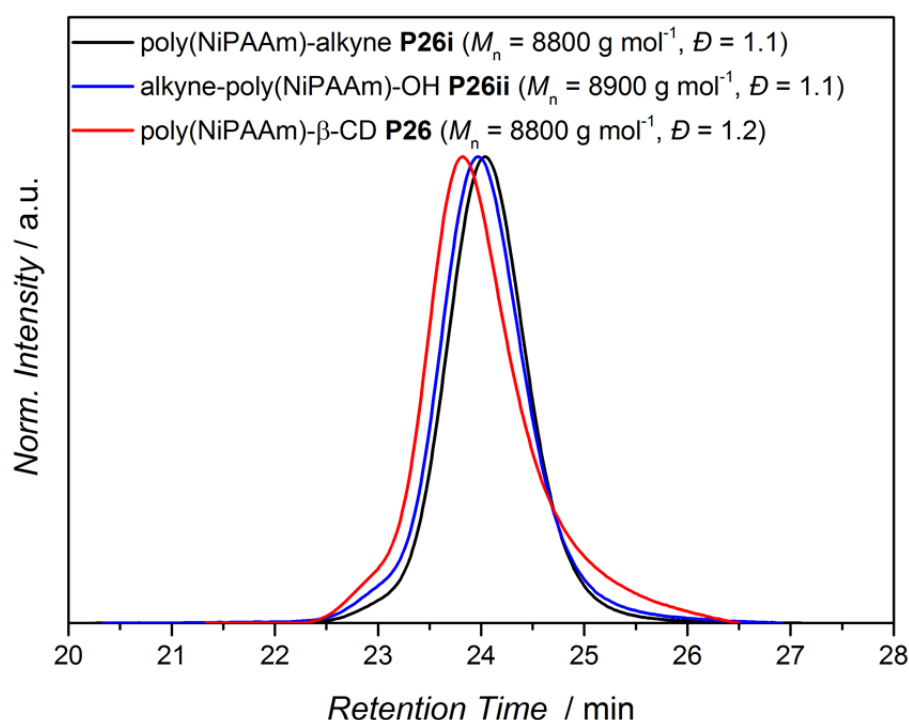


Figure B.5. SEC traces of poly(NiPAAm)-alkyne **P26i** (black), alkyne-poly(NiPAAm)-OH **P26ii** (blue) and poly(NiPAAm)- β -CD **P26** (red) measured in DMAC at 50 °C. Reproduced with permission from the American Chemical Society, 2015 (DOI: 10.1021/acsmacrolett.5b00485).

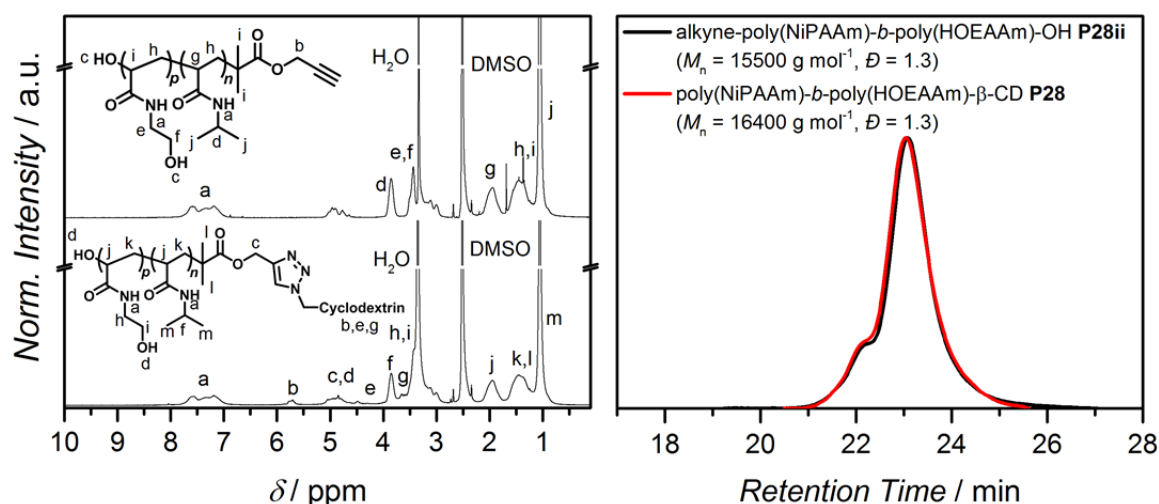


Figure B.6. Left) ^1H NMR (400 MHz, DMSO- d_6 , 25 °C) spectrum of alkyne-poly(NiPAAm)-*b*-poly(HOEAAM)-OH **P28ii** (top) and the final β -CD-functionalized poly(NiPAAm)-*b*-poly(HOEAAM)- β -CD **P28** (bottom), clearly showing the proton resonances of β -CD. Right) SEC traces of alkyne-poly(NiPAAm)-*b*-poly(HOEAAM)-OH **P28ii** (black) and poly(NiPAAm)-*b*-poly(HOEAAM)- β -CD **P28** (red) measured in DMAC at 50 °C. The picture was modified with permission from the American Chemical Society, 2015 (DOI: 10.1021/acsmacrolett.5b00485).

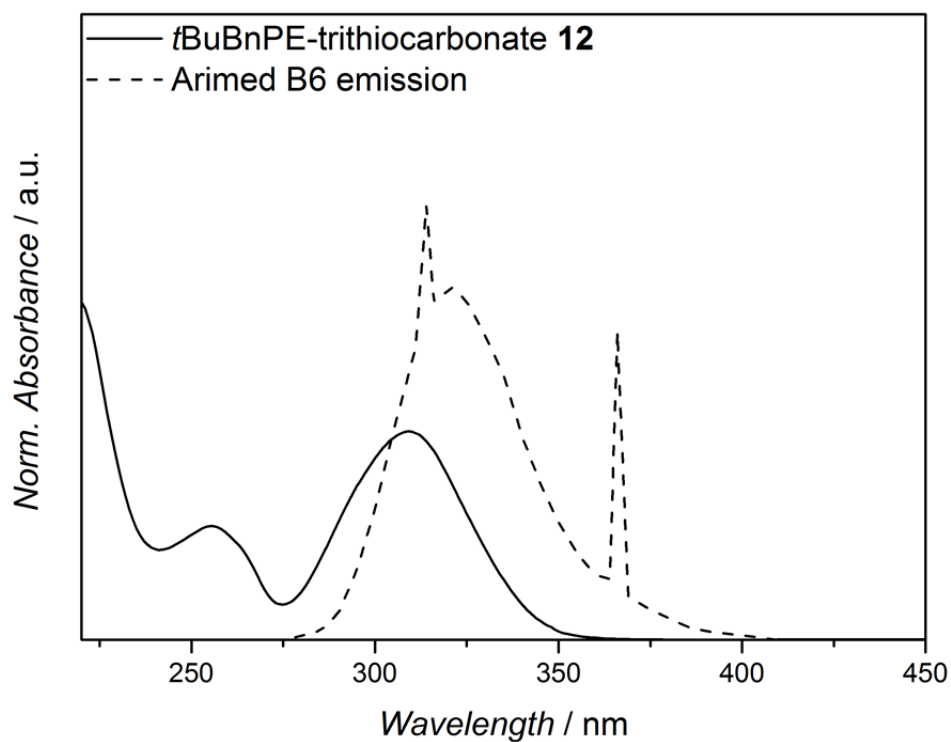


Figure B.7. Emission spectrum of the employed compact low-pressure fluorescent lamp (Arimed B6, 36 W) and the UV-Vis spectrum of the *t*BuBnPE-trithiocarbonate RAFT agent (**12**) measured in MeCN. Reproduced with permission from the American Chemical Society, 2015 (DOI: 10.1021/acsmacrolett.5b00485).

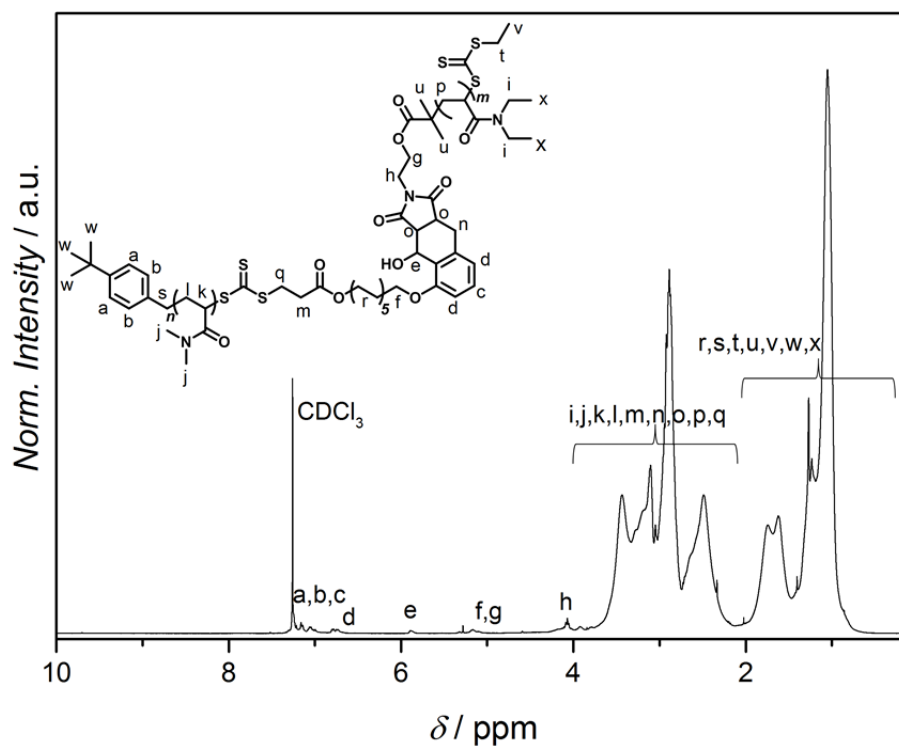


Figure B.8. ^1H NMR (400 MHz, CDCl_3) spectrum of the diblock copolymer poly(DMAAm)-*b*-poly(DEAAm) **P29**. Reproduced with permission from the American Chemical Society, 2015 (DOI: 10.1021/acsmacrolett.5b00485).

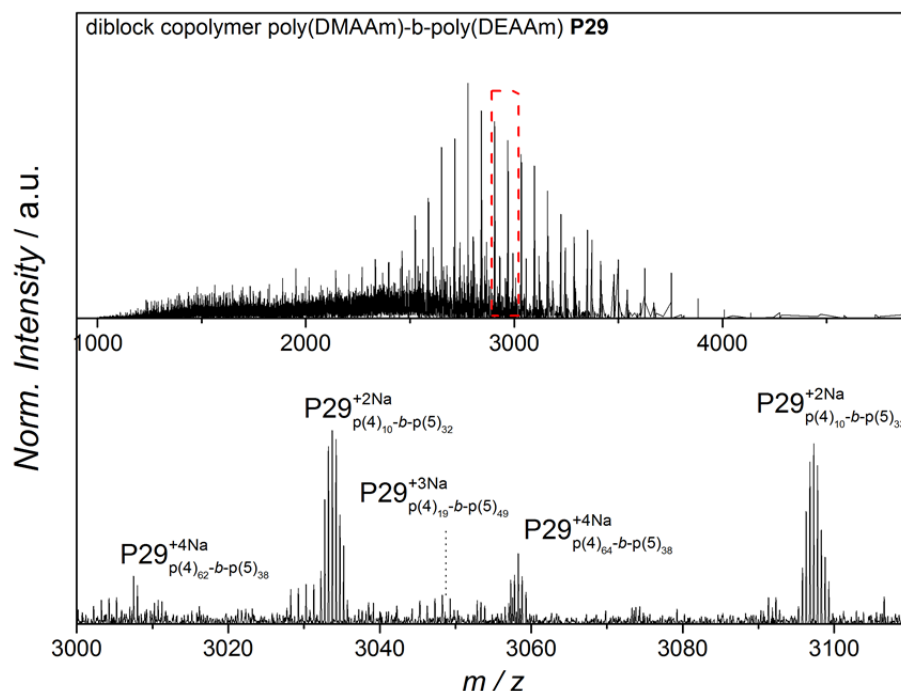


Figure B.9. ESI-MS spectrum of poly(DMAAm)-poly(DEAAm) **P29** and a magnification of the spectrum (below). The spectrum shows the double, triple and quadruple charged polymer chains of **P29** ionized with Na⁺. *It was noted that $\Delta m/z$ is very high and outside the resolution of the Orbitrap mass analyzer. The analyzed structure is a highly complex diblock copolymer and it is assumed that during ionization, for example, proton abstraction or similar processes occur. It was also note that the assigned peaks do not correspond to the single polymer blocks (**P23** and **P25**). On balance all analytical evidence (SEC, NMR and DLS) clearly points to the formation of the diblock copolymer **P29** and that the sub-Da deviation occurs during the ionization process. Reproduced with permission from the American Chemical Society, 2015 (DOI: 10.1021/acsmacrolett.5b00485).

Table B.2. Mass peak assignment for poly(DMAAm)-*b*-poly(DEAAm) **P29**. Experimental and theoretical m/z values for the labelled peaks shown in Figure B.9. Reproduced with permission from the American Chemical Society, 2015 (DOI: 10.1021/acsmacrolett.5b00485).

m/z_{exp}	assignment	chemical formula	m/z_{theo}	$\Delta m/z^*$
3007.499	$\text{p(DMAAm)}_{62}\text{-b-p(DEAAm)}_{38} + \text{Na}_4$	$[\text{C}_{623}\text{H}_{1117}\text{N}_{101}\text{Na}_4\text{O}_{108}\text{S}_6]^{4+}$	3006.822	0.677
3033.731	$\text{p(DMAAm)}_{10}\text{-b-p(DEAAm)}_{32} + \text{Na}_2$	$[\text{C}_{321}\text{H}_{571}\text{N}_{43}\text{Na}_2\text{O}_{50}\text{S}_6]^{2+}$	3033.575	0.156
3047.275	$\text{p(DMAAm)}_{19}\text{-b-p(DEAAm)}_{49} + \text{Na}_3$	$[\text{C}_{485}\text{H}_{873}\text{N}_{69}\text{Na}_3\text{O}_{76}\text{S}_6]^{3+}$	3047.483	0.208
3057.782	$\text{p(DMAAm)}_{64}\text{-b-p(DEAAm)}_{38} + \text{Na}_4$	$[\text{C}_{629}\text{H}_{1125}\text{N}_{105}\text{Na}_4\text{O}_{112}\text{S}_6]^+$	3056.836	0.946
3097.281	$\text{p(DMAAm)}_{10}\text{-b-p(DEAAm)}_{33} + \text{Na}_2$	$[\text{C}_{328}\text{H}_{584}\text{N}_{44}\text{Na}_2\text{O}_{51}\text{S}_6]^{2+}$	3097.125	0.156

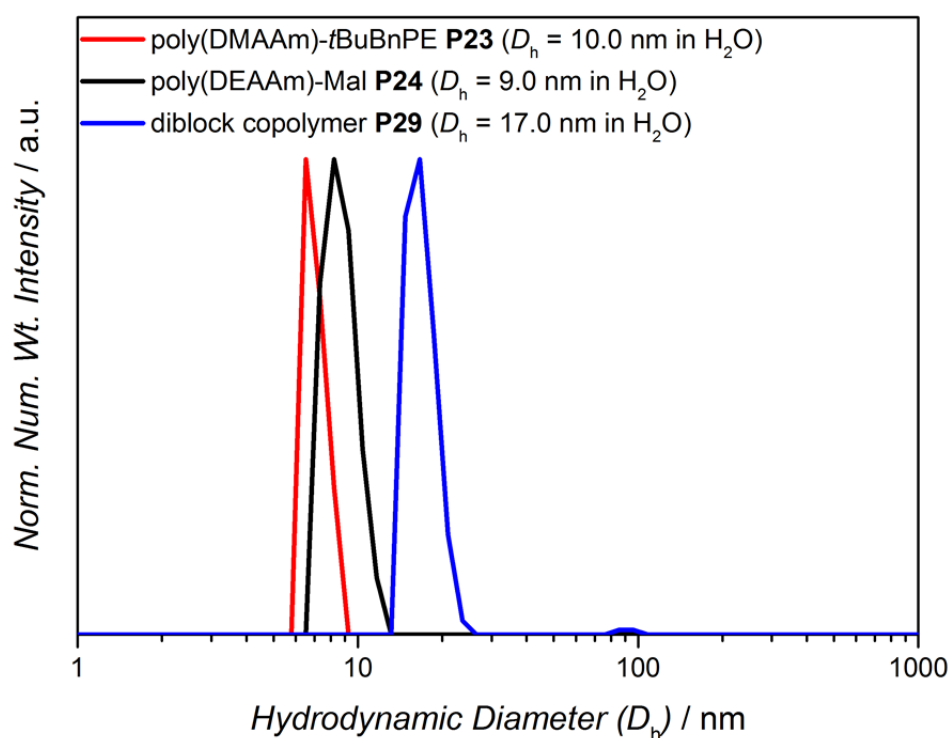


Figure B.10. DLS measurements at 25 °C in Milli Q water, showing number weighted size distributions of the single blocks: poly(DEAAm)-Mal **P24** and poly(DMAAm)-tBuBnPE **P23**, as well as the diblock copolymer **P29**. The samples were measured at a concentration of 0.06 mmol L⁻¹. Reproduced with permission from the American Chemical Society, 2015 (DOI: 10.1021/acsmacrolett.5b00485).

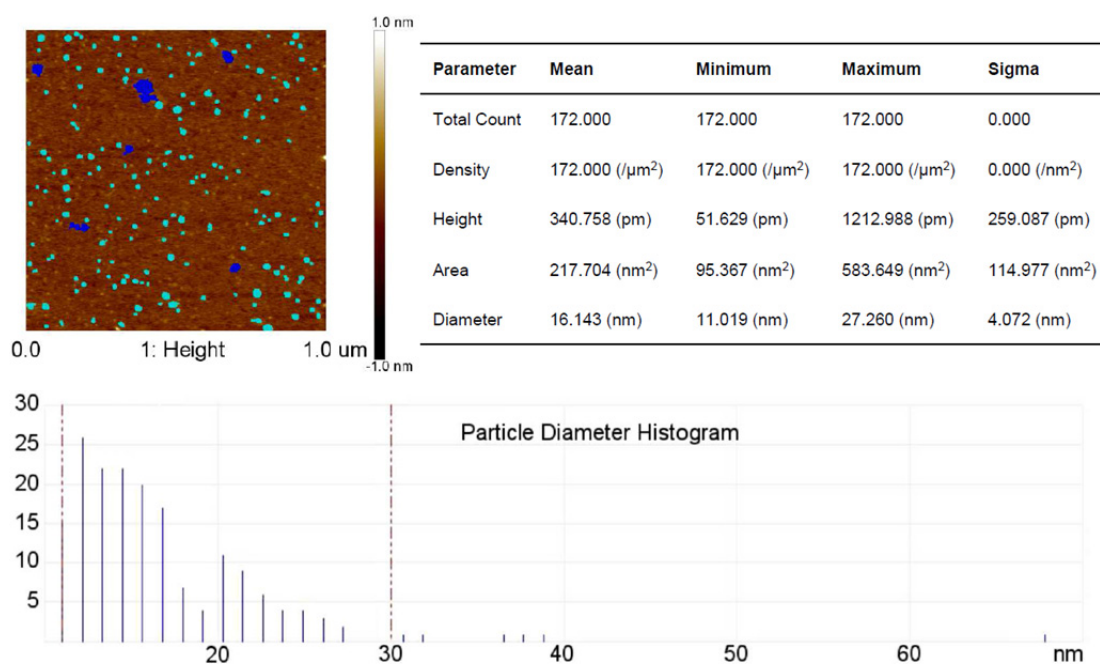


Figure B.11. 2D topographic image of the micelles (M42) along with the statistical data collected in a table, and a histogram of the particle diameters. The detected particles are colored in light blue. The spots colored in dark blue are agglomerates in the sample and were not considered in the analysis.

Particles analysis was performed from freshly cleaved mica surfaces with NanoScope Analysis 1.40 (Bruker). Reproduced with permission from the American Chemical Society, 2015 (DOI: 10.1021/acs.macromol.5b00923).

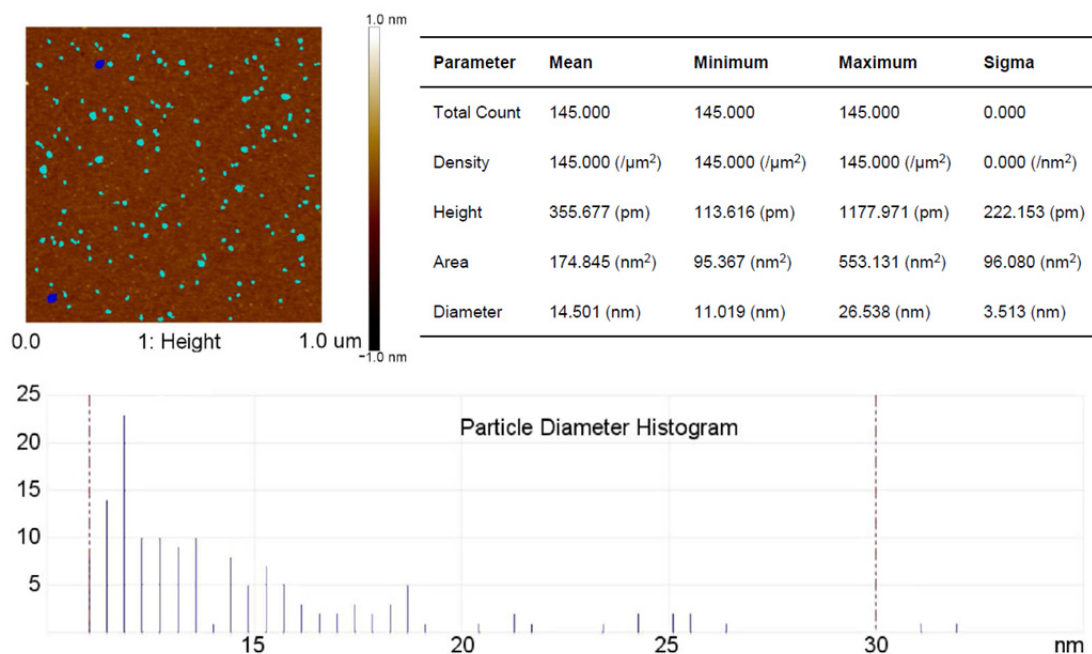


Figure B.12. 2D topographic image of the nanoparticles (**N43**) along with the statistical data collected in a table, and a histogram of the particle diameters. The detected particles are colored in light blue. The spots colored in dark blue are agglomerates in the sample and were not considered in the analysis. Particles analysis was performed from freshly cleaved mica surfaces with NanoScope Analysis 1.40 (Bruker). Reproduced with permission from the American Chemical Society, 2015 (DOI: 10.1021/acs.macromol.5b00923).

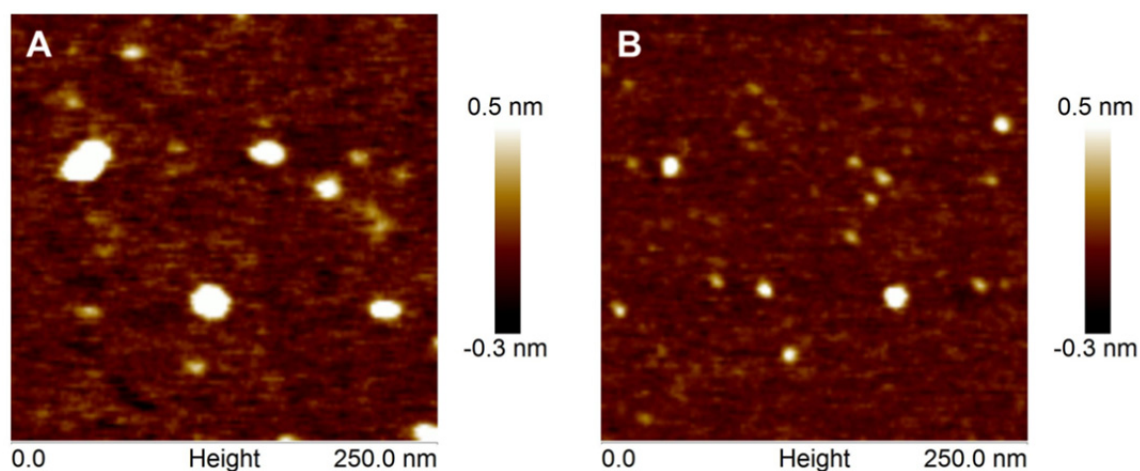


Figure B.13. Higher magnification AFM images of A) micelles (**M42**) and B) nanoparticles (**N43**). Reproduced with permission from the American Chemical Society, 2015 (DOI: 10.1021/acs.macromol.5b00923).

List of Publications

- [1] ***Photo-Induced Macromolecular Functionalization of Cellulose via Nitroxide Spin Trapping***
Delaittre, G.; Dietrich, M.; Blinco, J. P.; Hirschbiel, A.; Bruns, M.; Barner, L.; Barner-Kowollik, C. *Biomacromolecules* **2012**, *13*, 1700-1705.
- [2] ***Photo-Sensitive RAFT-Agents for Advanced Microparticle Design***
Kaupp M.; Tischer, T.; Hirschbiel A. F.; Vogt, A. P.; Geckle, U.; Trouillet, V.; Hofe, T.; Stenzel, M. H.; Barner-Kowollik, C. *Macromolecules* **2013**, *46*, 6858–6872.
- [3] ***Highly Efficient Photoluminescent Cu(I)-PyrPHOS-Metallopolymers***
Volz, D.; Hirschbiel, A. F.; Zink, D. M.; Friedrichs, J.; Nieger, M.; Baumann, T.; Braese, S.; Barner-Kowollik, C. *J. Mater. Chem. C* **2014**, *2*, 1457–1462.
- [4] ***Photolithographic Patterning of 3D-Formed Polycarbonate Films for Targeted Cell Guiding***
Hirschbiel, A. F.; Geyer, S.; Yameen, B.; Welle, A.; Nikolov, P.; Giselbrecht, S.; Scholpp, S.; Delaittre, G.; Barner-Kowollik, C. *Advanced Materials* **2015**, *27*, 2621-2626.
- [5] ***Photochemical Design of Stimuli Responsive Nanoparticles Prepared by Supramolecular Host-Guest Chemistry***
Hirschbiel, A. F.; Schmidt, B. V. K.; Krolla-Sidenstein, P.; Blinco, J.; Barner-Kowollik, C. *Macromolecules* **2015**, *48*, 4410-4420.

[6] *Access to Multiblock Copolymers via Supramolecular Host-Guest Chemistry and Photochemical Ligation*

Hirschbiel, A.F.; Konrad, W.; Schulze-Sünninghausen, D.; Wiedmann, S.; Luy, B.; Schmidt, B. V. K. J.; Barner-Kowollik, C. *ACS Macro Letters* **2015**, *4*, 1062-1066.

Conference Contributions

- [1] *Photolithographic Patterning of 3D-Formed Polycarbonate Films for Targeted Cell Guiding*
Hirschbiel, A. F.; Geyer, S.; Yameen, B.; Welle, A.; Nikolov, P.; Giselbrecht, S.; Scholpp, S.; Delaittre, G.; Barner-Kowollik, C. *European Polymer Congress 2015*, Dresden, Germany, 21 - 26th June 2015.

Danksagung

An dieser Stelle möchte ich allen Leuten danken, die mich während der drei Jahre begleitet und unterstützt haben.

Zuerst möchte ich mich bei Prof. Dr. Christopher Barner-Kowollik für die herzliche Aufnahme in seinen Arbeitskreis und die Betreuung dieser Arbeit bedanken. Auch dafür, dass er mir ermöglicht hat, drei Monate an der QUT in Australien zu verbringen, für seine Unterstützung und die Diskussionen möchte ich mich recht herzlich bedanken.

Dr. Bernhard Schmidt danke ich für die Unterstützung und Beratung während der zwei gemeinsamen Projekte, besonders auch für seinen Einsatz gegen Ende dieser Arbeit.

Dieser Dank gilt auch Dr. Guillaume Delaittre, der mir während des gemeinsamen Oberflächenprojekts zur Seite stand und auch sonst immer ein zuverlässiger Ansprechpartner war.

Dr. James Blinco danke ich für seine freundliche Aufnahme an der QUT und die Gelegenheit, meine Forschungsarbeiten in seinen Laboren fortzusetzen.

Auch Dr. Anja Goldmann, Frau Dr. Maria Schneider und Vincent Schüler, die die ganze Abteilung am Laufen halten, gilt mein herzlicher Dank.

Zusätzlich möchte ich mich auch bei meinen Kollaborationspartnern bedanken: dem Biologen-Team, Dr. Steffen Scholpp und Simone Geier für die Zelltests auf den Polycarbonat-Oberflächen, Dr. Peter Krolla-Sidenstein für die AFM-Messungen und die netten Treffen, Prof. Dr. Burkhard Luy und David Schulze-Sünninghausen für die

NOESY-Messungen, Dr. Stefan Giselbrecht und Dr. Pavel Nikolov für das Thermoformen der Polycarbonatfilme. Ganz besonderer Dank gilt auch Dr. Alexander Welle für die zahlreichen ToF-SIMS-Messungen und Dr. Basit Yameen für seine tollen Ratschläge und für seine Unterstützung.

Ich möchte mich auch bei Andrea Lauer und Waldemar Konrad für ihre gute Arbeit als Hiwi- und Vertiefenstudenten bedanken.

Des Weiteren danke ich dem gesamten Masseteam – Michi, Kai und Andrea – für die gute Zusammenarbeit.

Für das Korrekturlesen dieser Arbeit danke ich: Andrew Inglis, Anja Goldmann, Elena Frick, Eva Blaso, Jan Steinkönig, Kai Hildebrandt, Kai Pahnke, Mark Pfeifle und Mikela Trigilio.

Bedanken möchte ich mich auch bei meinen Kollegen: Elena, Eva, Kai H., Lukas, Andrea H., Andrea L., Kim, Paul, Christiane, Thomas T., Alexander H. und Corinna für die Gespräche, Diskussionen und Kaffeepausen.

Auch bei Mirja und Papia möchte ich mich für die schöne gemeinsame Zeit seit dem Studium bedanken.

Nicht zuletzt möchte ich mich von ganzem Herzen bei meiner Familie bedanken, die mich ständig unterstützt hat und auch viel Verständnis aufgebracht hat. Ganz besonders möchte ich mich an dieser Stelle bei meiner Mama, meiner Oma und Mark bedanken, der durch seine Unterstützung einen großen Teil zum Gelingen dieser Arbeit beigetragen hat.